An Observational Exploration of the Evolution of Angular Momentum in Close Detached Binary and Single Stars of Solar Type

by

Søren Christian Dalgaard Meibom

A dissertation submitted in partial fulfillment of the

requirements for the degree of

Doctor of Philosophy

(Astronomy)

at the

University of Wisconsin – Madison

2005

To my parents

- for building the foundation from where I can reach my goals

Acknowledgments

It is a pleasure to acknowledge the people who have directly or indirectly contributed to this work.

Starting with my family, I wish to thank my parents for a lifetime of love, support, and a never failing encouragement to pursue my goals. They have given me more than any child can expect and I dedicate this thesis to them as a token of my appreciation.

Sara, my wife and invaluable friend and companion through six years. Her love, patience, and dedication to me and our two children has been essential to the successful completion of this thesis.

Robert Mathieu, my thesis advisor and friend. In addition to his outstanding talents and skills in science, he is a considerate and good man and a great father who has been a role model for me in matters of life in general as well as in the world of astrophysics. I am thankful for all his insightful advice and guidance, and for his generous financial support that has made it possible for me to present my work and meet with colleagues all over the world. This thesis builds in many ways on his accomplishments in the field of binary stars and open clusters, and is one among many excellent theses that have resulted from the WIYN Open Cluster Study, of which he has been an effective leader. I am certain that I will continue to discover important lessons that he taught me in many years to come. Bob and his family has always been hospitable and has generously helped my family in many ways these very hectic last months.

Jean-Paul Zahn, whose brilliant work has greatly improved our understanding of the physics of tidal interactions in close binary stars. His contributions to this field has guided theoretical and observational efforts for decades including this thesis. It has been a great pleasure to get to know him and a honor to enter a collaboration with him.

Keivan Stassun, who welcomed and helped me from the first day I arrived in Madison. As a friend and a colleague, he has been important to my life as a graduate student and to the quality of this thesis work. I thank him for generously sharing his time and knowledge.

Sydney Barnes, a close friend whose taste in food, wine, and music is surpassed only by his talent and passion for science. Discussions with Sydney about astronomy and other matters have been invaluable to my work and well-being. He made me laugh and smile when it was most needed.

David James, a unique source of support, help, and wisdom about the world of astronomy and beyond. Our shared sense of humor and interests in astronomy and life have led to many memorable moments and will continue to do so for many years to come.

Chris Dolan, who taught me the process of deriving high-precision radial velocities from multi-object spectroscopic observations and willingly shared his vast knowledge of computer programming, and Aaron Steffen, with whom I studied for many exams and who is always ready to share his large knowledge about computer hardware and software. Aaron's help with formatting this thesis to meet the requirements of the graduate school was critical.

I am grateful to all faculty, staff, and fellow students of the University of Wisconsin - Madison Astronomy Department. The department is an exceptionally friendly and pleasant place to work. It is full of considerate and skilled people from whom I have received much help and learned many important skills.

I thank the members of the WIYN Open Cluster Study (WOCS) team. I have received much help from them and always enjoyed their company.

This thesis is based entirely on observational data from the WIYN telescopes. I express my appreciation for the high quality of these facilities and for the friendly and skilled observatory staff. I would like to thank the following people by name: George Jacoby, Diane Harmer, Charles Corson, Darryl Willmarth, and Heidi Schweiker. And I thank the many great telescope operators that I have worked with over the years.

I would have never crossed the Atlantic to work in the company of all these wonderful people, if not for the 3 year Ph.D fellowship I received from the Danish Research Agency (Forskningstyrelsen). The opportunity that fellowship gave me has truly changed my life and their service and support has been superb.

Finally, but most importantly, I wish to thank my "astronomical parents" Johannes Andersen and Birgitta Nordström from Copenhagen, Denmark. Their enthusiasm for astronomy was a deciding factor in my choice to pursue a career in this field. Their experience and generous help has had a very positive impact on my life and has been critical to my success.

Contents

List of Tables

List of Figures

Chapter 1

Introduction

In this thesis I study observationally the impact of a close binary companion on the evolution of rotational and orbital angular momentum of late-type stars.

For a given mass distribution and fixed total angular momentum, a detached binary system has the least mechanical energy when it rotates as a rigid body. This minimum energy state requires the two stars to have circular orbits and synchronized spins. If a detached binary does not have circular orbits or synchronized spins, then there exists no frame of reference in which all differential motions disappear and kinetic energy will continue to dissipate into heat and be radiated into space until the equilibrium state of both circular orbits and synchronized spins is reached.

In the closest binary stars ($a \lesssim 0.2$ AU) tides are introduced in the two stars by the gradient of their mutual gravitational pull. Viscous dissipation of kinetic energy introduces a phase shift in the tidal bulge, allowing a torque on the tilted mass distribution to drive an exchange of stellar and orbital angular momentum. The cumulative effects of such tidal interactions with time is referred to as tidal evolution. The characteristic signs of completed tidal evolution are: 1) Alignment of the stellar spin axes perpendicular to the orbital plane; 2) Synchronization of the rotation of the stars to the orbital motion; 3) Circularization of the orbits.

The main challenge for theoretical models of tidal evolution is to identify and understand the processes responsible for dissipation of kinetic energy within the stars. The efficiency of such mechanism(s) controls the rate and evolution of tidal circularization and synchronization. At the present time, the efficiency of the dissipation mechanisms employed by tidal theory cannot account

for observations of tidal evolution.

Observations of tidal circularization have been the primary constraint on tidal theory over the past 2 decades (e.g. Mathieu et al. 1992; Duquennoy et al. 1992; Melo et al. 2001; Latham et al. 2002; Mathieu et al. 2004). In particular, the distribution of orbital eccentricities with orbital periods (the $e - \log(P)$ diagram) has provided clear evidence for tidal circularization in homogeneous and coeval populations of binaries, and enabled a measure of the degree of circularization as a function of orbital period integrated over the lifetime of the binary population.

In comparison, observational data suitable for measuring the rate of tidal synchronization in late-type binaries are sparse. This is in part because, practically speaking, binary orbital elements are simpler to obtain than rotation periods for stars in binaries, but also because telescope and instrument capabilities in the past have favored rotational measurements of bright and rapidly rotating stars.

The observational study of tidal evolution is important for several reasons. First, the rate of tidal evolution depends on dissipative processes within the stars which in turn are sensitive to stellar interior structure. The interior structure and dissipative mechanisms are predicted by stellar and tidal theory (Zahn 1989; Terquem et al. 1998; Goodman & Dickson 1998; Savonije & Witte 2002). Observations of tidal circularization and synchronization, constraining tidal theory, are therefore fundamentally testing our understanding of stellar interior theory. Second, provided that we understand these dissipative processes, the observed properties of a given binary system can deliver important information about its evolutionary state, on its past history, and even on the conditions of its formation. Third, tidal synchronization of the observable surface layers is closely linked to the internal angular momentum transport in the star. Thus, the rate of synchronization of the surface layers can shed light on the coupling between those layers and the stellar interior. Fourth, the range in binary separations over which tidal synchronization can significantly affect stellar angular momentum evolution provides important information about the impact of binarity on stellar angular momentum evolution in late-type stars. Fifth, simultaneous observations of tidal synchronization and magnetic field tracers (X-rays, chromospheric emission, etc.) during rapid stellar evolution may enable determination of the evolution rates of stellar dynamos.

Finally, many of the recently discovered extra-solar planets, ("hot Jupiters") orbit close enough

to their host stars that significant tidal synchronization and circularization is expected. Tidal interactions in star-planet systems may therefore play an important role in determining the observed distributions of mass, orbital period, and eccentricity of extra-solar planets (Ogilvie & Lin 2004).

In binaries that are too wide for significant tidal evolution ($a \gtrsim 0.2$ AU) the stars might still affect each others angular momentum evolution. Models of the evolution of pre main-sequence (PMS) binaries with companions separated by less than the typical circumstellar disk radius ($a \lesssim 100$ AU) predict that the companion will truncate, and possibly tidally disrupt, the circumstellar disk. Accordingly, the lifetime of circumstellar disks for such binary configurations are expected to be short compared to those of wider binaries and single stars. Furthermore, recent theoretical models of low-mass PMS stars suggest that their rotational evolution is largely dictated by magnetic star-disk interactions ("magnetic disk-locking"). Consequently, the effect of a close companion on the disk lifetime in the PMS phase should ultimately reveal itself in the rotational evolution as the star approaches and settles on the main-sequence.

Published observational studies searching for a relation between binarity and stellar rotation are still few and their results are contradictory. A reliable detection or non-detection of a correlation between the presence of a close (0.2 AU $\lesssim$ a $\lesssim$ 100 AU) companion will provide additional insight into the PMS rotational evolution of late-type stars, particularly on the role of interactions between the companion and the circumstellar disk.

1.1 Theory of Tidal Evolution

The phenomenon of tides is familiar to us from the water-tides on earth. Tides in stars were first considered by Darwin (1879) who described the formation of stellar tides in close binary systems. Almost a century passed before tides in stars again were brought to the attention of the astronomical community in a series of thesis papers by (Zahn 1966a,b,c). Zahn's work was motivated by a compilation of orbital eccentricities of eclipsing binaries by Kopal & Shapley (1968). The data showed a striking relation between stellar mass/structure of the binary components and the degree of tidal circularization. This result led Zahn to develop what are still today the primary theories of tidal evolution in close binaries (Zahn 1970, 1975, 1977, 1989) - the *dynamical tide theory* and the *equilibrium tide theory*.

The equilibrium tide theory (Zahn 1989; Hut 1981; Zahn 1977) has been the primary theory used to explain tidal evolution in late-type main-sequence binaries. The theory was extended by Zahn & Bouchet (1989) to include tidal evolution during PMS evolution. The dynamical tide theory (Zahn 1977, 1975), which before 1998 was used to explain tidal evolution in early-type binaries, was recently applied to solar-type main-sequence binaries (Witte & Savonije 2002; Savonije & Witte 2002; Terquem et al. 1998; Goodman & Dickson 1998). Both theories predict the rate of tidal circularization and synchronization, although based on entirely different mechanisms for tidal dissipation.

In the equilibrium tide theory a star will adjust instantaneously to the perturbing force exerted by its companion. Consequently the tidal bulges will align with the line joining the two stars. However, if a dissipation mechanism exist causing friction to the tidal flow, then the tidal bulges will either lead or lag the companion in its orbit by an angle α if the star's angular rotation velocity ($\Omega_\star$) is either greater or smaller than the orbital angular velocity of the companion (ω). In solar-type stars turbulent viscosity is identified as the dissipation mechanism. The shear between the tidal flow and the convective motion causes the kinetic energy of the large-scale motions to cascade down to smaller and smaller scales until it is dissipated into heat. Now, $\alpha \propto (\Omega - \omega)/t_{diss}$, where t_{diss} is he characteristic time for the dissipative process. The tilted mass distribution result in a tidal torque (Γ) on the star, which will cause an exchange of stellar and orbital angular momentum and consequent tidal evolution ($\Omega \rightarrow \omega$, $e \rightarrow 0$). Figure 1.1 shows a schematic view of a close binary system, and equations (1.1), (1.2), and (1.3) give the expressions for the torque and the resulting characteristic times for tidal synchronization and circularization, respectively, in the equilibrium tide theory (Zahn 1989):

$$\Gamma = \frac{6(\Omega - \omega)}{t_{diss}} \; \lambda \; q^2 \; M \; R^2 \Big(\frac{R}{a}\Big)^6 \tag{1.1}$$

$$t_{sync} = \frac{t_{diss}}{6 \; \lambda_{sync} \; q^2} \; \frac{I}{M \; R^2} \; \Big(\frac{a}{R}\Big)^6 \tag{1.2}$$

$$t_{circ} = \frac{t_{diss}}{21 \; \lambda_{circ} \; q(1+q)} \; \Big(\frac{a}{R}\Big)^8. \tag{1.3}$$

Both times are strongly dependent on the ratio of the stellar radius (R) to the stellar separation (a), suggesting that the transition in period between circularized/non-circularized and synchronized/non-synchronized binaries will be well defined, and that significant tidal evolution will be restricted to the closest binaries. M denotes the stellar mass, I the moment of inertia, q the binary mass ratio, t_{diss} the viscous dissipation time, and $\lambda_{sync/circ}$ a structural constant whose value depends on the mass concentration within the stars and on where in the star the tidal torque is applied. The ratio of eqs. [1] and [2] gives that $t_{circ} \simeq 10^3 \times t_{sync}$ for a main-sequence binary with solar-type components. Tidal synchronization proceeds faster than circularization because the angular momentum of the stars ($\sim I\Omega << MR^2\Omega$) is much smaller than that of the orbits ($\sim Ma^2\omega$). ω and Ω are the orbital angular velocity and the stellar rotation angular velocity, respectively.

As $t_{sync} << t_{circ}$, stars in eccentric binaries will synchronize their spin angular velocities to a value Ω_{ps} close to the orbital angular velocity at periastron passage (ω_p) where the stellar separation is smallest. This is called "pseudo-synchronization" (Hut 1981). Hut (1981) derives an expression for Ω_{ps} by setting the tidal torque on the stars integrated over the eccentric orbit equal to zero.

A graphical illustration of tidal evolution from the birth line to the late main-sequence of an initial 5 day eccentric binary with two 1.0 $M_\odot$ stars is given by Zahn & Bouchet (1989) in their Figure 1 and shown here in Figure 1.2. The synchronization procceds rapidly and the system becomes pseudo-synchronized and subsequently circularized well before it reaches the zero-age main-sequence (ZAMS). As the stars contract onto the ZAMS they spin up while their convection zones retreat and the stellar radii decrease. Consequently, tidal breaking is no longer effective enough to prevent the star from spinning up as it approaches the ZAMS. Once settled on the main-sequence, synchronization resumes and is completed by an age of $\sim$ 1 Gyr.

A particularly interesting result from the models by Zahn & Bouchet (1989) is that in a solar-type binary all tidal circularization occurs during the PMS phase when the stars are large and deeply convective, and no measureable tidal tidal circularization occurs during the main-sequence phase. In effect, their model predict that the degree of tidal circularization in a binary population does not

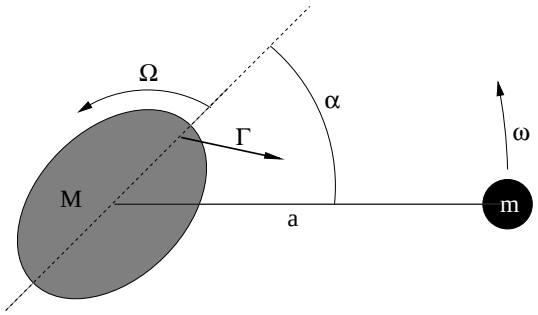

Fig. 1.1.— Schematic view of a binary system with a primary star with mass M and secondary star with mass m separated by a distance a. The rotational angular velocity of the primary star is denoted Ω while the orbital angular velocity of the secondary is denoted ω. In the example shown here $\Omega_\star > \omega$. The angle α represents the misalignment of the tides with respect to the line joining the centers of the two stars. This misalignment is due to the dissipation of tidal energy within the primary star and it results in a net torque Γ responsible for the exchange of angular momentum between the rotation of the primary star and the orbit of the secondary star.

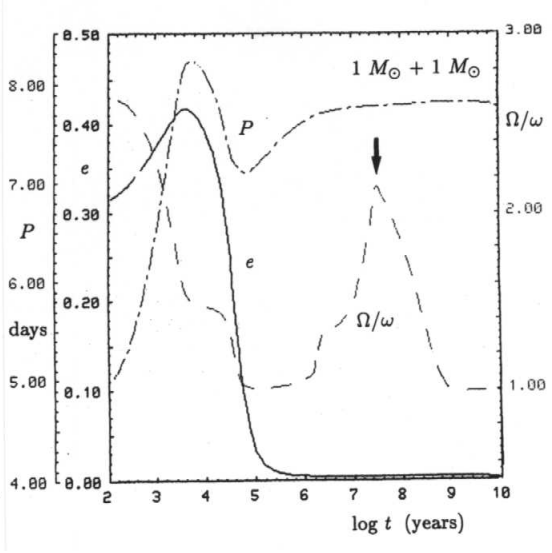

Fig. 1.2.— Figure 1 from Zahn & Bouchet (1989). Evolution in time of the eccentricity e, the orbital period P, and of the ratio between the rotational and orbital velocities (Ω/ω), for a system with two components of 1 $M_\odot$.

change with the population age. This was a surprise as all privious models had predicted ongoing tidal circularization throughout the main-sequence phase.

The dynamical tide is the result of excitation of oscillating internal gravity modes by the periodic tidal potential of the binary companion. The transfer of angular momentum between the companion's orbit and the star happens when the excited modes are thermally damped either near the radiative surface (early-type stars) or at the base of the convective envelope (late-type stars). Terquem et al. (1998) and Goodman & Dickson (1998) were the first to investigate the effect of dynamical tides in the radiative core of solar-type stars. Savonije & Witte (2002) and Witte & Savonije (2002) re-examined the idea and argued for the importance of resonance locking between stellar eigenmodes and tidally induced modes. The dynamical tide with resonance locking is currently the most efficient tidal dissipation mechanism for late-type stars on the main-sequence. However, the model predictions presented in Witte & Savonije (2002) do not include the PMS phase.

Figures 1 and 3 in Witte & Savonije (2002) show the evolution of orbital and stellar parameters for a pair of 1 $M_{\odot}$ stars according to their model. Evolution starts on the ZAMS. The stars in the initially 16-day, highly eccentric binary rotate super-synchronously. Figure 1.3 shows the evolution of the orbital eccentricity and the stellar rotation for this binary. Pseudo-synchronization is achieved within $\sim$ 500 Myr due to strong retrograde gravity modes. The orbital eccentricity declines by less than 10% in the same time. The spin-down is followed by a spin-up between 0.5-1.0 Gyr due to prograde modes, at which point a decrease in the stellar separation triggers efficient retrograde modes that forces the stars to spin down to sub-synchronous rotation at $\sim$ 3 Gyr. Eventually, circularization of the orbit leads to diminishing retrograde forcing and the stars approach synchronous rotation over the remainder of the main-sequence phase.

1.2 Observations of Tidal Evolution

As the orbital data for eclipsing binaries (Kopal & Shapley 1968) motivated Zahn's theoretical work, so did Zahn's efforts motivate a search for evidence for the predicted tidal evolution. For late-type main-sequence binaries the first response came from Koch & Hrivnak (1981) who presented the distribution of orbital eccentricities against their orbital periods (the $e - \log(P)$ diagram) for a large sample of spectroscopic and eclipsing late-type field binaries. The effect of tidal circularization

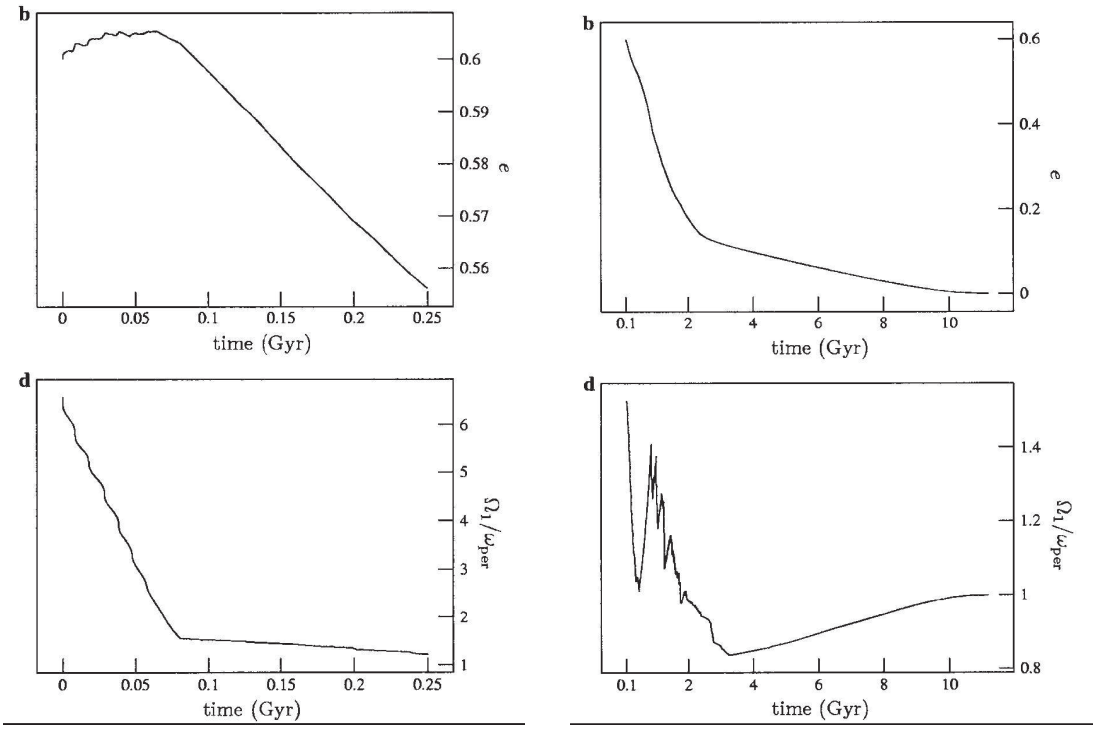

Fig. 1.3.— Model evolution of orbital and stellar parameters for a pair of 1 $M_{\odot}$ super-synchronous stars in a initially 16 day highly eccentric binary. Taken from Figure 1 and 3 in Witte & Savonije (2002).

was clear. Binaries with periods shortward of ∼6 days have circular orbits, while binaries with longer orbital periods displayed a distribution of non-zero eccentricities. The interest in tidal circularization of solar-type main-sequence binaries got an extra boost when a short conference paper by Mayor & Mermilliod (1984) presented a sharp transition from circular to eccentric binaries at a period of 5.7 days among main-sequence binaries in 4 intermediate-age clusters (see Figure 1.4). Next Mathieu & Mazeh (1988) showed a similar transition in the older open cluster M67 at 10.3 days, and suggested that the longer period was due to tidal circularization operating over a longer time interval (4.5 Gyr compared to $\sim$ 0.6 Gyr). Following a workshop in 1992 (Bettmeralp, Switzerland), which became a wide-ranging exploration of the $e - \log(P)$ diagram, the observed dependence of tidal cutoff periods (defined as the longest period circular orbit) on age was analyzed by Mathieu et al. (1992) and Duquennoy et al. (1992). Comparison to the predictions of several theoretical models showed that

no one theory of tidal circularization could explain the observed cutoff periods of both the young and old clusters.

Over the next decade most new orbital solutions were for PMS binaries. These were summarized by Melo et al. (2001) and a new PMS cutoff period of 7.6 days, compared to the preliminary value of 4.3 days used by Mathieu et al. (1992), was reported. Importantly, the observational data as of 1992 as well as the new PMS data suffered from a limited number of binaries in each population, and a lack of homogeneity in the primary stars of those binaries.

The advent of multi-object high-resolution spectrographs mounted on large telescopes, such as Hydra on WIYN, have stimulated extensive studies of cluster binary populations. A particularly important new result is the cutoff period of 15.0 days for the 7-Gyr cluster NGC188 (Mathieu et al. 2004). This cutoff period confirms that older clusters have cutoff periods significantly longer than young-to-intermediate age clusters, and thus suggests that tidal circularization is indeed ongoing during the main-sequence phase of evolution in contrast to the prediction by Zahn & Bouchet (1989).

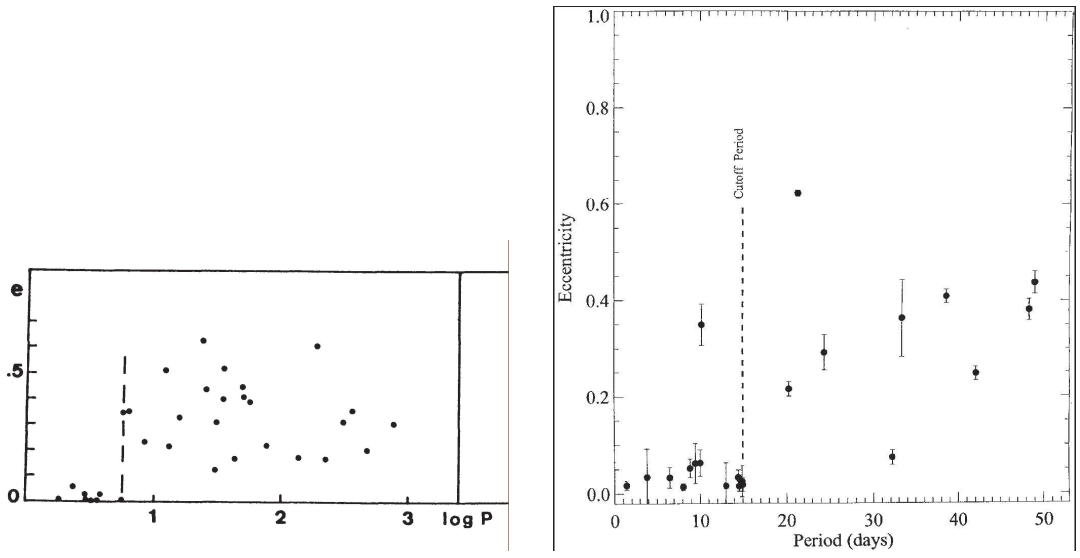

Fig. 1.4.— **Left** The $e - \log(P)$ diagram for main-sequence binaries in 4 intermediate-age clusters (Pleiades, Hyades, Praesepe, Coma Ber). The tidal cutoff period (longest period circular orbit) is 5.7 days. Source Mayor & Mermilliod (1984). **Right** The $e - \log(P)$ diagram for main-sequence solar-type binaries in NGC188. The tidal cutoff period is 15.0 days. Source: Mathieu, Meibom, & Dolan (2004).

With new superb data at hand and with the promising results of ongoing spectroscopic surveys of large coeval binary populations coming in, it is becoming increasingly important to make proper use of all information available from these data to constrain models of tidal circularization. A fundamental failing of the past on the observational side of this field has been the lack of well-determined uncertainties on the measured tidal circularization cutoffs. Without such uncertainties the meaningfulness of comparisons with theories is seriously compromised. In addition, the tidal cutoff period (the longest period circular orbit) so far used as the diagnostic for the degree of tidal circularization has several weaknesses: 1) It is vulnerable to systematic errors due to (near-)circular orbits in the initial binary population, and due to evolution histories involving more than tidal circularization (e.g., stellar evolution and stellar dynamics); 2) There is a systematic difference between the observed and true cutoff period which is a function of sample size; 3) It does not measure the circularization rates for typical binaries, but rather for those binaries with the initially lowest eccentricities; 4) This dependence on the initially lowest eccentricity binaries leads to an enhanced sampling error given a Gaussian-like initial eccentricity distribution; and 5) It does not make use of information in the eccentric orbits. It is a primary goal of this thesis to address these weaknesses as well as to provide new populations of large homogeneous and coeval binary populations at ages that will sample the gap between the PMS and the old main-sequence binary populations.

Relative to tidal circularization, the rate of tidal synchronization has received little attention. The observational efforts has primarily targeted early-type stars (e.g. Abt & Boonyarak 2004; Abt et al. 2002; Giuricin et al. 1984b,a; Levato 1974). This bias is mainly due to the difficulties of obtaining accurate rotation periods of late-type stars in a close binaries, particularly with the telescopes and instrumentation combinations available a decade or more ago. That has now changed, and with the availability of modern CCD detectors mounted on medium sized telescopes, extensive photometric surveys routinely measure rotation periods of late-type stars in young open clusters.

The rate of tidal synchronization provides an important second window on the efficiency of tidal interaction on late-type binaries. Only few (e.g. Giuricin et al. 1984c) have looked through that window. It is a key goal of this thesis to provide observations of stellar rotation in coeval populations of close binaries with late-type components, and thus lay the foundation for a new diagnostic of the

rate of tidal synchronization with qualities similar to the $e - \log(P)$ diagram.

In addition, the observational data resulting from this effort will offer rotation periods for single stars as well as binaries too wide for significant tidal interactions. These data will be used to study the effect of a close companion on star-disk interactions during the PMS phase, and the rotational evolution of late-type stars in general.

1.3 Thesis Structure

This section outlines the structure of the thesis and briefly states the purpose and content of each chapter. The introduction itself comprises Chapter 1 and motivates the work done while giving a brief overview of prior work in the field. Chapters 2, 3, and 4 represent the main achievements of the thesis work in the form of journal papers. Chapter 2 presents new and previously published data on tidal circularization. The interpretation of these data is discussed and a new diagnostic for the degree of tidal circularization is proposed. The results are compared to model predictions. Chapter 3 presents new data on tidal synchronization and introduce a new representation of such data useful for comparison between observations and theoretical expectations. We discuss deviations from the expected degree of tidal synchronization. Chapter 4 deals with the rotational evolution of late-type stars in general. It presents a proposed explanation for abnormally slowly rotating stars and a discussion of the effect of binary companions on circumstellar disks and consequently on the stellar rotational evolution during the pre main-sequence phase. Finally, Chapter 5 states what has been learned from this thesis and what future efforts will make important contributions to the field.

References

Abt, H. A., & Boonyarak, C. 2004, ApJ, 616, 562

Abt, H. A., Levato, H., & Grosso, M. 2002, ApJ, 573, 359

Darwin, G. H. 1879, The Observatory, 3, 79

Duquennoy, A., Mayor, M., & Mermilliod, J. C. 1992, in Binaries as Tracers of Stellar Formation. Proceedings of a Workshop held in Bettmeralp, Switzerland, Sept. 1991, in honor of Dr. Roger Griffin. Editors, Antoine Duquennoy, Michel Mayor; Publisher, Cambridge University Press, Cambridge, England, New York, NY, 1992. LC # QB821 .B55 1991. ISBN # 0521433584. P. 52, 1992, 52

Giuricin, G., Mardirossian, F., & Mezzetti, M. 1984a, A&A, 135, 393

—. 1984b, A&A, 131, 152

—. 1984c, A&A, 141, 227

Goodman, J., & Dickson, E. S. 1998, ApJ, 507, 938

Hut, P. 1981, A&A, 99, 126

Koch, R. H., & Hrivnak, B. J. 1981, AJ, 86, 438

Kopal, Z., & Shapley, M. B. 1968, Ap&SS, 1, 112

Latham, D. W., Stefanik, R. P., Torres, G., Davis, R. J., Mazeh, T., Carney, B. W., Laird, J. B., & Morse, J. A. 2002, AJ, 124, 1144

Levato, H. 1974, A&A, 35, 259

Mathieu, R. D., Duquennoy, A., Latham, D. W., Mayor, M., Mermilliod, T., & Mazeh, J. C. 1992, in Binaries as Tracers of Stellar Formation. Proceedings of a Workshop held in Bettmeralp, Switzerland, Sept. 1991, in honor of Dr. Roger Griffin. Editors, Antoine Duquennoy, Michel Mayor; Publisher, Cambridge University Press, Cambridge, England, New York, NY, 1992. LC # QB821 .B55 1991. ISBN # 0521433584. P. 278, 1992, 278

Mathieu, R. D., & Mazeh, T. 1988, ApJ, 326, 256

Mathieu, R. D., Meibom, S., & Dolan, C. J. 2004, ApJ, 602, L121

Mayor, M., & Mermilliod, J. C. 1984, in IAU Symp. 105: Observational Tests of the Stellar Evolution Theory, 411–+

Melo, C. H. F., Covino, E., Alcalá, J. M., & Torres, G. 2001, A&A, 378, 898

Ogilvie, G. I., & Lin, D. N. C. 2004, ApJ, 610, 477

Savonije, G. J., & Witte, M. G. 2002, A&A, 386, 211

Terquem, C., Papaloizou, J. C. B., Nelson, R. P., & Lin, D. N. C. 1998, ApJ, 502, 788

Witte, M. G., & Savonije, G. J. 2002, A&A, 386, 222

Zahn, J. P. 1966a, Annales d'Astrophysique, 29, 313

—. 1966b, Annales d'Astrophysique, 29, 489

—. 1966c, Annales d'Astrophysique, 29, 565

Zahn, J.-P. 1970, A&A, 4, 452

—. 1975, A&A, 41, 329

—. 1977, A&A, 57, 383

—. 1989, A&A, 220, 112

Zahn, J.-P., & Bouchet, L. 1989, A&A, 223, 112

Chapter 2

A Robust Measure of Tidal Circularization in Coeval Binary Populations: The Solar-Type Spectroscopic Binary Population in the Open Cluster M35

2.1 Abstract

We present a new homogeneous sample of 32 spectroscopic binary orbits in the young ($\sim$ 150 Myr) main-sequence open cluster M35. The distribution of orbital eccentricity vs. orbital period ($e - \log(P)$) displays a distinct transition from eccentric to circular orbits at an orbital period of $\sim$ 10 days. The transition is due to tidal circularization of the closest binaries. The population of binary orbits in M35 provide a significantly improved constraint on the rate of tidal circularization at an age of 150 Myr. We propose a new and more robust diagnostic of the degree of tidal circularization in a binary population based on a functional fit to the $e - \log(P)$ distribution. We call this new measure the *tidal circularization period*. The tidal circularization period of a binary population represents the orbital period at which a binary orbit with the most frequent initial orbital eccentricity circularizes (defined as $e = 0.01$) at the age of the population. We determine the tidal circularization period for M35 as well as for 7 additional binary populations spanning ages from the pre main-sequence ($\sim$ 3 Myr) to late main-sequence ($\sim$ 10 Gyr), and use Monte Carlo error analysis to determine the uncertainties on the derived circularization periods. We conclude that current theories of tidal circularization cannot account for the distribution of tidal circularization periods with population age.

2.2 Introduction

In a coeval population of binary stars the closest binaries (separations $\lesssim$ 0.5 AU) tend to have circular orbits, while wider binaries have orbits with a distribution of non-zero eccentricities. This trend holds true for binaries with early-type (North & Zahn 2003; Pan et al. 1998; Matthews & Mathieu 1992; Giuricin et al. 1984) as well as late-type (Mathieu et al. 2004; Latham et al. 2002; Melo et al. 2001; Mathieu et al. 1992) main-sequence components, for binaries with evolved stellar components (Mermilliod & Mayor 1992), and in the orbital eccentricity distribution of large planets around solar-type stars (http://exoplanets.org). The transition from eccentric to circular orbits is explained by dissipative tidal interactions caused by the reaction of the binary components to each other's gravitational field (tidal circularization: Hut 1981; Zahn 1977; Darwin 1879). The

theory of tidal interactions predicts that the timescale of circularization depends strongly on stellar separation. Consequently, for a coeval binary population, the transition from eccentric to circular orbits should occur at a well-defined binary period. However, despite the coeval nature of a star cluster, its population of short period binaries may be small in number and consist of systems with a distribution of initial eccentricities, masses, and stellar angular momenta. Accordingly, the size and heterogeneity of the binary population will add complexity and uncertainty to the observational determination of the tidal circularization period.

Nonetheless, the transition between eccentric and circular binary orbits provides an important constraint on the rate of tidal circularization as a function of orbital period, integrated over the lifetime of a binary population. Furthermore, the distribution of tidal circularization periods with population age enables us to study the evolution of tidal circularization with time.

The success of theoretical models describing the efficiency and the evolution of tidal circularization can be measured by their ability to "predict" the tidal circularization periods for binary populations of different ages. The differences between present-day models lie in the mechanism by which energy and angular momentum is transported between the binary components and their orbits. Currently, three theoretical models exist for the mechanism for tidal dissipation in late-type main-sequence stars: 1) *The equilibrium tide theory* describes retardation of the hydrostatic tidal bulge (equilibrium tide) due to the coupling of the tidal flow to the motion of turbulent eddies in the stellar convective envelope. This dissipative coupling is assumed to be responsible for a phase shift between the tidal bulge and the orbital motion of the binary stars. Because of the phase shifts a tidal torque is established between the two stars (Zahn 1977; Hut 1981); 2) *The theory of dynamical tides* describes the excitation and damping of gravity (g) waves in the radiative zones of stars due to the tidal forcing by the companion star (Savonije & Papaloizou 1983; Zahn 1977, 1975, 1970). This dissipation mechanism has been successfully applied to explain circularization of early-type main-sequence stars with radiative envelopes (Claret & Cunha 1997; Giuricin et al. 1984; Zahn 1977), and recently has also been applied to the radiative cores of late-type stars (Savonije & Witte 2002; Witte & Savonije 2002; Goodman & Dickson 1998; Terquem et al. 1998). Inclusion of resonance locking between the tidally forced modes and stellar eigenmodes provides increased efficiency of the tidal

coupling (Savonije & Witte 2002; Witte & Savonije 2002, 2001, 1999a,b); 3) A pure *hydrodynamical mechanism* has been proposed by Tassoul (2000, 1988) and Tassoul & Tassoul (1996). Tassoul suggests that hydrodynamical flows (large-scale meridional currents) induced by lack of symmetry about the rotation axis in the tidally perturbed star are responsible for the tidal torques on the component stars. This mechanism has been controversial on theoretical grounds (Rieutord 1992; Rieutord & Zahn 1997; Tassoul & Tassoul 1997).

Despite the developments in the theory of tidal circularization, the models still cannot account for the observed periods of circular orbits in solar-mass binary populations (e.g. Witte & Savonije 2002; Claret & Cunha 1997; Mathieu et al. 1992). To help along further progress of theoretical modeling there is a need for high quality observational data on large and coeval samples of binary stars, allowing for accurate determination of the transition from eccentric to circular orbits.

This paper presents a homogeneous ($M_{prim} \sim 1\ M_{\odot}$) sample of 32 spectroscopic binary orbits in the open cluster M35 (NGC 2168; $\alpha_{2000} = 6^h\ 9^m$, $\delta_{2000} = 24^o\ 20'$; $l = 186.59^o$, $b = 2.19^o$, distance $\simeq 850\ pc$). With an age similar to the Pleiades but approximately three times richer, M35 is a benchmark for stellar astrophysics at ~ 150 Myr (Deliyannis et al. 2004, in preparation). The age makes M35 an important testing ground for binary stars that have recently ended their pre main-sequence (PMS) phase where they were larger and fully convective. Thus M35 sets the initial state for main-sequence tidal circularization.

Section 2.3 describes the observations, instrument, and telescope used in the spectroscopic survey of M35. In Section 2.4 we present the distribution of orbital eccentricity as a function of orbital period in M35 (the $e - \log(P)$ diagram). In Section 2.5 we motivate and present a new robust method for determining the period at which the most frequent binary orbits circularize. We will call this the *tidal circularization period*. In Section 2.6 we discuss and compare our new diagnostic to the previous measure of tidal circularization, the tidal circularization cutoff period. We compare the precision and accuracy performance of both diagnostics and determine measurement uncertainties on the tidal circularization period. In Section 2.7 we determine the tidal circularization period for the binary population in M35, and in Section 2.8 we determine the circularization period for a series of published populations of late-type unevolved main-sequence binaries. In Section 2.9 we

carry out a comparison between current theoretical predictions of the efficiency and evolution of tidal circularization and the circularization periods derived in Sections 2.7 and 2.8. Section 2.10 summarizes and presents our conclusions.

2.3 Observations

M35 has been included in the WIYN Open Cluster Study (WOCS) program since 1997. The radial-velocity survey of the cluster will be described in detail in Meibom et al. (in preparation). We summarize the relevant points here. The initial selection of $\sim$ 2000 target stars was based on photometric membership in the cluster and proper-motion membership studies to $V \lesssim 15$ by McNamara & Sekiguchi (1986) and Cudworth (1971). Bjorkman & Mathieu (unpublished) completed astrometry and photometry to $V \sim 17$. Our radial-velocity study includes stars from $V \simeq 13$ to $V \simeq 16.5$, corresponding to a range in stellar mass from $\sim 1.4\ M_{\odot}$ ($(B-V)_0 \sim 0.37$) to $\sim 0.7\ M_{\odot}$ ($(B-V)_0 \sim 1.1$), with solar mass stars at V $\sim$ 15 ((B-V) $\sim$ 0.58). Masses are derived using the Yale (Y2) stellar evolution models (Yi et al. 2003). The cluster reddening ($E_{(B-V)} = 0.20$) was adopted from Deliyannis et al. 2004 (in preparation).

All spectroscopic data were obtained using the WIYN[1] 3.5m telescope at Kitt Peak, Arizona, USA. The telescope is equipped with a Multi-Object Spectrograph (MOS) consisting of a fiber optic positioner (Hydra) feeding a bench mounted spectrograph. The Hydra positioner is capable of placing $\sim$ 95 fibers in a 1-degree diameter field with a precision of $0.2''$. In the field of M35 approximately 82-85 fibers are positioned on stars while the remaining fibers are used for measurements of the sky background. We use the $3''$ diameter fibers optimized for blue transmission, and the spectrograph is configured with an echelle grating and an all-transmission optics camera providing high throughput at a resolution of $\sim$ 20,000. All observations were done at central wavelengths of 5130Å or 6385Å with a wavelength range of $\sim$ 200Å providing rich arrays of narrow absorption lines. Radial velocities with a precision of $\sim 0.5\ km\ s^{-1}$ (Meibom et al. 2001) are derived from the spectra via cross-correlation with a high S/N sky spectrum.

Telescope time granted from NOAO[2] and Wisconsin allowed for 3-4 observing runs per year

[1]The WIYN Observatory is a joint facility of the University of Wisconsin-Madison, Indiana University, Yale University, and the National Optical Astronomy Observatories.

[2]NOAO is the national center for ground-based nighttime astronomy in the United States and is operated by the

for M35, with each run typically including multiple observations on several sequential nights. Once identified, velocity variables are observed at a frequency appropriate to the timescale of their variation. At present the radial-velocity survey has resulted in a sample of 81 spectroscopic binaries: 32 members, 37 candidate members and 12 non-members. Of the 32 member binaries, 25 are single-lined (SB1) and 7 are double-lined (SB2) spectroscopic binaries. The orbital periods span from 2.25 days to 1115 days among the member binaries, corresponding to separations from ~ 0.04 to 2.5 AU assuming a 1 $M_{\odot}$ primary and a 0.5 $M_{\odot}$ secondary component. The 32 member binaries were identified in the 2MASS All Sky Survey based on equatorial coordinates. 2MASS ID's, astrometry, photometry, and orbital parameters are listed in Tables 2.1 and 2.2.

2.4 The Period-Eccentricity Distribution in M35

The new compilation of binary orbits in M35 greatly improves the constraint on tidal circularization at the early stage of the main-sequence phase. Prior to this publication, the small sample of binary orbits in the Pleiades provided only rough limits on the transition between eccentric and circular orbits at this age (Mermilliod et al. 1992). Figure 2.1 shows the distribution of orbital eccentricity (e) as a function of *log* orbital period (P) for the 32 spectroscopic binary members of M35. The shortest period binaries have orbital eccentricities consistent with circular orbits, while the orbits for longer period binaries show a distribution of non-zero eccentricities. The presumably primordial distribution of eccentricities for the longest period binaries is consistent with the Gaussian distribution observed in late-type main-sequence binary populations in other open clusters (Duquennoy et al. 1992), in the solar neighborhood (Duquennoy & Mayor 1991), and from the Galactic halo (Latham et al. 2002). The lack of high eccentricity orbits ($e \gtrsim 0.6$) among the long period binaries in M35 may be due in part to observational biases.

All binaries whose periods and eccentricities are plotted in Figure 2.1 are cluster members based on their radial velocities and location in the color-magnitude diagram (CMD). Fifteen have confirmation of membership from proper-motion measurements. A few binary systems deserve special attention and Figure 2.2 shows on a linear scale the distribution of orbital eccentricity vs. period

Association of Universities for Research in Astronomy (AURA), Inc. under cooperative agreement with the National Science Foundation.

Table 2.1. Astrometric, photometric data for binary members of M35.

2MASS ID[1]	MS ID[2]	Cd ID[3]	α (2000) h m s	δ (2000) ^{o} $'$ $''$	V	$B-V$	MP (%)[4]
06090257+2420447	249	402	06 09 02.550	+24 20 44.62	13.62	0.60	99
06090403+2423483	252	404	06 09 04.010	+24 23 48.26	13.31	0.63	99
06090521+2419309	259	410	06 09 05.180	+24 19 30.92	13.32	0.60	99
06090650+2413499	267	419	06 09 06.470	+24 13 49.90	14.62	0.75	97
06091099+2421515	301	447	06 09 10.960	+24 21 51.51	13.65	0.62	97
06092037+2412177	360	512	06 09 20.340	+24 12 17.74	13.64	0.62	99
06093861+2417394	463	612	06 09 38.590	+24 17 39.54	14.38	0.73	94
06083426+2421359	...	...	06 08 34.220	+24 21 35.73	16.03	1.16	...
06085047+2419382	...	...	06 08 50.440	+24 19 38.16	16.42	1.26	...
06090352+2417234	...	...	06 09 03.490	+24 17 23.36	15.95	1.10	...
06091557+2410422	...	...	06 09 15.540	+24 10 42.16	15.47	1.03	...
06091924+2417223	...	...	06 09 19.210	+24 17 22.37	15.53	0.92	...
06092436+2426200	...	...	06 09 24.330	+24 26 20.03	15.34	0.88	...
06084130+2426389	...	...	06 08 41.260	+24 26 38.88	16.10	1.14	...
06090444+2412441	...	...	06 09 04.410	+24 12 44.00	14.86	0.80	...
06093267+2415041	...	...	06 09 32.640	+24 15 04.14	14.26	0.67	...
06104368+2416089	...	...	06 10 43.680	+24 16 09.05	14.50	0.82	72
06101134+2426415	...	...	06 10 11.350	+24 26 41.42	15.32	1.02	...
06095563+2417454	...	...	06 09 55.627	+24 17 45.60	15.02	0.88	...
06094745+2423085	494	650	06 09 47.455	+24 23 08.56	13.63	0.67	90
06092221+2446528	...	...	06 09 22.217	+24 46 52.68	15.00	0.78	72
06092708+2413452	404	550	06 09 27.094	+24 13 45.12	13.80	0.73	98
06092536+2404037	...	541	06 09 25.363	+24 04 03.72	13.76	0.61	57
06085334+2432309	198	343	06 08 53.335	+24 32 30.80	14.32	0.67	96
06085441+2403081	...	...	06 08 54.418	+24 03 08.06	14.97	0.77	...
06083296+2408164	...	...	06 08 32.969	+24 08 16.30	15.05	0.78	...
06083082+2417547	...	...	06 08 30.818	+24 17 54.67	15.47	0.88	...
06083184+2410384	75	229	06 08 31.841	+24 10 38.35	14.57	0.74	89
06080751+2423413	9	122	06 08 07.500	+24 23 41.46	13.94	0.60	98
06074436+2430262	...	...	06 07 44.352	+24 30 26.10	15.23	0.82	...
06100456+2437000	...	...	06 10 04.562	+24 37 00.19	15.74	1.03	...
06083789+2431455	...	...	06 08 37.889	+24 31 45.48	15.95	1.05	...

References. — (1) 2MASS ID's; (2) McNamara & Sekiguchi (1986) ID's; (3) Cudworth (1971) ID's; (4) Proper motion membership probability by McNamara & Sekiguchi (1986); Cudworth (1971)

Table 2.2. Orbital data for binary members of M35.

2MASS ID[1]	Binary type	# RV's	γ (kms^{-1})	Period (days)	e	M_{prim} ($M_\odot$)	M_{sec} ($M_\odot$)	Spectral type
0447	SB1	32	−8.3	10.280	0.009 ±0.019	1.32	...	F7
3483	SB2	11/9	−8.7	22.490	0.155 ±0.017	1.28	1.01	M
9309	SB1	25	−8.4	2.703	0.028 ±0.028	1.32	...	F7
3499	SB1	18	−6.8	344.6	0.334 ±0.030	1.05	...	G0
1515	SB1	20	−7.7	58.02	0.502 ±0.029	1.28	...	F8
2177	SB2	15/7	−8.5	35.380	0.272 ±0.017	1.28	0.83	M
7394	SB1	18	−8.1	79.28	0.375 ±0.010	1.05	...	G0
1359	SB2	18/7	−7.9	56.14	0.353 ±0.026	0.77	0.77	M
9382	SB2	19/14	−5.3	24.108	0.219 ±0.013	0.69	0.66	M
7234	SB1	18	−7.5	156.9	0.594 ±0.024	0.77	...	K1
0422	SB1	36	−7.9	8.170	0.538 ±0.013	0.77	...	K1
7223	SB1	18	−8.8	795	0.208 ±0.045	0.86	...	G7
6200	SB1	22	−7.4	10.330	0.016 ±0.009	0.95	...	G3
6389	SB1	18	−6.9	18.426	0.276 ±0.016	0.77	...	K1
2441	SB1	15	−9.1	49.075	0.358 ±0.018	0.95	...	G3
5041	SB1	12	−7.46	7.088	0.003 ±0.005	1.19	...	F9
6089	SB1	17	−9.5	10.077	0.008 ±0.005	0.95	...	G3
6415	SB1	32	−6.4	14.524	0.246 ±0.044	0.86	...	G7
7454	SB1	18	−7.5	30.130	0.273 ±0.005	0.95	...	G3
3085	SB1	15	−6.9	1114.97	0.543 ±0.072	1.19	...	F9
6528	SB1	15	−8.6	8.010	0.041 ±0.032	0.95	...	G3
3452	SB2	20/15	−10.2	4.442	0.010 ±0.006	1.05	0.92	M
4037	SB2	24/20	−7.5	16.488	0.041 ±0.014	1.28	1.13	M
2309	SB1	15	−8.0	22.619	0.404 ±0.007	1.19	...	F9
3081	SB1	19	−7.45	12.280	0.550 ±0.003	1.05	...	G0
8164	SB1	17	−7.3	457.0	0.512 ±0.064	0.95	...	G3
7547	SB2	16/15	−10.3	18.590	0.429 ±0.009	0.95	0.89	M
0384	SB1	18	−7.1	475	0.507 ±0.021	1.05	...	G0
3413	SB1	19	−8.3	930	0.474 ±0.079	1.32	...	F7
0262	SB1	11	−6.9	473	0.309 ±0.121	0.95	...	G3
7000	SB1	16	−8.3	12.566	0.095 ±0.006	0.86	...	G7
1455	SB1	14	−8.1	2.247	0.010 ±0.008	0.77	...	K1

References. — (1) Last 4 digits of 2MASS ID's from Table 2.1

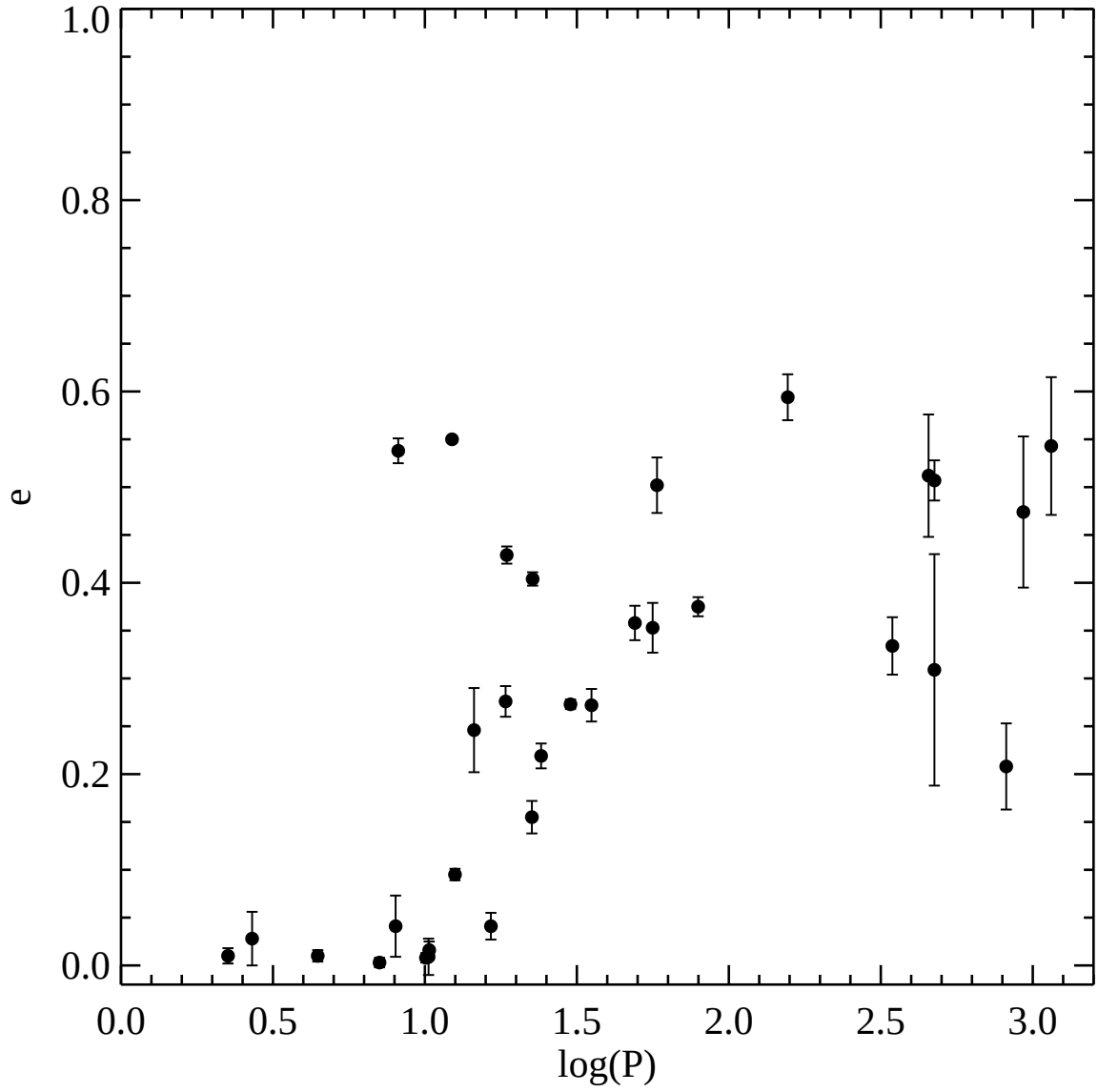

Fig. 2.1.— The distribution of orbital eccentricity (e) as a function of *log* orbital period (P) for 32 solar-type spectroscopic binary members in M35.

for binaries with periods less than 20 days. The last 4 digits of the 2MASS ID are used to label key binaries in Figure 2.2 and for reference in the text and in Tables 2.1 ans 2.2. Nine binary orbits have eccentricities less than $3 \times \sigma_e$ above $e = 0.0$, where σ_e denotes the error on the orbital eccentricity. We consider these binary orbits to be circular. Binary 4037 ($P_{orb} = 16.49$ days, $e = 0.041 \pm 0.014$) has the longest period among the binaries with circular orbits. Three circular binaries have orbital periods close to 10 days: 6089 ($P_{orb} = 10.08$ days, $e = 0.008 \pm 0.005$), 0447 ($P_{orb} = 10.28$ days, $e = 0.009 \pm 0.019$), and 6200 ($P_{orb} = 10.33$ days, $e = 0.016 \pm 0.009$). 4 binaries have eccentric orbits with periods shortward of the longest period circular orbit: 0422 ($P = 8.17$ days, $e = 0.538 \pm 0.013$), 3081 ($P = 12.28$ days, $e = 0.550 \pm 0.003$), 7000 ($P = 12.57$ days, $e = 0.095 \pm 0.006$), and 6415 ($P = 14.52$ days, $e = 0.246 \pm 0.044$).

Thus regardless of the homogeneity in age, metallicity and primary mass of the M35 binary population there is a ~ 8 day overlap in period between eccentric and circular binary orbits.

2.5 Determining the Circularization Period

The transition from eccentric to circular orbits observed in M35 is also found in observational studies of late-type main-sequence binary populations in well known open clusters such as the Pleiades (Mermilliod et al. 1992), the Hyades/Praesepe (Duquennoy et al. 1992; Mermilliod & Mayor 1999), M67 (Latham et al. 1992), and NGC188 (Mathieu et al. 2004), and in populations of PMS (Melo et al. 2001, and references therein), field (Duquennoy & Mayor 1991), and halo (Latham et al. 2002) binaries. This characteristic fingerprint of tidal circularization is an important observational constraint on the theory of tidal circularization. Consequently, determination of the period at which binary orbits becomes circular in a given binary population is critical to constraining theoretical models. However, determining this tidal circularization period is not straightforward in any of the above populations.

The longest period circular orbit has been the preferred measure over the past decade (e.g. Duquennoy et al. 1992) and has been referred to as the *tidal circularization cutoff period* (hereinafter: cutoff period). We argue here that the cutoff period is not the optimal measure of the transition between eccentric and circular orbits.

Populations of short period binaries vary in size and consist of systems with a distribution of

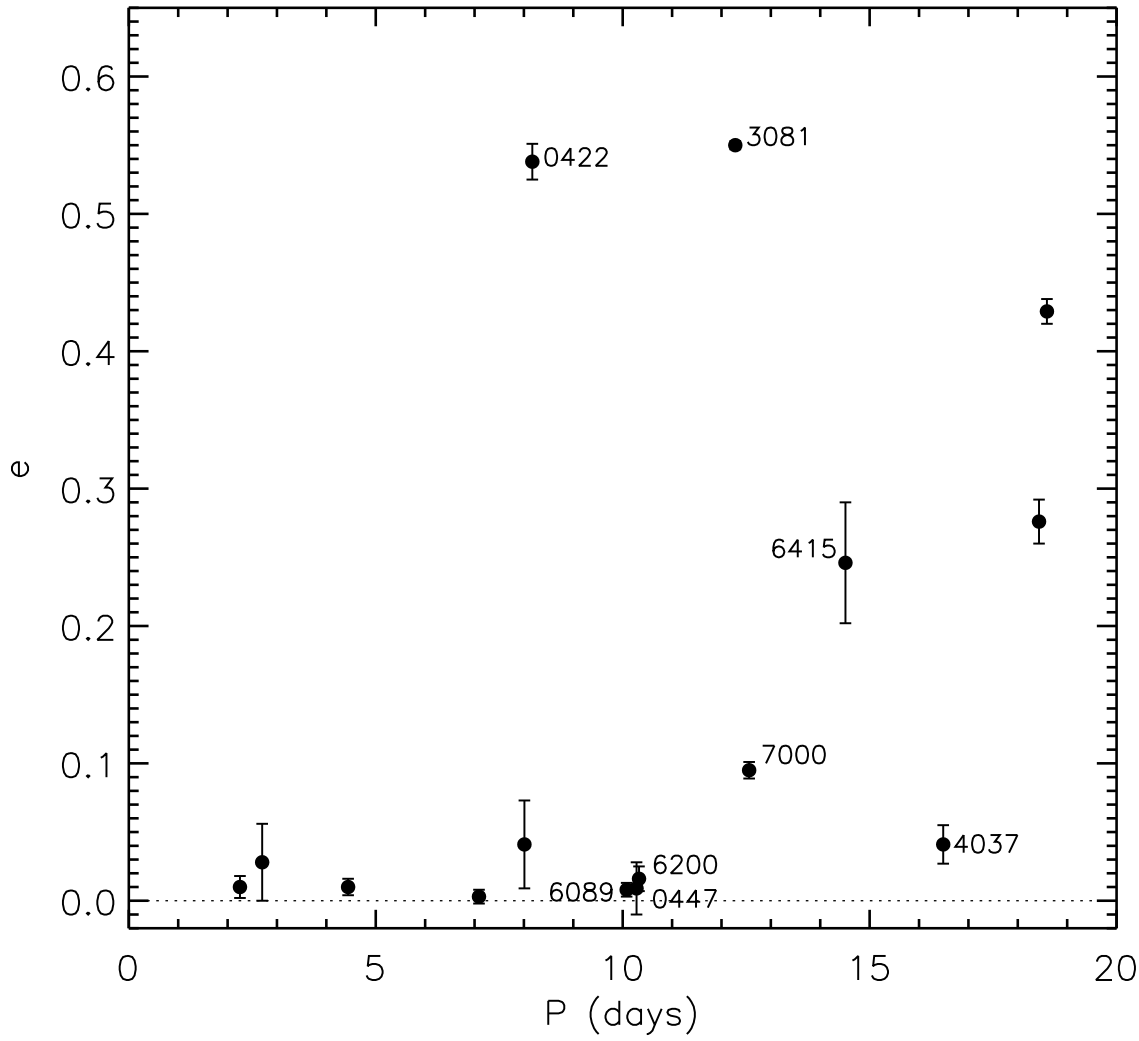

Fig. 2.2.— The eccentricity distribution of M35 binary orbits with periods shorter than 20 days. Numbers next to selected data refer to binary ID numbers in Tables 2.1 ans 2.2.

initial eccentricities. This is observed in the Gaussian distribution of orbital eccentricity at longer orbital periods where presumably orbital evolution has been minimal (Halbwachs et al. 2003; Duquennoy et al. 1992; Duquennoy & Mayor 1991). The Gaussian distribution of initial orbital eccentricities combined with the effects of tidal circularization will lead to an overlap in period-space between initially low eccentricity orbits that have been circularized and initially high eccentricity orbits not yet circularized. This overlap is indeed observed in all published populations of coeval binary orbits with the exception of the small sample in the Pleiades cluster (see Section 2.8, Figure 2.8). The width of this overlap was estimated by Mathieu & Mazeh (1988) based on the observed distribution of initial orbital eccentricities, and indeed, Duquennoy et al. (1992) showed that the existence of eccentric orbits in the Hyades/Praesepe populations with periods shorter than the longest period circular orbit can be explained due to incomplete tidal circularization of binaries with initially high orbital eccentricity. We similarly find through simulations of tidal circularization using the equilibrium tide theory by Zahn (1977) that eccentric orbits with periods shorter than the longest period circular orbit can be a result of high initial eccentricity ($e \gtrsim 0.5$).

For short-period binaries with low but non-zero orbital eccentricity ($0.0 \lesssim e \lesssim 0.1$), Mazeh (1990) suggests that the eccentricity is induced by the presence of a third companion star due to dynamical interactions different from tidal effects. However, most eccentric orbits with periods shorter than the longest period circular orbit have eccentricities between 0.1 and 0.6, and among the 4 binaries in M35 with moderate to significant eccentricities and periods shortward of the longest period circular orbit we see no indications in the stellar spectra of a third component.

Monte Carlo simulations of tidal circularization using the equilibrium tide theory by Zahn (1977) show that the longest period circular binary orbit defining the cutoff period is likely to originate from the low eccentricity tail of the initial Gaussian eccentricity distribution. Accordingly, the cutoff period does not measure tidal circularization of the most frequent binary orbit. We show in Figure 2.3 the $e - \log(P)$ diagram of a tidally circularized population of artificially generated binaries (grey diamonds). To focus on the process of tidal circularization, the lower limit on the initial orbital eccentricity was set to 0.05 (dotted horizontal line). The threshold of 0.05 is 2-3 times the typical error on orbital eccentricities determined from observations. The initial and final locations of the

longest period circular orbit are marked with an open and a filled circle, respectively.

Figure 2.3 also demonstrate that the probability of measuring the "true" cutoff period of a parent population of binaries is highly sensitive to the size of the observed binary population. Consequently, the value of the observed cutoff period will vary with the size of the population.

Furthermore, long period (P $\sim 2 \times 10^1 - 10^2$ days) circular ($e < 0.05$) or marginally circular ($e \lesssim 0.1$) orbits of unevolved binaries are observed in the majority of the published binary populations (see Section 2.8, Figure 2.8), indicating the possibility that binary stars can also form with very low eccentricity. While not included in Figure 2.3, the cutoff period is vulnerable to such primordial circular orbits.

Finally, the determination of the cutoff period makes no use of the information provided by eccentric orbits in the $e - \log(P)$ diagram.

Consequently we suggest that the cutoff period is not a robust measure of the state of tidal circularization in a coeval binary population.

So motivated, we propose a new method for determining the period of circularization of primordial eccentric binary orbits. We refer to this period as the *tidal circularization period*. Our proposed method will make use of the information provided by all binary orbits in a population by fitting to the observed period-eccentricity distribution a function of the form:

$$e(P) = \begin{cases} 0.0 & \text{if } P \leq P' \\ \alpha\big(1 - e^{\beta(P'-P)}\ \big)^{\gamma} & \text{if } P > P' \end{cases} \tag{2.1}$$

This mathematical function is motivated by the observed period-eccentricity distributions and by numerical modeling using the theory of Zahn (1977). The function is not physically derived but constructed to mimic the tidal circularization isochrone of the most frequently occurring eccentric binary orbits. Figure 2.4 shows the function in the $e - \log(P)$ diagram. The transition of the function from eccentric to circular orbits is managed by the $e^{\beta(P'-P)}$ term and the γ coefficient. γ controls the abruptness of the break from $e = 0$ at the period P' and β controls the overall steepness/slope of the transition. Our choices of β and γ are discussed in Section 2.6. The value of α ($\alpha = 0.35$) is set to ensure that $e(P > P')$ approaches a value of 0.35, the mean eccentricity of all observed binary orbits with periods longer than 50 days in the Pleiades, M35, Hyades/Praesepe, M67, and NGC188.

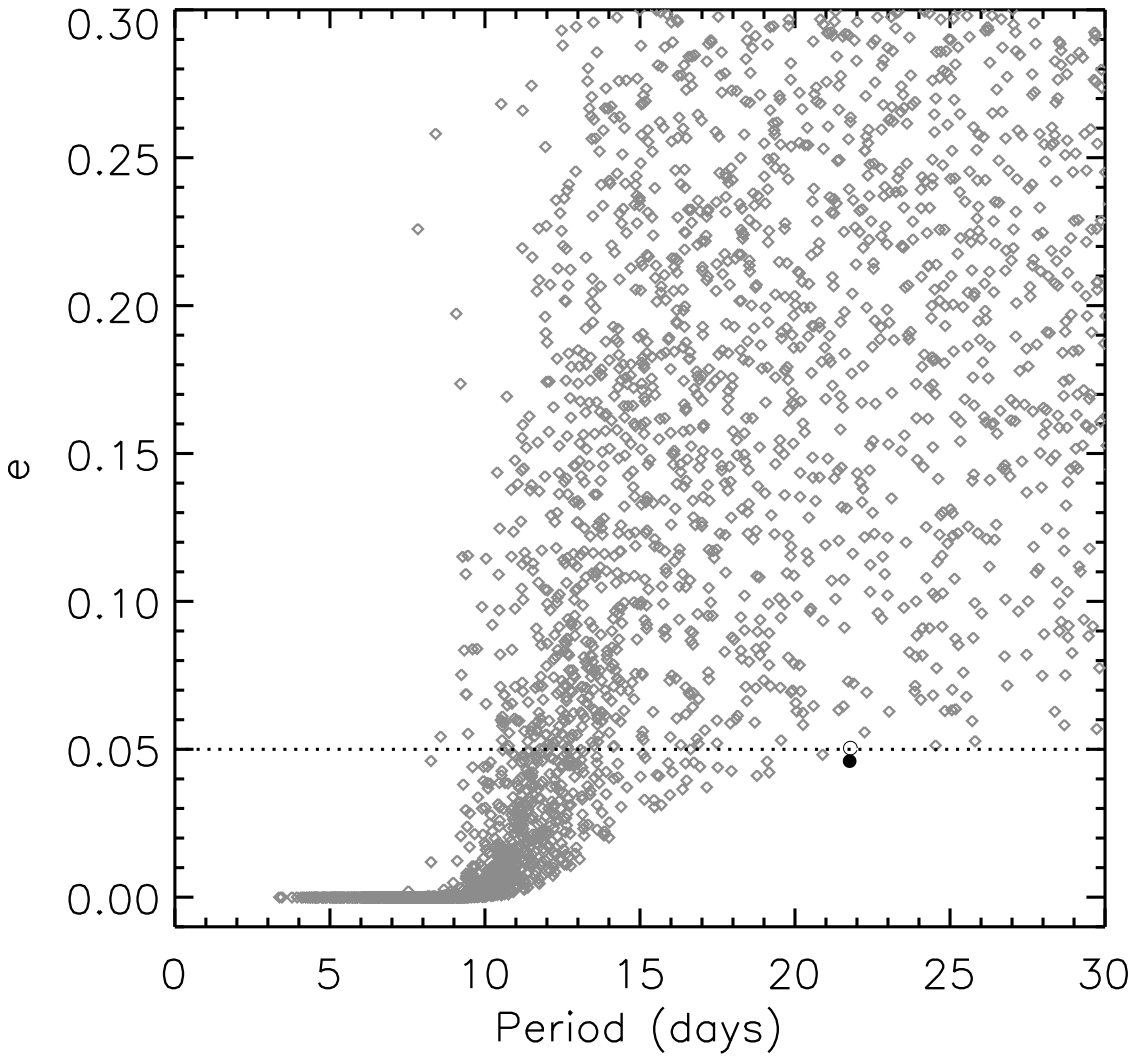

Fig. 2.3.— The $e - \log(P)$ diagram for a tidally circularized population of artificially generated binaries (grey diamonds). The lower limit on the initial orbital eccentricity is shown as a dotted line at $e = 0.05$. The initial and final locations of the longest period circular orbit are marked with an open and a filled circle, respectively.

For periods shortward of P' the function is set to 0.0 ($e(P < P') = 0.0$). We will hereafter refer to this function as the circularization function.

The value of P' determines the location of the onset of the rise in the circularization function. We determine the location of the circularization function in period by minimizing the total absolute deviation (δ) between the observed (e_i) and the calculated ($e(P_i)$) eccentricities,

$$\delta = \sum_{i=1}^{N} \mid e_i - e(P_i) \mid^{\eta} . \tag{2.2}$$

N denotes the number of binary orbits. The value of the exponent η controls the influence on P' by the binary orbits with maximum deviation from the circularization function. We found that $\eta > 1$ causes high sensitivity to the short period eccentric binaries, often leading to values of P' smaller than the period of the shortest period eccentric orbit. $\eta = 1$ leads to values of P' between the periods of the shortest period eccentric orbit and the longest period circular orbit. We use $\eta = 1$ when fitting the circularization function throughout this paper.

Figure 2.4 shows the circularization function fitted to an artificially generated sample of binary orbits. Tidal circularization of these binary orbits has been simulated by numerical integration of differential equations derived using equations (4.3) and (4.4) in Zahn (1977) (Note erratum by Zahn (1978)) and the assumptions by Duquennoy et al. (1992):

$$\frac{de}{dt} = \frac{-e}{AP^{16/3}} \tag{2.3}$$

$$\frac{dP}{dt} = \frac{-3e^2}{AP^{13/3}} \tag{2.4}$$

The constant A controls the effectiveness of tidal dissipation and thus the rate of tidal circularization. We set A so that numerical simulation of tidal circularization using equations (3) and (4) produce transitions from eccentric to circular orbits at periods similar to those observed.

The circularization function mimics the transition from eccentric to circular orbits of the "typical"binary ($0.3 < e_{ini} < 0.4$; highlighted in Figure 2.4). The tidal circularization isochrone for the typical binary is reproduced by the circularization function at $e = 0.01$. Thus we define the "tidal circularization period" (hereinafter circularization period or CP) as the period for which the best fit

circularization function has a value of 0.01 ($e(CP) = 0.01$). The choice of $e = 0.01$ as the threshold for circularization is also similar to the threshold chosen in theoretical simulations (see Section 2.9), and thus facilitates direct comparison between observations and theory.

Our estimate of the initial eccentricity of a binary orbit that circularizes with a period equal to the circularization period at the age of a binary population, is tied to the tidal theory of Zahn (1977). Deviations from the typical (most frequent) initial eccentricity depends on the value of the circularization period (the age of the binary population). By fitting the circularization function to rich distributions of tidally circularized binary orbits (as shown in Figure 2.4), we find that over the range of circularization periods of interest to this study, $\sim$ 5 days to 15 days, the range of initial eccentricities of the binaries represented by the resulting circularization periods is 0.2-0.5. This range of initial orbital eccentricities is centered on the mean of the observed Gaussian eccentricity distribution ($\bar{e} = 0.35$) and we conclude that according to the Zahn (1977) theory the circularization period represents the orbital period at which a binary orbit with the most frequent initial orbital eccentricity circularizes. The range of initial eccentricities from 0.2 to 0.5 also includes the initial eccentricity used in theoretical predictions of tidal circularization (see Section 2.9) facilitating direct comparison between these predictions and the observed circularization periods.

2.6 Evaluation of the Performance of the Tidal Circularization Period

In the following we test the performance of the circularization function and compare its performance to the cutoff period. Using a Monte Carlo approach, we generate 10,000 binary populations each with 20 binaries with periods between 10 and 50 days, corresponding to the number of known binary orbits in the M35 sample with orbital periods shorter than 50 days. Tidal circularization was simulated by numerical integration of the Zahn (1977) differential equations (eqs. [2.3] and [2.4] above). Initial orbital periods and eccentricities for each population were determined by random selection from a log-normal period distribution and a normal (Gaussian) eccentricity distribution. [3] We adopted the period distribution of Duquennoy & Mayor (1991) derived from solar-type binaries in the solar neighborhood, while the Gaussian eccentricity distribution ($\bar{e} = 0.35, \sigma = 0.21$) was determined by fitting the distributions of all orbital eccentricities from the Pleiades, M35, Hyades/Praesepe,

[3] Orbits randomly selected with an initially negative eccentricity were excluded.

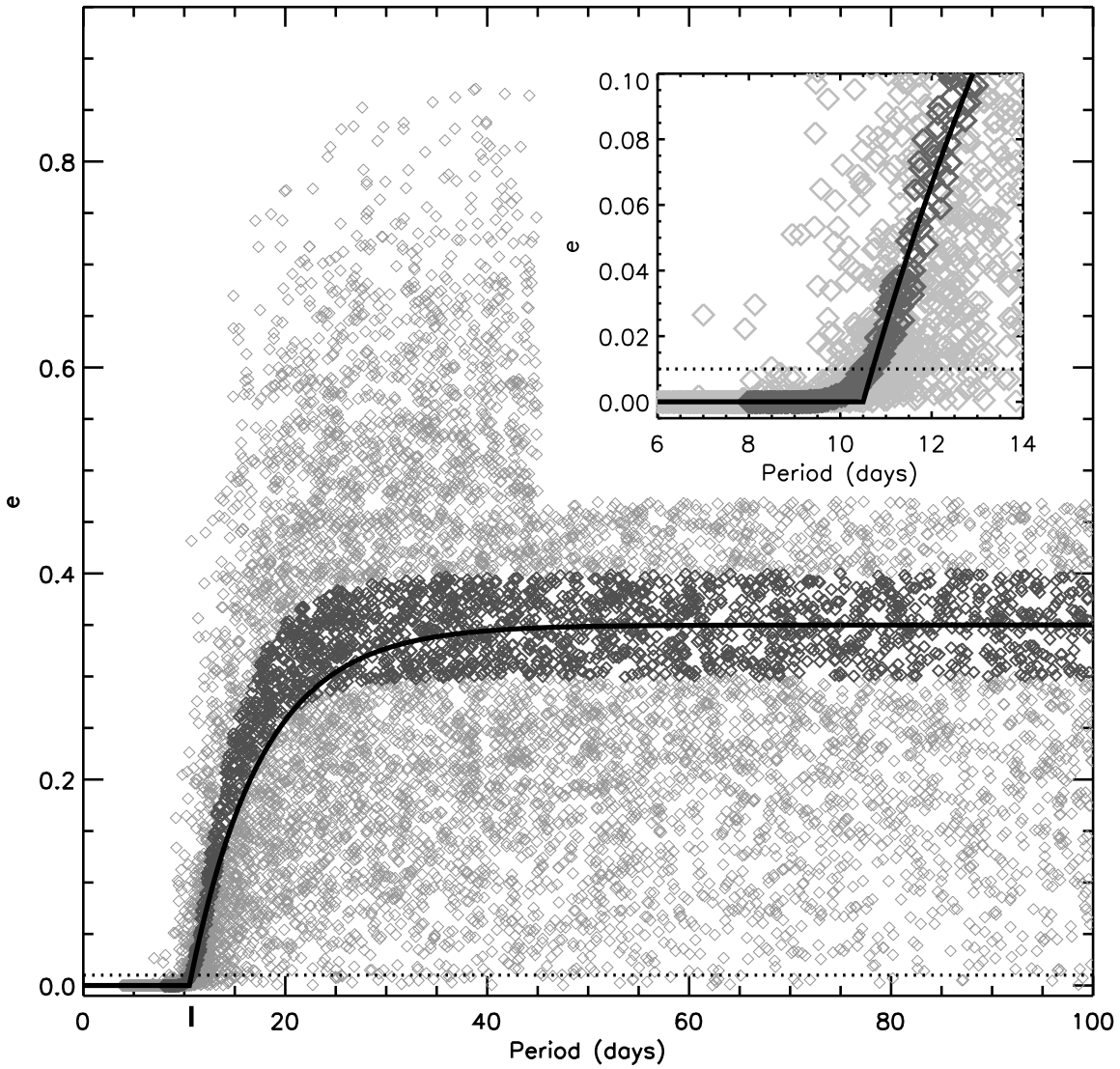

Fig. 2.4.— The circularization function (black solid line) fitted to an artificially generated sample of binary orbits (diamonds). Tidal circularization of these binary orbits has been simulated by numerical integration of the differential equations (2.3) and (2.4). Selection of the initial orbital periods and the initial orbital eccentricities is described in the main text. Binaries with the "typical" (most frequent) initial eccentricities between 0.3 and 0.4 are highlighted (dark diamonds). The circularization period (CP) is defined as the period at which the circularization function has a value of 0.01 ($e(CP) = 0.01$). $e = 0.01$ is marked by a horizontal dotted line and CP is marked by the vertical black line on the period axis. The insert is a close-up view of the transition-region.

M67, and NGC188 for orbits with periods longer than 50 days.

We ran the Monte Carlo experiment twice. The first time we excluded initially circular orbits ($e_i < 0.05$) to test the performance of the diagnostics in the absence of initially circular binaries. The second time we allowed for initially circular orbits to see the effect of such systems on the circularization and cutoff periods.

The distributions of circularization periods and cutoff periods resulting from the two Monte Carlo experiments described above allow us to determine the uncertainty on each of these measures. We will refer to the circularization period and the cutoff period derived from each binary population as the *observed* circularization period and the *observed* cutoff period. For reference two "parent" populations of $\sim 20,000$ binary orbits were generated and tidally evolved. We will refer to the circularization period and the cutoff period derived from these parent populations as the *true* circularization period and the *true* cutoff period.

Figure 2.5 show the distributions of the observed circularization periods (2.5a) and the observed cutoff periods (2.5b) derived for the 10,000 different binary populations *excluding* initially circular binary orbits. The true circularization period is shown in Figure 2.5a as a vertical solid line at 10.6 days. The distribution of circularization periods is slightly asymmetric with a tail at longer periods. Nonetheless, the true circularization period falls at the mode of the observed distribution. Thus, we take an observed circularization period as the best estimate of the true circularization period for any binary population.

The interval enclosing 2/3 of the observed circularization periods on either side of the mode is marked by dotted vertical lines, and hereafter called the 2/3-interval. We define the uncertainty on the true circularization period of a binary population as the $\pm$ period intervals that the true circularization period can be shifted before the observed circularization period must be drawn from outside of the 2/3-interval. The errorbars on the true circularization period can thus be determined by considering two limiting cases: i) The observed circularization period is located at the short-period boundary of the 2/3 interval; 1.0 days shortward of the mode. In that case the observed circularization period would underestimate the true circularization period by 1.0 days. We assign a positive errorbar of 1.0 days to the true circularization period. ii) The observed circularization

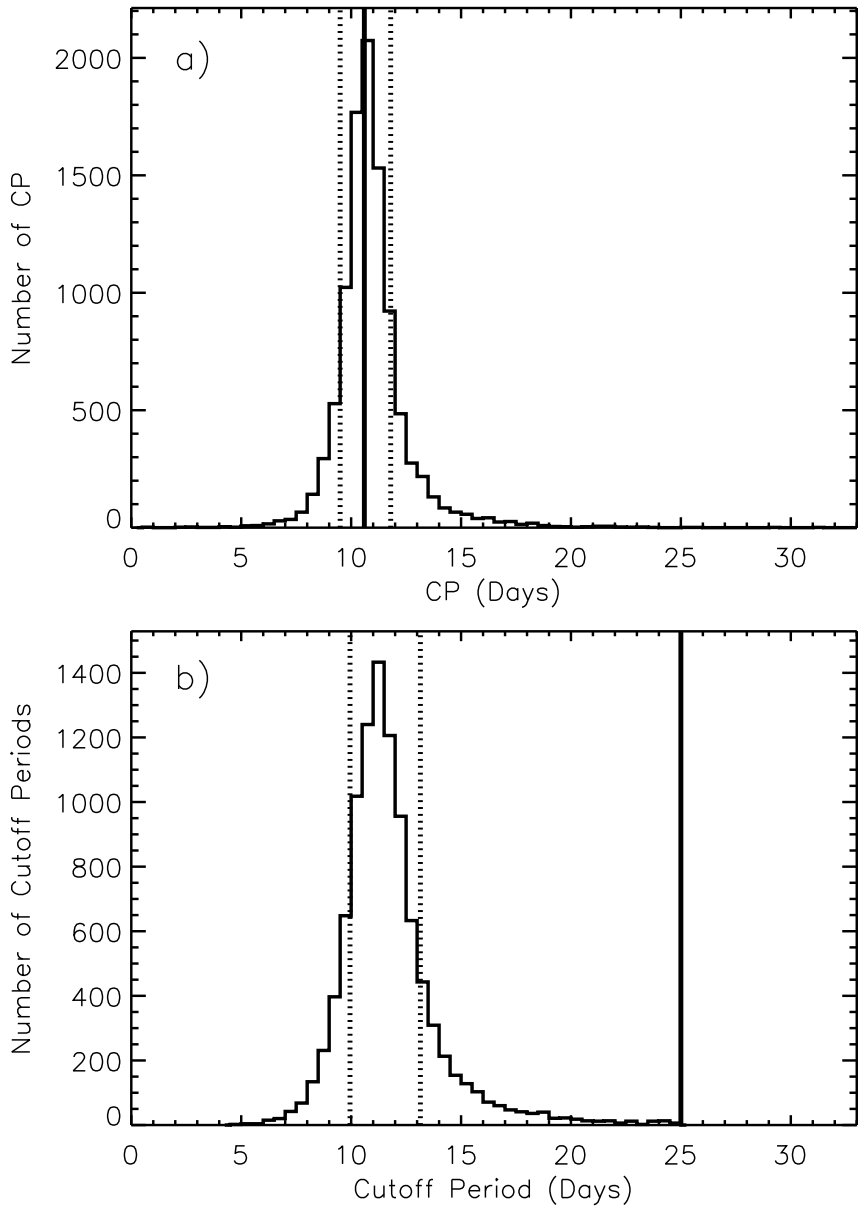

Fig. 2.5.— **a)** The distribution of circularization periods from 10,000 different binary populations each with 20 binary orbits with periods between 10 and 50 days. Only initially eccentric binary orbits ($e_i > 0.05$) were considered. The vertical solid line mark the location of the true circularization period determined from a "parent" population of $\sim$ 20,000 binary orbits (10.6 days). The interval containing 2/3 of all circularization periods around the mode is shown by the two vertical dotted lines at 9.6 and 11.8 days. **b)** The distribution of cutoff periods from the same 10,000 binary populations. The true cutoff period determined from the "parent" population of $\sim$ 20,000 binary orbits is marked by a vertical solid line at 25.0 days. The vertical dotted lines at 10.0 and 13.2 days mark the interval containing 2/3 of all cutoff periods around the mode at 11.3 days.

period is located at the long period boundary of the 2/3 interval; 1.2 days longward of the mode. In that case the observed circularization period would overestimate the true circularization period by 1.2 days. We assign a negative errorbar of 1.2 days to the true circularization period.

Accordingly, for a binary sample with $\sim$ 20 orbits shorter than 50 days (e.g. the M35 sample) the uncertainty range around the circularization period is + 1.0 days and - 1.2 days.

The cutoff period of each binary population is defined here as the period of the longest period binary with an eccentricity below 0.05. The distribution of observed cutoff periods in Figure 2.5b is also slightly asymmetric with a tail toward longer periods and a mode of 11.3 days. The true cutoff period is marked by a vertical solid line at 25 days. Necessarily, the observed cutoff periods are shorter than the true cutoff period, and the mode of the distribution falls 13.7 days shortward thereof.

The measurement uncertainty of the cutoff period is defined similarly to the circularization period. The 2/3-interval is marked by dotted vertical lines, and we define the uncertainty range around our estimate of the true cutoff period as the $\pm$ period intervals that the true cutoff period can be shifted before the observed cutoff period must be drawn from outside of the 2/3-interval. Accordingly, for a binary sample with 20 orbits shorter than 50 days (e.g. the M35 sample) the uncertainty range around the maximum likelihood estimate of the true cutoff period is + 1.3 days and - 1.9 days.

We wish to emphasize that the maximum likelihood observed circularization period and the true circularization period are the same, whereas the maximum likelihood observed cutoff period is offset from the true cutoff period by 13.7 days. The latter difference reflects a significant sample size dependence of the cutoff period that obscures the physical dependence of the age of the binary population.

In addition the Monte Carlo error analysis gives an error on the circularization period that is 1.0 day smaller than the error on the cutoff period. Thus we have shown that the circularization period is both more accurate and more precise than the cutoff period.

Next we consider binary populations *including* initially circular ($e < 0.05$) binary orbits drawn from the Gaussian parent eccentricity distribution. Figure 2.6 shows the distributions of the observed

circularization periods (2.6a) and the observed cutoff periods (2.6b) derived for 10,000 binary populations. All vertical lines represent the same quantities as in Figure 2.5. Note the small effect of initially circular orbits on the distribution of the observed circularization periods and on the true circularization period derived from the parent population. The uncertainty range around the maximum likelihood estimate of the true circularization period is + 1.0 days and - 1.5 days, somewhat inflated by the initially circular orbits.

In contrast, the distribution of cutoff periods is drastically changed by the presence of initially circular binary orbits ($e < 0.05$). The true cutoff period is undefined and a tail of cutoff periods longward of the distribution mode is produced.

In the presence of binaries with initially low eccentricity determination of the cutoff period is then dependent on the judgment of individual observers to define the eccentricity threshold between circular and eccentric systems and to select the binary defining the cutoff period. Examples of the effect of such judgments/selections on the value of the cutoff period will be given in Section 2.8 below.

Comparison of Figure 2.5 and Figure 2.6 clearly demonstrates the robustness of the circularization period and the vulnerability of the cutoff period. Determination of the circularization period uses the information from all binary orbits, circular as well as eccentric, and is thus less vulnerable to initially circular orbits. The cutoff period is determined from one binary orbit alone and is thus vulnerable to the presence of initially circular orbits in the binary population, contamination from binaries with anomalous evolutionary paths, and/or binaries that have been falsely classified as cluster members.

Importantly, the disadvantages of the cutoff period will be enhanced with larger binary populations, whereas the measurement uncertainty on the circularization period will decrease with increasing population size.

To enable ourselves and colleagues to quote errors on circularization periods to binary populations of different sizes and ages, we repeated the Monte Carlo error analysis (allowing for initially circular binary orbits) 9 times. For each of 3 different sample sizes (10, 20, and 30 binaries) we tidally evolved each of 10,000 samples so that the modes of the circularization period distributions were $\sim$ 5, 10, and 15 days. Errors on the circularization periods were derived in the manner explained

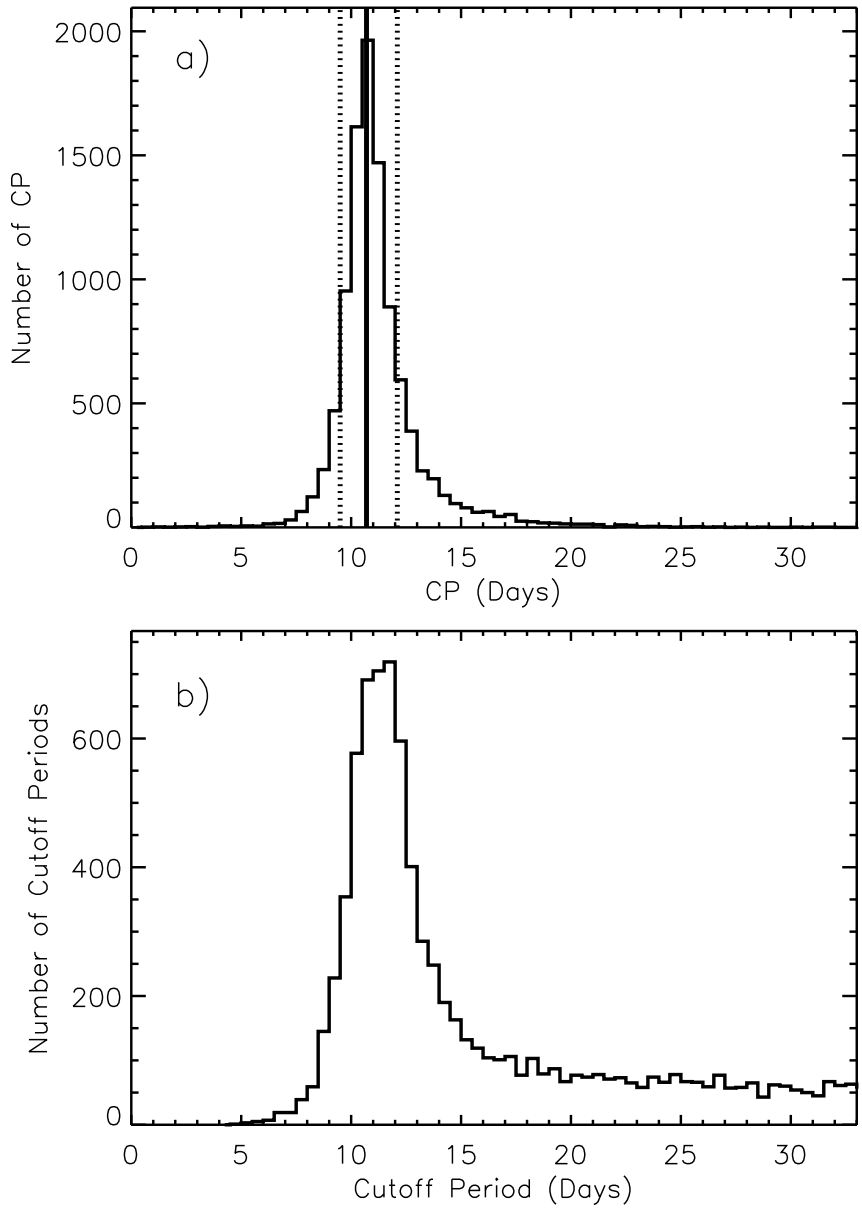

Fig. 2.6.— **a)** The distribution of circularization periods from 10,000 different binary populations each with 20 binary orbits with periods between 10 and 50 days. Initially circular binary orbits ($e_i < 0.05$) were included. All vertical lines represent the same quantities as in Figure 2.5. The estimated true circularization period is 10.7 days, and the interval containing 2/3 of all circularization periods around the mode range from 9.7 to 12.2 days. **b)** The distribution of cutoff periods from the same 10,000 binary populations.

above. Table 2.3 list the derived errors and can be used as a reference for colleagues studying tidal circularization in clusters not listed in this paper.

The coefficients β and γ in the circularization function (eq. [2.1]) controls the steepness/slope and the abruptness, respectively, of the function's transition from zero to non-zero eccentricities. Values of 0.14 for β and 1.0 for γ were adopted to minimize the width of the distributions of circularization periods resulting from the Monte Carlo experiments described above, and to minimize the sensitivity of the circularization period to the choice of eccentricity threshold ($e = 0.01$) between circular and eccentric orbits.

2.7 The Circularization Period in M35

After motivating, presenting and testing the circularization function and defining the circularization period, we are ready to apply this new diagnostic of tidal circularization to the population of binary orbits in M35.

Figure 2.7 show the period-eccentricity distribution in the $e - \log(P)$ diagram of M35. The circularization function resulting in the minimum total absolute deviation between observed and calculated eccentricities is over-plotted and the locations of the observed circularization period (CP) and it's uncertainty interval are marked. The horizontal dotted line marks $e = 0.01$. The observed circularization period for M35 is $10.2^{+1.0}_{-1.5}$ days. The errors quoted were derived in Section 2.6 and are listed in Table 2.3.

The M35 period-eccentricity distribution show striking similarities to the artificially generated distributions created using eqs. (3) and (4) and an initial Gaussian eccetricity distribution. In addition to the period overlap between eccentric and circular orbits described in Section 2.4, 3 circular

Table 2.3. Circularization Period Errors

Size of Binary Population	CP = 5 days Errors (days)	CP = 10 days Errors (days)	CP = 15 days Errors (days)
10 Binaries	+ 1.8 - 1.9	+ 1.5 - 3.1	+ 2.3 - 3.2
20 Binaries	+ 1.2 - 1.2	+ 1.0 - 1.5	+ 1.4 - 2.2
30 Binaries	+ 1.1 - 1.1	+ 0.8 - 1.1	+ 1.2 - 1.5

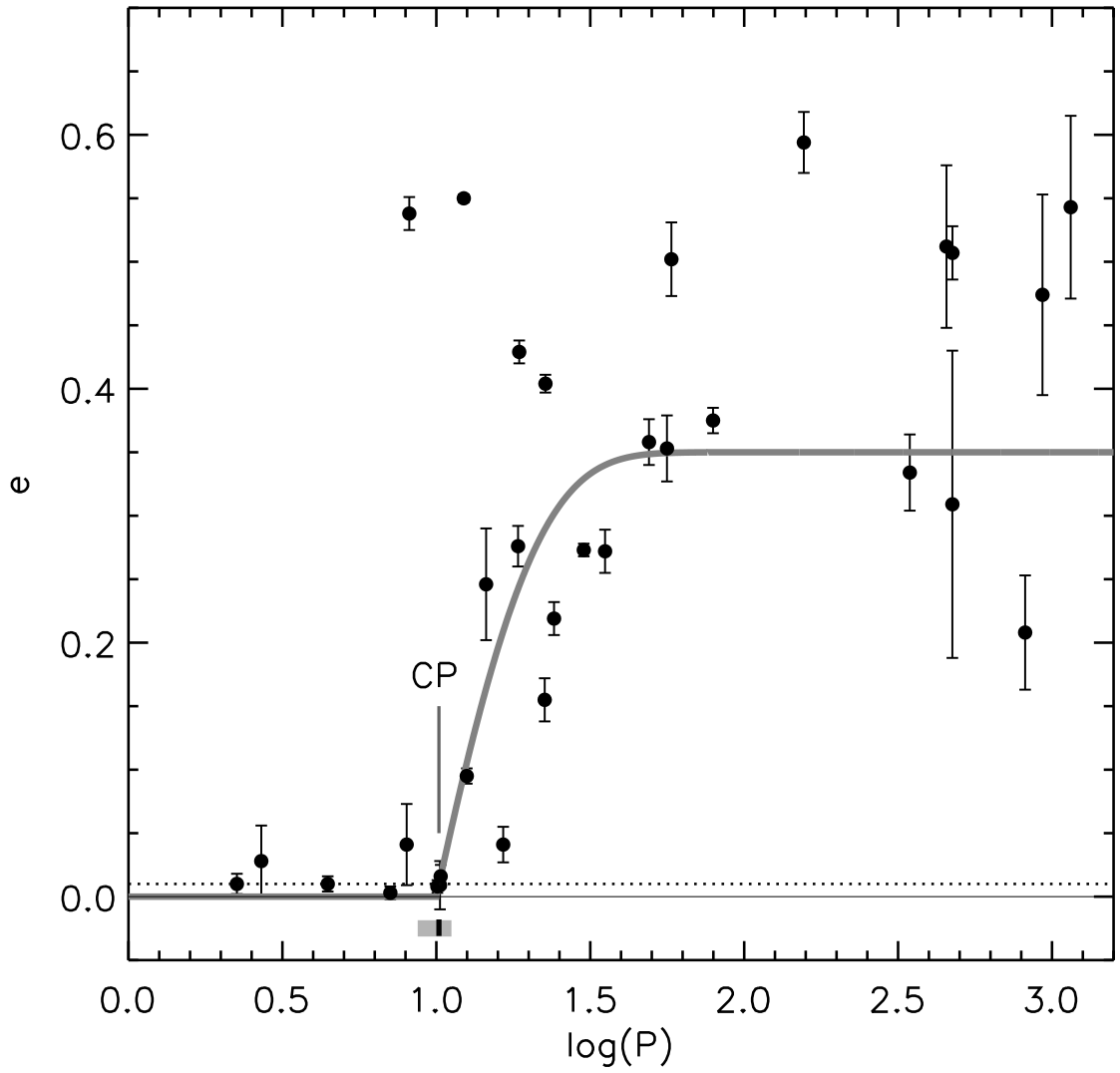

Fig. 2.7.— The distribution of orbital eccentricity (e) as a function of *log* orbital period (P) for 32 spectroscopic binary members of M35. The grey curve represent the best fit circularization function and the dotted horizontal line mark e = 0.01. The circularization period (CP) is marked at $\log(P) = 1.0$ (10.2 days) and it's uncertainty interval overplotted.

binaries with periods of ~ 10 days in M35 nicely represent the most frequent (typical) binaries located in the high density region at $e \lesssim 0.05$ and $P \sim 10$ days in Figure 2.4. The distribution of eccentricities of binaries with periods longer than ~ 10 days is consistent with a primordial Gaussian distribution and the circular binary (4037) with a period 16.49 days is likely to originate from the low eccentricity wing.

Therefore, M35 is a good example of the advantages of the circularization period in defining the transition between eccentric and circular binary orbits. The best fit circularization function takes advantage of the information provided by all binary orbits and provide a more robust determination of the circularization period for the typical binary orbit.

2.8 The Circularization Periods of 7 Additional Binary Populations

Below we briefly discuss and present the period-eccentricity distributions and determine circularization periods for 7 additional binary populations spanning ages from ~ 3 Myr (PMS binaries) to ~ 10 Gyr (Galactic halo binaries). Figure 2.8a-h show the orbital data of each individual population with the best-fit circularization function over-plotted and the circularization period with error marked. All results are listed in Table 2.4 here we briefly discuss each population in turn.

The PMS binary population (Figure 2.8a): The sample of 37 low-mass PMS binaries show the characteristic period overlap between eccentric and circular orbits. The orbital parameters are taken from Melo et al. (2001), and references to individual binaries can be found in their paper. The PMS sample is not strictly coeval, but cover an age range from $\sim$ 1-10 Myr (Melo et al. 2001). We determine a circularization period of $7.1^{+1.2}_{-1.2}$ days for the PMS binary sample. This value should be compared to the 7.56 day cutoff period determined by Melo et al. Note, that Melo et al. chose to disregard the circular orbit of binary RX J1301.0-7654a (P = 12.95 days ($\log(P) = 1.11$), $e = 0.04 \pm 0.02$; Covino, private communication) based on measurements of super-synchronous rotation of the individual binary components. Because the timescale for tidal synchronization is thought to be shorter than the timescale for circularization (Zahn 1977; Hut 1981), Melo et al. argue that the circular orbit of RX J1301.0-7654a might not be a result of tidal circularization. However, as mentioned by Melo et al., super-synchronous stellar rotation is an expected result of the transition from the PMS to the ZAMS due to conservation of angular momentum and a decline in the efficiency

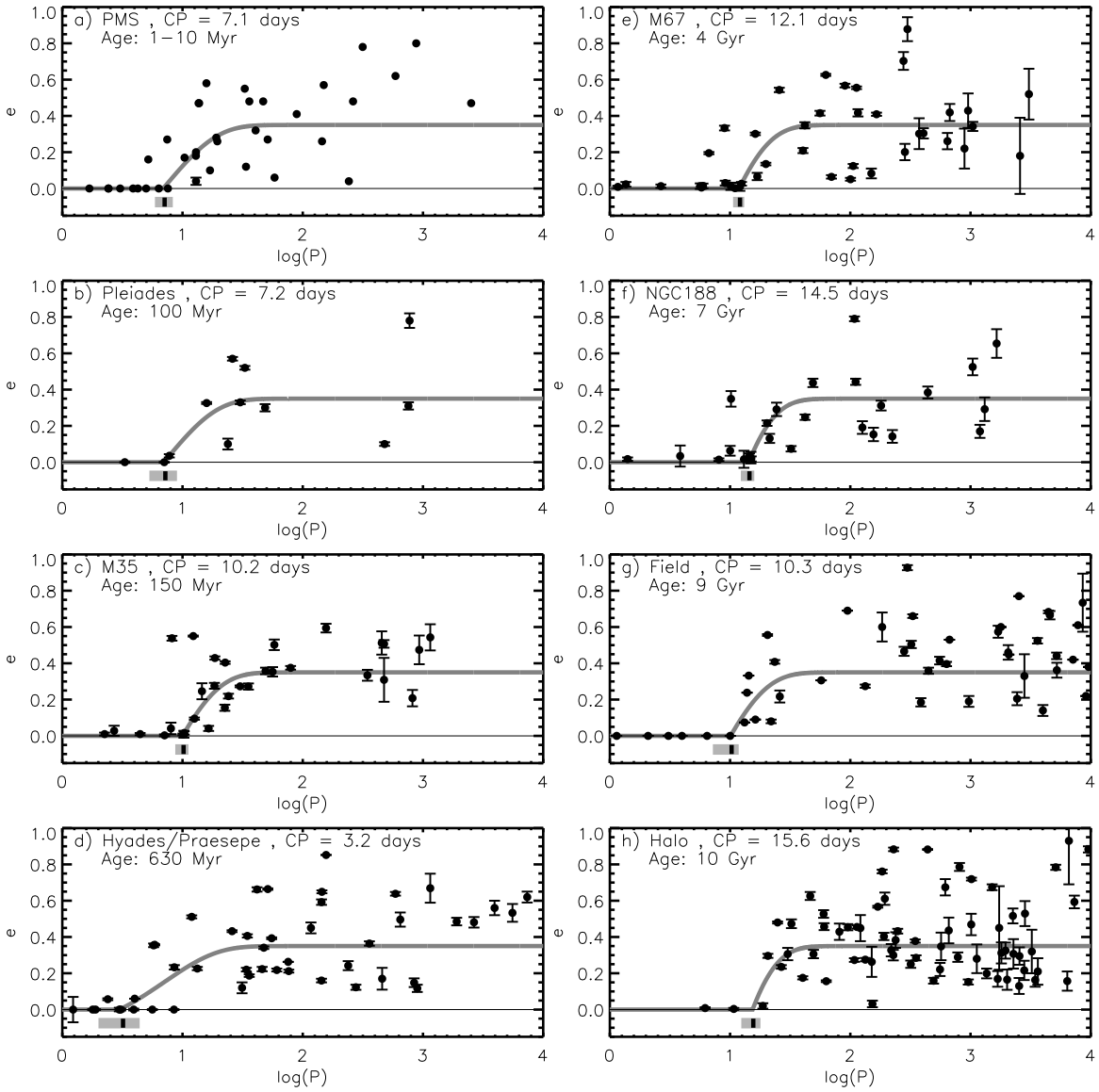

Fig. 2.8.— The period-eccentricity distributions for 8 late-type binary populations: **a)** PMS, **b)** Pleiades, **c)** M35, **d)** Hyades/Praesepe, **e)** M67, **f)** NGC188, **g)** field, and **h)** halo. Over-plotted each distribution is the best fit circularization function. A solid horizontal line mark e(P) = 0.00. The circularization period (CP) and it's uncertainty are marked on the period axis by a vertical black line and a grey bar, respectively. The circularization period and the age of the binary population are printed in each plot.

of tidal breaking as the stars contract. Thus we have chosen to include binary RX J1301.0-7654a. However, due to the robust nature of our new diagnostic, excluding binary RX J1301.0-7654a from the PMS sample causes only a 0.5 day decrease in the circularization period, whereas the longest period circular orbit would decrease by 5.39 days (from 12.95 to 7.56 days).

The Pleiades binary population (Figure 2.8b): The eccentricity distribution of 12 binary orbits in the $\sim$ 100 Myr Pleiades cluster provides poor sampling of the transition region. Also, unlike any other population included in this study, the Pleiades features a gap between the longest period circular and the shortest period eccentric orbit. By fitting the circularization function we make use of the information provided by the binary orbits on both sides of the gap, and determine a circularization period of $7.2^{+1.8}_{-1.9}$ days. This value should be compared to the 7.7 day cutoff period previously used for the Pleiades cluster. The orbital parameters shown in Figure 2.8b are taken from Mermilliod et al. (1997, 1992). The estimated masses for the binary primary components falls within $\sim 0.9\ M_{\odot} - 1.4\ M_{\odot}$.

The M35 binary population (Figure 2.8c): The distribution of orbital eccentricities in M35 (discussed above) is shown here for the purpose of comparison.

The Hyades/Praesepe binary populations (Figure 2.8d): The sample of 47 binary orbits in the $\sim$ 630 Myr Hyades/Praesepe twin clusters show 3 eccentric binaries shortward of the longest period circular orbit. The best fit circularization function is over-plotted and the circularization period of $3.2^{+1.2}_{-1.2}$ days is marked. The cutoff period for the Hyades/Praesepe sample has previously been set by the 8.49 day circular binary J331. J331 consist of two 0.5 $M_{\odot}$ components, and thus is substantially different from the binaries with approximately solar-mass components defining the transition regions in other binary populations. For this reason Mathieu et al. (1992) questioned whether binary J331 should be disregarded, as the difference in mass and stellar structure (depth of convective envelope) might have significantly altered the timescale of tidal circularization. We will not comment further on the effect of stellar mass here, but simply emphasize that while we have included binary J331, disregarding it leads to no noticeable change in the Hyades/Praesepe circularization period, compared to a -2.75 days change from 8.49 to 5.74 days in the Hyades/Praesepe cutoff period. The orbital parameters shown in Figure 2.8d are taken from Griffin et al. (1985, 1982);

Griffin & Gunn (1981, 1978) for Hyades binaries and Mermilliod & Mayor (1999); Mermilliod et al. (1992, 1990) for Praesepe binaries. The estimated masses for the the primary components of this sample falls within $\sim 0.5\ M_{\odot} - 1.5\ M_{\odot}$.

The M67 binary populations (Figure 2.8e): The sample of spectroscopic binaries in the old open clusters M67 contain stellar components ranging in evolution from the unevolved main-sequence to the tip of the giant branch (Mathieu, priv. comm.). As the rate of tidal circularization depends sensitively on stellar radius and the depth of the convection zone, we will consider only binaries in M67 with unevolved primary components. Figure 2.8e shows the distribution of orbital eccentricity vs. log orbital period for 39 unevolved binaries in M67. Two eccentric orbits are found shortward of the longest period circular orbit. The best fit circularization function is over-plotted and the circularization period of $12.1^{+1.0}_{-1.5}$ days is marked. The mass-range of the binary primary components is $\sim 0.9\ M_{\odot} - 1.2\ M_{\odot}$.

The NGC188 binary populations (Figure 2.8f): As for M67, the binary population in NGC188 contains evolved as well as unevolved stellar components. Again we will consider only binaries with unevolved primary components. The distribution of orbital eccentricity vs. log orbital period for 27 unevolved binary stars in NGC188 is shown in Figure 2.8f. The binary population contains a single eccentric system with a period shorter than the longest period circular binary. The circularization period of $14.5^{+1.4}_{-2.2}$ days is marked and the best fit circularization function is over-plotted. The orbital data shown in Figure 2.8f are taken from Mathieu et al. (2004). The mass-range of the primary components in this sample is $\sim 0.95\ M_{\odot} - 1.05\ M_{\odot}$.

The field binary population (Figure 2.8g): The orbital characteristics of 50 close solar-type binaries from the solar neighborhood (hereinafter: the field) is shown with the circularization period of $10.3^{+1.5}_{-3.1}$ days marked and the best fit circularization function over-plotted. The orbital data are taken from Duquennoy & Mayor (1991), who adopt an age range of 7-11 Gyr for the population of field binaries. We adopt 9 Gyr as the age of the field sample. However, the age of some individual binary systems are poorly known, thus despite the well-defined circularization period, the age-ambiguities of this sample makes it less reliable for probing the evolution of tidal circularization.

The Galactic halo binary population (Figure 2.8h): The orbital characteristics of 61 binaries

from the Galactic halo. The best fit circularization function is over-plotted and the circularization period of $15.6^{+2.3}_{-3.2}$ days is marked. The orbital data are taken from Latham et al. (2002). We adopt an age of 10 Gyr for the halo binary population. From a large sample of 171 high proper motion spectroscopic binaries, Latham et al. (2002) find no obvious differences between the binary characteristics in the halo and in the disk populations. The observed frequency is the same and the period distributions are consistent with the hypothesis that the binaries are drawn from the same parent population. Nonetheless, the halo binary population is not strictly coeval and the stars differ significantly in mass and metallicity from those of the open cluster/disk populations. Arguably, comparison of solar-mass/solar-metallicity tidal circularization theory to the halo cutoff period requires consideration of these differences.

It is important to note that in the majority of the binary populations discussed here, circular or marginally circular binary orbits are observed with periods from tens to hundreds of days longer than the circularization period. The selection of unevolved main-sequence binaries for each population suggest that these long period ($P \sim 10^1 - 10^2$ days) low eccentricity ($e \sim 0.05$) orbits are not a result of accelerated tidal circularization due to evolved primary components. The existence of long-period low eccentricity binaries in the PMS, Pleiades and M35 samples is a strong indication that binary stars can form with circular or marginally circular orbits, consistent with an initial Gaussian distribution of orbital eccentricities.

The binary populations shown in Figure 2.8 also show a high frequency of high-eccentricity orbits at periods shorter than the one or more circular orbits. The ability to reproduce such systems from binaries in the high-eccentricity tail of the initial Gaussian distribution by numerically integrating current theoretical models of tidal circularization (Duquennoy et al. 1992, Section 2.6 this paper), provide further support for the existence of an initial Gaussian distribution of orbital eccentricities.

2.9 Evolution of Tidal Circularization

While different tidal circularization theories agree that the timescale of circularization depends strongly on stellar separation, and that consequently a transition from eccentric to circular orbits is expected at a well-defined binary period, the different theories describe different mechanisms for the tidal dissipation leading to circularization. The mechanism and efficiency of tidal dissipation in a

given model reflects itself in the model's prediction of the rate of circularization and the evolution of the tidal circularization period. Observational determinations of the circularization periods in binary populations of different ages provide a critical test of the dissipation mechanism(s) responsible.

Detailed discussion of the distribution of circularization cutoff periods with age, and its ability to constrain tidal circularization theory, was given by Witte & Savonije (2002),Melo et al. (2001), and Mathieu et al. (1992). However, the addition of the new large binary populations of M35 and NGC188 (Mathieu et al. 2004), the introduction of a new robust measure of tidal circularization (the circularization period) with measured uncertainties, and the recent theoretical work on dynamical tides in late-type stars (e.g. Witte & Savonije 2002), motivate a fresh look at how the theory compares to the observations.

We show in Figure 2.9 the circularization periods for all binary populations discussed in this paper (solid/open circles) at their respective ages. Errorbars show the uncertainties on the circularization periods based on the Monte Carlo experiments described in Section 2.6.

With the exception of the Hyades/Praesepe population, the circularization periods of the coeval solar-type binary populations show a steady increase with age from the PMS and early main-sequence to the late main-sequence phase. The circularization period of the halo and field binaries follow this trend. However, due to the non-coevality and uncertainty in age of the field sample, and the differences in mass and metallicity of the stars in the halo sample, we choose not to include their circularization periods in the subsequent analysis.

The small value of the circularization period of the Hyades/Praesepe sample can be explained in part by the high number of short period eccentric binaries, in particular the two highly eccentric short period binaries (Hyades: HD30738, $P = 5.75$ days, $e = 0.354$; Praesepe: KW181, $P = 5.87$ days, $e = 0.357$). However, even in the absence of these two systems the Hyades/Praesepe circularization period will be 5.9 days and thus still deviate from the overall trend of increasing circularization periods with increasing age. We note that Duquennoy & Mayor (1991) draw attention to an excess of short period binaries ($\log(P) < 1$ day) in the Hyades period distribution when compared to distribution from their G-dwarf sample.

The predictions of main-sequence tidal circularization in the framework of both the equilibrium

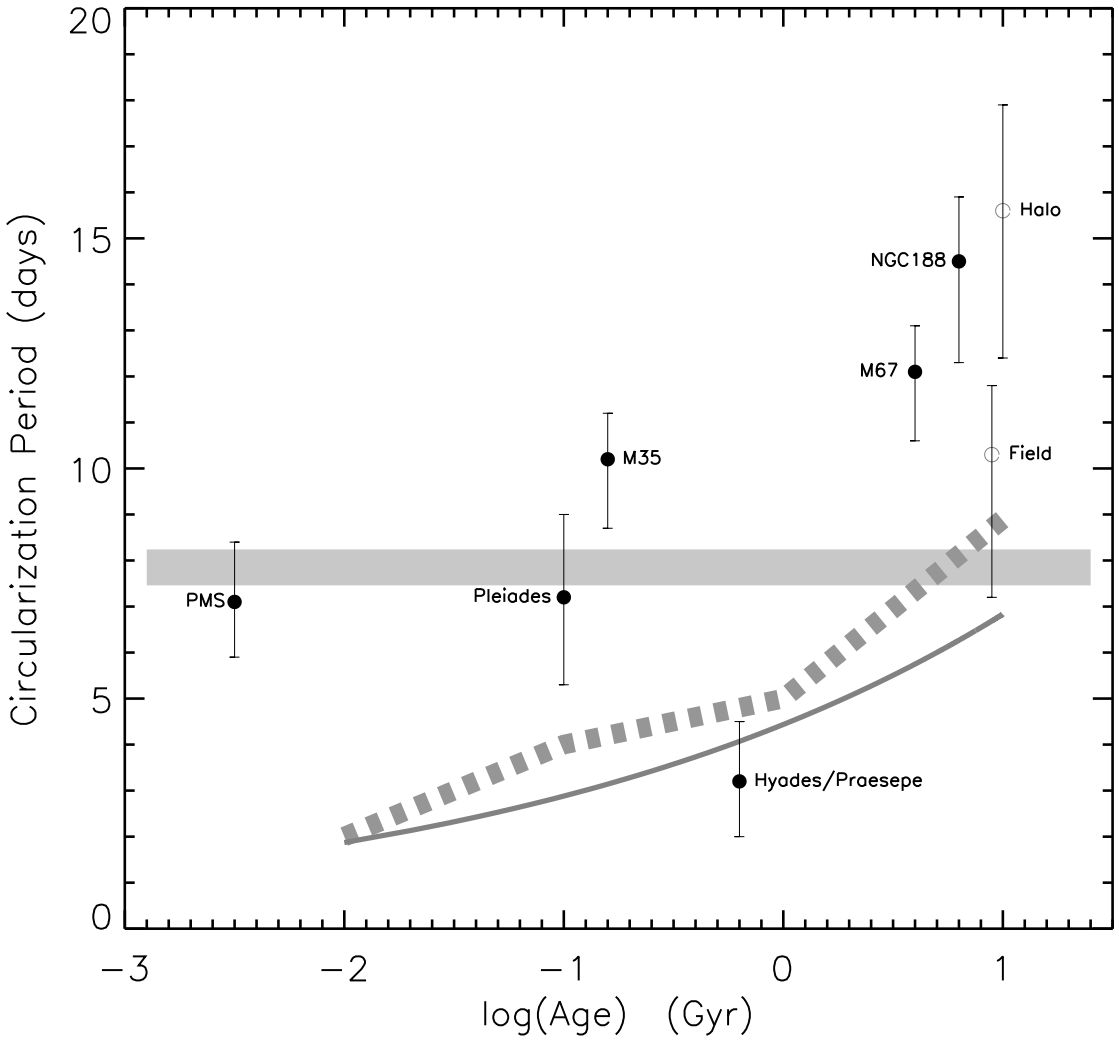

Fig. 2.9.— The distribution of circularization periods with age for 8 late-type binary population (solid/open circles). Errorbars represent the uncertainties on the circularization periods derived in Section 2.6. The solid curve shows the predicted cutoff period as a function of time based on main-sequence tidal circularization using the revised equilibrium tide theory by Zahn (1989) (Claret & Cunha 1997). The broad dashed band represent the predicted cutoff period period for initially super-synchronous 1 $M_{\odot}$ stars calculated in the framework of the dynamical tide model including resonance locking (Witte & Savonije 2002). The horizontal grey band represents the prediction by Zahn & Bouchet (1989) in which tidal circularization is significant only during the PMS phase.

tide theory and the dynamical tide theory are also shown in Figure 2.9, as is the prediction by Zahn & Bouchet (1989) including PMS tidal circularization. Note that these different theoretical predictions displayed in Figure 2.9 use different criteria for determination of the cutoff period. Claret & Cunha (1997, equilibrium tide theory) define the cutoff period at a given age as the longest orbital period for which the relative variation in the eccentricity is 0.5% of the initial value ($e_{ini} = 0.30$). Witte & Savonije (2002, dynamical tide theory) define the cutoff period as the longest orbital period for which a binary with 1 $M_{\odot}$ components has been circularized to $e < 0.01$. As such the predictions of Witte & Sovonije are upper limits on the circularization period. Zahn & Bouchet (1989, PMS tidal theory) define the cutoff period as the period at which a binary with component masses between 0.5 $M_{\odot} - 1.25$ $M_{\odot}$ and initial orbital eccentricity of 0.2 or 0.3 circularizes to $e < 0.005$. Recall that the circularization periods displayed in Figure 2.9 represent the orbital period at which a binary orbit with initial eccentricities in the range 0.2 - 0.5 evolves to $e = 0.01$ at the age of the population.

The equilibrium tide theory: Let us consider first the equilibrium tide theory using the dissipation mechanism by Zahn (1989). The equilibrium tide theory predicts active tidal circularization throughout the main-sequence phase, leading to longer cutoff periods with increasing population age (solid curve in Figure 2.9). However, as pointed out by Claret & Cunha (1997), an artificial enhancement of the turbulent dissipation is necessary to fit the observed cutoff periods. Comparison with the new circularization periods, again with the exception of the circularization period of the Hyades/Praesepe population, show a similar discrepancy between the observations and the theoretical predictions of pure main-sequence tidal circularization.

The grey horizontal band in Figure 2.9 shows the prediction by Zahn & Bouchet (1989) of tidal circularization including the PMS phase. Based on the reduced rate of tidal circularization derived by Zahn (1989), Zahn & Bouchet suggested that all tidal circularization occurs during the PMS phase when the stars have larger radii and deeper convective envelopes. They found that for main-sequence stars the efficiency of turbulent dissipation derived from the equilibrium tide theory is so small that tidal circularization following the PMS phase is negligible despite the Gyr timescales available. Their PMS tidal circularization theory predicts a range of cutoff periods between $\sim$ 7.2 - 8.5 days for binaries with components with masses between 0.5 - 1.25 $M_{\odot}$ and initial eccentricities

of either 0.2 or 0.3. Accordingly, all late-type main-sequence binaries should have circular orbits for period less than $\sim$ 8 days and (primordial) eccentric orbits at longer periods, independent of age.

The hypothesis that PMS tidal circularization alone sets a tidal cutoff period, independent of age, is *not* consistent with the observed distribution of circularization periods. We performed a χ^2 test fitting different constant theoretical circularization periods to the distribution of observed circularization periods. We find that there is less than a 1% probability that the observed circularization periods (excluding or including the field and halo samples) derive from a model predicting no evolution of the circularization periods with age. Repeating the χ^2 test for all binary populations but the Hyades/Praesepe population also tells us that there is less than 1% chance that the PMS, Pleiades, M35, M67, and NGC188 populations derive from a model predicting pure PMS circularization.

The dynamical tide theory: The predicted evolution of main-sequence tidal circularization using the dynamical tide theory with inclusion of resonance locking (Witte & Savonije 2002) is shown in Figure 2.9 as a broad dashed band. The width of the dashed band represents the range of predicted evolutions of the cutoff period for binaries with stellar components rotating at super-synchronous ($\Omega = 2\omega_p$), pseudo-synchronous ($\Omega = \omega_p$), and orbital ($\Omega = \omega$) speeds. Ω, ω_p, and ω denote the initial stellar angular velocity, the orbital angular velocity at periastron, and the average orbital angular velocity, respectively. The masses of the binary components used by Witte & Savonije are 1 $M_\odot$.

Regardless of stellar rotation velocity, the dynamical tide theory with inclusion of the resonance locking mechanism (Witte & Savonije 2002) appears to predicts slightly more efficient tidal circularization than the equilibrium tide theory throughout the main-sequence phase. However, Witte & Savonije (2002) define the cutoff period as the longest orbital period for which a binary has been circularized to $e < 0.01$. This definition implies that the predicted cutoff periods are likely set by binaries with low initial orbital eccentricities, and thus are not directly comparable to the predictions by Claret & Cunha (1997). Still there is a discrepancy between the predicted level of circularization and the distribution of observed circularization periods. For the special case of very slowly rotating stars, the calculations of Witte & Savonije (2002, not shown in Figure 2.9) offer a near match to the circularization periods of Pleiades, M35, M67 and NGC188. However, the required stellar rotation

periods are of order 100 days for stars in close binary systems with ages between 0.1 and 10 Gyr. Such very slow rotations would be unexpected and thus needs to be observationally established.

The slopes of the main-sequence tidal circularization models match the increase in circularization period seen in Figure 2.9. Thus if the efficiency of tidal dissipation were to be artificially enhancement for both the equilibrium tide and the dynamical tide theories, the predicted main-sequence evolution for both theories would be in agreement with the observed increase in circularization period for all populations but the Hyades/Praesepe.

The hybrid scenario: The lack of success of both PMS and main-sequence tidal circularization theories to account for the observations of tidal circularization motivated the suggestion of a "hybrid scenario" (Mathieu et al. 1992). The hybrid scenario is heuristic and was motivated by a distribution of cutoff periods that appeared age-independent for populations younger than $\sim$ 1 Gyr while showing a positive correlation with age for populations older than $\sim$ 1 Gyr. The hybrid scenario suggest that tidal circularization in binary populations younger than $\sim$ 1 Gyr derive from PMS tidal circularization, and that after the passage of $\sim$ 1 Gyr the integrated main-sequence tidal circularization begins to circularize binaries with orbital periods of $\sim$ 10 days.

Considering the new distribution of circularization periods the need for a hybrid scenario is uncertain. With the exception of the Hyades/Praesepe population the observed circularization periods increase with age from the PMS and throughout the main-sequence phase. A χ^2 test shows that there is less than 1% probability that the circularization periods for populations younger than $\sim$ 1 Gyr derive from a model predicting no main-sequence tidal circularization. Excluding the Hyades/Praesepe sample result in χ^2 value of $\sim$ 1. Thus, the current distribution of circularization periods for the youngest binary populations cannot distinguish between a model predicting an age-independent circularization period or a model predicting a continuous increase in the circularization period from the PMS onward.

If tidal circularization is in fact active throughout the main-sequence phase, the question remains which if any of the suggested dissipation mechanisms is responsible. Either the equilibrium or the dynamical tide mechanisms, or perhaps both in combination, could be responsible for the circularization of binary orbits during the main-sequence phase. However, unless both mechanisms

are at work simultaneously, more efficient tidal dissipation is needed in both the equilibrium and the dynamical tide theories. We note that PMS tidal circularization is still needed to explain the 7.1 day circularization period of the PMS sample, and that an increase in the efficiency of turbulent dissipation of the equilibrium tide theory presumably will affect circularization during the PMS as well.

Alternatively, assuming pure PMS tidal circularization, the differences in circularization periods among the binary populations in Figure 2.9 could be due to differences in initial stellar and circumstellar conditions. Goodman & Dickson (1998) speculate that perhaps the differences in mass and/or metallicity between the younger disk binaries and the older disk and halo binaries could be the cause of differences in cutoff periods set during the PMS phase. While the ranges of primary stellar masses and metallicities of the populations included in this study are similar, other stellar/circumstellar and binary/circumbinary parameters might be of importance to the efficiency and duration of tidal circularization during the PMS phase. The strong dependence of the efficiency of circularization on stellar rotation displayed in the dynamical tide theory by Witte & Savonije (2002) is a powerful example of how differences in initial conditions may affect the evolution of tidal circularization.

It is difficult to draw secure conclusions about the evolution of tidal circularization based on only 6 circularization periods. The future observational goal is to further populate the age vs. circularization period diagram (Figure 2.9) with reliable circularization periods at carefully selected ages based on large samples of binary orbits from homogeneous coeval binary populations. Following the present study and the recent publication of binary orbits in NGC188 (Mathieu et al. 2004), we plan to contribute (work in progress) such circularization periods at the ages of the young open cluster M34 ($\sim$ 250 Myr) and the intermediate age open cluster NGC6819 ($\sim$ 2.5 Gyr). By inspection of Figure 2.9 it is evident that these future circularization periods will greatly improve the observational constraint on future theoretical models and predictions of tidal circularization in close late-type binary stars.

The future goal for theory of tidal circularization in late-type main-sequence stars is to construct models that combine PMS tidal circularization with main-sequence tidal circularization, and

predict more efficient tidal circularization in binaries with main-sequence components to account for the observed evolution of circularization.

2.10 Summary and Conclusions

In a coeval population of binary stars the closest binaries tend to have circular orbits, while wider binaries have orbits with a distribution of non-zero eccentricities. Determination of the orbital period to which binaries have been circularized is an important observational constraint on theoretical models seeking to explain the dissipation mechanism(s) responsible for tidal circularization. Coeval populations of short-period binary orbits are therefore key observational contributions.

However, despite homogeneity in age, mass and metallicity, a population of short-period binaries may be small in size and will consist of systems with a distribution of initial eccentricities. The size of a binary population will affect the uncertainty on its circularization period. The initial eccentricity of a circular binary with a period equal to the circularization period is unknown, but can be estimated through the use of theoretical models. Proper comparison between observed and theoretical circularization periods thus require measurement uncertainties on the observed circularization periods and information about the initial eccentricities of the binaries that circularize at those periods.

The primary contributions of this study are: 1) a new population of solar-type spectroscopic binary orbits for the 150 Myr open cluster M35; 2) a new diagnostic to determine the period of circularization of the most frequently occurring binary; 3) an evaluation of the performance of this new diagnostic providing measurement uncertainties on the resulting circularization periods and information about the initial eccentricity of the binaries that circularize at that period; and 4) a comparison of the distribution of circularization periods from 8 binary populations to the predictions from theoretical models.

The new sample of 32 spectroscopic binary orbits in the "Pleiades age" ($\sim$ 150 Myr) open cluster M35 greatly improves the constraint on tidal circularization at the early stage of the main-sequence phase. Prior to this study, the small sample of binary orbits in the Pleiades provided only very rough limits on the transition between eccentric and circular orbits at this age.

Monte Carlo simulations of tidal circularization using the equilibrium tide theory by Zahn

(1977) were used to create artificial $e - \log(P)$ distributions. These simulations, together with the $e - \log(P)$ distributions of M35 and 7 additional published binary populations, were used to critically assess the adequacy of the tidal circularization cutoff period (the period of the longest period circular binary) to measure the degree of tidal circularization. We conclude that the cutoff period is not an optimal measure of the transition between eccentric and circular orbits because of the following disadvantages:

- The simulations of tidal circularization using the equilibrium tide theory by Zahn (1977) show that the cutoff period is likely to originate from the low eccentricity tail of an initial Gaussian eccentricity distribution. Therefore, the cutoff period does not represent the period of circularization of the most frequently occurring binary orbit.

- The expected value of the observed cutoff period of a population of binaries varies with the size of the population.

- The cutoff period is vulnerable to the presence of circular orbits that are not a measure of tidal effects, such as primordial circular binary orbits or orbits of binaries with anomalous evolutionary paths.

- Determination of the cutoff period makes no use of the information provided by eccentric orbits in the $e - \log(P)$ diagram.

Motivated by the need for a more robust determination of the orbital period at which a binary orbit with the most frequent initial orbital eccentricity circularizes, we introduce the circularization function and the circularization period. The functional shape of the circularization function (eq. [2.1]) is fixed and mimics the transition from eccentric to circular orbits in the $e - \log(P)$ diagram (Figure 2.4). The circularization period is defined as the period for which the circularization function has a value of 0.01 ($e(CP) = 0.01$). The location in period of the circularization function thus determines the circularization period. The advantages of the circularization function/period are:

- Numerical simulations of tidal circularization using the equilibrium tide theory by Zahn (1977) show that the circularization period is the period at which a binary with the most frequent initial eccentricity ($e \sim 0.35$) evolves to $e = 0.01$ at the age of the population.

- The circularization period is determined from all binary orbits (circular and eccentric), and so is less vulnerable to primordial circular binaries or binaries with anomalous evolutionary paths.
- The observed circularization period is the best estimate of the true circularization period independent of the size of the binary population.

Monte Carlo error analysis allows us to examine the distribution of the circularization periods. From this analysis we estimate and provide the uncertainty on the circularization period as a function of the size of the binary sample and of the value of the circularization period. We note that even in the absence of initial circular binaries and/or contamination from binaries with anomalous evolutionary paths, the Monte Carlo error analysis show that the uncertainty on the circularization period is smaller than the uncertainty on the cutoff period. Thus we conclude that the circularization period is both more accurate and more precise than the cutoff period.

We present the circularization periods for M35 and 7 additional binary populations ranging in age from $\sim$ 3 Myr to $\sim$ 10 Gyr. With the exception of the circularization period of the Hyades/Praesepe population, the distribution of circularization periods with age show a steady increase from the PMS to the late main-sequence.

We compare the distribution of circularization periods to the predictions by theoretical models. The models of main-sequence tidal circularization using either the equilibrium tide theory (Zahn 1989) or the dynamical tide theory with resonance locking (Witte & Savonije 2002) both predict longer cutoff periods with increasing population age in agreement with the trend in the distribution of circularization periods. **However, the predicted circularization periods fall significantly below the observed circularization periods.** This suggest that the efficiency of the dissipation in these models is too low.

A model including PMS tidal circularization (Zahn & Bouchet 1989) predicts negligible circularization during the main-sequence phase. This prediction is not consistent with the observed distribution of circularization periods.

The need for a hybrid scenario as proposed by (Mathieu et al. 1992) is uncertain. The current distribution of circularization periods for the youngest binary populations cannot distinguish between a model predicting an age-independent circularization period or a model predicting a continuous

increase in the circularization period from the PMS onward.

The goal for future theories of tidal circularization in late-type main-sequence binaries is to combine PMS and main-sequence circularization in one model that can account for the circularization periods observed at all ages.

References

Claret, A., & Cunha, N. C. S. 1997, A&A, 318, 187

Cudworth, K. M. 1971, AJ, 76, 475

Darwin, G. H. 1879, The Observatory, 3, 79

Duquennoy, A., & Mayor, M. 1991, A&A, 248, 485

Duquennoy, A., Mayor, M., & Mermilliod, J. C. 1992, in Binaries as Tracers of Stellar Formation. Proceedings of a Workshop held in Bettmeralp, Switzerland, Sept. 1991, in honor of Dr. Roger Griffin. Editors, Antoine Duquennoy, Michel Mayor; Publisher, Cambridge University Press, Cambridge, England, New York, NY, 1992. LC # QB821 .B55 1991. ISBN # 0521433584. P. 52, 1992, 52

Giuricin, G., Mardirossian, F., & Mezzetti, M. 1984, A&A, 134, 365

Goodman, J., & Dickson, E. S. 1998, ApJ, 507, 938

Griffin, R. F., Griffin, R. E. M., Gunn, J. E., & Zimmerman, B. A. 1985, AJ, 90, 609

Griffin, R. F., & Gunn, J. E. 1978, AJ, 83, 1114

—. 1981, AJ, 86, 588

Griffin, R. F., Mayor, M., & Gunn, J. E. 1982, A&A, 106, 221

Halbwachs, J. L., Mayor, M., Udry, S., & Arenou, F. 2003, A&A, 397, 159

Hut, P. 1981, A&A, 99, 126

Latham, D. W., Mathieu, R. D., Milone, A. A. E., & Davis, R. J. 1992, in ASP Conf. Ser. 32: IAU Colloq. 135: Complementary Approaches to Double and Multiple Star Research, 155

Latham, D. W., Stefanik, R. P., Torres, G., Davis, R. J., Mazeh, T., Carney, B. W., Laird, J. B., & Morse, J. A. 2002, AJ, 124, 1144

Mathieu, R. D., Duquennoy, A., Latham, D. W., Mayor, M., Mermilliod, T., & Mazeh, J. C. 1992, in Binaries as Tracers of Stellar Formation. Proceedings of a Workshop held in Bettmeralp, Switzerland, Sept. 1991, in honor of Dr. Roger Griffin. Editors, Antoine Duquennoy, Michel Mayor; Publisher, Cambridge University Press, Cambridge, England, New York, NY, 1992. LC # QB821 .B55 1991. ISBN # 0521433584. P. 278, 1992, 278

Mathieu, R. D., & Mazeh, T. 1988, ApJ, 326, 256

Mathieu, R. D., Meibom, S., & Dolan, C. J. 2004, ApJ, 602, L121

Matthews, L. D., & Mathieu, R. D. 1992, in ASP Conf. Ser. 32: IAU Colloq. 135: Complementary Approaches to Double and Multiple Star Research, 244

Mazeh, T. 1990, AJ, 99, 675

McNamara, B., & Sekiguchi, K. 1986, AJ, 91, 557

Meibom, S., Barnes, S. A., Dolan, C., & Mathieu, R. D. 2001, in ASP Conf. Ser. 243: From Darkness to Light: Origin and Evolution of Young Stellar Clusters, 711

Melo, C. H. F., Covino, E., Alcalá, J. M., & Torres, G. 2001, A&A, 378, 898

Mermilliod, J.-C., Bratschi, P., & Mayor, M. 1997, A&A, 320, 74

Mermilliod, J. C., & Mayor, M. 1992, in Binaries as Tracers of Stellar Formation. Proceedings of a Workshop held in Bettmeralp, Switzerland, Sept. 1991, in honor of Dr. Roger Griffin. Editors, Antoine Duquennoy, Michel Mayor; Publisher, Cambridge University Press, Cambridge, England, New York, NY, 1992. LC # QB821 .B55 1991. ISBN # 0521433584. P. 183, 1992, 183

Mermilliod, J.-C., & Mayor, M. 1999, A&A, 352, 479

Mermilliod, J.-C., Rosvick, J. M., Duquennoy, A., & Mayor, M. 1992, A&A, 265, 513

Mermilliod, J.-C., Weis, E. W., Duquennoy, A., & Mayor, M. 1990, A&A, 235, 114

North, P., & Zahn, J.-P. 2003, A&A, 405, 677

Pan, K., Tan, H., & Shan, H. 1998, A&A, 335, 179

Rieutord, M. 1992, A&A, 259, 581

Rieutord, M., & Zahn, J. 1997, ApJ, 474, 760

Savonije, G. J., & Papaloizou, J. C. B. 1983, MNRAS, 203, 581

Savonije, G. J., & Witte, M. G. 2002, A&A, 386, 211

Tassoul, J. 1988, ApJ, 324, L71

—. 2000, Stellar rotation (Stellar rotation / Jean-Louis Tassoul. Cambridge ; New York : Cambridge University Press, 2000. (Cambridge astrophysics series ; 36))

Tassoul, J.-L., & Tassoul, M. 1996, Fundamentals of Cosmic Physics, 16, 337

Tassoul, M., & Tassoul, J. 1997, ApJ, 481, 363

Terquem, C., Papaloizou, J. C. B., Nelson, R. P., & Lin, D. N. C. 1998, ApJ, 502, 788

Witte, M. G., & Savonije, G. J. 1999a, A&A, 341, 842

—. 1999b, A&A, 350, 129

—. 2001, A&A, 366, 840

—. 2002, A&A, 386, 222

Yi, S. K., Kim, Y., & Demarque, P. 2003, ApJS, 144, 259

Zahn, J.-P. 1970, A&A, 4, 452

—. 1975, A&A, 41, 329

—. 1977, A&A, 57, 383

—. 1978, A&A, 67, 162

—. 1989, A&A, 220, 112

Zahn, J.-P., & Bouchet, L. 1989, A&A, 223, 112

Table 2.4. Distribution of Circularization Periods with Population Age

Binary Population	log(*Age*) (Gyr)	Circularization Period (days)
PMS Binaries	-2.5	$7.1^{+1.2}_{-1.2}$
Pleiades	-1.0	$7.2^{+1.8}_{-1.9}$
M35	-0.8	$10.2^{+1.0}_{-1.5}$
Hyades/Praesepe	-0.2	$3.2^{+1.2}_{-1.2}$
M67	0.6	$12.1^{+1.0}_{-1.5}$
NGC188	0.8	$14.5^{+1.4}_{-2.2}$
Field Binaries	0.95	$10.3^{+1.5}_{-3.1}$
Halo Binaries	1.00	$15.6^{+2.3}_{-3.2}$

Chapter 3

An Observational Study of Tidal Synchronization in Solar-Type Binary Stars in the Open Clusters M35 and M34

3.1 Abstract

We present rotation periods for the solar-type primary stars in 13 close ($a \lesssim 5$ AU) single-lined spectroscopic binaries with known orbital periods (P) and eccentricities (e). All binaries are members of the open clusters M35 (NGC2168; $\sim$ 150 Myr) and M34 (NGC1039; $\sim$ 250 Myr). The binary orbital parameters and the rotation periods of the primary stars were determined from time-series spectroscopy and time-series photometry, respectively. Knowledge of the ages, orbital periods, and eccentricities of these binaries combined with the rotation periods and masses of their primary stars makes them particularly interesting systems for studying the rates of tidal circularization and synchronization. Our sample of 13 binaries includes 6 with orbital periods shortward of 13 days ($a \lesssim 0.12$ AU). The stars in these binaries orbit sufficiently close that their spins and orbits have evolved toward synchronization and circularization due to tidal interactions. We investigate the degree of tidal synchronization in each binary by comparing the angular rotation velocity of the primary stars ($\Omega_\star$) to the angular velocity expected if the primary star was synchronized ($e = 0$) or pseudosynchronized ($e > 0$) with the orbital motion (Ω_{ps}). We compare the observed binaries to the evolution expected from tidal theory. Four of the 6 closest binaries do not meet the theoretical expectations. Two binaries with circular orbits are not synchronized, and 2 binaries with eccentric orbits are not pseudo-synchronized. The remaining 2 binaries have both reached the equilibrium state of both a circularized orbit and synchronized rotation.

3.2 Introduction

Tidal and dissipative forces in close detached binary stars drive an exchange of angular momentum between the rotation of the stars and their orbital motion. The cumulative effects of such tidal interactions with time is referred to as tidal evolution. Characteristic signs of tidal evolution are: 1) Alignment of the stellar spin axes perpendicular to the orbital plane; 2) Synchronization of the rotation of the stars to the orbital motion; 3) Circularization of the orbits. In a population of coeval detached late-type binary stars tidal evolution can be observed among the closest binaries ($a \lesssim 0.2$ AU).

Observations of *tidal circularization* have been the primary constraint on tidal theory over the past 2 decades (e.g. Meibom & Mathieu 2005; Mathieu et al. 2004; Latham et al. 2002; Melo et al. 2001; Duquennoy et al. 1992; Mathieu et al. 1992). In particular, the distribution of orbital eccentricities with orbital periods (the $e - \log(P)$ diagram) has provided clear evidence for tidal circularization in homogeneous and coeval populations of binaries, and enabled a robust measure of the degree of circularization as a function of orbital period integrated over the lifetime of the binary population. (Meibom & Mathieu 2005) define the *tidal circularization period* of a binary population as the longest orbital period to which binaries with initial eccentricities of e=0.35 circularize at the age of the population. The distribution of tidal circularization periods with age show an increase from ~ 7 days at the pre main-sequence phase to ~ 15 days at the late main-sequence phase. Importantly, current theories of tidal circularization cannot account for the distribution of tidal circularization periods with population age. The theoretically predicted circularization periods (Zahn 1989; Zahn & Bouchet 1989; Witte & Savonije 2002) fall significantly below the observed circularization periods of the oldest binary populations, indicating that the rate of tidal circularization in these models is too low (see Meibom & Mathieu 2005).

In comparison, the amount of observational data suitable for measuring the rate of *tidal synchronization* in late-type binaries is sparse. This is in part because binary orbital elements are simpler to obtain than rotation periods for stars in binaries. Even so, observations of the synchronization of the stars in a binary system provide a second window on the tidal effects on that system, and one of major importance for several reasons. First, tidal theory makes explicit predictions for the relative rates of tidal circularization and synchronization that can be straightforwardly tested (Witte & Savonije 2002; Zahn & Bouchet 1989). For a typical binary the two rates differ and the predicted evolutionary paths from an asynchronous, eccentric binary to a synchronized and circular binary take the stars in and out of synchronism during the evolutions of the stars, their orbital separation, and their orbital eccentricity (see Figure 1 in Zahn & Bouchet (1989) and Figures 1 and 3 in Witte & Savonije (2002)). Second, the range in binary separations over which tidal synchronization can significantly affect the stellar angular momentum evolution provides an important constraint on the impact of binarity on stellar angular momentum evolution in late-type stars. Third, synchronization

of the observable surface layers is closely linked to the internal angular momentum transport in the star. Thus, the rate of synchronization of the surface layers can shed light on the coupling between those layers and the stellar interior. Fourth, simultaneous observations of tidal synchronization and magnetic field tracers (X-rays, chromospheric emission, etc.) during rapid stellar evolution may enable determination of the evolution rates of stellar dynamos.

Finally, significant tidal synchronization and circularization is expected in the many star-planet systems where the planets orbits very close to their late-type host stars (i.e., "hot Jupiter" systems). Tidal interactions in star-planet systems may therefore play an important role in determining the observed distributions of mass, orbital period, and eccentricity of extra-solar planets (Ogilvie & Lin 2004).

To date, most published studies of synchronization have focused on early-type binaries (e.g. Abt & Boonyarak 2004; Abt et al. 2002; Giuricin et al. 1984b,a; Levato 1974). This emphasis is due, in part, to telescope and instrument capabilities which in the past have favored bright and rapidly rotating stars. Also, the use of archived data on eclipsing binaries has introduced a bias toward higher mass stars.

However, a few recent studies of tidal synchronization, e.g Giuricin et al. (1984c), Claret et al. (1995) and Claret & Cunha (1997), include binaries with late-type main-sequence primary stars. These studies represent important contributions to the study of tidal synchronization. Giuricin et al. studied 43 detached double-lined eclipsing and non-eclipsing binaries with at least one late-type stellar component. However, in half of the binaries the primary or secondary star, or both, have evolved off the main sequence. They found that the observed degree of synchronism was in agreement with the theoretical predictions of Zahn (1977). In their study stellar rotation was derived from either line-broadening ($v \sin(i)$) or from periodic brightness variations.

We note that, for non-eclipsing binaries, the stellar rotation velocities measured from line broadening are less suitable for constraining models of tidal synchronization, because of the ambiguities introduced by the unknown inclination of the rotation axis and non-rotational line-broadening due to the secondary spectrum.

Claret et al. and Claret & Cunha studied tidal synchronization using eclipsing binary data

from Andersen (1991), of which 10 systems have late-type stellar components. The two studies compared the observed binary parameters against the model predictions of Tassoul (1988) and Zahn (1989), respectively, and found general agreement between the observed level of synchronization and the predicted timescales for synchronization. All astrophysical parameters required to determine the theoretical time-scale for which synchronization is achieved were obtained by comparing theoretical models (Claret 1995; Claret & Gimenez 1995) directly to each star of the Andersen sample. Rotation velocities ($v \sin(i)$) for all stars were derived from line-broadening.

Knowledge of binary ages is critical in order to measure the rate and evolution of tidal synchronization. Furthermore, because of the sensitive dependence of tidal effects to stellar radius, knowledge of the stellar evolutionary state and history is essential for testing tidal evolution. For example, tidal theory predicts that the pre main-sequence (PMS) and the early main-sequence ($t \lesssim 500$ Myr) are the most active phases of tidal evolution, the PMS phase because of the large radii and deep convective envelopes, and the early main-sequence phase because the stars are spinning super-synchronously after contracting onto the zero-age main sequence. Similarly, post-main-sequence evolution of one or both components of a binary greatly increases the rate of tidal evolution.

Thus an optimal binary sample for the study of tidal evolution would comprise a coeval population of late-type binaries with accurate information about age, evolutionary stage, orbital parameters, and rotational angular velocities of the stars. Arguably such binary samples with ages $t \lesssim 500$ Myr are particularly interesting. Given these needs, young open clusters are superb laboratories for the study of tidal evolution.

So motivated, we have undertaken parallel spectroscopic and photometric surveys of the open clusters M35 and M34 to derive orbital periods and eccentricities as well as stellar rotation periods for late-type binaries. M35 (150 Myr; von Hippel et al. 2002; Deliyannis 2005) and M34 (250 Myr; Steinhauer 2005) provide populations of close late-type binaries with ages during the most active phase of tidal evolution, making them attractive targets for observational testing of models of tidal synchronization. M35, in particular, provides a rich population of close binaries which has allowed determination of a well-defined tidal circularization period at $10.2^{+1.0}_{-1.5}$ days (Meibom & Mathieu 2005). Indeed, 8 out of the 9 M35 binaries with periods less than ~ 10 days have been circularized

to eccentricities less than 0.05. In M34, our ongoing spectroscopic survey has led to the discovery of 5 circular binaries ($e < 0.1$) with periods of less than 5.5 days. A tidal circularization period has not yet been determined for M34.

We begin by briefly introducing the current theories of tidal evolution in Section 3.3. Section 3.4 outlines our observational program and Section 3.5 describe our observational results. In Section 3.6 we address potential complications of measuring the rotation periods of stars in close binary systems. In Section 3.7 we evaluate the degree of tidal synchronization and circularization for the closest binaries in M35 and M34 and introduce the $\log(\Omega_\star/\Omega_{ps}) - \log(P)$ diagram which presents the dependence on stellar separation. We compare the observed tidal evolution of individual binaries to the predictions of current tidal theory in Section 3.8. Section 3.9 summarizes and presents our conclusions.

3.3 Model Predictions of Tidal Synchronization

We will discuss our observational results in the context of two different theoretical models of tidal evolution in solar-type binaries: 1) The equilibrium tide theory (Zahn 1989; Hut 1981; Zahn 1977) which has been the primary theory used to explain tidal evolution in main-sequence binaries with late-type components, but which also has been extended by Zahn & Bouchet (1989) to include tidal evolution during PMS evolution; 2) The dynamical tide theory (Zahn 1977, 1975) which before 1998 was used primarily to explain tidal evolution in binaries with early-type stars, but recently has been applied to binaries with solar-type components (Witte & Savonije 2002; Savonije & Witte 2002; Terquem et al. 1998; Goodman & Dickson 1998). Both theories make predictions about the rate of tidal synchronization and circularization, and Zahn & Bouchet (1989) and Witte & Savonije (2002) make explicit predictions assuming a specified set of initial stellar and binary conditions. However, the physical mechanism responsible for tidal dissipation is fundamentally different in the two models.

In the equilibrium tide theory the characteristic times for tidal synchronization and circularization are (Zahn 1989)

$$t_{sync} = \frac{t_{diss}}{6\ \lambda_{sync}\ q^2}\ \frac{I}{M\ R^2}\ \left(\frac{a}{R}\right)^6 \tag{3.1}$$

$$t_{circ} = \frac{t_{diss}}{21\ \lambda_{circ}\ q(1+q)} \left(\frac{a}{R}\right)^8 \tag{3.2}$$

Both times are strongly dependent on the ratio of the stellar radius (R) to the stellar separation (a) and thus restrict significant tidal evolution to the closest binaries. Here M denotes the stellar mass, I the moment of inertia, q the binary mass ratio, t_{diss} the viscous dissipation time, and $\lambda_{sync/circ}$ a structural constant whose value depends on the mass concentration within the stars and on where in the star the tidal torque is applied. From the ratio of eqs. [3.1] and [3.2] it can be estimated that $t_{circ} \simeq 10^3 \times t_{sync}$ for a binary with solar-type components. The process of tidal synchronization proceeds faster than circularization primarily because the angular momentum of the individual stars ($\sim I\Omega << MR^2\Omega$) is much smaller than that of the orbit ($\sim Ma^2\omega$). Here ω and Ω are the orbital angular velocity and the stellar rotation angular velocity, respectively.

In an initially eccentric binary the stars will synchronize their spin angular velocities to a value Ω_{ps}, close to (within $\sim 20\%$) the orbital angular velocity at periastron passage (ω_p) where the stellar separation is the minimized. This is referred to as pseudo-synchronization. An expression for Ω_{ps} can be derived by setting the tidal torque on the stars integrated over the eccentric orbit equal to zero (see Hut 1981).

$$\Omega_{ps} = \frac{1 + \frac{15}{2}e^2 + \frac{45}{8}e^4 + \frac{5}{16}e^6}{(1+e)^2\ (1 + 3e^2 + \frac{3}{8}e^4)}\ \omega_p \tag{3.3}$$

$$\omega_p = \omega\ \frac{(1+e)^2}{(1-e^2)^{3/2}} \tag{3.4}$$

A detailed graphical illustration of the tidal evolution of a binary with two 1.0 $M_\odot$ stars is given by Zahn & Bouchet (1989). In their model, pseudosynchronization is achieved in less than 100,000 years, the stars then spin up due to less efficient tidal braking as the convection retreats and the stars contract onto the ZAMS. Once the star has settled on the main-sequence synchronization resumes and is completed by an age of $\sim$ 1 Gyr.

Similarly, Witte & Savonije present in their Figures 1 and 3 the tidal evolution of a binary with two 1.0 $M_\odot$ stars in the framework of the dynamical tide theory. Their eqs. [10], [11], and [12] give the differential equations governing the changes in orbital eccentricity, semi-major axis, and

stellar rotation velocity. In their model, starting at the ZAMS, pseudo-synchronization is gradually achieved within $\sim$ 500 Myr, followed by a spin-up between 0.5-1.0 Gyr and then spin-down to sub-synchronous rotation at $\sim$ 3 Gyr. The stars approach complete synchronization over the remainder of the main-sequence lifetime.

3.4 Observations and Data Reduction

We have conducted two parallel observational programs on the open clusters M35 and M34: 1) High precision radial-velocity surveys to identify binaries and determine their orbital parameters; 2) Comprehensive photometric time-series surveys to determine stellar rotation periods from light modulation by star-spots on the surfaces of the late-type primary stars.

3.4.1 Time-Series Spectroscopy

M35 and M34 have been included in the WIYN Open Cluster Study (WOCS; Mathieu 2000) since 1997 and 2001, respectively. As part of WOCS the solar-type stars in both clusters have been targets in extensive radial-velocity surveys to determine cluster membership and to detect binary stars. A detailed description of the radial-velocity surveys of these two clusters will follow in later papers; we give here the most relevant information.

All spectroscopic data were obtained using the WIYN [1] 3.5m telescope at Kitt Peak, Arizona, USA. The telescope is equipped with a Multi-Object Spectrograph (MOS) consisting of a fiber optic positioner (Hydra) feeding a bench mounted spectrograph. The Hydra positioner is capable of placing $\sim$ 95 fibers in a 1-degree diameter field with a precision of $0.2''$. In the field of M35 and M34 approximately 82-85 fibers are positioned on stars while the remaining fibers are used for measurements of the sky background. We use the $3''$ diameter fibers optimized for blue transmission, and the spectrograph is configured with an echelle grating and an all-transmission optics camera providing high throughput at a resolution of $\sim$ 20,000. All observations were done at central wavelengths of 5130Å or 6385Å with a wavelength range of $\sim$ 200Å providing rich arrays of narrow absorption lines. Radial velocities with a precision of $\sim 0.2\ kms^{-1}$ are derived from the spectra via cross-correlation

[1] The WIYN Observatory is a joint facility of the University of Wisconsin-Madison, Indiana University, Yale University, and the National Optical Astronomy Observatories.

with a high S/N sky spectrum (Hole et al. 2005; Meibom et al. 2001).

The initial selection of target stars was based on photometric cluster membership in the color-magnitude diagrams (see Figure 3.1). For M35 proper-motion membership studies to $V \lesssim 15$ by McNamara & Sekiguchi (1986) and Cudworth (1971) were used as well. The target list for M35 includes stars of type mid F to mid K, corresponding to a range in stellar mass from $\sim 1.4\ M_{\odot}$ ($V_0 \simeq 12.5$, $(B-V)_0 \simeq 0.4$) to $\sim 0.7\ M_{\odot}$ ($V_0 \simeq 16$, $(B-V)_0 \simeq 1.1$), with solar-mass stars at $V_0 \sim 15$. In M34 stars of type early F to early M were observed corresponding to a range in stellar mass from $\sim 1.5\ M_{\odot}$ ($V_0 \simeq 12.0$, $(B-V)_0 \sim 0.3$) to $\sim 0.4\ M_{\odot}$ ($V_0 \simeq 16.5$, $(B-V)_0 \sim 1.5$), with solar mass stars at $V_0 \sim 13.5$.

Telescope time granted from Wisconsin and NOAO[2] allowed for 3-4 spectroscopic observing runs per year per cluster, with each run typically including multiple observations on several sequential nights. Once identified, velocity variables are observed at a frequency appropriate to the timescale of their variation. At present the radial-velocity survey of M35 has resulted in a sample of 50 spectroscopic binaries for which orbital solutions have been derived. The orbital periods span 2.25 days to 3112 days corresponding to separations from 0.04 to ~ 5 AU, assuming a 1 $M_{\odot}$ primary star and a 0.5 $M_{\odot}$ secondary star. In M34 orbital parameters have been derived for 20 spectroscopic binaries spanning orbital periods from 2.26 to 1210 days. This paper is based on a subset of those binaries that are described in detail below.

3.4.2 Time-Series Photometry

We have photometrically surveyed stars in a $\sim 40' \times 40'$ region centered on M35 and M34. The photometric data were obtained using the WIYN 0.9m telescope [3] at Kitt Peak equipped with a $2k \times 2k$ CCD camera. The complete dataset is composed of images from two different but complementary observing programs. Images of the two clusters were acquired by the first author from December $1^{st} - 17^{th}$ 2002 with a frequency of approximately once per hour for the about six hours per night

[2]NOAO is the national center for ground-based nighttime astronomy in the United States and is operated by the Association of Universities for Research in Astronomy (AURA), Inc. under cooperative agreement with the National Science Foundation.

[3]The 0.9m telescope is operated by WIYN Inc. on behalf of a Consortium of ten partner Universities and Organizations (see http://www.noao.edu/0.9m/general.html)

that the clusters airmasses were below 1.5. In addition, one image per night was obtained in a queue-scheduled (synoptic) observing program from October 2002 to March 2003. We reduced our CCD frames using the standard IRAF CCDRED package. We used the IRAF GASP package to compute a simple linear transformation of pixel coordinates to equatorial coordinates for each frame, using as reference approximately 30 stars from the Digitized Sky Survey per frame. Our derived stellar positions show a frame-to-frame scatter of less than $0\farcs1$ in each direction. We identified stellar sources using the IRAF DAOFIND task and performed PSF photometry using the DAOPHOT package. Figure 3.2 displays the standard deviation as a function of V magnitude for stars in the field of M35. A relative photometric precision of $\sim 0.5\%$ is obtained for stars with $12 \lesssim V \lesssim 15$, with slightly poorer precision at the $V = 16\fm5$ faint-limit of the spectroscopic study. For M35 the result of the photometric survey is a database of differential photometric V-band light curves for ~ 14000 stars with $12 \lesssim V_0 \lesssim 19.5$. At the present time only the photometric data on M35 have been reduced and analyzed. The photometry for star 6214 in M34 presented in this paper is kindly provided by Barnes (2005).

We employed the Scargle (1982) periodogram analysis to detect periodic variability in the light curves (see Stassun et al. 1999). For each candidate star, we generate a set of 100 synthetic light curves, each consisting of normally distributed noise with a nightly and a night-to-night dispersion representative of our data. We compute a periodogram for each test light curve and take the maximum observed power level in these 100 periodograms as the level of 1% false-alarm probability (FAP). We adopt this measure of FAP as our basic criterion for accepting or rejecting detected photometric variability; we accept only periods whose periodogram signals are stronger than the power corresponding to the 1% FAP level. From our database we have determined stellar rotation periods for 443 stars. Of these, 259 have one or more radial-velocity measurements (the remainder being below the faint limit of the spectroscopic survey or photometric non-members), 203 are photometric and spectroscopic members of M35, and 12 are members of binary systems with known orbital parameters. Meibom et al. (2005) present and describe in more detail our photometric data, the reduction thereof, and the methods used for detecting periodic variability.

3.5 Observational Results

We present the spectroscopic and photometric results for 12 binaries in M35 and 1 binary in M34. These binaries are single-lined spectroscopic systems with well-determined orbital periods and eccentricities. The rotation periods of their primary stars are determined from periodic variations in their light curves, presumably due to spots on the stellar surfaces. The mass of the primary star in each binary has been estimated from 150 Myr and a 250 Myr Yale isochrones (Yi et al. 2003) fitted to the cluster sequences of M35 and M34, respectively. Photometry and values for cluster reddening for both clusters were provided by Deliyannis (2005) and Steinhauer (2005). Tables 3.1 and 3.2 lists all observational results for the 13 binaries together with the derived orbital angular velocities and stellar rotation angular velocities needed for studying tidal synchronization. Figure 3.1 shows the color-magnitude diagram (CMD) of M35. The locations of these 12 binaries are marked as black dots. Five M35 binaries discussed in detail below are labeled with the last 4 digits of their respective 2MASS ID's. The 150 Myr isochrone is corrected for reddening and extinction and a distance modulus of $9\overset{\mathrm{m}}{.}8$ (Kalirai et al. 2003). Relevant model masses are marked along the isochrone.

All 13 binaries are photometric and radial-velocity members of M35 or M34. Figure 3.3 shows the distributions of measured radial-velocities for the two clusters. Gaussian functions have been simultaneously fitted to the cluster and field components of each distribution. The radial-velocity cluster membership probability (P_{RV}) of each of the 13 binary stars is calculated following the formalism by Vasilevskis et al. (1958)

$$P_{RV} = \frac{C(RV)}{C(RV) + F(RV)} \tag{3.5}$$

where $C(RV)$ and $F(RV)$ represent the values of the Gaussian fit to the cluster and field distributions, respectively, for the center-of-mass radial-velocity of a binary.

Figure 3.4 shows the distributions of radial-velocity membership probabilities for stars in the fields of M35 and M34. In both clusters the separation between members and non-members is distinct. Less than 10% of the stars have probabilities placing them between the member and non-member peaks, corresponding to radial-velocities on the wings of the cluster distributions.

Of particular interest to our study of tidal synchronization are the 6 binaries with orbital

Table 3.1. Photometric and Spectroscopic Results for the 13 Binaries in M35 and M34

ID [a]	V_o	$(B-V)_o$	γ $(km\ s^{-1})$	P_{RV} [b] %	P_{orbit} (Days)	e	σ_e
06090257+2420447	13.016	0.403	-8.30	94	10.28	0.009	0.019
06090306+2420095	14.369	0.655	-6.92	90	3112.67	0.394	0.118
06090306+2419361	15.150	0.802	-9.25	91	637.03	0.234	0.025
06090352+2417234	15.351	0.896	-6.74	88	156.60	0.580	0.034
06091557+2410422	14.867	0.834	-6.14	76	8.17	0.649	0.022
06091924+2417223	14.933	0.724	-8.86	93	795.30	0.255	0.056
06092436+2426200	14.741	0.678	-7.36	93	10.33	0.016	0.009
06095563+2417454	14.420	0.680	-7.54	94	30.13	0.273	0.005
06085441+2403081	14.368	0.565	-7.45	93	12.28	0.550	0.003
06082017+2421514	14.259	0.544	-8.16	94	2324.11	0.199	0.093
06074436+2430262	14.634	0.624	-7.04	91	476.21	0.389	0.046
06083789+2431455	15.354	0.855	-8.08	93	2.25	0.010	0.008
02410615+4246219[c]	15.323	1.000	-7.27	94	4.39	0.063	0.033

[a]Stellar 2MASS ID.

[b]The radial velocity membership probability (P_{RV}) calculated using the formalism by Vasilevskis et al. (1958).

[c]M34 binary.

Table 3.2. Photometric and Spectroscopic Results for the 13 Binaries in M35 and M34

ID [a]	P_{rot}^{prim} (Days)	$\delta(P_{rot}^{prim})$ (Days) [b]	M_{prim} ($M_\odot$)	ω ($rad\ day^{-1}$) [c]	$\Omega_\star$ ($rad\ day^{-1}$)	$\Omega_\star/\Omega_{ps}$ [d]	$\log(\Omega_\star/\Omega_{ps})$ [e]
0447	2.30	0.02	1.4	0.611	2.73	4.46	0.65
0095	2.48	0.01	1.1	0.002	2.54	625.66	2.80
9361	4.70	0.07	1.0	0.010	1.34	101.74	2.01
7234	2.38	0.02	0.9	0.040	2.64	17.52	1.24
0422	3.71	0.06	0.9	0.769	1.76	0.45	-0.35
7223	5.25	0.08	1.0	0.008	1.20	108.47	2.04
6200	10.13	0.39	1.1	0.609	0.62	1.02	0.01
7454	2.84	0.03	1.1	0.209	2.22	7.29	0.86
3081	6.03	0.12	1.1	0.512	1.04	0.61	-0.21
1514	2.56	0.02	1.2	0.003	2.45	731.43	2.86
0262	4.26	0.07	1.1	0.013	1.48	56.47	1.75
1455	2.29	0.02	0.9	2.794	2.74	0.98	-0.01
6219[f]	8.03	0.10	0.7	1.431	0.78	0.53	-0.28

[a]Last 4 digits of stellar 2MASS ID from Table 3.1

[b]The estimated uncertainty of the stellar rotation period ($\delta(P_{rot}^{prim})$).

[c]Average orbital angular velocity.

[d]Measured rotational angular velocity of the primary star.

[e]Ratio of the measured rotational angular velocity to the expected pseudo-synchonism rotational angular velocity.

[f]M34 binary.

periods in the range from 2.25 days to 12.28 days. The stars in these 6 systems are close enough that their spins and orbits have evolved due to tidal interactions. The orbital parameters were first presented in Meibom & Mathieu (2005). The photometric light curves are shown below and the derived rotation periods are presented in Table 3.2. The uncertainty ($\pm\delta P$) on the rotation periods were determined using the expression for the periodogram resolution (Kovacs 1981)

$$\delta P = P^2 \frac{3\sigma}{4T\sqrt{N}A} \tag{3.6}$$

where σ is the uncertainty in the data, T is the total time spanned by the data, N is the number of independent data points, and A is the amplitude of the detected signal. When estimating rotation period uncertainties we made the conservative assumption that only data from separate nights are truly independent and set the value of N to the number of nights of data in the light curve. We describe here in detail the observational results for those 6 systems.

Binary 1455: 14 radial-velocity measurements have been obtained of this binary over ~ 600 orbital cycles. With an orbital period of only 2.25 days this is the shortest period binary found in our survey of M35. The orbit is circular with $e = 0.010 \pm 0.003$. Figure 3.5 (left) shows the orbital solution overplotted on the radial-velocity data phased to the 2.25 day period. The CMD location of binary 1455 is on the cluster main sequence slightly above the position on the 150 Myr isochrone corresponding to a mass of $\sim 0.9\ M_{\odot}$. We use $0.9\ M_{\odot}$ as an estimate for the mass of the primary star as there is no sign of the secondary star in the spectra/cross-correlation function of this binary. The radial-velocity cluster membership probability (P_{RV}, eq. [3.5]) of binary 1455 is 94%.

The phased light curve shown in Figure 3.5 (right) is based on 96 photometric measurements obtained over 15 nights in December 2002. The maximum periodogram power corresponds to a period of 2.29 ± 0.02 days. We note that phasing the photometric measurements with the binary orbital period of 2.25 days rather than the independently determined value of 2.29 days produces only a subtle change of the light curve. When including the synoptic data a total of 156 measurements were obtained from October 2002 to March 2003. The same rotation period was found using all 156 measurements, but the phased light curve is noisier, presumably due to the varying quality of the synoptic data and possibly due to irregularities in the spot modulation over the longer timescale.

Binary 6214: Figure 3.6 (left) shows the orbital solution overplotted on 15 radial-velocity measurements over ~ 160 orbital cycles. The data have been phased to a 4.39 day period. The orbit is indistinguishable from circular with an eccentricity of 0.063 ± 0.033. We estimate the mass of the primary star to be $\sim 0.7\ M_{\odot}$ using the fit of a 250 Myr Yale isochrone to the M34 cluster sequence. The radial-velocity cluster membership probability of binary 6214 is 94%.

The phased light curve shown in Figure 3.6 (right) is based on 55 photometric measurements over 15 nights. The data were kindly provided by Barnes (2005). The maximum power in the periodogram corresponds to a period of 8.03 ± 0.1 days, roughly twice the orbital period. We note that phasing the photometric measurements with the binary orbital period of 4.39 days does not lead to well-phased data.

Binary 0422: The radial velocity of this binary has been measured 41 times over ~ 330 orbital cycles. The high eccentricity of the orbit makes it difficult to observe during the short periastron passage. One observation has been obtained close to periastron passage, allowing a better determination of the orbital eccentricity. The cross-correlation function from this observation revealed a second spectral component with peak-height about two thirds that of the primary peak and a radial-velocity of $-8.8\ km\ s^{-1}$, consistent with cluster membership. We suggest therefore that this is a triple system consisting of a close binary and a distant tertiary star. The radial-velocity curve for the binary, phased to a period of 8.17 days, is shown in Figure 3.7 (left). The velocity of the tertiary star is marked as a circle at phase 0.04. Overplotted is the best fit orbital solution with an eccentricity of 0.649 ± 0.022. The center-of-mass velocity is $-6.14\ km\ s^{-1}$ ($\sim 2\ \sigma_{cluster}$ away from the $-8.1\ km\ s^{-1}$ cluster velocity), corresponding to a radial velocity membership probability of 76%. This deviation from the cluster velocity may be partly due to the dynamical influence of the triple system. The system is located $\sim 0\overset{\mathrm{m}}{.}5$ above the cluster main sequence, likely due to the combined light of the close binary and the tertiary star. Because the tertiary star is fainter than the primary in binary 0422, we assume that it is also redder and we estimate the mass of the primary star in binary 0422 by assuming that in the absence of the tertiary star the binary will be on the main-sequence fainter and bluer than the triple system. We note however, that these assumptions have no large effect on the estimated $1.0\ M_{\odot}$ of the primary star.

Binary 0422 was imaged 126 times, 74 of which fell within 15 nights in December 2002. The phased light curve shown in Figure 3.7 (right) is based on those 74 photometric measurements. The rotation period corresponding to the maximum periodogram power is 3.71 ± 0.06 days. A slightly shorter rotation period of 3.56 days is found using all 126 photometric measurements, but the light curve is noisier. Again, the added noise is presumably due to the varying quality of the synoptic data and possibly due to irregularities in the spot modulation over the longer time-scale.

Binary 0447: The orbital parameters of this binary were determined from 32 radial-velocity measurements over $\sim$ 150 orbital cycles. The 10.28 day orbit is circular with an eccentricity of 0.009 ± 0.019. Figure 3.8 (left) shows the orbital solution overplotted on the phased radial-velocity data. The color and V magnitude of binary 0447 places it on the cluster main sequence at the blue limit of our sample of M35 stars. This position corresponds to a mass of $\sim 1.4\ M_{\odot}$ on the 150 Myr Yale isochrone. The radial-velocity cluster membership probability is 94%. Furthermore, the measured Lithium abundance for this star is consistent with cluster membership (Steinhauer & Deliyannis 2004).

The phased light curve shown in Figure 3.8 (right) is based on 84 photometric measurements from the 15 nights in December 2002. The rotation period corresponding to the maximum periodogram signal is 2.30 ± 0.02 days. A slightly shorter rotation period of 2.2 days is found when including the synoptic data.

Binary 6200: Like binary 0447 this binary has a circular orbit ($e = 0.016 \pm 0.009$) with a period of $\sim$ 10 days. Figure 3.9 (left) shows the orbital solution overplotted on the radial velocity data phased to the 10.33 day period. The orbital parameters are determined from 22 radial velocities over $\sim$ 120 orbital cycles. The location of binary 6200 on the M35 cluster sequence corresponds to a mass of $\sim 1.1\ M_{\odot}$. The radial-velocity cluster membership probability is 93%.

Figure 3.9 (right) shows the phased light curve of binary 6200 based on 86 photometric measurements from December 2002. A total of 138 measurements were made from October 2002 to March 2003. The maximum periodogram power corresponds to a period of 10.13 ± 0.39 days. The same period was found using all 138 brightness measurements, but the periodic signal is noisier. We note the structure in the light curve between phase 0.6 and 0.8. This secondary signal is presumably

due to a second group of photospheric spots.

Binary 3081: The orbital solution for binary 3081 is based on 19 radial-velocity measurements over ~ 70 cycles, and gives an orbital period of 12.28 days and an orbital eccentricity of 0.550 ± 0.003. Figure 3.8 (left) shows the orbital solution overplotted on the phased radial velocity data. We estimate the mass of the primary star to be $\sim 1.1\ M_{\odot}$. The radial-velocity cluster membership probability is 93%.

Figure 3.10 (right) shows the phased light curve based on 133 photometric measurements from December 2002. The rotation period corresponding to the maximum periodogram power is 6.03 ± 0.12 days. The grouping of the data in the phased light curve is caused by the integer value of the rotation period and the data sampling frequency. The V magnitude of binary 3081 is $14\overset{\text{m}}{.}37$ and its amplitude of variability is $0\overset{\text{m}}{.}02$; approximately 4 times the expected photometric error (see Figure 3.2).

3.6 The Potential Photometric Effects of Binarity

The brightness variations in a binary may be caused by effects other than spots on the surface of the primary star. We are not concerned with stellar eclipses as they produce a characteristic and easily detectable photometric effect that with little difficulty can be distinguished from spot modulation. However, other phenomena may cause photometric variability similar to that of spots on the primary star. We identify here two potential sources of photometric variability and estimate the influence of each of these effects on our ability to determine the rotation period of the primary stars from spot modulation.

3.6.1 The Effect of Spots on the Secondary Star

Let us first consider the effect of a spot on the surface of the secondary star. Because all of the binaries presented here are single-lined spectroscopic binaries, we will assume that the V band ($\sim$ 5000Å) flux of the secondary star is at least a factor of 5 less than that of the primary. We further assume that the spot on the secondary star produces an observed peak-to-peak brightness variation of the secondary of $0\overset{\text{m}}{.}15$ in the V-band, equivalent to the largest periodic signals observed in M35. The spot on the secondary, by itself, will then result in a $0\overset{\text{m}}{.}02$ peak-to-peak variation in the brightness of the binary.

The observed peak-to-peak brightness variations of the binaries presented in this paper are in the range from $\sim 0\overset{\mathrm{m}}{.}02 - 0\overset{\mathrm{m}}{.}12$. Therefore, to assign the observed variability of these binaries to spots on the secondary will require the combination of a heavily spotted secondary star (flux reduction of up to 75%) and a quiet (spot-less) primary star. Such a combination seems unlikely. The detected photometric variability is thus likely to result from spots on the primary star.

If, in a binary, both stellar spins have been synchronized or pseudo-synchronized to the orbital motion, then photometric variability at the $\sim 0\overset{\mathrm{m}}{.}02$ level can be due to spots on both stars that appear in phase as seen by the observer. Arguably, stars in the majority of young solar-type binaries rotate out of phase and non-synchronous to their eccentric orbital motion. The variability, if any, in the combined light of such binaries will derive from an out-of-phase superposition of the periodic signals caused by spots on both stars. Photometric time-series studies of solar-type main-sequence stars typically detect periodic variability at the level of $\sim 0\overset{\mathrm{m}}{.}02 - 0\overset{\mathrm{m}}{.}2$, and we know from the results presented here that such photometric variability is not confined to single stars. Therefore, we argue that the photometric variability detected in this and other studies comes from one star, either a single star or the primary star in a binary system. We conclude that the periodic variabilities detected in the light curves of the unevolved single-lined M35 and m34 binaries are caused by spots on the solar-type primary stars, and are therefore reliable measures of their rotation periods.

3.6.2 The Effect of Tidal Deformation

Another potential source of brightness variability in a binary star is the change in brightness due to tidally induced changes in the projected surface area of the stars. When a star becomes oblate due to the gravitational forces in the binary systems, its projected surface area, as seen by an observer, will change as it revolves. The change in area will depend on the binary mass ratio, the stellar separation, and on the inclination of the orbit to the line of sight. For a circularized binary the resulting brightness variation will be sinusoidal with a period equal to half the orbital period. For a binary with an eccentric orbit the brightness will increase at periastron passage and the light curve will deviate from a sinusoidal shape.

Zahn (1992) estimates the elevation, δR, of a tide on a star with mass M and radius R raised by a companion with mass m at a distance d, as $\delta R/R \simeq q(R/d)^3$, where $q = m/M$ is the binary

mass ratio. We assume again that $M = 1.0\ M_{\odot}$ and $m = 0.7\ M_{\odot}$ and that the orbital period is 2.25 days (as in our shortest period binary). Then $d = 0.04$ AU and $\delta R \simeq 0.08\ R_{\odot}$. To estimate an upper limit on the consequent photometric variation we assume that the binary is seen "edge on" ($i = 90^{o}$), and that the radius of the stellar disk increases/decreases by δR when the line joining the two stars is perpendicular/parallel to the line of sight. The resulting maximum difference in projected surface area of both stars corresponds to a brightness difference of $\sim 0\overset{\text{m}}{.}02$ for the binary.

Note that this upper limit estimate for the variability introduced by tidal distortion is for a stellar separation corresponding to our shortest period binary. The effect will decrease rapidly with stellar separation and thus will be negligible for all binaries other than 1455. Binary 1455 has a 2.25 day circular orbit and so the photometric variability due to tidal distortion in this system should have a period of 1.125 days and an amplitude of $\sim 0\overset{\text{m}}{.}02$. The light curve of 1455 actually varies with a period of 2.3 days and with an amplitude of $0\overset{\text{m}}{.}08$.

We conclude from this analysis that the periodic variability in our binary light curves can not be due to a tidally induced change in the projected surface areas of the stars.

3.7 The $\log(\Omega_{\star}/\Omega_{ps}) - \log(P)$ Diagram

In this section we wish to present our observational results in a way that facilitates comparison with predictions of tidal theory. In that spirit, we introduce in Figure 3.11 the $\log(\Omega_{\star}/\Omega_{ps}) - \log(P)$ diagram. ¿From our observational results we can derive for each binary the average orbital angular velocity ($\omega = 2\pi/P_{orb}$) and the rotational angular velocities of the primary star ($\Omega_{\star} = 2\pi/P_{rot}^{prim}$). With reference to Section 3.3, eqs. [3.3] and [3.4], we can calculate, for a given binary, the theoretical pseudo-synchronization angular velocity (Ω_{ps}). As a diagnostic of the degree of tidal synchronization in a binary system we use the ratio of $\Omega\star$ to Ω_{ps}

$$\frac{\Omega_{\star}}{\Omega_{ps}} = \frac{(1 + 3e^2 + \frac{3}{8}e^4)\ (1 - e^2)^{3/2}}{1 + \frac{15}{2}e^2 + \frac{45}{8}e^4 + \frac{5}{16}e^6} \frac{P_{orb}}{P_{rot}^{prim}} \tag{3.7}$$

The base 10 logarithm of $\Omega\star/\Omega_{ps}$ ($\log(\Omega_{\star}/\Omega_{ps})$) has a useful behavior for analyses. Synchronous and pseudo-synchronous binaries will lay on the line represented by $\log(\Omega_{\star}/\Omega_{ps}) = 0$. We refer to that line as the *synchronization line*. Super-synchronous binaries ($\Omega\star > \Omega_{ps}$) will have $\log(\Omega_{\star}/\Omega_{ps}) > 0$, while sub-synchronous binaries ($\Omega\star < \Omega_{ps}$) have $\log(\Omega_{\star}/\Omega_{ps}) < 0$. Figure 3.11 shows $\log(\Omega_{\star}/\Omega_{ps})$

for all 13 binary stars as a function of their orbital periods and Table 3.2 lists the values of $\Omega_\star/\Omega_{ps}$ and $\log(\Omega_\star/\Omega_{ps})$. We discuss here the degree of tidal synchronization in each of the 6 binaries with orbital periods less than 13 days.

Binary 1455: The similarity of the orbital period (2.25 days) and the rotation period of the primary star (2.29 ± 0.02 days) suggest that the primary in binary 1455 is synchronized to the circular orbital motion. Binary 1455 is thus both tidally circularized and synchronized at the age of 150 Myr, and lay on the synchronization line in Figure 3.11 ($\Omega_\star/\Omega_{ps} = 0.98$).

Binary 6214: This 250 Myr M34 binary has a circular orbit with a period of 4.39 days but the primary star is rotating sub-synchronously at 8.03 ± 0.1 days, corresponding to 53% of the orbital angular velocity ($\Omega_\star/\Omega_{ps} = 0.53$, $\log(\Omega_\star/\Omega_{ps}) = -0.28$).

Binary 0422: This 150 Myr M35 binary has not been circularized and has a highly eccentric orbit ($e = 0.65$) with a period of 8.17 days. The primary star in 0422 is not pseudo-synchronized and rotates with a sub pseudo-synchronous period of 3.71 ± 0.06 days, corresponding to 45% of Ω_{ps} ($\Omega_\star/\Omega_{ps} = 0.45$, $\log(\Omega_\star/\Omega_{ps}) = -0.35$).

Binary 0447: The 10.28 day orbit of this M35 binary is circular. The rotation period of the primary star is super-synchronous at 2.30 ± 0.02 days ($\Omega_\star/\Omega_{ps} = 4.46$, $\log(\Omega_\star/\Omega_{ps}) = 0.65$).

Binary 6200: This M35 binary has a circular 10.33 day orbit and synchronized primary star. The primary star is rotating once every 10.13 ± 0.39 days corresponding to $\Omega_\star/\Omega_{ps} = 1.02$ or $\log(\Omega_\star/\Omega_{ps}) = 0.01$.

Binary 3081: The primary star of this M35 binary follows a highly eccentric ($e = 0.55$) orbit with a period of 12.3 days, while its rotation period of 6.03 ± 0.12 days correspond to sub-synchronous rotation ($\Omega_\star/\Omega_{ps} = 0.61$, $\log(\Omega_\star/\Omega_{ps}) = -0.21$).

3.8 Discussion

Explicit predictions for tidal evolution based on the equilibrium or dynamical theories (Section 3.3) are published for only a few initial orbital and stellar parameters. Ideally, model predictions would exist for a fine grid of such parameters, allowing for direct comparison with the different binaries observed in M35 and M34. In the absence of such theoretical framework we must compare our observations of tidal evolution to predictions derived from more global findings of tidal theory. One

such finding is the difference in the timescales for tidal synchronization and tidal circularization in a given binary system. Primarily due to the difference between stellar and orbital angular momentum, the timescale for tidal synchronization is approximately 3 orders of magnitude smaller than the timescale for tidal circularization for constant stellar structure. From this finding we can formulate two expectations for *main-sequence* tidal evolution in a coeval sample of binaries: 1) The rotation of a star in a circularized binary should be synchronized to the orbital angular velocity; and 2) The rotation of a star in an eccentric binary should be pseudo-synchronized ($\Omega_\star = \Omega_{ps}$) if the orbital period is similar to or shorter than the tidal circularization period.

In the $\log(\Omega_\star/\Omega_{ps}) - \log(P)$ diagram for M35 and M34, these expectations correspond to all of the shortest period binaries ($P_{orb} \lesssim 13$ days) being located on the synchronization line. Inspection of Figure 11 immediately shows that this is not the case.

The two shortest period binaries, 1455 in M35 and 6214 in M34, both have circular orbits, as expected. Furthermore, the primary star of the shortest period binary, 1455, is indeed synchronized, in agreement with the first expectation. In marked contrast, the primary star of 6214 is rotating sub-synchronously in a circular orbit, and thus runs counter to the most basic expectation of main-sequence tidal evolution. We note that the circular orbit of 6214 is not a surprise; the 4.4 day period is less than half that of the tidal circularization period of M35, and 3 additional circular binaries have been found in M34 with periods between 4 and 5.5 days. Thus it is the newly discovered sub-synchronism that requires explanation.

The M35 binaries 0447 and 6200 provide another important comparison. Both have circular orbits at essentially the same 10.3 day period. However, the primary star of 6200 is rotating synchronously, as expected, while the primary of 0447 is rotating super-synchronously by more than a factor 4. This super-synchronism is unexpected based both on the circular orbit of 0447 and on comparison with 6200, its near-twin in period, eccentricity, and age. Perhaps of importance is the difference in the primary masses; 1.4 $M_\odot$ for 0447 and 1.1 $M_\odot$ for 6200. This difference in mass, and thus interior structure, of the primary stars can potentially translate into a difference in the mechanism and efficiency for tidal dissipation, in the internal angular momentum transport, and in the rate of external angular momentum loss (e.g., wind loss). Binaries 0447 and 6200 thus provide a

remarkable test of the role of stellar mass and structure in tidal evolution.

The third diagnostic pair of binaries are the M35 eccentric binaries 0422 and 3081. 0422 has a period of 8.2 days, shorter than the tidal circularization period of M35, yet retains an eccentricity of 0.65. 3081 has a period of 12.3 days, slightly longer than the M35 tidal circularization period, and has an eccentricity of 0.55. Both binaries represent the best cases in our sample to study evolution to pseudo-synchronization. In fact, neither have achieved pseudo-synchronization; both are rotating sub-synchronously by factors of 1.7 to 2.2. As such they both are counter to the second expectation of pseudo-synchronism for periods near the tidal circularization period.

The primaries of 3 of these 6 binaries are observed to rotate sub-synchronously. Stellar differential rotation and spots at high latitudes could lead to observed sub-synchronous rotation not representative of the rotation at the stellar equator. Using the sun as a reference, the difference in rotation period between the equator (25 days) and a latitude of 60^o (32 days) of a solar-type star is 7 days. The angular rotation velocity determined from brightness variations due to a spot at 60^o latitude will thus be about 25% less than if the spot were located at the equator. Assuming that this is the case for the primary stars in binaries 6214, 0422, and 3081, and thus increasing $\Omega_\star$ of the primary stars in these binaries by 25%, leads to $\Omega_\star/\Omega_{ps}$ ratio of 0.66, 0.75, and 0.57, respectively, for binaries 6214, 3081, and 0422. Such corrections are not sufficient to bring these binaries into synchronous or pseudo-synchronous rotation. We conclude from these estimates that the sub-synchronous rotation observed in the 3 binaries can not be explained due to differential rotation and that spots at high latitude, unless differential rotation with latitude is more severe in younger stars as compared to the sun.

To summarize, among six young (150-250 Myr), short-period (< 13 days), solar-type binaries, only two have both reached the equilibrium state of both a circularized orbit and synchronized rotation. Among the exceptions we find binaries with circular orbits that are not synchronized, and binaries with eccentric orbits that are not pseudo-synchronized. As a set, these six binaries present a challenging case study for tidal evolution theory. Here we begin that conversation with brief considerations of stellar evolution, stellar dynamics, tidal evolution theory, and initial conditions. None is capable of explaining all of the binaries.

Given the young ages of M34 and M35, in fact solar-mass stars have not been on the main sequence for long; hence the assumption of constant interior structure made at the beginning of this section likely should be abandoned and the impact of pre-main-sequence evolution considered. In fact, super-synchronous rotation at the age of M35 is predicted by Zahn & Bouchet (1989) for a circular 7.8 day period binary comprising two 1.1 $M_{\odot}$ stars. In their model the super-synchronous rotation on the early main-sequence is a result of a weakened tidal torque as the convective envelope of the primary retreats during late PMS evolution. Consequently the primary star is not tidally locked as its radius decreases, and the star spins up as it evolves to the main sequence. Perhaps this is the explanation for the super-synchronous rotation of binary 0447. Arguably its difference from binary 6200 can be attributed to a smaller convective envelope of the higher mass primary star in 0447, and thus relatively less tidal coupling than in 6200. We note that the ratio of $\Omega_{\star}$ to ω for 0447 is almost 3 times the ratio predicted by Zahn & Bouchet at the age of m35, but their model calculation is a for a lower-mass star in any case. Indeed, arguably the synchronization of the 1.1 $M_{\odot}$ in 6200 with a 10.3 day period is a more significant contradiction with the Zahn & Bouchet model.

Our findings for the binaries 0422 and 3081 may also reflect on the dynamical evolution of the cluster. M35 is a rich cluster with a relaxation time of order 100 Myr years (Mathieu 1983). It is likely that some binaries in the cluster core have gone through resonant gravitational encounters and stellar exchanges. Typically such encounters lead to hard, highly eccentric orbits for the binary products, and so perhaps the eccentric binaries 0422 and 3081 are such products. If so, the most massive stars - i.e., the primary stars - are the most likely to have been exchanged into the binary. As such, they would have experienced tidal torques for a time smaller than the age of the cluster, and indeed may retain their rotation periods from the time of the encounters. In this scenario that both are sub-synchronous is essentially the result of chance selection of those rotation periods from the single star population.

Finally, we note that the null hypothesis that the rotation periods of the primary stars are not at all influenced by tidal effects cannot be definitively ruled out. We show in Figure 3.11 two intervals, one bounded by diagonal dotted lines and the other bounded by diagonal solid lines. The interval framed by solid lines represents $\log(\Omega_{\star}/\Omega_{ps})$ corresponding to $P_{rot}^{prim} = 4.3$ days (the

median observed rotation period for stars in M35; Chapter 4) for $0.05 < e < 0.65$ (the observed range of non-zero orbital eccentricities in M35 (Meibom & Mathieu 2005)). The interval framed by dotted lines represents $\log(\Omega_\star/\Omega_{ps})$ corresponding to $e = 0.35$ (the mean of the observed eccentricity distribution in M35) and $1 < P_{rot}^{prim} < 15$ days (the range in rotation periods in M35). All of the M34 and M35 primary stars with measured rotation periods fall within these intervals, and thus are not distinguishable from the rotation periods of single stars. For the binaries with periods greater than 30 days, we presume that the rotation periods of the primaries in fact are set by the same mechanisms as in the single stars.

Might the same be said for the six binaries with periods of less than 30 days? The low rotation periods of the primary stars in both of the eccentric binaries 0422 and 3081 might derive simply from the same causes of such periods in single stars. In fact, the rate of tidal evolution in high eccentricity binaries may be slower than for binaries with low eccentricities. In a highly eccentric orbit tidal interactions are essentially confined to a short time interval around periastron passage. If the duration of the tidal perturbation at periastron passage is shorter than the convective turnover time, the efficiency of tidal coupling may be significantly reduced (Goodman & Oh (1997), Goldman & Mazeh (1991), and Zahn (1989)). Duquennoy et al. (1992) and Meibom & Mathieu (2005) conjecture that eccentric binaries with periods at or below the tidal circularization period, such as 0422 and 3081, might be the result of high primordial eccentricities ($e \gtrsim 0.7$). Perhaps the consequently reduced rate of tidal evolution has allowed the rotational evolution of the primary stars to be little different from that of single stars.

We find it far less plausible that the rotational evolutions of the primaries of the four binaries with circular orbits have not been altered by tidal effects. Two of these binaries would have to fall on the synchronization line by chance, while the circular orbits of the other two are strong evidence for substantial action by tidal forces since the formation of the system.

The observed rotational and orbital states of the 6 close M35 and M34 binaries pose interesting and different challenges to current tidal theory. To properly test tidal theory, models must be run with stellar and binary parameters tailored to fit the observed systems. Furthermore, ingredients such as internal stellar angular momentum transport and external wind loss should be included in

such models, as both helioseismic observations of the Sun (e.g. Goode et al. 1991; Eff-Darwich et al. 2002) and observations of rotation of late-type stars in general (e.g. Barnes (2003); Soderblom et al. (1993)) suggest that angular momentum is transported between the convective envelope and the radiative core in such stars.

3.9 Summary and Conclusions

Tidal forces in close detached binaries drive an exchange of angular momentum between the stars and their orbital motion. With time the binary system will approach an equilibrium state in which the stellar spin axes are aligned perpendicular to the orbital plane, the stellar spins are synchronized to the orbital motion, and the stellar orbits are circular.

Tidal theory makes global and explicit predictions about tidal evolution in close solar-type binaries. However, current models cannot account for the level of tidal circularization observed in the oldest populations of solar-type binaries, indicating that the theoretical rates of tidal evolution are too small. The same models predict that the process of tidal synchronization proceeds faster than tidal circularization by about three orders of magnitude. Observations of tidal synchronization therefore provide an important additional constraint on these models and the dissipation mechanisms they employ. Importantly, observing the rate of tidal synchronization also promises to shed light on physical processes of stars, such as internal and external angular momentum transport and the evolution of stellar dynamos.

To study tidal synchronization requires knowledge about the orbital velocities and rotational velocities of one or both stars in a binary. We present rotation periods for the solar-type primary stars in 13 single-lined binaries with known orbital periods and eccentricities. All 13 binaries are radial-velocity and photometric members of the young open clusters M35 (150 Myr) and M34 (250 Myr). The stellar rotation periods are derived from high-precision (0.5%) relative time-series photometry obtained from 2 weeks of classically scheduled observations combined with $\sim$ 6 months of queue-scheduled monitoring.

We compare the rotational angular velocity of each primary star ($\Omega_\star$) to the angular velocity required for the star to be (pseudo-) synchronized (Ω_{ps}). We use the value of $\Omega_\star/\Omega_{ps}$ as a measure of the degree of tidal synchronization and present that measure as a function of the binary orbital

period (P) in a $\log(\Omega_\star/\Omega_{ps}) - \log(P)$ - diagram.

The longest period binaries are unaffected by tidal interactions and the distribution of $\log(\Omega_\star/\Omega_{ps})$ fall within the interval expected from the dispersion in the observed stellar and orbital parameters. In contrast, our previous studies of tidal circularization in these clusters have shown that binaries with periods of ~ 10 days and less have been affected by tidal interactions. Considering theoretical predictions that the rate of tidal synchronization exceeds that of tidal circularization by of order a factor 1000, for constant stellar interior structure it is expected that 1) circularized binaries should also be synchronized; and 2) the shortest period eccentric binaries should be pseudo-synchronized. Consequently, all binaries with periods shortward of ~ 10 days should fall on or near the synchronization line ($\log(\Omega_\star/\Omega_{ps}) = 0$) in the $\log(\Omega_\star/\Omega_{ps}) - \log(P)$ - diagram.

However, 4 of the 6 binaries in M35 and M34 with orbital periods less than ~ 13 days offer interesting challenges to our understanding of tidal evolution in solar-type binaries:

- The 10.28 day orbit of M35 binary 0447 has been circularized, but the primary star rotates highly super-synchronously. As an important comparison, the M35 binary 6200 has been both circularized and synchronized at an orbital period of 10.33 days.

- Both primary stars in the M35 highly eccentric binaries 0422 ($P_{orb} = 8.17$ days) and 3081 ($P_{orb} = 12.28$ days) are rotating slower than their pseudo-synchronization speeds.

- Orbiting in a 4.39 day circular orbit, the primary star in the M34 binary 6214 is rotating sub-synchronous.

Only binaries 1455 and 6200 meet the expectations of tidal theory with 2.25 and 10.33 day circular orbits and synchronized primary stars.

At the present time, theoretical models make detailed predictions for only a few configurations of binary orbital and stellar parameters. Specific models must be run with carefully chosen initial orbital and stellar parameters to attempt to reproduce the observed tidal evolution at 150 Myr and 250 Myr.

We propose explanations for the observed binary and stellar parameters within the framework of current theory of stellar and tidal evolution, stellar dynamics, and observed stellar and binary

initial conditions. Specifically we suggest that the super-synchronous rotation of binary 0447 might be explained by PMS and main-sequence tidal evolution (Zahn & Bouchet 1989) and the relatively high mass and shallow convection zone of the primary star. We also note that that the sub-synchronous rotation of the primary stars in binary 0422 and 3081 might be due to either dynamical stellar interactions and/or reduced tidal dissipation in highly eccentric systems. We offer no explanation of the sub-synchronous and circular binary 6214, but find it unlikely that the parameters of binary 6214 together with the 3 other circularized binaries are the result of chance initial conditions.

Populating the $\log(\Omega_\star/\Omega_{ps}) - \log(P)$ diagram with coeval homogeneous populations of binary stars sets the beginning of a new era in observational studies of tidal synchronization. With time, the $\log(\Omega_\star/\Omega_{ps}) - \log(P)$ diagram for binary populations spanning in age from the PMS to the late main-sequence phase will become an important observational tool tracing the evolution of tidal synchronization in a way similar to the $e - \log(P)$ diagram in studies of tidal circularization. While at this early time, the limited number of binaries that can be placed in the diagram does not allow us to determine a "tidal synchronization period" marking the transition between synchronous and asynchronous systems, the degree of tidal synchronization in individual binaries provide interesting challenges to tidal theory. The success of theoretical models can be measured by their ability to predict the observed orbital and rotational evolution of these binary stars.

References

Abt, H. A., & Boonyarak, C. 2004, ApJ, 616, 562

Abt, H. A., Levato, H., & Grosso, M. 2002, ApJ, 573, 359

Andersen, J. 1991, A&A Rev., 3, 91

Barnes, S. A. 2003, ApJ, 586, 464

—. 2005, Priviate communication.

Claret, A. 1995, A&AS, 109, 441

Claret, A., & Cunha, N. C. S. 1997, A&A, 318, 187

Claret, A., & Gimenez, A. 1995, A&AS, 114, 549

Claret, A., Gimenez, A., & Cunha, N. C. S. 1995, A&A, 299, 724

Cudworth, K. M. 1971, AJ, 76, 475

Deliyannis, C. P. 2005, in preparation.

Duquennoy, A., Mayor, M., & Mermilliod, J. C. 1992, in Binaries as Tracers of Stellar Formation. Proceedings of a Workshop held in Bettmeralp, Switzerland, Sept. 1991, in honor of Dr. Roger Griffin. Editors, Antoine Duquennoy, Michel Mayor; Publisher, Cambridge University Press, Cambridge, England, New York, NY, 1992. LC # QB821 .B55 1991. ISBN # 0521433584. P. 52, 1992, 52

Eff-Darwich, A., Korzennik, S. G., & Jiménez-Reyes, S. J. 2002, ApJ, 573, 857

Giuricin, G., Mardirossian, F., & Mezzetti, M. 1984a, A&A, 135, 393

—. 1984b, A&A, 131, 152

—. 1984c, A&A, 141, 227

Goldman, I., & Mazeh, T. 1991, ApJ, 376, 260

Goode, P. R., Dziembowski, W. A., Korzennik, S. G., & Rhodes, E. J. 1991, ApJ, 367, 649

Goodman, J., & Dickson, E. S. 1998, ApJ, 507, 938

Goodman, J., & Oh, S. P. 1997, ApJ, 486, 403

Hole, K. T., Mathieu, R. D., Latham, D. W., & Meibom, S. 2005, submitted to AJ

Hut, P. 1981, A&A, 99, 126

Kalirai, J. S., Fahlman, G. G., Richer, H. B., & Ventura, P. 2003, AJ, 126, 1402

Kovacs, G. 1981, Ap&SS, 78, 175

Latham, D. W., Stefanik, R. P., Torres, G., Davis, R. J., Mazeh, T., Carney, B. W., Laird, J. B., & Morse, J. A. 2002, AJ, 124, 1144

Levato, H. 1974, A&A, 35, 259

Mathieu, R. D. 2000, in ASP Conf. Ser. 198: Stellar Clusters and Associations: Convection, Rotation, and Dynamos, 517–+

Mathieu, R. D., Duquennoy, A., Latham, D. W., Mayor, M., Mermilliod, T., & Mazeh, J. C. 1992, in Binaries as Tracers of Stellar Formation. Proceedings of a Workshop held in Bettmeralp, Switzerland, Sept. 1991, in honor of Dr. Roger Griffin. Editors, Antoine Duquennoy, Michel Mayor; Publisher, Cambridge University Press, Cambridge, England, New York, NY, 1992. LC # QB821 .B55 1991. ISBN # 0521433584. P. 278, 1992, 278

Mathieu, R. D., Meibom, S., & Dolan, C. J. 2004, ApJ, 602, L121

McNamara, B., & Sekiguchi, K. 1986, AJ, 91, 557

Meibom, S., Barnes, S. A., Dolan, C., & Mathieu, R. D. 2001, in ASP Conf. Ser. 243: From Darkness to Light: Origin and Evolution of Young Stellar Clusters, 711

Meibom, S., & Mathieu, R. D. 2005, ApJ, 620, 970

Meibom, S., Mathieu, R. D., & Stassun, K. G. 2005, in preparation.

Melo, C. H. F., Covino, E., Alcalá, J. M., & Torres, G. 2001, A&A, 378, 898

Ogilvie, G. I., & Lin, D. N. C. 2004, ApJ, 610, 477

Savonije, G. J., & Witte, M. G. 2002, A&A, 386, 211

Scargle, J. D. 1982, ApJ, 263, 835

Soderblom, D. R., Stauffer, J. R., MacGregor, K. B., & Jones, B. F. 1993, ApJ, 409, 624

Stassun, K. G., Mathieu, R. D., Mazeh, T., & Vrba, F. J. 1999, AJ, 117, 2941

Steinhauer, A. 2005, in preparation.

Steinhauer, A., & Deliyannis, C. P. 2004, ApJ, 614, L65

Tassoul, J. 1988, ApJ, 324, L71

Terquem, C., Papaloizou, J. C. B., Nelson, R. P., & Lin, D. N. C. 1998, ApJ, 502, 788

Vasilevskis, S., Klemola, A., & Preston, G. 1958, AJ, 63, 387

von Hippel, T., Steinhauer, A., Sarajedini, A., & Deliyannis, C. P. 2002, AJ, 124, 1555

Witte, M. G., & Savonije, G. J. 2002, A&A, 386, 222

Yi, S. K., Kim, Y., & Demarque, P. 2003, ApJS, 144, 259

Zahn, J.-P. 1975, A&A, 41, 329

—. 1977, A&A, 57, 383

—. 1989, A&A, 220, 112

Zahn, J.-P. 1992, in Binaries as Tracers of Stellar Formation. Proceedings of a Workshop held in Bettmeralp, Switzerland, Sept. 1991, in honor of Dr. Roger Griffin. Editors, Antoine Duquennoy, Michel Mayor; Publisher, Cambridge University Press, Cambridge, England, New York, NY, 1992. LC # QB821 .B55 1991. ISBN # 0521433584. P. 253, 1992, 278

Zahn, J.-P., & Bouchet, L. 1989, A&A, 223, 112

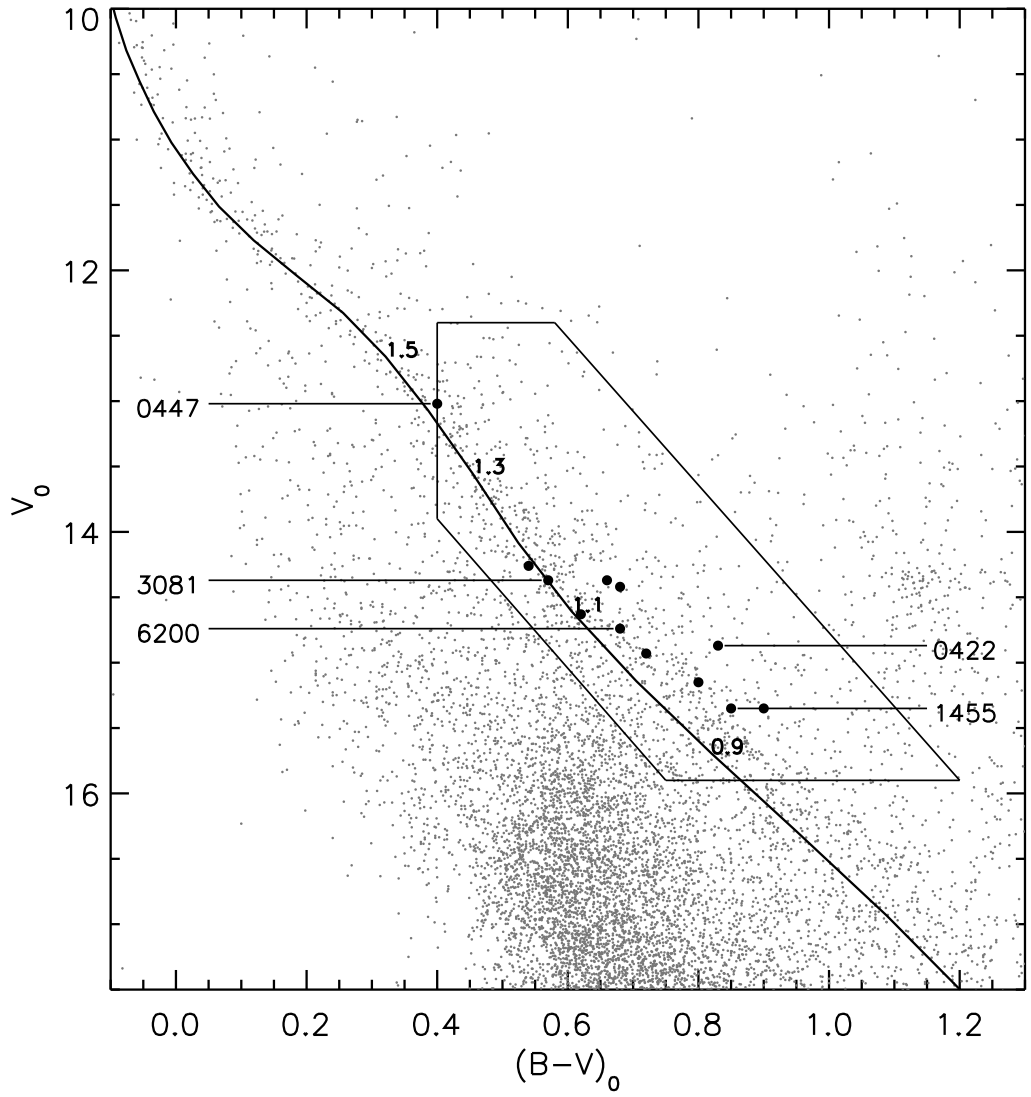

Fig. 3.1.— The color-magnitude diagram of M35. The photometry and the cluster reddening ($E_{(B-V)} = 0.2$) was provided by Deliyannis (2005). The 12 binaries with known rotation periods of their primary stars are marked as black dots. The 5 binaries with orbital period shortward of 13 days are labeled with the last 4 digits of their respective 2MASS ID's. The 150 Myr isochrone overplotted has been corrected for reddening and extinction and a distance modulus of $9\overset{m}{.}8$ (Kalirai et al. 2003). Relevant isochrone masses are marked. The stars included in our spectroscopic survey fall within the region outlined.

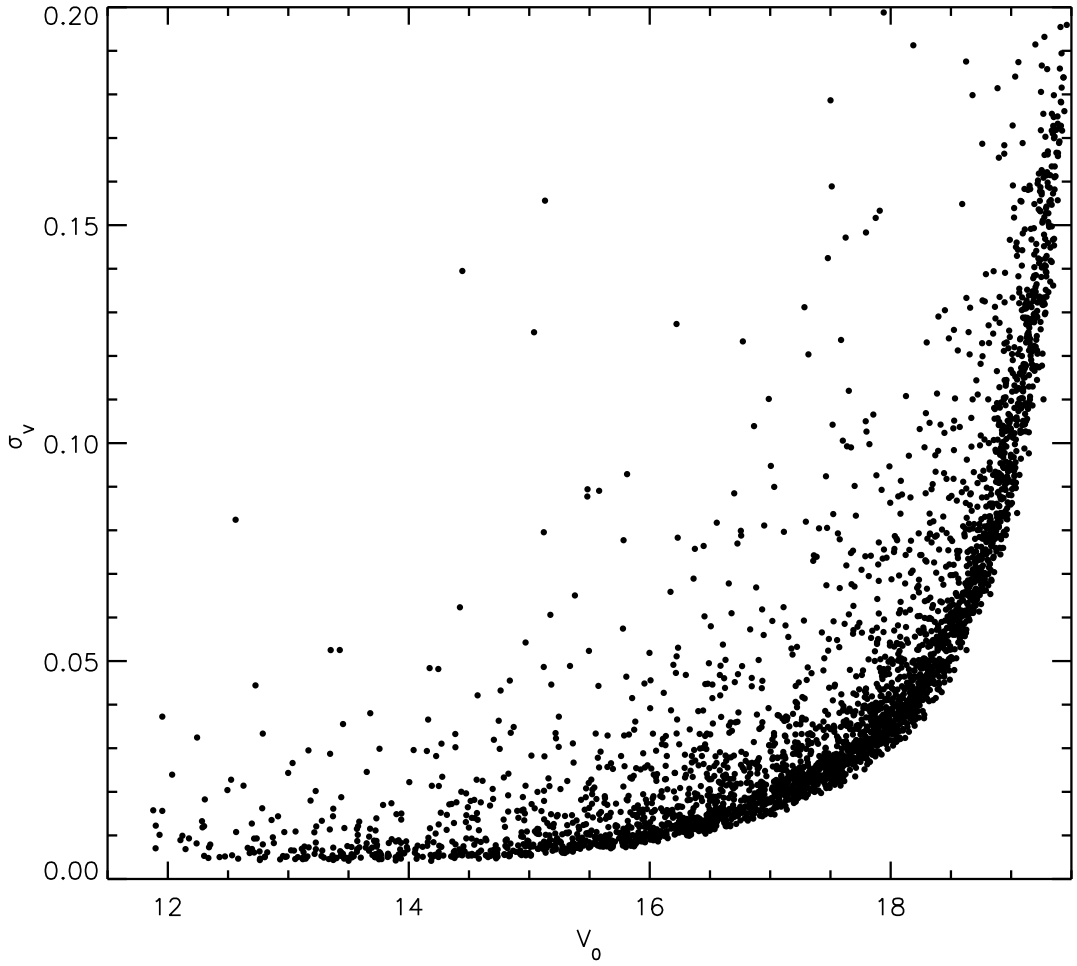

Fig. 3.2.— The standard deviation of the instrumental V magnitudes as a function of the true V magnitude (V_0) for stars in the field of M35. A first-order estimate of the true V magnitude has been obtained by applying a correction of $-3\overset{\mathrm{m}}{.}238$, equivalent to the mean difference between the instrumental V magnitude and the V magnitude from Deliyannis (2005), plus an extinction correction of $3 \times E_{(B-V)} = 0\overset{\mathrm{m}}{.}6$ (Deliyannis 2005). A relative photometric precision of $\sim 0.5\%$ is obtained for stars with $12\overset{\mathrm{m}}{.}0 \lesssim V \lesssim 15\overset{\mathrm{m}}{.}0$.

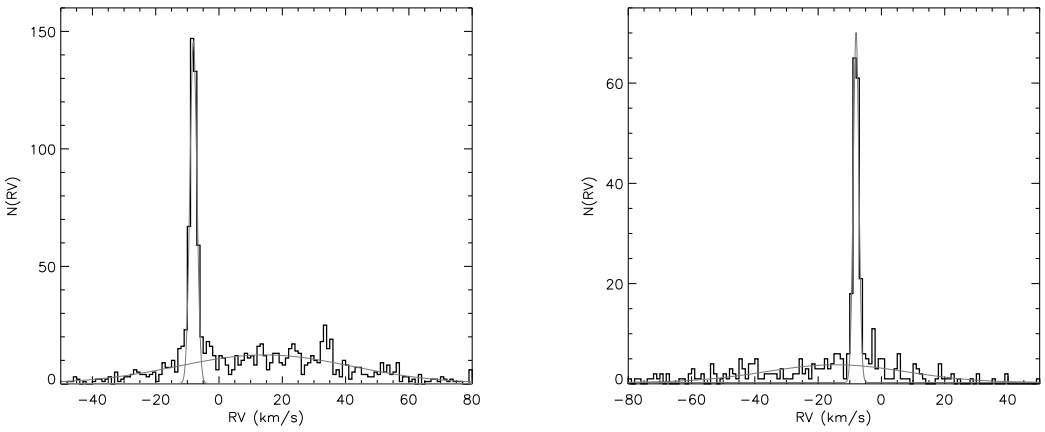

Fig. 3.3.— The distributions of radial-velocities for stars in the fields of M35 (left) and M34 (right). Two Gaussian functions (grey solid curves) have been simultaneously fitted to the cluster and field components of each distribution.

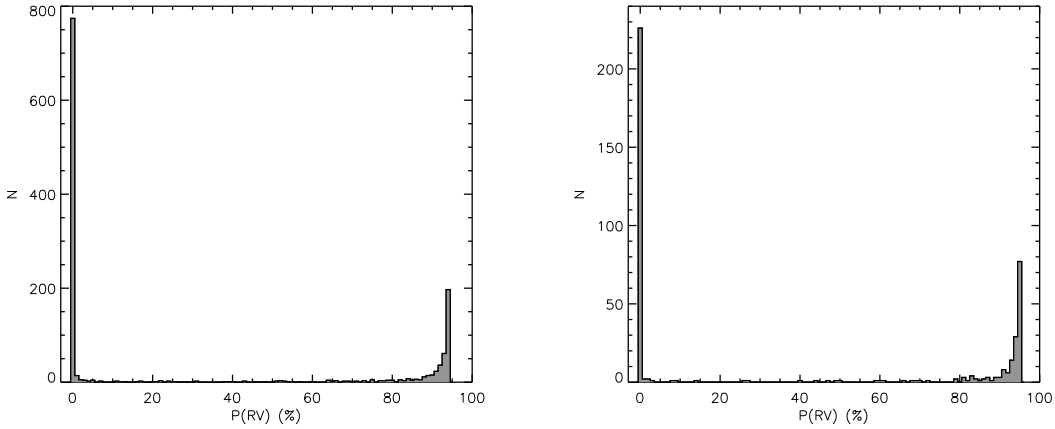

Fig. 3.4.— The distributions of radial-velocity membership probabilities (P(RV)) for stars in the fields of M35 (left) and M34 (right). Cluster members and non-members are easily identified as two distinct peaks in the distributions. The space between the peaks is populated by stars with radial-velocities corresponding to the wings of the cluster distributions.

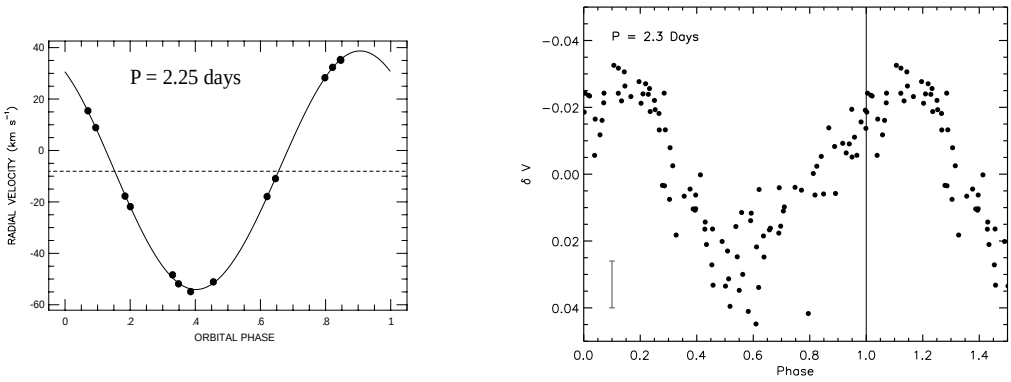

Fig. 3.5.— **Left:** The radial velocity measurements of binary 1455 phased to an orbital period of 2.25 days. The best fit orbital solution is overplotted. The orbit is circular with an eccentricity of only 0.010 ± 0.003. **Right:** The differential V-band photometry for binary 1455 phased to a period of 2.29 ± 0.02 days, corresponding to the maximum periodogram power. The vertical solid line indicates a phase value of 1.0, and the errorbar in the lower left-hand corner represent $\pm$ the typical photometric error at the V magnitude of binary 1455.

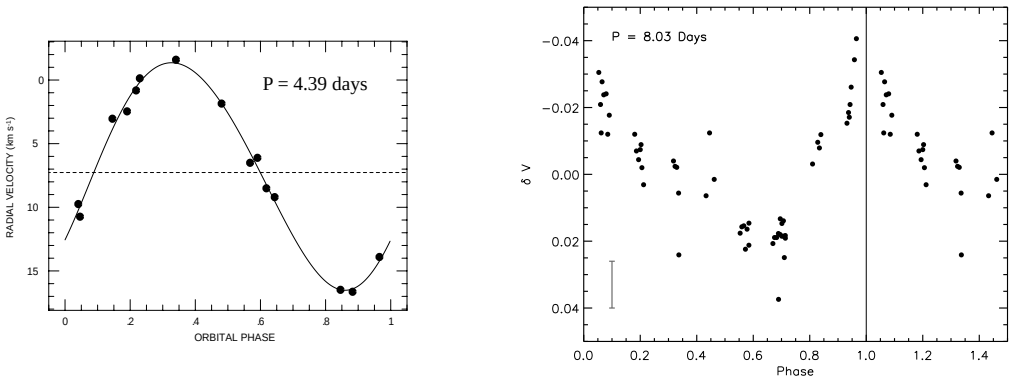

Fig. 3.6.— **Left:** The radial velocity measurements of binary 6214 phased to an orbital period of 4.39 days. The best fit orbital solution is overplotted. The orbit is circular with an eccentricity of 0.063 ± 0.033. **Right:** The differential V-band photometry for binary 6214 (Barnes 2005) phased to a period of 8.03 ± 0.1 days. The vertical solid line indicates a phase value of 1.0, and the errorbar in the lower left-hand corner represent $\pm$ the typical photometric error at the V magnitude of binary 6214 (Barnes 2005).

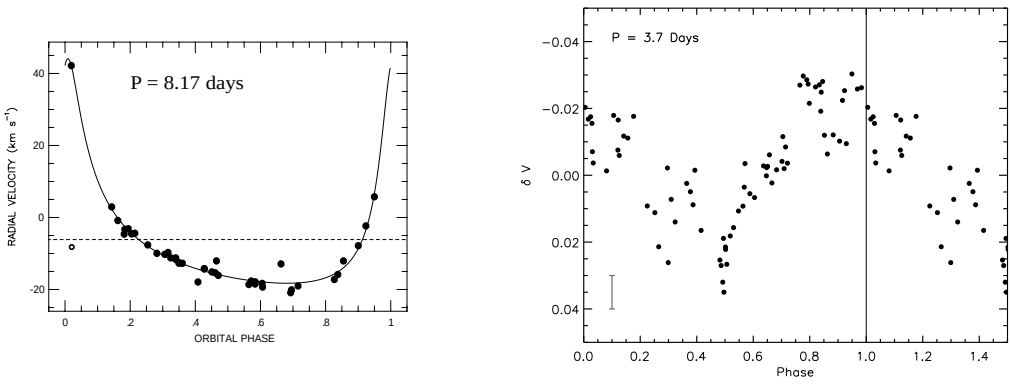

Fig. 3.7.— **Left:** The radial velocity measurements of binary 0422 phased to an orbital period of 8.17 days. The best fit orbital solution is overplotted. The orbit is highly eccentric ($e = 0.649 \pm 0.022$). One observation was obtained at periastron passage (maximum velocity separation) revealing a third spectral component. The velocity of the tertiary component is marked as an open circle at phase 0.04. **Right:** The differential V-band photometry for binary 0422 phased to a period of 3.71 ± 0.06 days. The vertical solid line indicates a phase value of 1.0, and the errorbar in the lower left-hand corner represent $\pm$ the typical photometric error at the V magnitude of binary 0422.

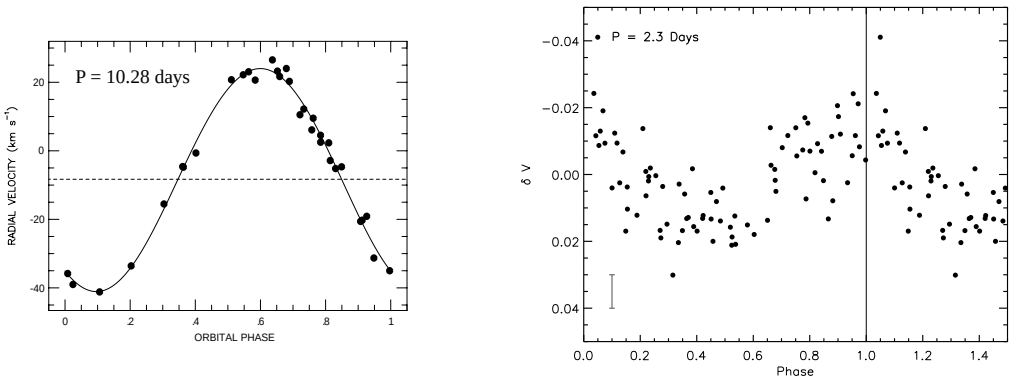

Fig. 3.8.— **Left:** The radial velocity measurements of binary 0447 phased to an orbital period of 10.28 days. The best fit orbital solution is overplotted. The orbit is circular ($e = 0.009 \pm 0.019$). **Right:** The differential V-band photometry for binary 0447 phased to a period of 2.30 ± 0.02 days, corresponding to the maximum periodogram power. The vertical solid line indicates a phase value of 1.0, and the errorbar in the lower left-hand corner represent $\pm$ the typical photometric error at the V magnitude of binary 0447.

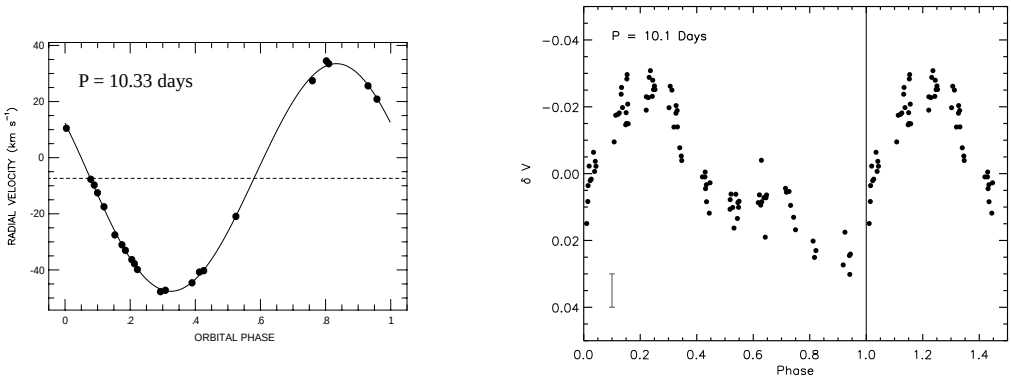

Fig. 3.9.— **Left:** The radial velocity measurements of binary 6200 phased to an orbital period of 10.33 days. The best fit orbital solution is overplotted. The orbit is circular ($e = 0.016 \pm 0.009$). **Right:** The differential V-band photometry for binary 6200 phased to a period of 10.13 ± 0.39 days, corresponding to the maximum periodogram power. The vertical solid line indicates a phase value of 1.0, and the errorbar in the lower left-hand corner represent $\pm$ the typical photometric error at the V magnitude of binary 6200.

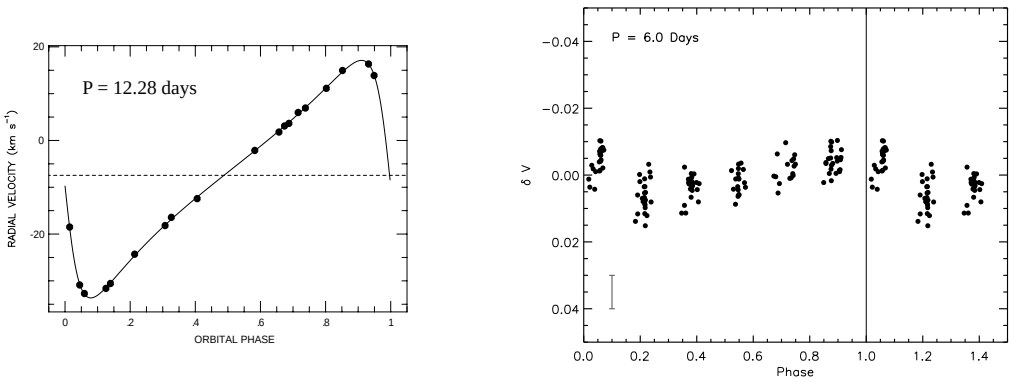

Fig. 3.10.— **Left:** The radial velocity measurements of binary 3081 phased to an orbital period of 12.28 days. The best fit orbital solution is overplotted. The eccentricity of the orbit is 0.016 ± 0.009. **Right:** The differential V-band photometry for binary 3081 phased to a period of 6.03 ± 0.12 days, corresponding to the maximum periodogram power. The vertical solid line indicates a phase value of 1.0, and the errorbar in the lower left-hand corner represent $\pm$ the typical photometric error at the V magnitude of binary 3081.

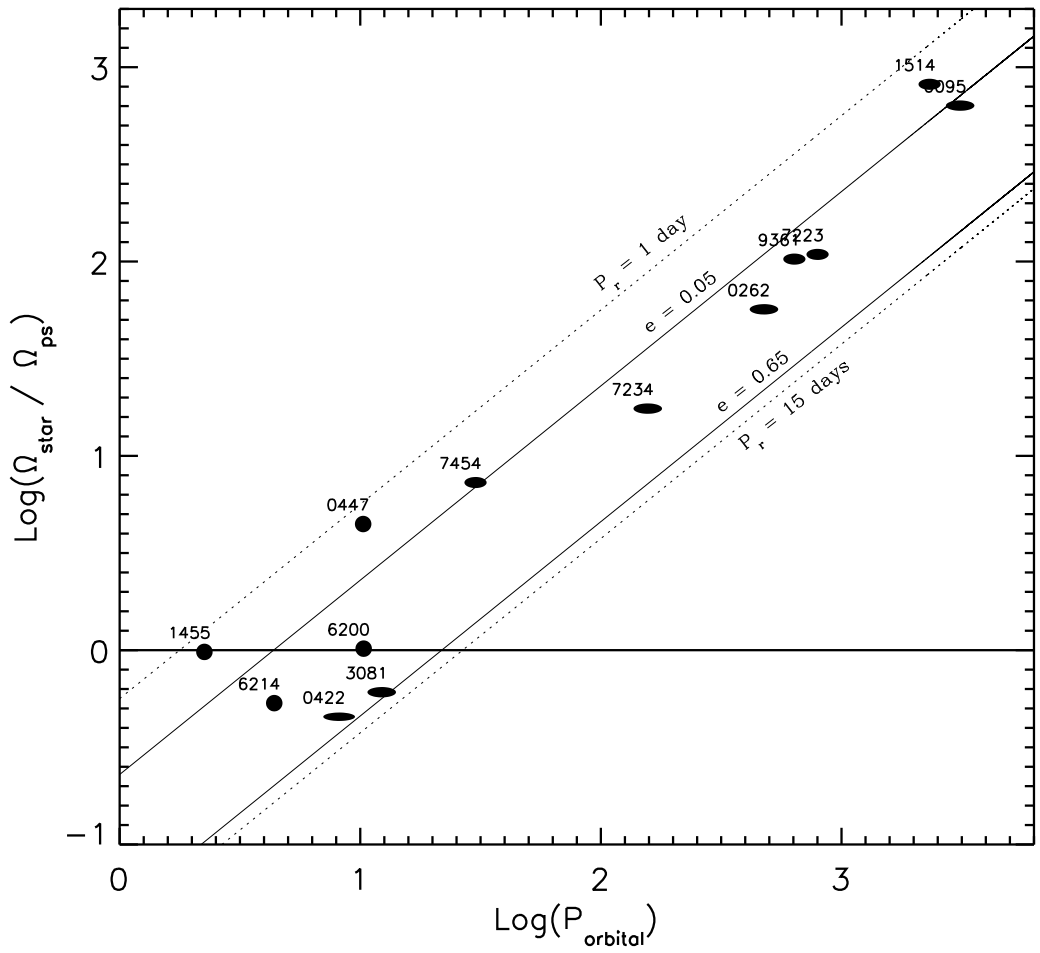

Fig. 3.11.— The $\log(\Omega_\star/\Omega_{ps}) - \log(P)$ diagram for M35 and M34. $\log(\Omega_\star/\Omega_{ps})$ is plotted as a function of orbital period for all 13 binaries. The shape of the plotting symbols are indicative of the orbital eccentricity of each binary. A solid horizontal line (the synchronization line) mark $\log(\Omega_\star/\Omega_{ps}) = 0$, the location in the diagram for synchronized or pseudo-synchronized binaries ($\Omega\star = \Omega_{ps}$). $\log(\Omega_\star/\Omega_{ps}) > 0$ for super-synchronous binaries and $\log(\Omega_\star/\Omega_{ps}) < 0$ for sub-synchronous binaries. The interval framed by solid lines represents $\log(\Omega_\star/\Omega_{ps})$ corresponding to $P_{rot}^{prim} = 4.3$ days and $0.05 < e < 0.65$. The interval framed by dotted lines represents $\log(\Omega_\star/\Omega_{ps})$ corresponding to $e = 0.35$ and $1 < P_{rot}^{prim} < 15$ days.

Chapter 4

The Effect of Stellar Mass and Binarity on The Rotational Evolution of Late-Type Stars in The Open Cluster M35

4.1 Abstract

We present the results of an extensive photometric time-series survey over a $40' \times 40'$ field centered on the 150 Myr open cluster M35. We report rotation periods for 443 stars within this field. Spectroscopic and multi-band photometric surveys over the same region have enable determination of photometric and radial-velocity cluster membership as well as identification of short-period ($P \lesssim$ 4500 days) binary stars. Of the 443 rotators, we find 310 stars to be late-type members of M35, corresponding to ∼16% of the cluster population within the brightness-limits of our photometric survey. The resulting distribution of rotation periods spans from $\sim 0.1 - 15$ days. We find that the 310 stars lie primarily on two distinct sequences when their rotation periods are plotted against their stellar color (mass). The well-defined sequences and the fractional numbers of stars on each sequence provide strong support for a hydromagnetic mechanism recently proposed by S. A. Barnes to explain the rotational evolution of late-type stars. A set of calibrated rotational isochrones, as defined by Barnes, fit well to the two sequences in the M35 color-period diagram, suggesting that an accurate age-estimate can be determined for a coeval stellar population based on the degree of stellar rotational evolution. We use the M35 color-period diagram to estimate characteristic timescales for the spin-down of G and K dwarfs. Ten M35 stars are rotating with rates that are abnormally slow compared to similar cluster stars. We propose that these stars are primary stars in close binaries and that tidal interactions are responsible for the slower than expected rotation. Finally, the rotation period distribution from 17 primary stars in close (a $\lesssim$ 5 AU), but non-synchronized, binaries is compared to the rotation period distribution from 53 single stars or primary stars in wide binaries (a $\gtrsim$ 5 AU). The probability that the two distributions derive from the same parent distribution is 0.11%. The primary stars in the close binary stars rotate on average faster than the single stars. The statistically significant difference between the two period distributions is *not* due to tidal interactions in the close binaries, and thus suggest that a close companion can, perhaps indirectly, affect the rotational evolution of a late-type star.

4.2 Introduction

Observational surveys of stellar rotation have revealed that young (age $\lesssim$ 500 Myr) late-type main-sequence stars in coeval populations rotate with rates ranging over two orders of magnitude from near their breakup velocities to velocities similar to that of our Sun. Understanding why some young stars deplete their angular momentum faster than others - which physical processes are at play, when, and to what extent - is a primary mandate for stellar evolution research.

The general notion that main-sequence stars of mid F-type or later are slow rotators with surface velocities of the order 10 $km\ s^{-1}$ or less (the Schatzman (1962) break), was dramatically changed with the discovery from photometric measurements (by Alphenaar & van Leeuwen (1981), van Leeuwen & Alphenaar (1982), and Meys et al. (1982)) of K dwarfs in the Pleiades rotating with periods of a few tenths of a day. Their finding challenged the understanding of the early angular momentum evolution for late-type stars, and led to an increasing interest in the angular momentum evolution of these rapid rotators and of late-type main-sequence stars in general.

Over the past two decades numerous observational surveys have contributed pieces to the puzzle of the large dispersion in rotation rates, and in the process found fascinating relations between surface rotation and stellar mass and age. Observations of mainly projected rotation velocities ($v \sin(i)$) of late-type stars in α Persei (50 Myr; Stauffer et al. (1985, 1989)), the Pleiades (100 Myr; Soderblom et al. (1983); Stauffer et al. (1984); Benz et al. (1984); Stauffer & Hartmann (1987); Soderblom et al. (1993a)), and the Hyades (625 Myr; Soderblom (1982); Benz et al. (1984); Radick et al. (1987)), but also some photometric studies of the Hyades (Lockwood et al. 1984; Radick et al. 1987), were first to provided a more detailed picture of the morphology of the velocity distribution at different ages. The rotation velocity distributions confirmed the coexistence of slow and rapidly rotating stars in α Persei and the Pleiades, but showed an absence of rapid rotators in the Hyades. Furthermore, the rapid rotators in the young clusters were found primarily among K and M dwarfs and not among G dwarfs. The emerging evidence for an age- and mass-dependence of the fastest rotators, prompted Stauffer et al. (1984), and later Soderblom et al. (1993b), to suggest that decoupling of the convective envelope from the radiative stellar core might be responsible for the observed spin-down and mass dependence. The mass, and thus spin-down rate, of the convective envelope is inversely

proportional to the stellar mass, allowing G dwarfs to spin down before K and M dwarfs and all rapid rotators to spin down by the age of the Hyades.

The decoupling of the envelope from the core had developed in the rotating stellar models of Endal & Sofia (1981) and later in the models of Pinsonneault et al. (1990), MacGregor & Brenner (1991), Barnes & Sofia (1996), and Sills et al. (2000). However in these models the decoupled zones cannot reconnect once decoupled. The concept of decoupling, if permanent, is therefore in conflict with helioseismic observations of the sun as a solid-body rotator (Gough 1982; Duvall et al. 1984; Goode et al. 1991; Eff-Darwich et al. 2002). Soderblom et al. (1993b) further noted that in order for the slow rotators in the Pleiades not to rotate too slowly by the age of the Hyades, they need to draw from an interior reservoir of angular momentum - a faster spinning core. Reconnection of the envelope and core - in accordance with helioseismic observations of the sun - might thus be required to explain the evolution of the slow rotators beyond the age of the Pleiades.

Understanding the formation of the rapid rotators is a separate problem. The fastest spinning stars in the young clusters cannot be explained from Skumanich-style spin-down (Skumanich 1972) of the fastest spinning T Tauri stars. The rapid rotators can be explained only by introducing saturation (MacGregor & Brenner 1991) of the angular momentum loss via stellar winds (Schatzman 1962). Stauffer & Hartmann (1987), Barnes & Sofia (1996), and Bouvier et al. (1997a) implemented such "magnetic saturation" and found that the saturation threshold needed was dependent on the stellar mass, with lower mass stars needing saturation at lower angular velocities. Support for the idea of magnetic saturation has been found in diagnostics of magnetic activity, i.e., coronal X-ray flux, chromospheric CaII emission, and the size of photospheric stars pots, which all appear to saturate at high, but different, rotation rates. However, the physical meaning of saturation is still unclear.

A popular explanation for the large dispersion of rotation periods and particular for the slower rotators in the observed distributions originates from the work of Koenigl (1991) and Edwards et al. (1993) on star-disk interactions in the pre main-sequence (PMS) phase. The magnetic interaction between young stars and their disks ("magnetic disk-locking") provide a means to brake the spin-up of the central star while transferring angular momentum from the star to the disk (e.g. Najita 1995, and references therein). Observational support for the disk-locking model, has been found in the

form of bimodalities in the rotation period distributions for stars in Orion and NGC2264, combined with indicators for the presence of circumstellar disks (see Herbst et al. (2000), Herbst & Mundt (2005; astro-ph/0508009) and references therein). However, other researchers have argued against the presence of bimodality and the disk correlation in similar data (Stassun et al. 1999; Rebull 2001). When inspected by Barnes (2001), the rotation rates of the host stars of extra-solar planets appear not to be distinguishable from those of a sample of nearby field stars, as one might expect if disk interaction is responsible for creating slow rotators. These conflicting results are curious, and it is not yet clear how to connect the rotational observations of PMS and young main-sequence stars, and in particular how to explain the very rapid main-sequence rotators, in terms of star-disk interactions.

Taking advantage of the results from an increasing number of photometric monitoring programs, Barnes (2003) proposes a different interpretation of the rotation period data. Barnes identifies and interprets emerging sub-populations in the distributions of stellar rotation period versus stellar color for several coeval populations of late-type stars. The photometric data, free of several ambiguities present in the $v \sin(i)$ data, provides a clearer picture of the dependencies of stellar rotation on stellar age and mass (color). Barnes (2003) identifies sequences of fast and intermediate/slow rotators in the color-period diagram, and explains their changing appearance with population age in terms of the changing nature of the stellar magnetic field and consequent change in the transport of angular momentum from the stellar envelope to the stellar core and to the stellar wind. This new approach combines the basic ideas of de-coupling of the stellar core and envelope with coupling or re-connection of the two zones through a global dynamo-field. Importantly, this scenario parts with the need for magnetic disk-locking to explain the intermediate and slow rotators.

Efforts to model the observed evolution of angular momentum from the PMS to the zero-age main-sequence (ZAMS) have essentially treated this as a single-star problem (e.g. Koenigl 1991; Bouvier et al. 1993; Shu et al. 1994; Ostriker & Shu 1995). Observational evidence suggests that most, if not all, stars form in binary or multiple systems (e.g. Duquennoy & Mayor 1991; Mermilliod et al. 1992; Ghez et al. 1993). Forming stars in pairs is perhaps also the most natural way to account for the orders of magnitude difference in angular momentum between a collapsing cloud core and a star (Larson 2002). Indeed, the typical amount of angular momentum of a star-forming cloud core is

comparable to that of a wide binary (Bodenheimer 1995).

The presence of a nearby companion is expected to shorten the duration of the star-disk interactions by truncation and disruption of the circumstellar disk (Pringle 1991; Artymowicz et al. 1991; Artymowicz 1992). It has therefore been speculated that, pending the validity of the magnetic disk-braking theory, young main-sequence stars in binaries ought to be rotating on average faster than corresponding single stars. However, Armitage & Clarke (1996) find that a solar-type star with a binary companion orbiting between $\sim$ 1-8 AU will experience a prolonged period of star-disk interactions and thus evolve to rotate slower than a similar single star or a similar star in a wider binary system. From observations, Stauffer & Hartmann (1987) find that rapid rotators are less often displaced above the Pleiades main-sequence, and Bouvier et al. (1997b) find no significant difference between the distribution of rotational velocities of single and binary stars in the Pleiades. However, Patience et al. (2002) argues that the rotational velocities for solar-type binaries in α Persei with separations between 10 and 60 AU are significantly higher than those of wider systems, suggesting that companions may act to change the rotational evolution of young stars. Again, the conflicting results are curious, and more observations of stellar rotation in close binary stars are needed to gain understanding about the affect of binarity on the angular momentum evolution of solar-type stars.

We present in this paper the results of extensive photometric and spectroscopic surveys of stars in the field of the open cluster M35 (NGC 2168). M35 is a rich ($\sim$ 2700 stars; Barrado y Navascués et al. (2001)), 150-180 Myr (Barrado y Navascués et al. 2001; von Hippel et al. 2002; Kalirai et al. 2003; Deliyannis 2005) northern hemisphere cluster located $\sim$ 800-900 pc (Barrado y Navascués et al. 2001; Kalirai et al. 2003) toward the galactic anticenter ($\alpha_{2000} = 6^h\ 9^m$, $\delta_{2000} = 24^o\ 20'$; $l = 186.^\circ59$, $b = 2.^\circ19$). The age and large population of late-type stars makes M35 particularly interesting from the point of view of studying the evolution of stellar rotation in single and binary stars. Slightly older than the Pleiades but much richer, M35 will be important in delineating the phase of rotational evolution between the zero-age main-sequence and the age of the Hyades ($\sim$ 625 Myr). At the distance of M35 the majority of cluster members are confined to within a $\sim 0.5^o$ diameter field, facilitating photometric and spectroscopic observations of a large number of stars. The combination of time-series and multi-band photometry with spectroscopic (radial-velocity) data, enable us to explore not

only the rotation period distribution and the color-period diagram for late-type members of M35, but also investigate the effect of a companion on the rotational evolution of stars in close binaries.

We begin in Section 4.3 by describing our time-series photometric observations, their reduction, our method for determining periodic photometric variability, and the data from the literature to which we can compare our derived rotation periods. In Section 4.4 we present our spectroscopic observations, our method for determining stellar radial-velocities and deriving cluster membership probabilities, and the overlap with the photometric data. In Section 4.5 we describe the multi-band photometric data for M35 and present the M35 color-magnitude diagram with the location of all detected rotators highlighted. Section 4.6 gives a full representation of our results and discusses their implications for various questions relating to the evolution of angular momentum in single and binary stars. We summarize our conclusions in Section 4.7.

4.3 Observations and Data Reduction

Except for the Sun, information about stellar rotation comes from observations of stellar photospheres (although the field of astroseismology is poised to change that in the near future). Rotation manifests itself directly through Doppler broadening of photospheric absorption lines, or for late-type stars from modulation of the stellar light by cool spots or hot plages on the photosphere, appearing and disappearing with each rotation . The former technique has the advantage that rotational information can be acquired from a single spectroscopic observation. The disadvantages are a limited sensitivity to slowly rotating stars, the ambiguities introduced by the unknown inclination of the rotational axis with respect to the line of sight, the necessity of measuring or calculating stellar radii, and the vulnerability to the non-rotational effects in the spectrum from a binary companion. The latter (photometric) technique eliminates the ambiguity of the axial inclination and is sensitive to rotation velocities from near breakup to as slow as solar. The disadvantages are the time- and labor-intensive nature of the observing programs, and the inherent restriction to (bias toward) stars with spots.

Our scientific goals are critically dependent on being able to determine high precision rotation periods for both rapidly and slowly rotating stars, and to determine such rotation periods for stars in binary systems. Time-series photometry was therefore the natural choice for our observational

program.

We have photometrically surveyed stars in a region approximately $40' \times 40'$ centered on the open cluster M35 over the time-span of ∼145 days. The photometric data were obtained using the WIYN [1] 0.9m telescope [2] at Kitt Peak National Observatory equipped with a $2k \times 2k$ CCD camera. The field of view of this instrument is $20.5' \times 20.5'$ and observations where obtained over a 2×2 mosaic. The complete dataset is composed of images from two different but complementary observing programs. Images of the same field were acquired by the first author with a frequency of approximately once per hour for 5-6 hours per night from 2-17 December 2002. In addition, one image per night was obtained in a queue-scheduled (synoptic) observing program from October 2002 to March 2003. The result is a database of differential photometric V-band light curves for more than 14000 stars with $12 \lessapprox V \lessapprox 20$. From this database we derive rotation periods for 443 stars.

Figure 4.1 shows the region surveyed (solid square) and the spatial distribution of the 443 rotators. The region is roughly coincident with that of Deliyannis (2005) in which they obtained UBVRI CCD photometry for ∼ 19000 stars (dashed square). Also shown is the spatial extent (circle) of our spectroscopic survey described in Section 4.4 (circle). The photometric survey region is located within the spectroscopic survey region so as to optimize the overlap with known short period spectroscopic binaries (see Meibom & Mathieu 2005; Meibom et al. 2005).

4.3.1 Photometric Time-Series Observations

The photometric dataset presented in this study is composed of images from two complementary observing programs. The high-frequency program ran over 16 full nights from the 2-17 December 2002. In each night we observed all four frames in the 2×2 mosaic with a frequency of approximately once per hour for the six hours that the cluster's airmass was below 1.5. The sampling frequency of the December run allow us to detect photometric variability with periods ranging from less than a day to about 8-10 days.

The second low-frequency observing program ran over 143 nights from 22 October 2002 to 11

[1] The WIYN Observatories are joint facilities of the University of Wisconsin-Madison, Indiana University, Yale University, and the National Optical Astronomy Observatories.

[2] The 0.9m telescope is operated by WIYN Inc. on behalf of a Consortium of ten partner Universities and Organizations (see http://www.noao.edu/0.9m/general.html)

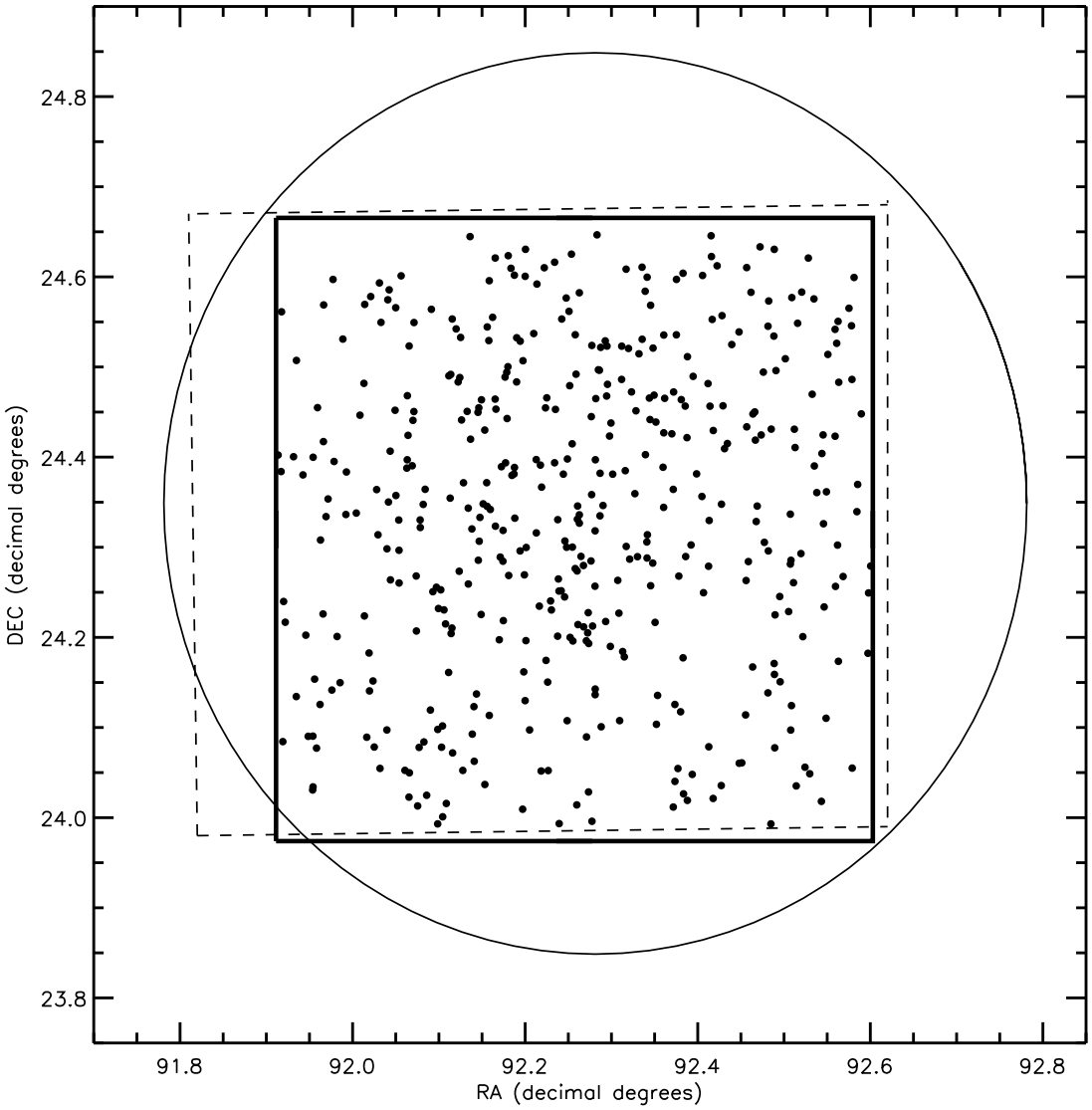

Fig. 4.1.— The locations and spatial extents of the photometric and spectroscopic surveys used in this study. The innermost solid square denotes the $40' \times 40'$ region of our time-series photometric survey. Within it we show the distribution of the 445 rotators (filled black circles). The dashed rectangle shows the region of the multi-band photometric study by Deliyannis (2005) and the circle represents the 1-degree diameter field of our spectroscopic survey of M35 (Braden et al. 2005).

March 2003. Over this period of time, interrupted only by bad weather and scheduled instrument changes, each of the four frames in the 2×2 mosaic were observed once per night. The observations

were queue-scheduled (synoptic) and carried out by the astronomer(s) on duty. The long time-span of this program provides data suitable for detecting periodic variability of up to $\sim$ 75 days, and for testing the long term stability of short-period photometric variations.

Figure 4.2 display a sample light curve of the combined data from both programs. Filled symbols represent the high-frequency observations and open symbols represent the low-frequency (synoptic) observations. All observations were done through a Johnson V-band filter.

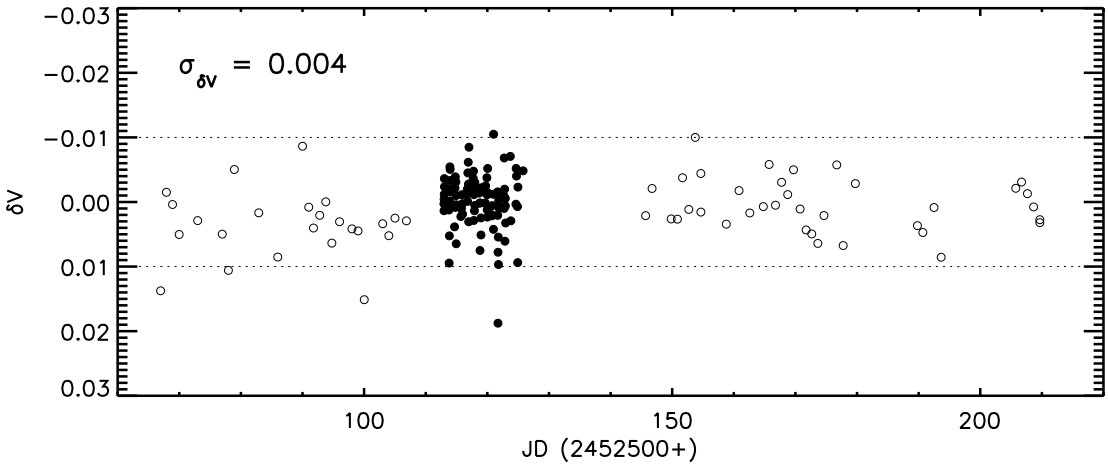

Fig. 4.2.— Sample light curve from our photometric database for a $V \simeq 14$ magnitude photometrically stable star. Filled symbols represent measurements from the high-frequency December 2002 observing run and open symbols represent the low-frequency (synoptic) observations. The data span a total of 143 days. The star was observed in all 157 images of the north-east quadrant of the 2×2 mosaic. The standard deviation (σ_V) of the 157 measurements is $0\overset{\mathrm{m}}{.}004$, representative of our best photometric precision. The horizontal dotted lines denote $\delta V = \pm 0\overset{\mathrm{m}}{.}01$.

4.3.2 Basic Reductions, PSF Photometry, and Light Curves

We reduced our CCD frames using the standard IRAF CCDRED package. We used the IRAF STSDAS GASP package to compute a simple linear transformation of pixel coordinates to equatorial coordinates for each frame, using as reference approximately 35 stars per frame from corresponding Digitized Sky Survey images. Our derived stellar positions show a typical frame-to-frame scatter of

$0\overset{''}{.}09$ in Right Ascension and $0\overset{''}{.}07$ in Declination.

Stellar sources were identified on all frames using the IRAF DAOFIND algorithm. We performed PSF photometry using the IRAF DAOPHOT package. Approximately 30 PSF stars were used to determine the best analytical PSF and to calculate a residual lookup table for each frame. We extract instrumental magnitudes for all detected objects and assemble a raw light curve (a time-series of instrumental magnitudes) for each star. A particular star may fail to appear on a given frame for various reasons. For example, stars near the edges of our frames may be missed on some exposures because of telescope pointing errors, while bright stars near the CCD saturation limit and the faintest stars near the selected detection limit may be missed because of variations in seeing, sky brightness, and sky transparency. Our light curves are therefore inhomogeneous to varying degrees, with some detected objects appearing on every frame, others appearing only on half or less. To ensure our ability to perform reliable time-series analysis on stars in our database, we have eliminated stars that appear on fewer than half of the total number of frames (typically stars near the edges of our CCD frames and/or stars near our magnitude limits). The resulting database contains 14022 sources with approximately $12 \lesssim V_0 \gtrsim 19.5$ and minimum 75 photometric measurements over ~ 143 nights. V_0 being a first order estimate of the true V magnitude obtained by applying a correction of the mean difference between the instrumental V magnitude and the V magnitude from Deliyannis (2005) plus an extinction correction of $3 \times E_{(B-V)} = 0\overset{m}{.}6$.

We apply the Honeycutt (1992) algorithm for differential CCD photometry to our raw light curves to remove non-stellar frame-to-frame photometric variations. We favor this technique for differential photometry because it does not require a particular set of comparison stars to be chosen a priori, nor does it require a star to appear in every frame.

The sample light curve in Figure 4.2 shows a $V \sim 14$ magnitude photometrically stable star. The standard deviation from 157 photometric measurements is $0\overset{m}{.}004$, representative of our best photometric precision. Figure 4.3 show the standard deviation of all photometric measurements as a function of the V magnitude for stars in the field of M35. The lower envelope of the distribution for stars with $12 \lesssim V \lesssim 15$ display our best relative photometric precision of $\sim 0.5\%$.

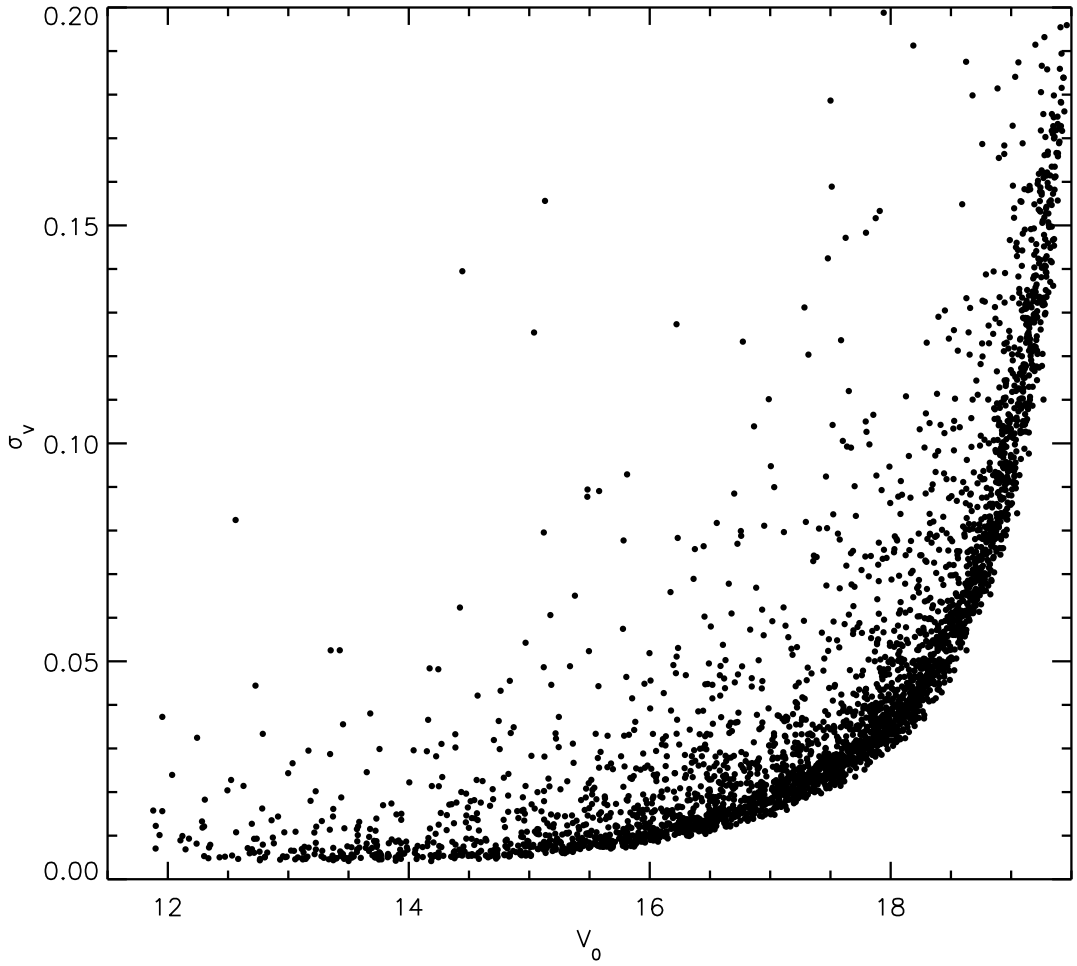

Fig. 4.3.— The standard deviation of the instrumental V magnitudes as a function of the true V magnitude (V_0) for stars in the field of M35. A first-order estimate of the true V magnitude has been obtained by applying a correction of $-3\overset{\text{m}}{.}238$, equivalent to the mean difference between the instrumental V magnitude and the V magnitude from Deliyannis (2005), plus an extinction correction of $3 \times E_{(B-V)} = 0\overset{\text{m}}{.}6$ (Deliyannis 2005). A relative photometric precision of $\sim 0.5\%$ is obtained for stars with $12\overset{\text{m}}{.}0 \lesssim V \lesssim 15\overset{\text{m}}{.}0$.

4.3.3 Photometric Period Detection

Periodic photometric variability, presumably due to spots on a rotating stellar surface, is a commonly used and measure of the stellar rotation period. In this section we describe the method

by which we detect periodic variability in our synoptic photometric database. We also discuss our assessment of the quality of these periods. We report periods for 443 stars in our sample.

We employed the Scargle (1982) periodogram analysis to detect periodic variability in the light curves because of its ability to handle unevenly sampled data. We apply the periodogram to search a grid of 5000 frequencies corresponding to periods between 0.1 day and 90 days. The lower search limit was set at the Nyquist critical frequency for our high-frequency data ($f_c = 1/(2\delta t) \simeq 2$ hours $\simeq 0.1$ day), while the upper limit was set at 90 days because a star with a 90-day period would complete about 1.5 cycle if it has data spanning all 143 nights.

Typically, a false alarm probability (FAP), the probability that a signal detected at a certain power level could have been produced by statistical fluctuation, is quoted as the statistical measure of confidence in a detected period. An analytical expression for estimating a FAP is given bye Scargle (1982) and Horne & Baliunas (1986). However, these methods are not entirely suitable when applied to synoptic studies of young stars because they only test against random fluctuations of a purely statistical nature (i.e., measurement errors) and additionally do not account for correlated fluctuations intrinsic to the source such as variability on timescales long compared to the sampling frequency. For such objects our repeated measurements during a single night are not independent and uncorrelated. Consequently, these analytical expressions estimating a FAP will likely overestimate the significance of any measured periodic variability.

Hence, we employ a two-dispersion Monte Carlo method for estimating the FAP of our detected periods, as per Herbst & Wittenmyer (1996). For each candidate star, we generate a set of 100 synthetic light curves, each consisting of normally distributed noise with two dispersions: one representing the variability of the candidate star during a night and one representing the night-to-night variability of the candidate star. We estimate the former by taking the mean of each night's standard deviation, and we estimate the latter by taking the standard deviation of nightly means. In this way, the test light curves have the freedom to vary on timescales that are long compared to our sampling interval, allowing them to mimic the random slow variability of stellar origin that could produce spurious periodic behavior over our limited observing window. We compute a periodogram for each test light curve and take the maximum observed power level in these 100 periodograms as the level

of 1% FAP. We adopt this measure of FAP as our basic criterion for accepting or rejecting detected photometric variability; we accept only periods whose periodogram signals are stronger than the power corresponding to the 1% FAP level. With this technique we have determined stellar rotation periods for 443 stars in our database. All rotation periods are listed in Table B.1 in Appendix B.

We do not have multiple seasons of observation or observations in multiple filters at our disposal by which to assess the credibility of our rotation periods. However, the good quality of our detected periods is supported by an observed correlation between photometric period and rotational line broadening within a subset of 16 stars. Figure 4.4 shows the projected rotation velocities measured by Barrado y Navascués et al. (2001) for 16 stars with known rotation periods. Each of the 16 stars have been included in our spectroscopic survey (described in Section 4.4) and have between 1 and 4 radial-velocity measurements. The standard deviations ($\sigma_{RV} \lesssim 1\ km\ s^{-1}$) and the radial-velocity membership probabilities ($P(RV) \geq 60$) suggest that all 16 stars are single and members of M35. The shortest period stars ($P_r \lesssim 2.5$ days) show increasing $v \sin(i)$ with decreasing rotation period. For rotation periods of ~ 4 days or longer the upper limits on the projected rotation velocities are consistent with slower rotation. For comparison, the solid, dashed, and dotted curves indicate the relation between rotation period and the projected rotational velocity for a solar-like star with a 90^o, 70^o, and 50^o inclination of the rotational axis, respectively. Thus, for all 16 stars, the projected rotation velocities are consistent with the measured rotation periods.

4.4 The Spectroscopic Survey

Critical to any study of stars in open clusters is the ability to determine the likelihood that individual stars are or are not physically associated with the cluster, and thus share the same age, distance, and initial chemical composition. For the purpose of the current study, cluster membership allows us to determine the ages and masses of our sample of stars with detected rotation periods. In this section we determine cluster membership from measurements of stellar radial velocities. This work has the added benefit of providing information about stellar multiplicity.

M35 has been included in the WIYN Open Cluster Study (WOCS; Mathieu (2000)) since 1997. As part of WOCS more than 6000 spectra has been obtained of approximately 1500 solar-type stars in M35. From this extensive radial-velocity survey we have 1) calculated cluster membership

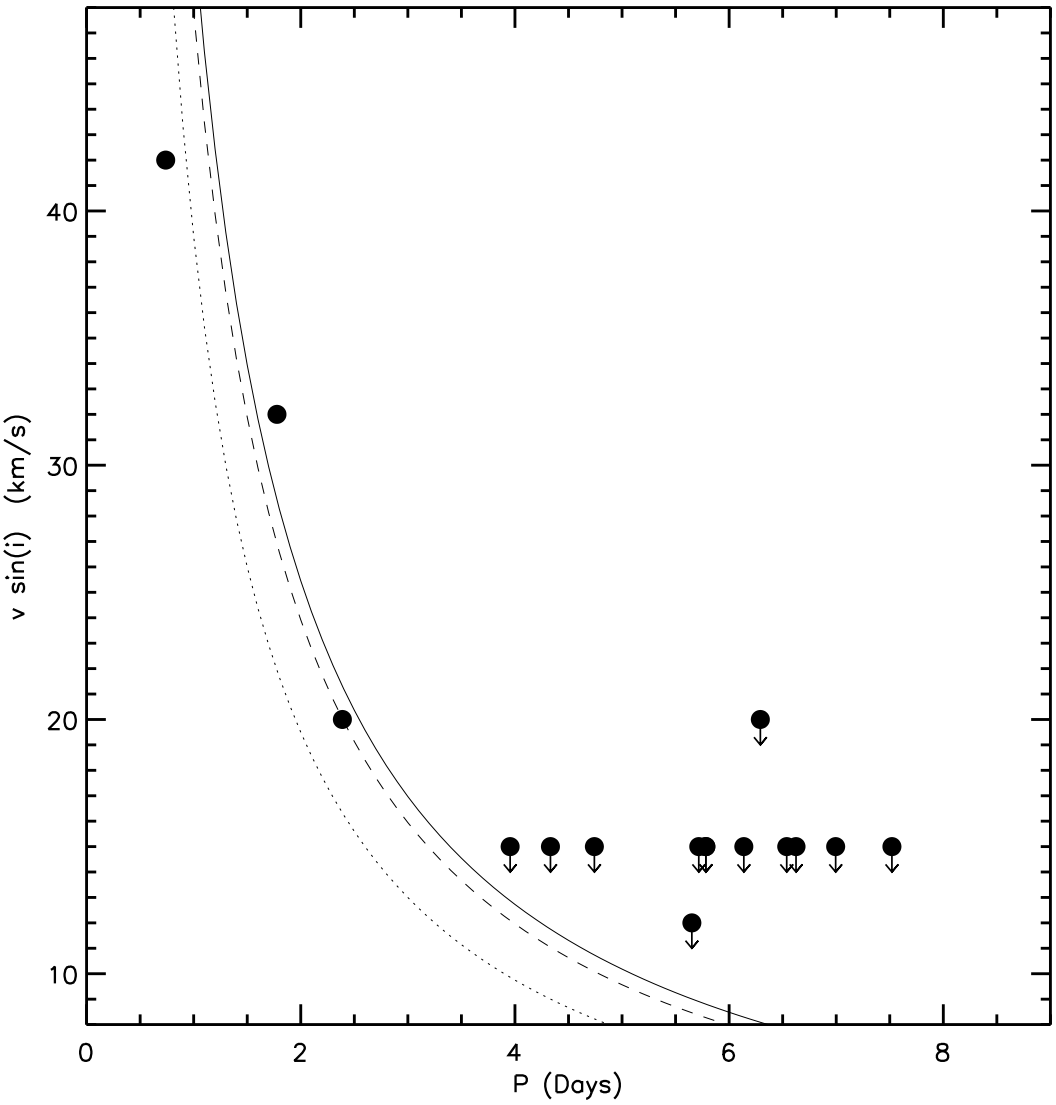

Fig. 4.4.— Projected rotation velocities (Barrado y Navascués et al. 2001) plotted against the measured rotation period for 16 stars in M35. All stars have $P(RV) \geq 60\%$ and none of the 16 stars are spectroscopic binaries. For comparison, the solid, dashed, and dotted curves indicate the relation between rotation period and the projected rotational velocity for a solar-like star with a 90^o, 70^o, and 50^o inclination of the rotational axis, respectively. The rotation periods and the projected rotation velocities are consistent for all 16 stars.

probability; 2) detected cluster binary stars; and 3) determined orbital parameters for the closest binaries. A detailed description of the radial-velocity survey will be presented in Braden et al. (2005); we give here the most relevant information.

The initial selection of M35 target stars for the spectroscopic survey used photometric and proper-motion criteria. Stars with $12\overset{m}{.}5 \lesssim V_0 \leq 16.0$ and $(B-V)_0 \gtrsim 0.4$ that fall on or less $\sim 1\overset{m}{.}0$ above the cluster main-sequence were selected. In stellar mass this selection corresponds to stars from $\sim 1.4\ M_\odot$ ($V_0 \simeq 12.4$, $(B-V)_0 \simeq 0.4$) to $\sim 0.7\ M_\odot$ ($V_0 \simeq 16$, $(B-V)_0 \simeq 1.1$), with solar mass stars at $V_0 \sim 15$. Proper motion studies of M35 by McNamara & Sekiguchi (1986) and Cudworth (1971) have faint-limits of $\sim 14\overset{m}{.}5 - 15\overset{m}{.}0$ in V. We excluded all stars with proper motion membership probabilities ($P(PM)$) less than 10%.

All spectroscopic data were obtained using the WIYN 3.5m telescope equipped with a multi-object fiber optic positioner (Hydra) feeding a bench mounted spectrograph. For M35 typically 82-85 fibers are positioned on stars within the 1-degree diameter field, while the remaining fibers are used for measurements of the sky background. We use the $3''$ diameter fibers optimized for blue transmission, and the spectrograph is configured with an echelle grating and an all-transmission optics camera providing high throughput at a resolution of $\sim$ 20,000. All observations were done at central wavelengths of 5130Å or 6385Å with a wavelength range of $\sim$ 200Å providing rich arrays of narrow absorption lines. Radial velocities with a precision of $\lesssim 0.5\ km\ s^{-1}$ (Hole et al. 2005; Meibom et al. 2001) are derived from the spectra via cross-correlation with a high S/N sky spectrum.

At present the radial-velocity survey of M35 has resulted in a sample of 50 spectroscopic binaries for which orbital solutions have been derived. The orbital periods span 2.25 days to $\sim$4500 days, corresponding to separations from 0.04 to $\sim$ 6 AU assuming a 1 $M_\odot$ primary and a 0.5 $M_\odot$ secondary component.

Of the 443 stars with rotation periods presented in this study, 259 have one or more radial-velocity measurements (the remainder being below our faint limit of the spectroscopic survey or photometric non-members). The radial-velocity cluster membership probability (P_{RV}) of each star is calculated using the formalism by Vasilevskis et al. (1958)

$$P_{RV} = \frac{C(RV)}{C(RV) + F(RV)} \tag{4.1}$$

where $C(RV)$ and $F(RV)$ represent the values of a dual Gaussian fit to the cluster and field radial velocity distributions, respectively. The mean or center-of-mass radial velocity of a single or binary star was used when calculating the membership probability. In M35 a radial velocity equal to the cluster velocity gives a membership probability of 94% and deviations of 1σ, 2σ, and 3σ from the mean of the Gaussian distribution of cluster velocities correspond to membership probabilities of 91%, 70%, 18%, respectively. Figure 4.5 shows the distribution of radial-velocity membership probabilities for stars in M35. The insert in Figure 4.5 shows the distribution of proper-motion membership probabilities from McNamara & Sekiguchi (1986) and Cudworth (1971). We have adopted $P(RV) \geq 50\%$ as the criteria for cluster membership. The proper-motion membership probability ($P(PM)$) is considered if available, with $P(PM) \geq 50\%$ as the criteria for cluster membership.

Of the 259 rotators with one or more radial-velocity measurement, 203 are radial-velocity members of M35 ($P(RV) \geq 50\%$) and 20 of those 203 stars are also proper-motion members ($P(PM) \geq 50\%$). Importantly, 14 rotators are members of binary systems for which we have determined binary orbital parameters. Twelve of these 14 binaries have been discussed in detail in Meibom et al. (2005) in the context of tidal synchronization. Two were excluded from that discussion because of large uncertainties on the orbital eccentricities. Five rotators are members of candidate binaries and 53 rotators are single stars. These single and binary rotators will be the focus of our discussion on the effect of binarity on stellar angular momentum evolution in Section 4.6.5.

4.5 UBVRI Photometry and the M35 Color-Magnitude Diagram

Figure 4.6 shows the (V-I) vs. V CMD for M35. The photometry was kindly provided by Deliyannis (2005). They obtained UBVRI data in a $23' \times 23'$ central field and BVRI data in a 2×2 mosaic for a total of $40' \times 40'$. All images were taken with the WIYN 0.9m telescope, and absolute PSF photometry was performed using the IRAF DAOPHOT package Landolt standard stars. The location in the M35 CMD of the 443 stars for which we have determined rotation periods are highlighted with large black dots in Figure 4.6. We utilize the well-defined cluster sequence in the CMD to assign photometric membership to 344 rotators located between the solid lines above and

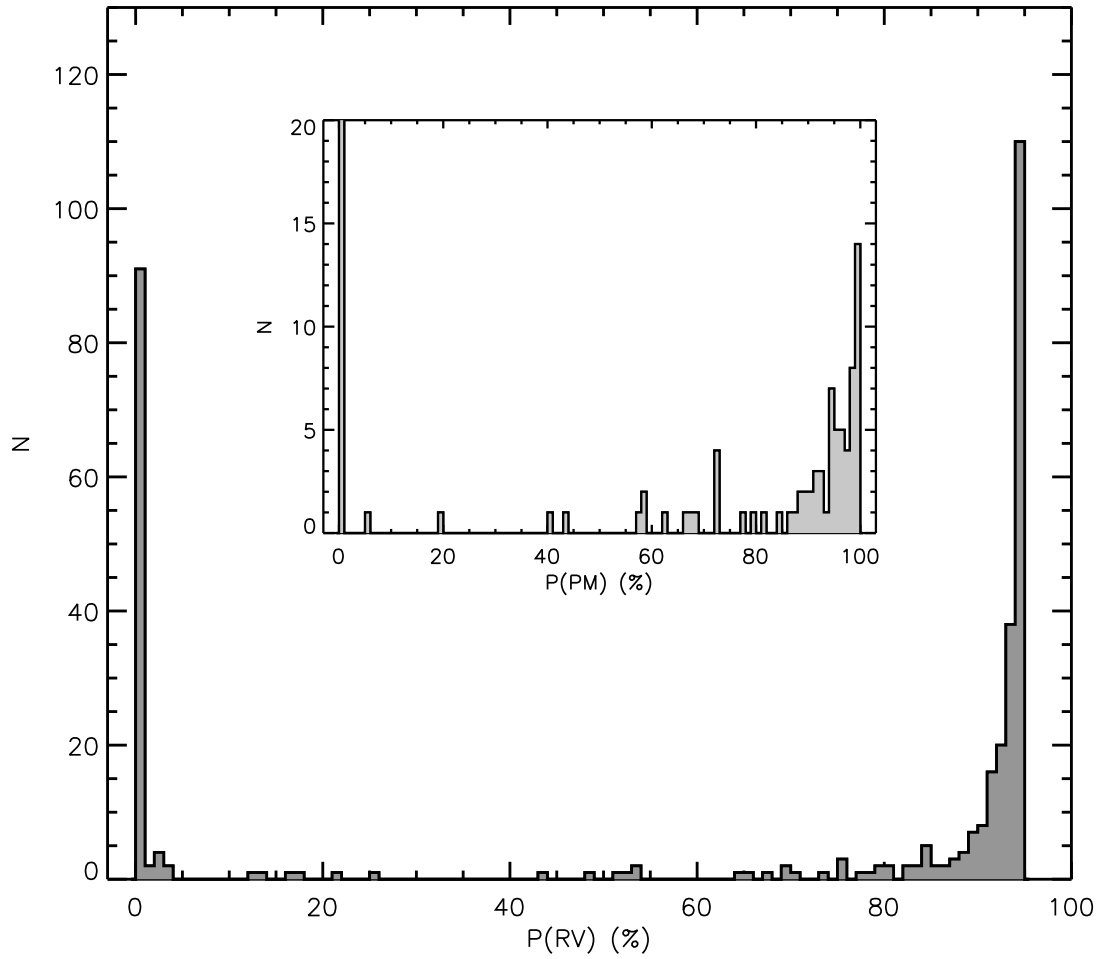

Fig. 4.5.— The distribution of radial-velocity membership probabilities. The insert shows the distribution of proper-motion membership probabilities from McNamara & Sekiguchi (1986); Cudworth (1971).

below the cluster main-sequence. The faint limits on photometric membership are put at the lower envelope of the cluster sequence and the bright limits are set to allow for a sequence of binaries $\sim 0\overset{\mathrm{m}}{.}75$ brighter. Due to the breadth of the blue ($(V-I) \lesssim 1.1$) part of the cluster main-sequence we were forced to be somewhat generous in our photometric membership criteria in that part of the CMD. Consequently a small sample of 11 stars fall suspiciously below the cluster main-sequence. None of these stars were radial-velocity and/or proper-motion members of M35 and we changed their status

to photometric non-members. An additional 23 photometric members have 3 or more radial-velocity measurements and a radial-velocity membership probability (P(RV)) of less than 50%. Those 23 stars were also removed from the list of photometric members. The final number of stars selected as photometric members of M35 is 310. The insert in Figure 4.6 shows the location in the M35 CMD of radial-velocity members (203 stars; open symbols), and radial-velocity and proper-motion members (20 stars; filled symbols). One star ($V_0 \simeq 16\overset{\text{m}}{.}7, (V-I)_0 \simeq 1\overset{\text{m}}{.}6$) falls above the bright limit for photometric membership but is a radial-velocity member based on a single measurement.

4.6 Results and Discussion

We present in this section our observational results and discuss their implications for the various questions relating to the evolution of angular momentum in single and binary stars. Specifically, we consider 1) the distribution of stellar rotation periods in M35; 2) the dependence of rotation period on stellar mass (the color-period diagram); and 3) the effect of a stellar companion on the early evolution of stellar rotation.

4.6.1 The Rotation Period Distribution

We have determined rotation periods on the basis of periodic photometric variability for 443 stars in the field of the open cluster M35. We designate 310 of the 443 stars as being photometric late-type members of M35, corresponding to ∼16% of the cluster population within the brightness limits of our photometric survey. Of the 310 photometric members, 202 have independently confirmed membership from one or more radial-velocity measurements. In this section we describe the rotation-period distribution of the 310 cluster members and inspect the short- and long-period extremes of the period distribution to assess the appropriateness of the upper and lower limits in our period search.

Figure 4.7 presents the distribution of rotation periods in M35, which spans more than 2 orders of magnitude from $\sim$ 0.1 days to $\sim$ 15 days. The distribution has structure, in particular a narrow peak at approximately 1 day and a broader and shallower population centered at about 6 days. We will discuss the origins of this structure in detail when we examine the distribution of rotation periods as a function of stellar color (mass) in Section 4.6.2.

In Figure 4.8 we display the short-period extreme of the rotation period distribution with

an increased resolution of 0.1 day. The dashed and grey histograms, respectively, represent all stars with detected rotation periods and all cluster members with detected rotation periods. The distribution shows that we are capable of detecting rotation periods down to the pseudo-Nyquist period-limit of about 2 hours ($\sim$ 0.08 day) resulting from our typical sampling cadence of about 1 hr^{-1}. The distribution of rotation periods for cluster members falls off shortward of 0.3-0.4 days. Only two member stars have rotation periods between 0.1 days and 0.2 days, corresponding to surface rotational velocities of 50% or more of their breakup velocities ($v_{br} = \sqrt{(GM_\star/R_\star)}$). We argue based on this inspection of the short-period tail of the distribution that the lower limit of 0.1 days for our period search was set appropriately for the stars in M35. (Two field stars have rotation periods below 0.1 day as a result of follow-up inspection of their individual data/light curves).

The long-period extremes of the period distributions for members and non-members (see Appendix C) show that the long time-span of the synoptic data enable us to detect the rotation of stars with periods beyond the $\sim$10 days typically found to be the upper limit in photometric surveys over 2-3 weeks. We report the detection of 16 stars with rotation periods longer than 10 days, and a longest detected rotation period of 23.2 days. From Figure 4.7 it seems evident that the rotation-period distribution of the 150 Myr M35 population has a physical upper limit of $\sim$10 days, well below the upper limit of our period search. We note that this statement is true only if the $\sim$16% of the clusters late-type population presented here, is a representative sample of the late-type stellar population in M35. The small sample of stars with periods above 10 days will be discussed further in Section 4.6.4.

4.6.2 Rotational Evolution and the Color-Period Diagram

We next analyze the rotation period distribution as a function of stellar mass, or equivalently for main-sequence stars, the stellar color index. Diagrams showing the rotational velocity as a function of stellar color appeared first in the literature for $v \sin(i)$ studies of the Pleiades (e.g. Stauffer & Hartmann 1987; Soderblom et al. 1993a) and provided evidence for sub-populations in the distribution of projected rotational velocities with color. The emerging structure in the distribution of rotational velocities with color led Soderblom et al. (1993a) to propose the idea of core-envelope decoupling and reconnection, to explain in particular the population of slow rotators.

Figure 4.9 presents the rotation periods for the 310 photometric members of M35 against their $B-V$ color index (hereinafter the color-period diagram). The colors are taken from the deep multi-band photometry by Deliyannis (2005, Section 4.5) and stellar masses are estimated using a 150 Myr Yale stellar evolutionary model (Yi et al. 2003) fit to the Deliyannis color-magnitude diagram. Radial-velocity members ($P(RV) \geq 50\%$) of M35 are highlighted in black and stars with proper-motion membership probability above 50% ($P(PM) \geq 50\%$) are marked with squares.

The structure in the M35 color-period diagram is striking. The majority of the stars fall on two sequences. One sequence starts at the blue end at $(B-V)_0 \simeq 0.5$ ($M_\star \simeq 1.2\ M_\odot$) and $P_r \simeq 2$ days, and forms a rich diagonal band of stars whose periods are increasing with (B-V). This sequence terminates at about $(B-V)_0 \simeq 1.2$ ($M_\star \simeq 0.65\ M_\odot$) and $P_r \simeq 10$ days. The second sequence consists of a tight sequence of rapid rotators ($P_r \lesssim 1$ day) extending from $(B-V)_0 \simeq 0.7-0.8$ ($M_\star \simeq 0.9-1.0\ M_\odot$) to $(B-V)_0 \simeq 1.5$ ($M_\star \lesssim 0.5\ M_\odot$). This well defined sequence of rapid rotators shows a small but steady decrease in rotation period with increasing color. A smaller number of stars are distributed in between the two sequences, and 10 stars have rotation periods that are abnormally slow, placing them above the rich diagonal band in Figure 4.9. The two primary loci of stars in the M35 color-period diagram provide an evident explanation for the structure observed in the one-dimensional period distribution (Section 4.6.1).

Similar structure in cluster color-period diagrams were recently discussed by Barnes (2003). From a compilation of rotation-period data Barnes produced color-period diagrams for cluster populations of mid F to early M dwarfs over a range of ages from the 30 Myr to 600 Myr. He further extended the age range to 800 Myr and solar age by inclusion of the (non-coeval) "young" and "old" populations of Mount Wilson stars (Baliunas et al. 1996). We show in Figure 4.10 Figure 1 from Barnes (2003) which displays the color-period diagrams for the coeval stellar populations considered by Barnes. Barnes identified distinct sequences and gaps in the color-period diagrams and noticed a progressive evolution of the location and richness of these sequences. We give here a brief summary of the results from Barnes (2003) most relevant to the current study.

Barnes named the broad diagonal sequence of stars with rotation periods increasing with color as the *interface* sequence (or I sequence) and the narrow sequence of rapidly rotating stars as the

convective sequence (or C sequence). The dependence on color (mass) and age of the rotation periods of the stars on the two sequences led Barnes to suggest an underlying mechanism for the rotational evolution of these late-type stars. Specifically, he argued that stars on the C sequence have radiative cores and convective envelopes that are decoupled, and that the evolution of their surface rotation rates is governed primarily by the moments of inertia of the convective envelope and by inefficient wind-loss of angular momentum (spin-down) driven by a small-scale convective (turbulent) magnetic fields. On the other hand, stars on the I sequence have large-scale (sun-like) magnetic fields provided by interface dynamos that also couple the cores and envelopes of these stars. The rotational evolution of the I sequence stars is primarily governed by the moments of inertia of the entire stars and more efficient angular momentum loss due to stronger winds driven by the dynamo field (i.e., a Skumanich (1972) style spin-down). Accordingly, Barnes suggests that a late-type star, in which the core and envelope are decoupled as it settles on the ZAMS, will evolve from the C sequence through the gap and onto the I sequence when the rotational shear between the stellar core and envelope establish a large-scale dynamo field that in turn couples the two zones. Higher mass stars have thinner convective envelopes with smaller moments of inertia than low mass stars, and thus leave the C sequence sooner. Stars that are either fully radiative or fully convective will remain as rapid rotators.

Based on the observed evolution of the shape and location of the two sequences and the fractional numbers of stars on each sequence, Barnes argued that the color-period diagram can be used in ways similar to the color-magnitude diagram. In that spirit Barnes followed the evolution of stars from the C sequence through the gap and onto the I sequence by counting stars on the two sequences and in the gap for each coeval population. He provided estimates for the timescales of stellar spin-down on each sequence as a function of stellar mass and for a time-scale over which stars move through the gap. He further constructed a set of rotational isochrones to be fit to the two sequences in the color-period diagram, giving a new "rotational" age of the stellar population.

With one of the largest samples of stellar rotation periods, M35 represents an excellent new opportunity to test and apply the ideas set forth by Barnes (2003). It is immediately evident from Figure 4.9 and Figure 4.10 that M35 shows perhaps the most striking example yet of the I and C sequences. In the following we compare the M35 color-period diagram to those of younger and older

cluster populations. We then apply the analytical tools developed by Barnes to the M35 color-period diagram. Specifically, we: 1) estimate the times it takes for all G and K dwarfs, respectively, to leave the C sequence; 2) calculate the characteristic timescales for stellar spin-down of G and K dwarfs on the C sequence; 3) determine the relative fractions of stars on the C and I sequences and in the gap and place M35 in the "Fraction vs. Age" diagram (Figure 3 in Barnes 2003); and 4) fit the proposed rotational isochrones (Barnes 2003) to the M35 sequences using an independently determined age for M35. Finally, we propose a new explanation for the abnormally slowly rotating stars located above the M35 I sequence.

When compared to color-period diagrams of younger and older clusters (see Figure 4.10), the M35 color-period diagram (Figure 4.9) shows convincing support of the idea that stars evolve from the C sequence through the gap and onto the I sequence, and that the timescale for this evolution is inversely proportional to the stellar mass. In M35 few G dwarfs are found on the C sequence and in the gap, while the I sequence is rich in G dwarfs and well defined. The M35 C sequence and gap are rich in K dwarfs, whereas the I sequence is less densely populated with stars in that color- (mass-) range. The lack of C sequence G dwarfs seen in M35 is already apparent at 100 Myr in the Pleiades color-period diagram although the Pleiades I sequence is not as rich and well defined as the M35 I sequence. These observations indicate that the timescale for G dwarfs to evolve off the C sequence and onto the I sequence is approximately 100-150 Myr. Correspondingly, the rich population of K dwarfs on the M35 C sequence is gone by the age of NGC3532. In NGC3532 the early and mid K dwarfs have evolved off the C sequence and onto a well defined I sequence, leaving only few early and mid K dwarfs in the gap. The NGC3532 C sequence and gap, however, is populated by late K dwarfs. These observations imply that all early to mid K dwarfs evolve onto the I sequence on a timescale between 150 and 300 Myr, or approximately twice the time required for G dwarfs. Finally, by the age of the Hyades only few late K or early M dwarfs have been found on the C sequence or in the gap, suggesting that such stars evolve off the C sequence and possibly onto the I sequence over less than 600 Myr, or twice the time required for the early to mid K dwarfs.

We can also use the M35 color-period diagram to measure the characteristic exponential timescales for the rotational evolution of stars on the C sequence. Our ability to detect rotation

periods over more than two orders of magnitude combined with spectroscopic and photometric membership information makes the M35 color-period diagram particularly suitable for such timescale estimates by counting stars on the two sequences and in the gap. When counting the number of stars we use the following criteria. Stars located in the color-period diagram between the lines represented by $P_r = 10(B-V)_0 - 2.5 \pm 2.0$ and with periods above 1.5 days were counted as I sequence stars. Stars redder than $(B-V)_0 = 0.6$ and with periods between 0 and 1.5 days were counted as C sequence stars. Stars located below $P_r = 10(B-V)_0 - 4.5$ and with periods above 1.5 days were counted as gap-stars. These selection criteria are subjective and although the sequences are well defined the I sequences, in particular, becomes broader and less well-defined redward of $(B-V)_0 \simeq 1.0$. However, due to the large number of rotation periods found in M35, the small number of stars that might be moved from the gap to the I sequence and vice versa will not influence the relative fractions and thus the timescales in any significant way.

We count the number of stars on the C sequence (N) and the total number of stars on the C and I sequences plus in the gap (N_0) within the color intervals corresponding to G and K dwarfs. Using 150 Myr as the age of M35 we derive $\tau_C^G = 60$ Myr and $\tau_C^K = 140$ Myr as the characteristic exponential timescales for stellar spin-down on the C sequence for G and K dwarfs, respectively.

Figure 4.11 adds M35 to Figure 3 in Barnes (2003) which show the evolution with time of the relative fractions of stars with $0.5 \leq (B-V)_0 \leq 1.5$ on the I sequence, C sequence, and C sequence plus gap stars. M35 fits remarkably well with the evolutionary trends previously seen for the I and C sequence populations. M35 is the youngest cluster for which the number of stars on the I sequence exceed the number of stars on the C sequence. In fact, we find in M35 that the I sequence contains twice as many stars as the C sequence, whereas in the Pleiades Barnes finds that the fractions of I and C sequence stars are approximately equal. We conclude that the I sequence is the dominant sequence overall after about 100 Myr.

4.6.3 Fitting Rotational Isochrones to the M35 Color-Period Diagram

The color- and time-dependence on the abundance and morphology of the I and C sequences inspired Barnes (2003) to construct a set of rotational isochrones for late-type stars. A heuristic functional form was chosen to represent the color dependence of each sequence at a given age (see

Barnes (2003) eqs. [10] and [15]). The function defines a one-parameter family, with that parameter being the age of the stellar population. The resulting curves in the color-period plane represent a set of rotational isochrones.

The well-defined sequences in the M35 color-period diagram together with the independently determined stellar-evolution age for M35 of 150 Myr (von Hippel et al. 2002; Deliyannis 2005), make possible a suitable test of the rotational isochrones proposed by Barnes. We show in Figure 4.12 the rotational isochrones for an age of 150 Myr overplotted on the M35 color-period diagram. The isochrones fit the M35 I and C sequences very well, suggesting that the rotational isochrones proposed by Barnes can indeed provide an accurate age-estimate for a coeval stellar population based on a well populated color-period diagram.

4.6.4 Prediction: Tidal Evolution in Close Binaries Responsible for Abnormally Slow Rotators

Ten stars in the M35 color-period diagram do not fit into the scenario described by Barnes (2003) and discussed above. These stars are located above the I sequence and are rotating with rates that are abnormally slow compared to their fellow stars located on the I sequence or below. All 10 stars are photometric members of M35 and 2 are photometric and spectroscopic members. We note that in NGC3532 a similar pattern is seen with 7 stars located above the I sequence. Why has the rotational evolution of these stars deviated significantly from that of most similar stars in M35? We propose that tidal interactions with a close stellar companion, synchronizing the stellar spins to the orbital motions, is responsible for the slower than expected rotation of these stars. Accordingly, we predict that the 10 stars in M35 are the primary stars in binaries with periods of approximately 10-15 days.

This proposition finds support from 2 of the 10 stars which are both photometric and radial-velocity members of M35. Located in the color-period diagram at $(B-V)_0 = 0.68$ and $P_r = 10.13$ days is the primary of a circular binary ($e = 0.016$) with an orbital period of 10.33 days. The rotation of the primary star in this binary has been synchronized to the orbital motion of the companion (Meibom et al. 2005), forcing it to rotate more slowly than a similar mass but single star in M35. Located closer to the M35 I sequence at $(B-V)_0 = 0.57$ and $P_r = 6.03$ days is the primary star of a highly

eccentric ($e = 0.55$) binary with an orbital period of 12.28 days. The rotation of the primary star in this binary has not yet been pseudo-synchronized (synchronized to the average angular velocity near periastron; Meibom et al. (2005), but the tidal evolution within this binary is presumably responsible for its location above the I sequence. Continued tidal evolution of this binary will circularize the orbit and synchronize the stellar spins to the orbital motions (Hut 1981; Zahn 1989; Witte & Savonije 2002) likely moving the location of the primary star even higher above the I sequence.

In addition to the two spectroscopic binaries, 3 of the remaining 8 slow rotators are photometric binaries. Spectroscopic observations of those stars and of the remaining 5 stars will be carried out in the near future to determine their status as binary or single stars, and in the case of binarity, the degree of tidal evolution.

4.6.5 The Effect of Binarity on the Stellar Angular Momentum Evolution

Stars in the closest binary stars continue to affect each others angular momentum evolution by tidal interactions throughout the PMS and main-sequence phases (e.g. Duquennoy et al. 1992; Mathieu et al. 1992; Melo et al. 2001; Meibom & Mathieu 2005). Such tidal interactions drive an exchange of stellar and orbital angular momentum at rates that are highly sensitive to the stellar separation and thus effective only in the closest binary stars ($a \lesssim 0.2$ AU). However, in wider binaries, the two stars may still indirectly influence each others rotational evolution through tidal and resonant gravitational interactions with the circumstellar and circumbinary disks.

Models of star-disk interactions in close binaries ($a \lesssim 100$ AU) predict that the presence of a companion star will truncate (Artymowicz & Lubow 1994; Armitage & Clarke 1996) and potentially tidally disrupt (Pringle 1991; Artymowicz 1992) the circumstellar disks. It has also been suggested that a gravitational torque on the circumstellar disk by the orbiting companion can lead to an enhanced rate of mass-accretion onto the star (Papaloizou & Terquem 1995; Korycansky & Papaloizou 1995). These models thus predict that the mass, size, and lifetime of circumstellar disks may be reduced for stars in close binaries as compared to wider binaries and single stars.

Observationally, the spectral energy distributions of some but not all, close PMS binaries, Jensen & Mathieu (1997) see indications of cleared gaps or holes in the circumbinary disks. Also, millimeter-wave flux from binaries with separations on the order of $\sim 50-100$ AU is reduced compared

with that of wider binaries or single stars (Jensen et al. 1994, 1996). However, measurements of infrared excess has provided evidence that circumstellar material can survive the binary formation process (Mathieu 1994; Simon & Prato 1995).

If indeed a binary companion does affect the mass, size, and lifetime of circumstellar disks, and if star-disk interactions play a key role in the rotational evolution of late-type stars, e.g. as suggested in the theory of magnetic star-disk interactions (Koenigl 1991; Bouvier et al. 1993; Shu et al. 1994; Ostriker & Shu 1995), one will expect to observe a relationship between binarity and stellar rotation on the ZAMS. However, the effect of binarity, and our ability to observe it, may depend on both stellar and binary parameters such as age, binary semi-major axis, and binary mass-ratio.

Bouvier et al. (1997b) and Patience et al. (2002) searched for a relationship between rotational velocity and binarity among late-type dwarfs in the Pleiades and α Persei, respectively. Bouvier et al. (1997b) studied 25 binaries ($a \simeq 10 - 1000$ AU) among 144 G and K dwarf members of the Pleiades. The binaries were identified as close photometric pairs in near-infrared images using adaptive optics. The physical separation was computed from the projected separation and the distance to the Pleiades from Mermilliod et al. (1992). Bouvier et al. used projected rotational velocities of the primary binary components and the single stars from Stauffer et al. (1984), Stauffer & Hartmann (1987), Soderblom et al. (1993a), Allain et al. (1996), and Queloz et al. (1998). They found no evidence for a relationship between binarity and rotation in the Pleiades. Their study showed that the fraction of binaries among slow and fast rotators of the Pleiades is the same, and that the distribution of $v \sin(i)$ among primaries of binary systems is the same as among single stars.

In a similar study Patience et al. (2002) explored a relation between rotation and binarity in α Persei. Using high-angular-resolution speckle imaging they surveyed 71 solar-type stars and detected 16 binaries with separations ranging from 10 to 581 AU. Like Bouvier et al. (1997b) they found no statistically significant difference between the ratio of binaries among the fast and slow rotators in α Persei. However, Patience et al. did report that, based on a two-sample K-S test, the distribution of projected rotational velocities for binaries with separations between 10-60 AU is different at the 98% level from the distribution of projected rotational velocities for wider binaries. The 4 close binaries in their sample have values of $v \sin(i)$ higher than any of the 12 wider binaries (see their Figure 10)

and Patience et al. thus argued that their data reveal a trend of increased rotational velocity with smaller binary separation. As noted by Patience et al., their result is preliminary and needs to be confirmed. In fact, the size of their sample of binaries with separations less than 60 AU (4 binaries) is the minimum for a K-S test to be meaningful (Press et al. 1992).

The results by Bouvier et al. and Patience et al. are contradictory. Both studies detect samples of binaries with comparable sizes and similar distributions of separations, and both studies were conducted using imaging techniques that made them unable to detect binaries closer than about 10 AU. Our spectroscopic survey of M35 is sensitive to binaries with separations of less than ~ 5 AU and thus explore a new interesting domain of even closer binaries. The relative sizes and lifetimes of PMS circumstellar and circumbinary disks is predicted to be sensitive to the binary semi-major axes. Importantly, in binaries with semi-major axes of $\sim$5 AU or less, the truncated circumstellar disks may be tidally disrupted or accreted on short timescales compared to larger disks in wider binaries. Accordingly, the rotational evolution of the binary components may differ.

Using the photometric and spectroscopic data for the late-type stars in M35 we wish to test for a relationship between binarity and stellar rotation. Of the 202 stars with rotation periods and radial-velocity membership, 155 stars have 3 or more radial-velocity measurements. Three or more radial-velocities allow us to test for variability indicative of a close companion star. More precisely, we can spectroscopically distinguish stars with a close stellar companion ($a \lesssim 5$ AU) and stars that are either single or have a stellar companion at a distance of approximately 5 AU or more (hereinafter called "single"). We apply the following criteria for determining whether a star is single or member of a binary system:

Single star: $N_{RV} \geq 3$, $\sigma_{RV} \leq 0.5\ km\ s^{-1}$, and photometrically single.

Binary star: $N_{RV} \geq 3$ and $\sigma_{RV} \geq 1.5\ km\ s^{-1}$.

where N_{RV} denotes the number of radial-velocity measurements, σ_{RV} the standard deviation of these measurements, and "photometrically single" refers to a star being located on the "single" star cluster sequence in the M35 CMD.

The two radial-velocity thresholds are justified based on our radial-velocity measurement precision of $\lesssim 0.5\ km\ s^{-1}$. Stars with $\sigma_{RV} \leq 0.5\ km\ s^{-1}$ therefore are stable at or below the 1 σ level,

and stars with $\sigma_{RV} \geq 1.5\ km\ s^{-1}$ vary at or above the 3 σ level. We have not considered stars in the grey-zone between single and binary: $0.5\ km\ s^{-1} \gtrsim \sigma_{RV} \lesssim 1.5\ km\ s^{-1}$. On the basis of these criteria we find 53 single stars and 19 binary stars from the sample of 155 stars with rotation periods. Of the 19 binaries 14 have known orbital parameters and their binary status is secure (see Meibom & Mathieu 2005). In 2 of the 14 binaries the stellar rotation of the primary star has been tidally synchronized to the orbital motion of the companion (Meibom et al. 2005). We will exclude those 2 binaries for the purposes of the discussion here as we are concerned with effects other than tidal interactions. Of the 5 remaining binaries 3 have radial-velocity standard deviations of 8.3 $km\ s^{-1}$, 5.9 $km\ s^{-1}$, and 5.1 $km\ s^{-1}$ (based on N_{RV} = 24, 12, and 10, respectively) significantly above 1.5 $km\ s^{-1}$. Orbital solutions will likely be determined for these systems within 1 or 2 observing seasons. The remaining 2 binaries have standard deviations of 1.8 $km\ s^{-1}$ and 1.6 $km\ s^{-1}$ based on 3 and 4 velocities, respectively. Careful inspection of each individual spectrum and cross-correlation function (peak) leaves no reason to doubt the quality of the derived radial velocities for these two stars, and so we keep the stars in the binary-star sample. We refer to Table 2.1 in Meibom & Mathieu (2005) for orbital data on the 14 binaries with orbits.

By design, our spectroscopic observing program is targeting close binary stars and thus gives lower priority to stars with radial-velocity variations within the expected uncertainty. Accordingly, the 53 single stars have only between 3 and 5 velocity measurements. The minimum separation in time of any pair of velocity measurements of the 53 stars is $\sim$ 50 days. The small velocity dispersions of these stars are therefore not a result of insufficient time-sampling of the velocity curve. Still, we cannot rule out the possibility that these stars are indeed long period binaries. By inspection of the radial-velocity data for our longest period binaries in M35 with known orbital parameters, we find that only for binaries with $a \gtrsim 5$ AU is one likely to measure 3 consecutive radial-velocities, 50 days or more apart, with a standard deviation of less than 0.5 $km\ s^{-1}$. We thus propose a conservative empirical lower limit of $\sim$ 5 AU on the separation of potential binaries among the 53 stars.

We show in Figure 4.13 the rotation-period distributions of the single stars (grey histogram) and of the binary stars (excluding the 2 tidally synchronized systems; transparent histogram). The distribution of rotation periods for the single stars is well defined and "bell-shaped" (a least squares

fit of a Gaussian function to the single star distribution is shown in Figure 4.13). The distribution have a mean value of 4.6 days with a standard error on the mean of 0.18 days. The distribution of rotation periods for the binary stars, while less well-defined, appears to have a definite peak at approximately 3 days, and the mean of the 17 rotation periods does fall at 3.1 days. The mean of the binary rotation-period distribution thus fall more than 8 σ shortward of the mean of the single star distribution, suggesting that the binary star distribution is not drawn from the same parent distribution as the single star distribution.

A non-parametric statistical test of the difference of the two distributions is the Kolmogorov-Smirnov (K-S) test. We performed a two-sample K-S test of the single star rotation period distribution against the binary star rotation period distribution. The result in that there is only a 0.11% probability that the two distributions derive from the same parent distribution. We performed a second two-sample K-S test of the single star rotation period distribution against a more conservative sample of binary rotation periods including only binaries with known orbital parameters. The result of this second K-S test is a 1.4% probability that the two distributions derive from the same parent distribution.

The analysis of the period distributions for single and binary stars lead us to conclude that there is a statistical significant difference between the two distribution in their current shape and size. The offset of the binary star distribution toward shorter rotation period suggest that the primary stars in close binaries ($a \lesssim 5$ AU) rotate on average faster than single stars or than primary stars in binaries with separations of ~ 5 AU or more. Note, that the on average faster rotation is not due to tidal synchronization as synchronized binaries were excluded.

This result is interesting because it provides a new observational constraint on models of star-disk interactions and their affect on the angular momentum evolution of late-type stars in the PMS phase. The role of star-disk interactions in controlling the angular momentum evolution of late-type stars has received much theoretical and observational attention over the past two decades. Interactions between a PMS star and its disk has become an essential feature of most models of angular momentum evolution of solar-like stars, while, at the same time, the concept has been questioned on observational and theoretical grounds. Over the same period of time, models of star-disk interactions

have predicted that a close binary companion will affect the lifetime of circumstellar disks. These model predictions in combination with observations of high binary frequencies among PMS as well as main-sequence stars, call for observations of stellar rotation in close binary stars.

An interesting and relevant example of theoretical work modeling the effect of binarity on star-disk interactions and thus stellar rotation, was presented by Armitage & Clarke (1996). They construct models for the rotational evolution of solar-mass single and binary PMS stars whose spin is regulated by magnetic disk-braking. One result of their models is that stars in binaries with separations between $\sim$ 1-8 AU can retain a circumstellar ring of gas and dust between the corotation radius and the binary truncation radius. The particles in the ring are trapped by an inner magnetic torque from the star and an outer tidal torque from the companion. The existens of such a quasi-stable ring of disk material enable prolonged magnetic coupling between the star and the ring, and thus prolonged magnetic breaking of the stellar spin as compared to single stars. Consequently, in the models by Armitage & Clarke, stars in binaries with separations of $\sim$ 1-8 AU evolve to rotate slower than single stars of same age and mass.

The effect of binarity on stellar rotation observed for binaries in M35 is opposite to the effect predicted in the model by Armitage & Clarke. However, in general, models of magnetic star-disk interaction predict that shortening of the lifetime of a circumstellar disk due to truncation and/or tidal disruption by a close companion, will lead to faster stellar rotation on the ZAMS than for a similar single star (e.g. Bouvier et al. 1993). This was the hypothesis discussed and tested by Bouvier et al. (1997b) and Patience et al. (2002).

The results presented here for M35 is perhaps the strongest evidence yet for faster rotation among binary primary stars as compared to single stars of the same age and mass. The result suggest that a companion star within $\sim$ 5 AU does affect the rotational evolution of a late-type star in a way that leads to on average faster rotation at 150 Myr. Within the framework of current models of PMS stellar evolution, this finding imply that the lifetime of circumstellar disks in binaries with semi-major axes $\lesssim$ 5 AU is shorter than for single stars or stars in wider binaries.

Conceivably, other mechanisms controlling stellar rotational evolution, such as the hydromagnetic mechanism discussed above, can diminish or "blur" the influence of a close companion on

star-disk interactions during the PMS phase. The observable difference in the rotational evolution between single and close binary stars may thus diminish and become less significant with the age of the stellar population. Observational surveys of stellar rotation in close binaries and single stars in coeval populations of ages spanning from the ZAMS to the late main-sequence will be needed to find out.

4.7 Summary and Conclusions

The coexistence of ultra-fast and slowly rotating stars in young coeval populations of late-type main-sequence stars, discovered in the 1980's, fueled an interest in the early angular momentum evolution of such stars. Models of stellar rotational evolution, seeking to explain the large dispersion in stellar rotation rates and an emerging dependence of rotation rate on stellar mass, were until recently constrained by observational data that suffered from small stellar samples and/or ambiguities inherent to measurements of projected rotational velocities. Over the past decade, time-series photometric surveys of young open clusters have provided direct measures of stellar rotation for an increasing number of late-type stars. The result is a manifestation of well-defined relations between stellar surface rotation and stellar mass and age .

However, most stars, if not all, form in binary or multiple systems. Still, efforts to model the observed rotational evolution of late-type stars has primarily treated this as a single-star problem. Some theoretical and observational studies have been carried out to predict and search for the effect of binarity on the rotational evolution of late-type stars. To date, the observational studies searching for a relation between binarity and rotation have done so only among binaries wider than 10 AU, and the results are contradictory.

We have presented the results of an extensive time-series photometric survey and an ongoing spectroscopic survey of the solar- and late-type stars in the rich young open cluster M35 (NGC2168). M35 is particularly interesting from the point of view of studying early angular momentum evolution as it is slightly older than the Pleiades but much richer, and thus delineates the active phase of rotational evolution between the ZAMS and the Hyades.

We have obtained photometric light curves for 14022 stars with $12 \lesssim V \lesssim 20$ over a $40' \times 40'$ field centered on M35. We have determined the rotation periods for 443 stars. Of these 310 are

photometric members of M35, corresponding to $\sim$ 16% of the total number of cluster stars within the brightness limits of our photometric survey.

From our spectroscopic data we find that 202 of the 310 photometric members are also radial-velocity members of M35. We further use the spectroscopic data to identify short-period ($P \lesssim 4500$ days) binary stars among the M35 rotators. Among 155 M35 rotators with 3 or more radial-velocity measurements, we report 53 to be single stars or wide binaries ($a \gtrsim 5$ AU) and 19 to be close binary stars ($a \lesssim 5$ AU). (The remaining 83 stars do not meet out criteria for being either single or binary stars.) We compare the rotation period distributions of single and close binary primary stars to look for an affect of binarity on stellar angular momentum evolution.

The primary results of our study are:

1. With 310 rotation periods for late-type members, M35 appears as a new key cluster in studies of stellar angular momentum evolution. The 310 rotators span periods over two orders of magnitude from 0.1 day, or close to the breakup velocity, up to 15 days. The M35 color-period diagram displays the most striking example of rotational sequences yet published. The 310 rotators lay primarily on two sequences, defined by Barnes (2003) as the Interface (I) and the convective (C) sequences. The M35 color-period diagram supports the idea proposed by Barnes that stars evolve from the C sequence and onto the I sequence, and that the timescale for this evolution is inversely proportional to the stellar mass. The rotational isochrones proposed by Barnes fit the M35 I and C sequences well, suggesting that the rotational isochrones can indeed provide an accurate age-estimate for a coeval stellar population based on a well populated color-period diagram. Furthermore, M35 fits well on the general trend of a diminishing number of stars on the C sequence and a growing number of stars on the I sequence observed by Barnes in coeval populations spanning ages from the ZAMS to the age of the Hyades.

2. From the M35 color-period diagram we estimate that the characteristic exponential timescale for rotational evolution on the C sequence is 60 Myr and 140 Myr for G and K dwarfs, respectively. These timescales may offer valuable constraints on the rates of internal and external angular momentum transport and on the evolution rates of stellar dynamos in late-type stars of different masses.

3. We propose that 10 M35 stars rotating with rates that are abnormally slow compared

to their fellow stars, and thus located above the I sequence in the color-period diagram, can be explained by tidal synchronization of the stellar rotation to the orbital motion of a close stellar companion. Accordingly, we predict that the 10 stars are the primary stars in binaries with periods of approximately 10-15 days.

4. We find a statistically significant difference between the rotation period distributions for 53 single stars or primary stars in wide ($a \gtrsim 5$ AU) binaries and 17 primary stars in close ($a \lesssim 5$ AU) binary stars. The rotation period distribution of the primary stars is offset toward shorter rotation periods with respect to the rotation period distribution of the single stars. The observed difference is not due to tidal interactions as tidally synchronized binaries were excluded.

The latter result suggest that a companion star within ~ 5 AU does affect the rotational evolution of a late-type star in a way that leads to on average faster rotation at 150 Myr. Importantly, the spectroscopic binaries in M35 explore a domain of binary separations in which truncated circumstellar disks are expected to be tidally disrupted or accreted onto their host stars rapidly compared to disks in wider binaries or around single stars. Therefore, in such binaries, the time over which star-disk interactions can act to control (brake) stellar spin-up may be reduced compared to the duration of effective star-disk interaction in wider binaries or for single stars. Consequently, in the framework of current models of PMS angular momentum evolution, primaries belonging to the closest binary systems are expected to reach the ZAMS rotating faster than single stars or primaries in wider binaries. However, a recent model of PMS angular momentum evolution suggest that the lifetimes of circumstellar disks in the closest binaries can exceed those in wider binaries because magnetic and tidal torques can retain disk-material between the corotation radius and the binary truncation radius. Still other models suggest prolonged circumstellar disk lifetimes in close binaries due to replenishment of disk-material from a circumbinary disk.

The observation in M35 of a statistical significant difference between the rotation period distributions for the closest binaries and for single stars or wider binaries, thus provide a valuable constraint on models of PMS rotational evolution of solar-type stars. Assuming, as the models do, that the rotational evolution of low-mass PMS stars is largely dictated by the interactions between the star and its circumstellar disk, the on average faster rotation among the M35 primary stars in

binaries with separations $\lesssim 5$ AU suggest that the life-times of circumstellar disks in such systems is shorter than for single stars or for stars in wider binaries.

References

Allain, S., Bouvier, J., Mayor, M., Queloz, D., Mermilliod, J. C., Fernandez, M., & Martin, E. L. 1996, in ASP Conf. Ser. 109: Cool Stars, Stellar Systems, and the Sun, 353–+

Alphenaar, P., & van Leeuwen, F. 1981, Informational Bulletin on Variable Stars, 1957, 1

Armitage, P. J., & Clarke, C. J. 1996, MNRAS, 280, 458

Artymowicz, P. 1992, PASP, 104, 769

Artymowicz, P., Clarke, C. J., Lubow, S. H., & Pringle, J. E. 1991, ApJ, 370, L35

Artymowicz, P., & Lubow, S. H. 1994, ApJ, 421, 651

Baliunas, S., Sokoloff, D., & Soon, W. 1996, ApJ, 457, L99+

Barnes, S., & Sofia, S. 1996, ApJ, 462, 746

Barnes, S. A. 2001, ApJ, 561, 1095

—. 2003, ApJ, 586, 464

Barrado y Navascués, D., Deliyannis, C. P., & Stauffer, J. R. 2001, ApJ, 549, 452

Benz, W., Mayor, M., & Mermilliod, J. C. 1984, A&A, 138, 93

Bodenheimer, P. 1995, ARA&A, 33, 199

Bouvier, J., Cabrit, S., Fernandez, M., Martin, E. L., & Matthews, J. M. 1993, A&A, 272, 176

Bouvier, J., Forestini, M., & Allain, S. 1997a, A&A, 326, 1023

Bouvier, J., Rigaut, F., & Nadeau, D. 1997b, A&A, 323, 139

Braden, E., Mathieu, R. D., & Meibom, S. 2005, in preparation.

Cudworth, K. M. 1971, AJ, 76, 475

Deliyannis, C. P. 2005, in preparation.

Duquennoy, A., & Mayor, M. 1991, A&A, 248, 485

Duquennoy, A., Mayor, M., & Mermilliod, J. C. 1992, in Binaries as Tracers of Stellar Formation. Proceedings of a Workshop held in Bettmeralp, Switzerland, Sept. 1991, in honor of Dr. Roger Griffin. Editors, Antoine Duquennoy, Michel Mayor; Publisher, Cambridge University Press, Cambridge, England, New York, NY, 1992. LC # QB821 .B55 1991. ISBN # 0521433584. P. 52, 1992, 52

Duvall, T. L., Dziembowski, W. A., Goode, P. R., Gough, D. O., Harvey, J. W., & Leibacher, J. W. 1984, Nature, 310, 22

Edwards, S., Strom, S. E., Hartigan, P., Strom, K. M., Hillenbrand, L. A., Herbst, W., Attridge, J., Merrill, K. M., Probst, R., & Gatley, I. 1993, AJ, 106, 372

Eff-Darwich, A., Korzennik, S. G., & Jiménez-Reyes, S. J. 2002, ApJ, 573, 857

Endal, A. S., & Sofia, S. 1981, ApJ, 243, 625

Ghez, A. M., Neugebauer, G., & Matthews, K. 1993, AJ, 106, 2005

Goode, P. R., Dziembowski, W. A., Korzennik, S. G., & Rhodes, E. J. 1991, ApJ, 367, 649

Gough, D. O. 1982, Nature, 298, 334

Herbst, W., Rhode, K. L., Hillenbrand, L. A., & Curran, G. 2000, AJ, 119, 261

Herbst, W., & Wittenmyer, R. 1996, Bulletin of the American Astronomical Society, 28, 1338

Hole, K. T., Mathieu, R. D., Latham, D. W., & Meibom, S. 2005, submitted to AJ

Honeycutt, R. K. 1992, PASP, 104, 435

Horne, J. H., & Baliunas, S. L. 1986, ApJ, 302, 757

Hut, P. 1981, A&A, 99, 126

Jensen, E. L. N., & Mathieu, R. D. 1997, AJ, 114, 301

Jensen, E. L. N., Mathieu, R. D., & Fuller, G. A. 1994, ApJ, 429, L29

—. 1996, ApJ, 458, 312

Kalirai, J. S., Fahlman, G. G., Richer, H. B., & Ventura, P. 2003, AJ, 126, 1402

Koenigl, A. 1991, ApJ, 370, L39

Korycansky, D. G., & Papaloizou, J. C. B. 1995, MNRAS, 274, 85

Larson, R. B. 2002, MNRAS, 332, 155

Lockwood, G. W., Thompson, D. T., Radick, R. R., Osborn, W. H., Baggett, W. E., Duncan, D. K., & Hartmann, L. W. 1984, PASP, 96, 714

MacGregor, K. B., & Brenner, M. 1991, ApJ, 376, 204

Mathieu, R. D. 1994, ARA&A, 32, 465

Mathieu, R. D. 2000, in ASP Conf. Ser. 198: Stellar Clusters and Associations: Convection, Rotation, and Dynamos, 517–+

Mathieu, R. D., Duquennoy, A., Latham, D. W., Mayor, M., Mermilliod, T., & Mazeh, J. C. 1992, in Binaries as Tracers of Stellar Formation. Proceedings of a Workshop held in Bettmeralp, Switzerland, Sept. 1991, in honor of Dr. Roger Griffin. Editors, Antoine Duquennoy, Michel Mayor; Publisher, Cambridge University Press, Cambridge, England, New York, NY, 1992. LC # QB821 .B55 1991. ISBN # 0521433584. P. 278, 1992, 278

McNamara, B., & Sekiguchi, K. 1986, AJ, 91, 557

Meibom, S., Barnes, S. A., Dolan, C., & Mathieu, R. D. 2001, in ASP Conf. Ser. 243: From Darkness to Light: Origin and Evolution of Young Stellar Clusters, 711

Meibom, S., & Mathieu, R. D. 2005, ApJ, 620, 970

Meibom, S., Mathieu, R. D., & Stassun, K. G. 2005, in preparation.

Melo, C. H. F., Covino, E., Alcalá, J. M., & Torres, G. 2001, A&A, 378, 898

Mermilliod, J.-C., Rosvick, J. M., Duquennoy, A., & Mayor, M. 1992, A&A, 265, 513

Meys, J. J. M., Alphenaar, P., & van Leeuwen, F. 1982, Informational Bulletin on Variable Stars, 2115, 1

Najita, J. 1995, in Revista Mexicana de Astronomia y Astrofisica Conference Series, 293–+

Ostriker, E. C., & Shu, F. H. 1995, ApJ, 447, 813

Papaloizou, J. C. B., & Terquem, C. 1995, MNRAS, 274, 987

Patience, J., Ghez, A. M., Reid, I. N., & Matthews, K. 2002, AJ, 123, 1570

Pinsonneault, M. H., Kawaler, S. D., & Demarque, P. 1990, ApJS, 74, 501

Press, W. H., Teukolsky, S. A., Vetterling, W. T., & Flannery, B. P. 1992, Numerical recipes in FORTRAN. The art of scientific computing (Cambridge: University Press, —c1992, 2nd ed.)

Pringle, J. E. 1991, MNRAS, 248, 754

Queloz, D., Allain, S., Mermilliod, J.-C., Bouvier, J., & Mayor, M. 1998, A&A, 335, 183

Radick, R. R., Thompson, D. T., Lockwood, G. W., Duncan, D. K., & Baggett, W. E. 1987, ApJ, 321, 459

Rebull, L. M. 2001, AJ, 121, 1676

Scargle, J. D. 1982, ApJ, 263, 835

Schatzman, E. 1962, Annales d'Astrophysique, 25, 18

Shu, F., Najita, J., Ostriker, E., Wilkin, F., Ruden, S., & Lizano, S. 1994, ApJ, 429, 781

Sills, A., Pinsonneault, M. H., & Terndrup, D. M. 2000, ApJ, 534, 335

Simon, M., & Prato, L. 1995, ApJ, 450, 824

Skumanich, A. 1972, ApJ, 171, 565

Soderblom, D. R. 1982, ApJ, 263, 239

Soderblom, D. R., Jones, B. F., & Walker, M. F. 1983, ApJ, 274, L37

Soderblom, D. R., Stauffer, J. R., Hudon, J. D., & Jones, B. F. 1993a, ApJS, 85, 315

Soderblom, D. R., Stauffer, J. R., MacGregor, K. B., & Jones, B. F. 1993b, ApJ, 409, 624

Stassun, K. G., Mathieu, R. D., Mazeh, T., & Vrba, F. J. 1999, AJ, 117, 2941

Stauffer, J. R., Hartmann, L., Soderblom, D. R., & Burnham, N. 1984, ApJ, 280, 202

Stauffer, J. R., & Hartmann, L. W. 1987, ApJ, 318, 337

Stauffer, J. R., Hartmann, L. W., Burnham, J. N., & Jones, B. F. 1985, ApJ, 289, 247

Stauffer, J. R., Hartmann, L. W., & Jones, B. F. 1989, ApJ, 346, 160

van Leeuwen, F., & Alphenaar, P. 1982, The Messenger, 28, 15

Vasilevskis, S., Klemola, A., & Preston, G. 1958, AJ, 63, 387

von Hippel, T., Steinhauer, A., Sarajedini, A., & Deliyannis, C. P. 2002, AJ, 124, 1555

Witte, M. G., & Savonije, G. J. 2002, A&A, 386, 222

Yi, S. K., Kim, Y., & Demarque, P. 2003, ApJS, 144, 259

Zahn, J.-P. 1989, A&A, 220, 112

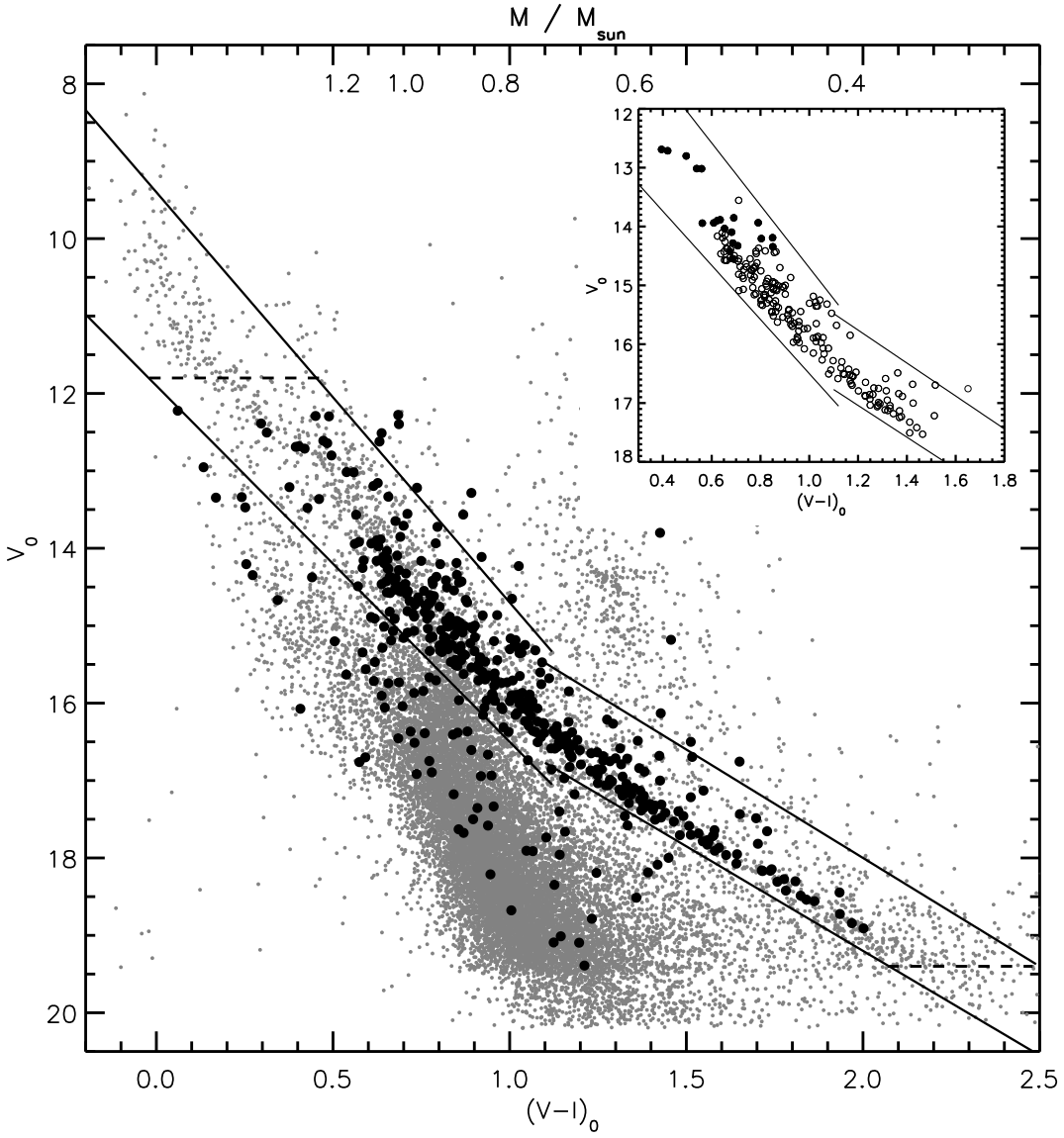

Fig. 4.6.— The M35 $(V-I)_0$ vs. V_0 color-magnitude diagram. Photometry was provided by Deliyannis (2005). The 443 stars with rotation periods are highlighted with solid black dots. Stars located between the solid lines above and below the cluster sequence are considered photometric members of M35. The horizontal dashed lines mark the bright and faint limit of our time-series photometric survey. Note that the faint limits for proper-motion and radial-velocity surveys are $V_0 \simeq 14.5$ and $V_0 \simeq 17.5$, respectively. The upper x-axis gives stellar masses corresponding to the color on the lower x-axis. Masses are derived using a 150 Myr Yale isochrone. The insert shows the location of stars that are photometric and radial-velocity members (203 stars; open symbols), and stars that photometric, radial-velocity, and proper-motion members (20 stars; filled symbols).

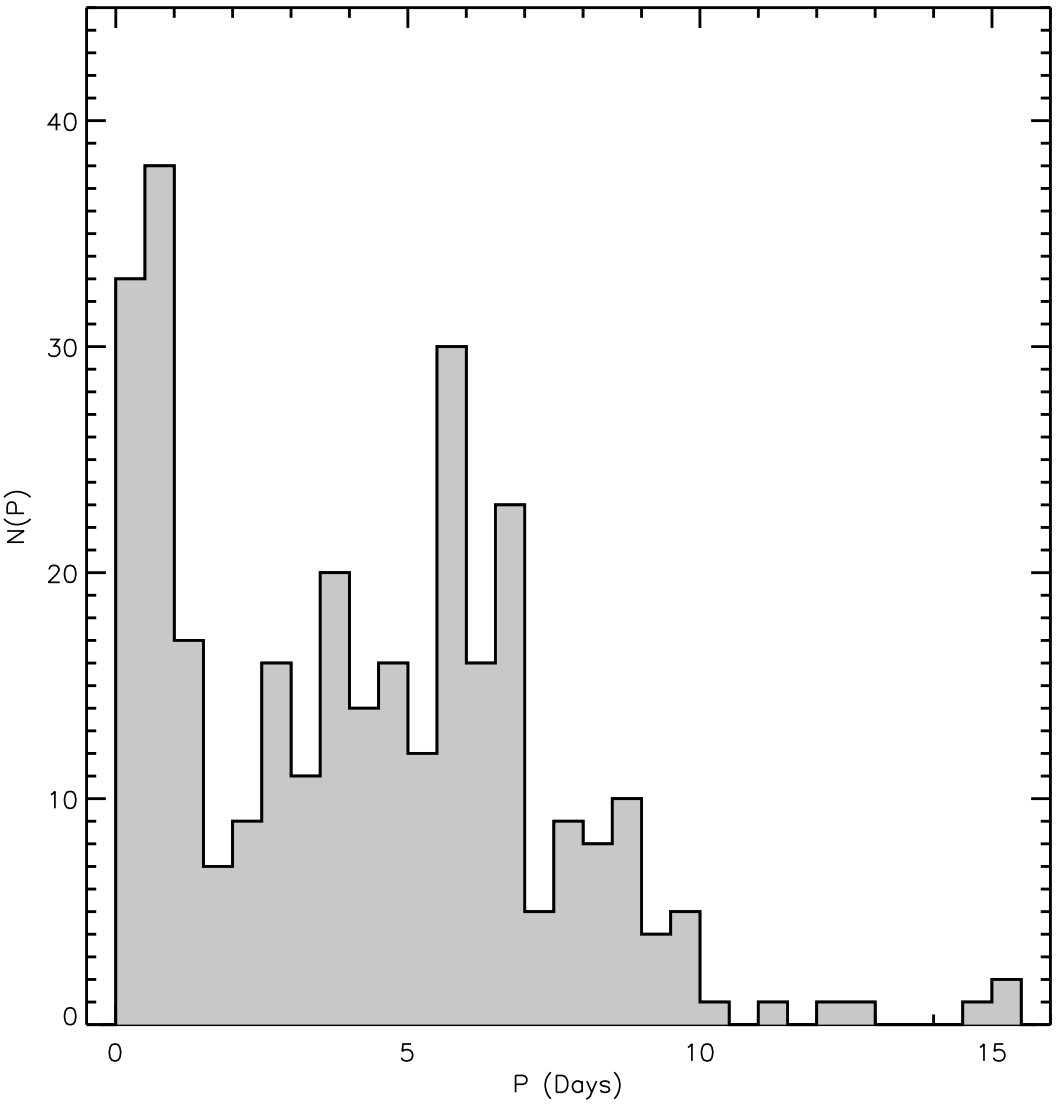

Fig. 4.7.— The distribution of rotation periods for the sample of 310 cluster members. The distribution show a large dispersion from $\sim$ 0.1 days to $\sim$ 15 days, and some structure with a distinct a distinct peak at $\sim$ 1 day and a shallower and broader peak centered at about 6 days.

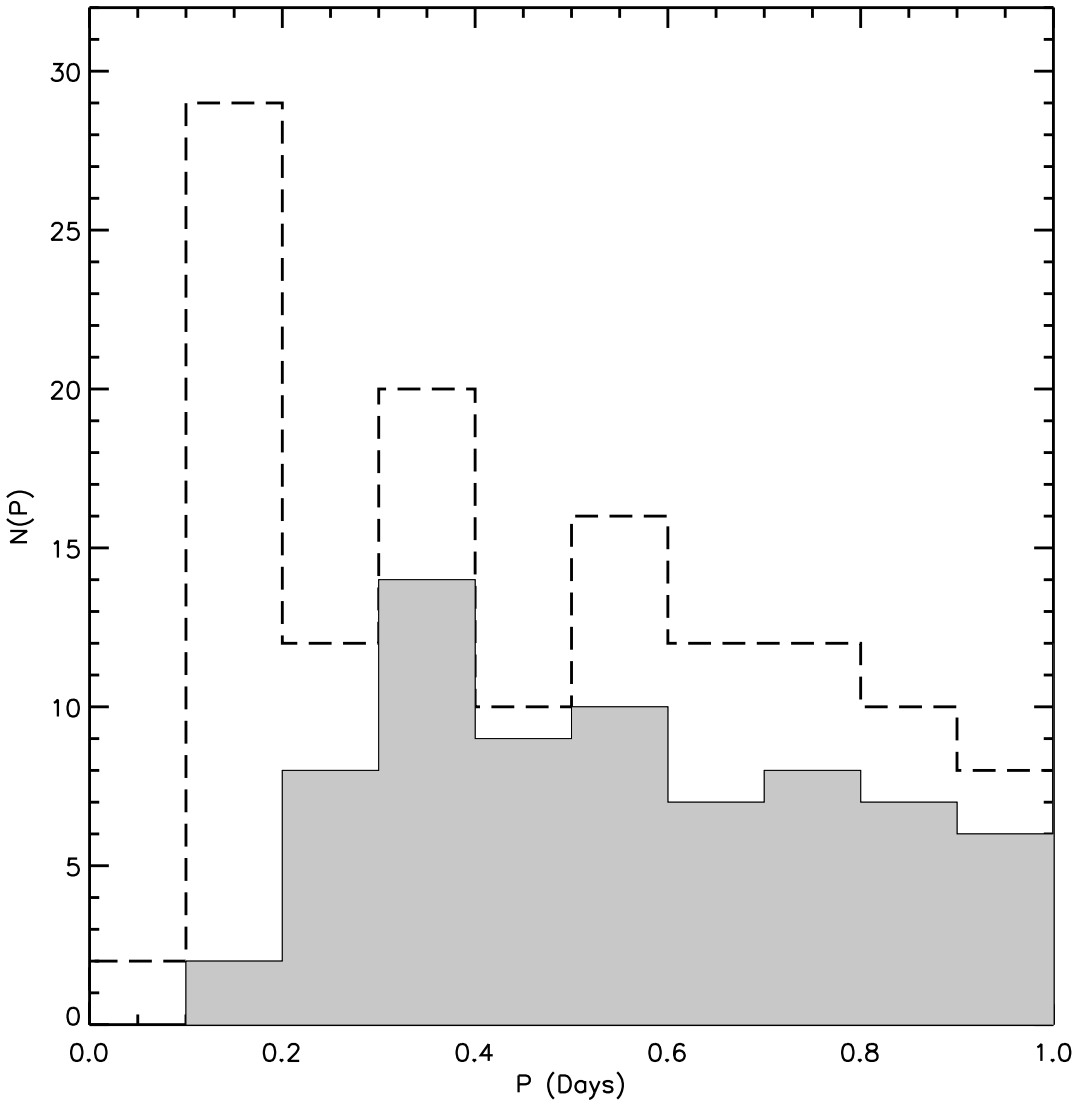

Fig. 4.8.— The short-period end of the M35 rotation-period distribution. The rotation periods have been binned in 0.1 day bins. The white (outlined by a dashed line) histogram represents all rotators in our sample. The grey histogram represents stars that are members of M35.

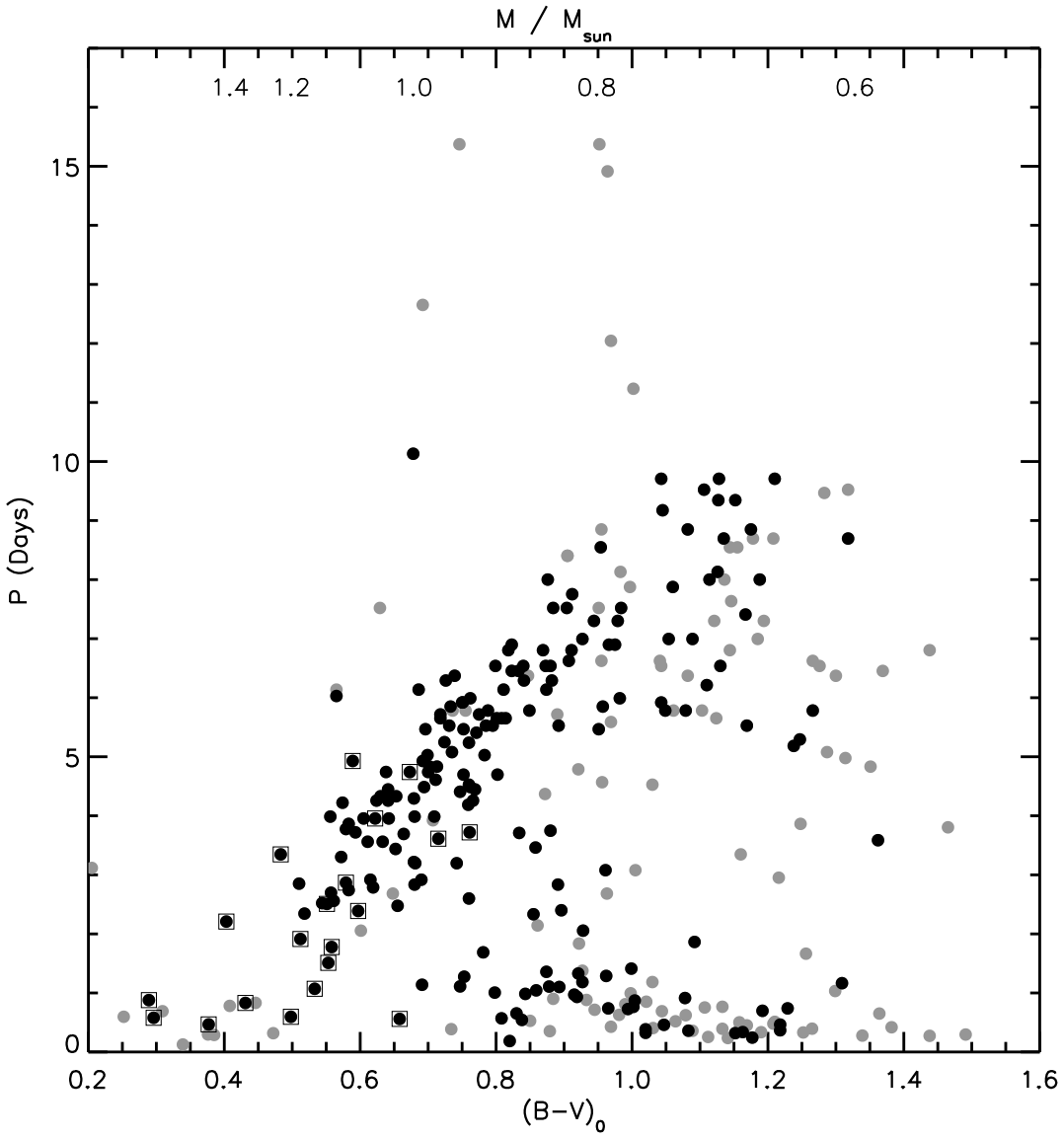

Fig. 4.9.— The distribution of stellar rotation periods with (B-V) color. All stars are photometric members of M35. Spectroscopic members of M35 are highlighted using black symbols and stars with additional proper-motion membership are marked with squares. The upper x-axis gives stellar masses corresponding to the color on the lower x-axis. Masses are derived using a 150 Myr Yale isochrone.

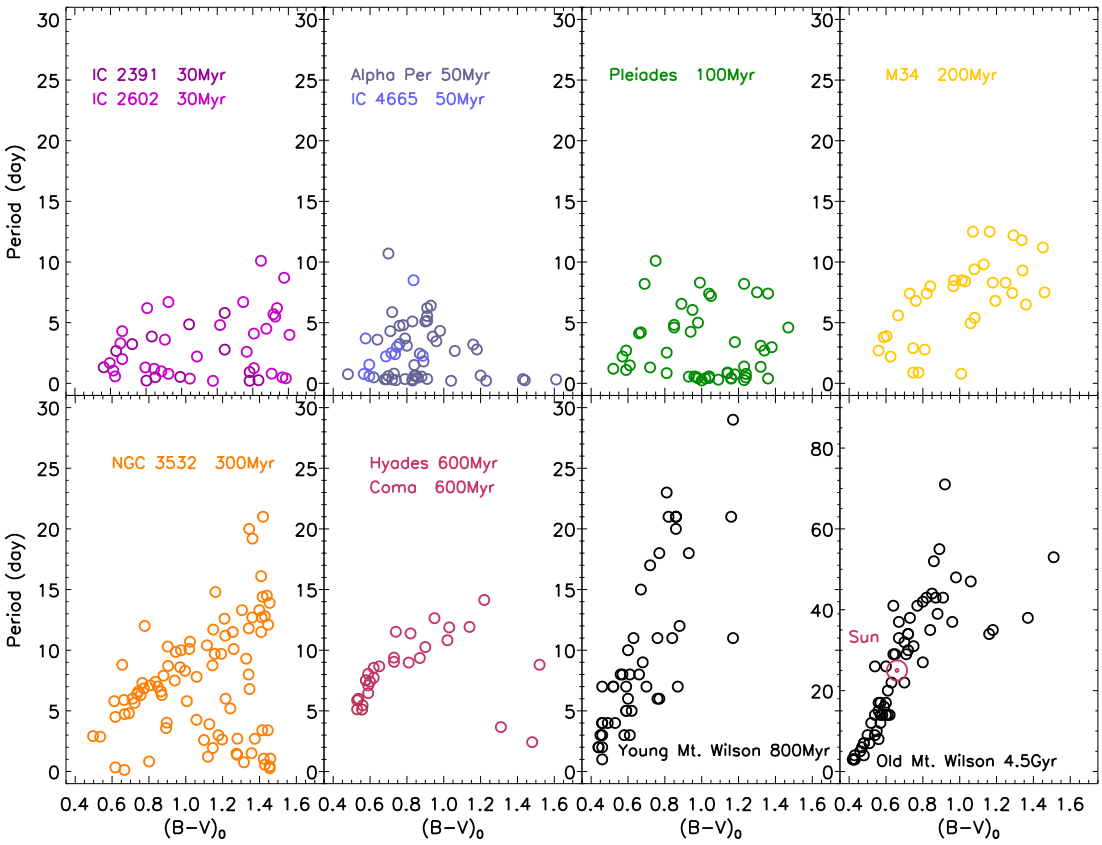

Fig. 4.10.— Figure 1 from Barnes (2003). Color-period diagrams for a series of open clusters younger and older than M35, and for the young and old Mount Wilson stars. Note the change in scale for the old Mount Wilson

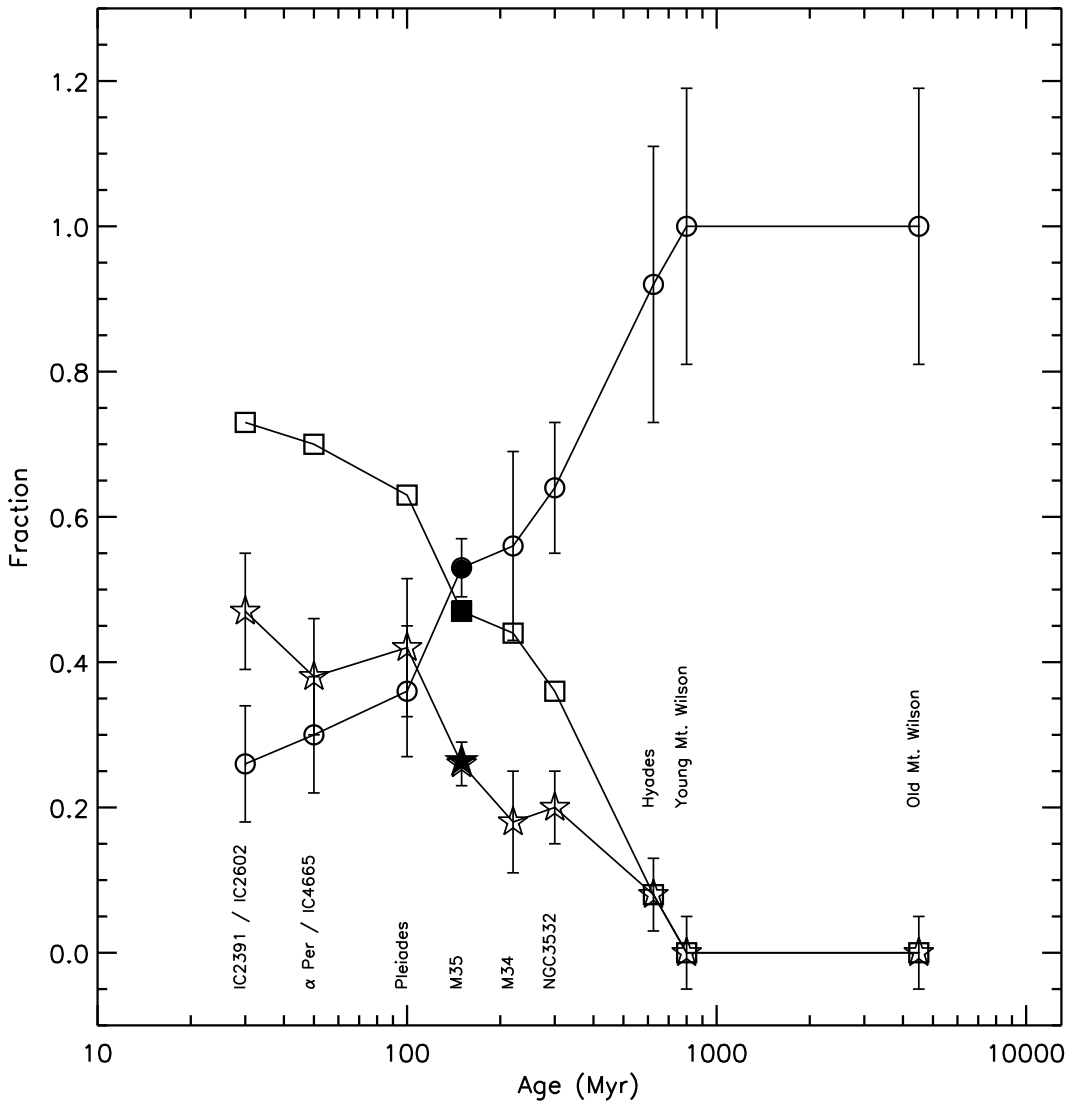

Fig. 4.11.— Reproduction of Figure 3 Barnes (2003) with M35 data added. Fractions of stars with $0.5 \geq (B-V)_0 \leq 1.5$ on the I sequence (circles), the C sequence (stars). The squares represent the relative fraction of the sum of C sequence and gap stars. The filled symbols show the relative fraction of stars in M35.

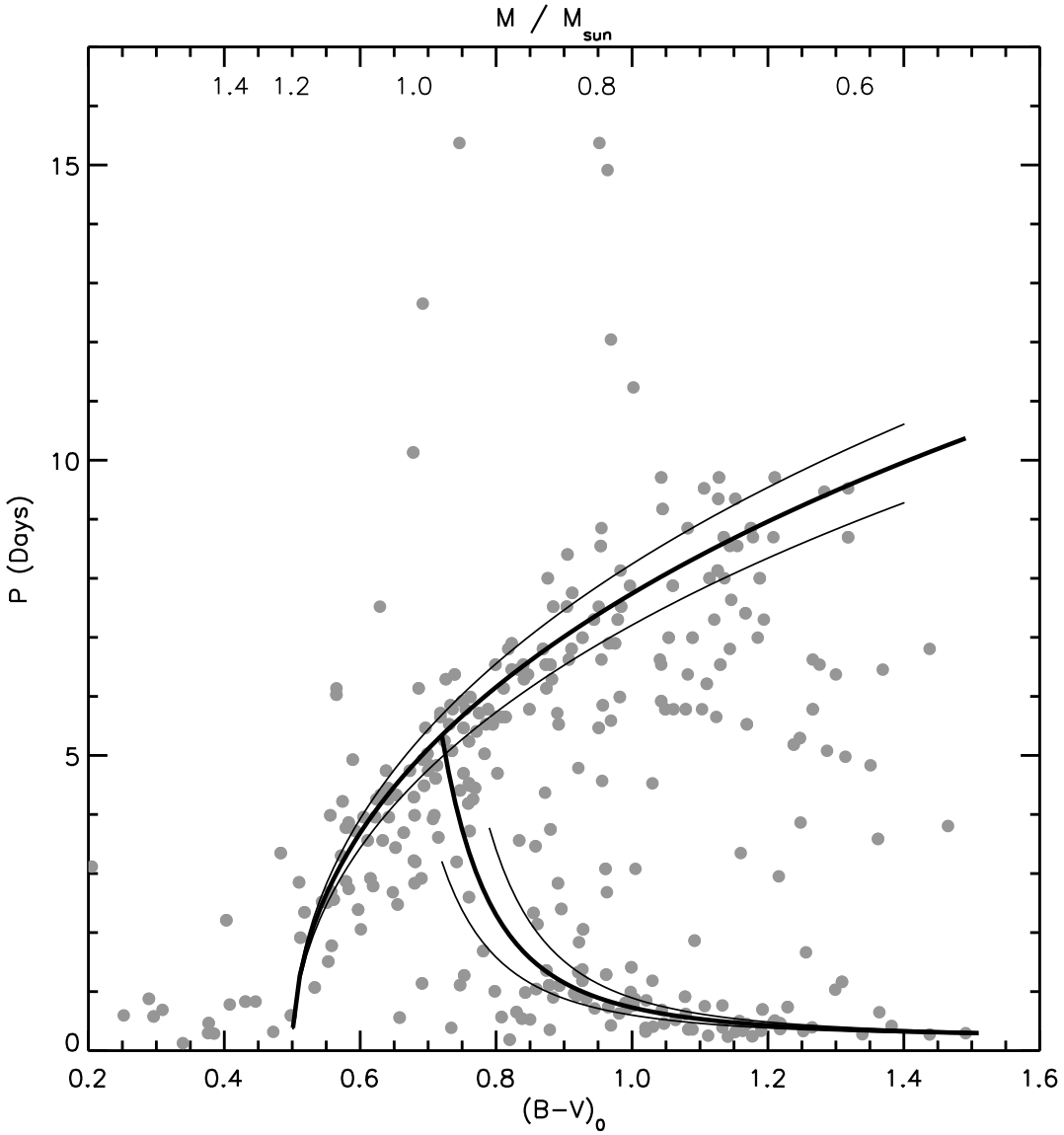

Fig. 4.12.— The distribution of stellar rotation periods with (B-V) color. All 310 cluster members with rotation periods are plotted using grey symbols. The 150 Myr rotational isochrones (Barnes 2003) are overplotted as thick black solid curves. To illustrate the sensitivity to age we show a 130 Myr and a 170 Myr isochrone as thin curves flanking the 150 Myr rotational isochrone. The upper x-axis give stellar masses corresponding to the color on the lower x-axis. Masses are derived using a 150 Myr Yale isochrone.

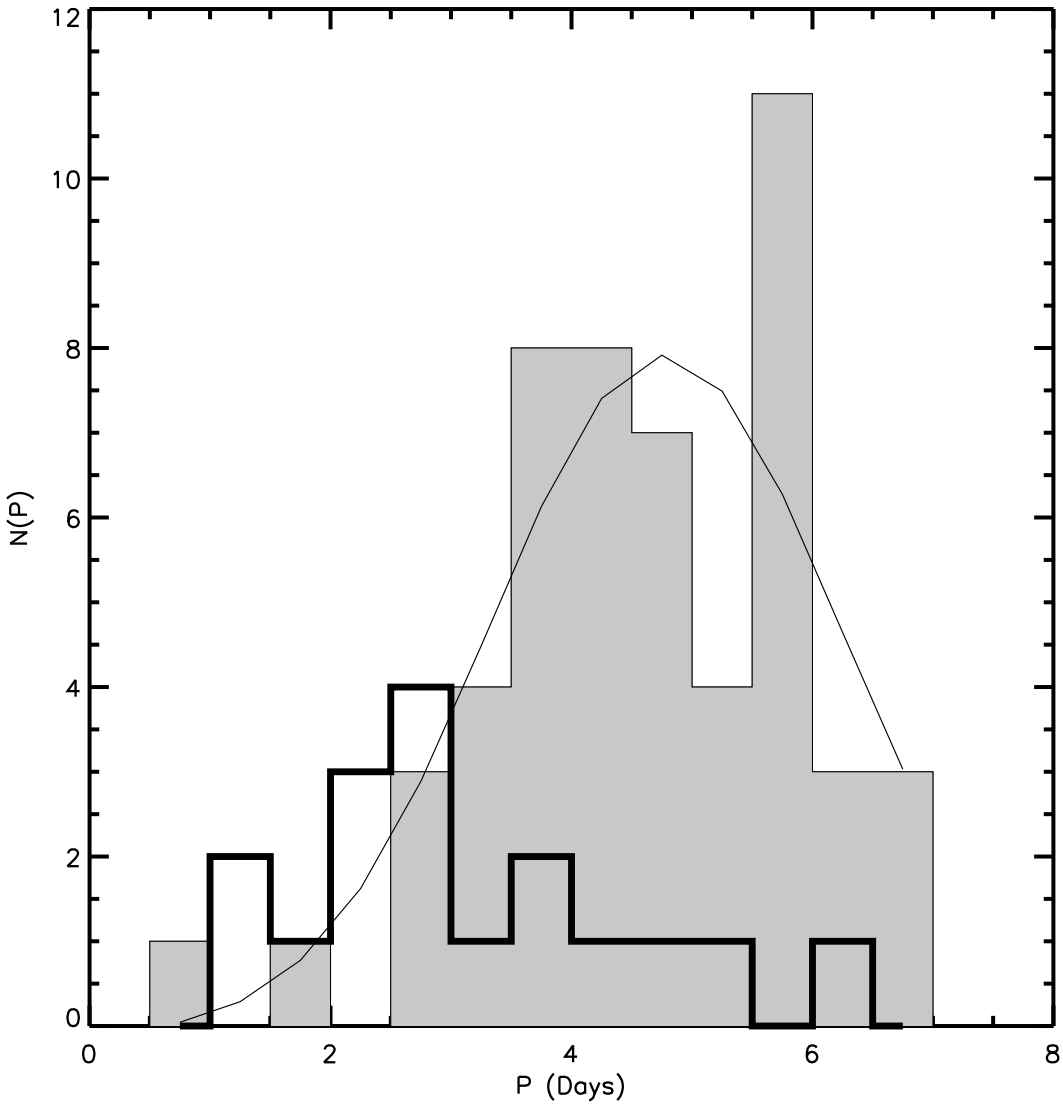

Fig. 4.13.— The distribution of rotation periods for single stars ($N_{RV} \geq 3$ and $\sigma_{RV} \leq 0.5\ km\ s^{-1}$; grey histogram) and binary stars ($N_{RV} \geq 3$ and $\sigma_{RV} \geq 1.5\ km\ s^{-1}$; transparent histogram). The best least squares fit of a Gaussian function to the single star distribution is shown as a solid curve. A Kolmogorov-Smirnov test comparing the cumulative distribution of both samples give a 0.11% probability that the two distributions derive from the same parent distribution.

Chapter 5

Summary, Conclusions, and Ideas for Future Work

It is now time to examine the results of this thesis and ask what it is we have learned. The primary goal was to study the impact of a close binary companion on the evolution of stellar and orbital angular momentum of solar-type stars in close detached binaries. Specifically we have studied tidal evolution (circularization and synchronization) in close detached late-type binaries, and the non-tidal effects of binarity and the stellar mass on the rotational evolution of late-type stars. The contributions presented are observational and significant effort has been put into developing improved observational diagnostics to better constrain theoretical models and thus to improve our understanding of the physical mechanisms responsible for the observed trends.

The thesis was divided into three chapters each representing the main areas of interest. Using the same structure and order, we present here the conclusions of this work together with ideas for future work.

5.1 Tidal Circularization

The theory of tidal circularization has had many important successes. Nonetheless, for binaries with solar-type primary stars, model predictions have not been consistent with the observed rate of tidal circularization. While discrepancies between observations and model predictions have posed a challenge to tidal theory, the lack of well-determined uncertainties on the observed degree of tidal circularization in a given binary population has compromised the comparison of theory and observations. Also, small binary populations, the distribution of primordial orbital eccentricities, and

heterogeneity in the masses of binary primary stars, adds complexity and uncertainty to the task of measuring the degree of tidal circularization in any given population of coeval binaries.

The primary contributions of this thesis are: 1) a new population of solar-type spectroscopic binary orbits for the 150 Myr open cluster M35; 2) a new diagnostic - the *tidal circularization period* - to determine the period of circularization of the most frequently occurring binary; 3) an evaluation of the performance of this new diagnostic providing measurement uncertainties on the resulting circularization periods and information about the initial eccentricity of the binaries that circularize at that period; and 4) a comparison of the distribution of circularization periods from 8 binary populations to the predictions from theoretical models.

The results of these contributions are displayed in Figure 9 in Chapter 2. From that figure the following conclusions are drawn. First, the oldest binary populations have tidal circularization periods that are significantly longer than those of the young and intermediate-age binary populations. Second, the data are consistent with a linear progression of circularization period with log age from the pre main-sequence (PMS) phase to $\sim$7 Gyr, or alternatively, with the hybrid scenario as suggested by Mathieu et al. (1992). Third, no current theory of tidal circularization can account for the observed magnitudes and distribution of tidal circularization periods with age. The models of main-sequence tidal circularization using either the equilibrium tide theory (Zahn 1989) or the dynamical tide theory with resonance locking (Witte & Savonije 2002) both predict circularization periods that fall significantly below the observed circularization periods. The model by (Zahn & Bouchet 1989) including PMS tidal circularization predicts negligible circularization during the main-sequence phase and is not consistent with the observed circularization periods for the old binary populations of M67 and NGC188 nor with the circularization period of M35. Consequently, the observational data suggest that tidal circularization is active throughout the main-sequence phase, and that the efficiency of the dissipation mechanisms employed by the models are too low.

A future observational goal is to further populate the age vs. circularization period diagram with reliable circularization periods at carefully selected ages based on large samples of binary orbits from homogeneous coeval binary populations. Also, expanding the observational parameter space to include close binaries among low-mass main-sequence stars will provide simplified, fully convective,

stellar interior structures that will not be affected by dynamical tides. Thus such low-mass binaries should provide tests of well-defined aspects of tidal theory. Furthermore, as emphasized by the work of Zahn & Bouchet (1989), it is critical that the very dynamic period of tidal evolution during the PMS stage of stellar evolution be well constrained by a coeval and homogeneous (in mass) population of close PMS binaries. Such a population has not yet been established observationally. Finally, the secondary star plays as important a role in the tidal evolution of a binary as the primary star, and model predictions make specific assumptions about both the primary and secondary binary components. Most spectroscopic binaries presented in this thesis are single-lined, and thus the masses and other parameters of the secondary stars are poorly determined. Intentional efforts to convert single-lined spectroscopic binaries into double-lined systems will greatly improve our ability to observationally test tidal theory.

5.2 Tidal Synchronization

Observations of tidal synchronization provide an important additional constraint on models of tidal evolution and the dissipation mechanisms they employ.

This thesis contributes rotation periods for the solar-type primary stars in 13 single-lined binaries with known orbital periods and eccentricities. All 13 binaries are radial-velocity and photometric members of the young open clusters M35 and M34 (250 Myr) and thus have ages corresponding to the most active phase of main-sequence tidal evolution.

As a measure of the degree of tidal synchronization the ratio of the rotational angular velocity of each primary star ($\Omega_\star$) to the angular velocity required for the star to be (pseudo-) synchronized (Ω_{ps}) is calculated for each binary. $\Omega_\star/\Omega_{ps}$ is presented as a function of the binary orbital period (P) in a $\log(\Omega_\star/\Omega_{ps}) - \log(P)$ - diagram.

Tidal theory predicts that the process of tidal synchronization proceeds faster than tidal circularization by about three orders of magnitude. Thus, for constant stellar interior structure, it is expected that 1) circularized binaries should also be synchronized, and 2) the shortest period eccentric binaries should be pseudo-synchronized. A model including PMS tidal evolution (Zahn & Bouchet 1989) predicts super-synchronous stars in circularized binaries on the zero-age main-sequence (ZAMS). The primary stars in the 6 binaries in M35 and M34 with orbital periods less than $\sim$ 13 days,

are thus expected to be either synchronized, pseudo-synchronized ($\log(\Omega_\star/\Omega_{ps}) = 0$), or to rotate super-synchronously ($\log(\Omega_\star/\Omega_{ps}) > 0$). Two binaries have been both circularized and synchronized and thus meets the expectations. In one circular binary the primary star rotates super-synchronously. In 3 binaries, including one circular, the primary stars are rotating sub-synchronous. The 6 binaries offer interesting challenges to tidal theory, specifically with respect to the role of stellar mass (structure) and initial orbital eccentricity on the tidal evolution of a binary system. We propose explanations for the observed binary and stellar parameters of the 6 systems within the framework of current theory of stellar and tidal evolution, theory of stellar dynamics, and observed stellar and binary initial conditions.

At the present time, theoretical models make detailed predictions for only a few configurations of binary orbital and stellar parameters. Specific models must be run with carefully chosen initial orbital and stellar parameters to attempt to reproduce the observed tidal evolution at 150 Myr and 250 Myr.

Populating the $\log(\Omega_\star/\Omega_{ps}) - \log(P)$ diagram with coeval homogeneous populations of binary stars sets the beginning of a new era in observational studies of tidal synchronization, and will be an important goal for future observational work.

5.3 Non-tidal Effects of Binarity on Stellar Rotation

Magnetic coupling between a PMS star and its disk have become an essential feature of most models of angular momentum evolution of solar-like stars. The interaction between young stars and their disks provide a means to brake the spin-up of the star while transferring angular momentum from the star to the disk. However, most stars, if not all, form in binary or multiple systems, and models of star-disk interactions in close binaries ($a \lesssim 100$ AU) predict that the presence of a companion star will truncate and potentially tidally disrupt the circumstellar disks. These models thus predict that the mass, size, and lifetime of circumstellar disks may be reduced for stars in close binaries as compared to wider binaries and single stars.

If indeed a binary companion does affect the mass, size, and lifetime of circumstellar disks, and if star-disk interactions play a key role in the rotational evolution of late-type stars, one might expect to observe a relationship between binarity and stellar rotation on the ZAMS.

This thesis presents a statistically significant difference between the rotation period distributions for 53 single stars or primary stars in binaries with separations of 5 AU or more and 17 primary stars in close ($a \lesssim 5$ AU) binary stars in M35. The rotation period distribution of the primary stars is offset toward shorter rotation periods with respect to the rotation period distribution of the single stars. The observed difference is not due to tidal interactions as tidally synchronized binaries were excluded. This result suggests that a companion star within ~ 5 AU does affect the rotational evolution of a late-type star in a way that leads to on average faster rotation at 150 Myr. In the framework of current models of PMS angular momentum evolution this result support the idea that the lifetimes of circumstellar disks in such close binaries are shorter than for single stars or for stars in wider binaries.

5.4 The Rotational Evolution of Late-Type Stars

Models of stellar rotational evolution were until recently constrained by observational data that suffered from small stellar samples and/or ambiguities inherent to measurements of projected rotational velocities. Time-series photometric surveys of young open clusters have over the past decade provided direct measures of stellar rotation for an increasing number of late-type stars. The result is a manifestation of well-defined relations between stellar surface rotation and stellar mass and age.

A main contribution of this thesis is an extensive time-series photometric survey of late-type stars in M35, resulting in rotation periods for 310 cluster members. The M35 color-period diagram displays two well-defined sequences of stars, corresponding to the I and C sequences defined by Barnes (2003). M35 fits well on the general trend of a diminishing number of stars on the C sequence and a growing number of stars on the I sequence observed by Barnes in coeval populations spanning ages from the ZAMS to the age of the Hyades. Therefore, the M35 color-period diagram offers strong support for the idea proposed by Barnes that stars evolve from the C sequence and onto the I sequence, and that the timescale for this evolution is inversely proportional to the stellar mass. The rotational isochrones proposed by Barnes fit the M35 I and C sequences well, suggesting that the rotational isochrones can indeed provide an accurate age-estimate for a coeval stellar population based on a well populated color-period diagram.

The M35 color-period diagram is well suited for an estimate of the characteristic exponential timescale for rotational evolution on the C sequence for G and K dwarfs. Timescales of 60 Myr and 140 Myr are determined for G and K dwarfs, respectively. These timescales may offer valuable constraints on the rates of internal and external angular momentum transport and on the evolution rates of stellar dynamos in late-type stars of different masses.

Finally, 10 M35 stars rotating with rates that are abnormally slow compared to their fellow stars. It is proposed in this thesis that tidal synchronization of the stellar rotation to the orbital motion of a close stellar companion is responsible for the abnormally slow rotation. Accordingly, it is predicted that the 10 stars are the primary stars in binaries with periods of approximately 10-15 days.

The color-period diagram promises to become a powerful tool to reveal the physical mechanisms controlling the rotational evolution of late-type stars, much like the color-magnitude diagram has guided models of stellar evolution. Comprehensive photometric surveys of rich open clusters, providing stellar rotation periods and color-indices for mid F to late M dwarfs, should therefore be high priority for future observational studies of stellar angular momentum evolution.

References

Barnes, S. A. 2003, ApJ, 586, 464

Mathieu, R. D., Duquennoy, A., Latham, D. W., Mayor, M., Mermilliod, T., & Mazeh, J. C. 1992, in Binaries as Tracers of Stellar Formation. Proceedings of a Workshop held in Bettmeralp, Switzerland, Sept. 1991, in honor of Dr. Roger Griffin. Editors, Antoine Duquennoy, Michel Mayor; Publisher, Cambridge University Press, Cambridge, England, New York, NY, 1992. LC # QB821 .B55 1991. ISBN # 0521433584. P. 278, 1992, 278

Witte, M. G., & Savonije, G. J. 2002, A&A, 386, 222

Zahn, J.-P. 1989, A&A, 220, 112

Zahn, J.-P., & Bouchet, L. 1989, A&A, 223, 112

Appendix A

PHASED LIGHT CURVES

This appendix presents the light curves for the 443 stars in the field of M35. The light curves have been divided into 3 groups according to the amplitude of the photometric variation. Each group of light curves are thus presented with a δV range on the ordinate that is appropriate for the amplitudes within that group. Stars with the largest photometric variability are shown first. Each page display 25 light curves.

For each star we show the data from the high-frequency survey as black symbols and data from the low-frequency (synoptic) survey as grey symbols. The stellar ID is given in the upper left corner of each plot. The period to which the data are phased (the rotation period) is given in the upper right corner. The 2-5 letter code in the lower right corner inform about the stars membership status.The codes have the following meaning: Photometric Member (PM), Photometric Non-Member (PNM), Photometric and Spectroscopic Member (PSM), and Photometric Member but Spectroscopic Non-Member (PMSNM). A horizontal grey line in each plot mark $\delta V = 0.0$ and a vertical grey line marks a phase of 1.0.

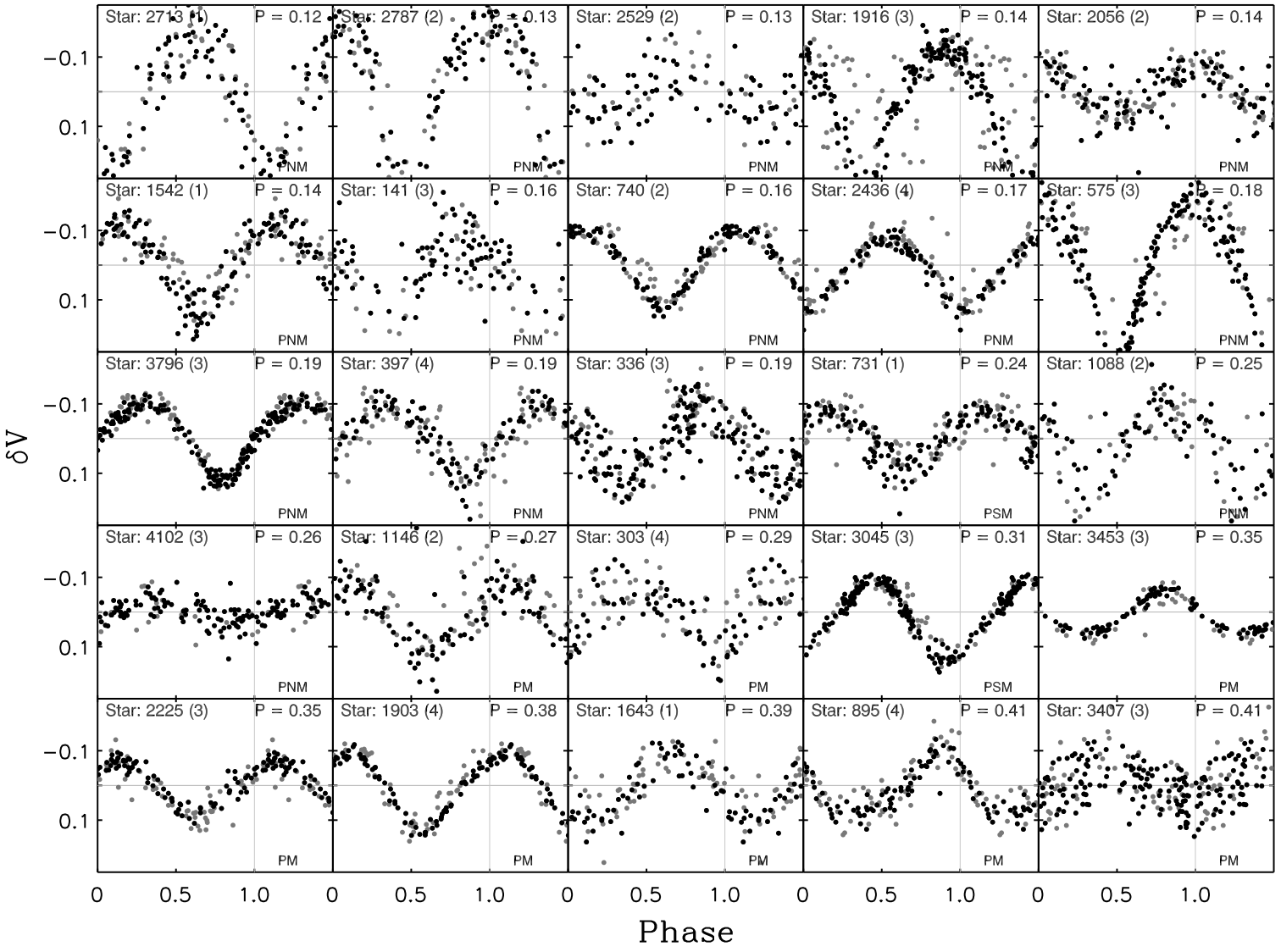
Star: 2713 (1) P = 0.12
Star: 2787 (2) P = 0.13
Star: 2529 (2) P = 0.13
Star: 1916 (3) P = 0.14
Star: 2056 (2) P = 0.14
Star: 1542 (1) P = 0.14
Star: 141 (3) P = 0.16
Star: 740 (2) P = 0.16
Star: 2436 (4) P = 0.17
Star: 575 (3) P = 0.18
Star: 3796 (3) P = 0.19
Star: 397 (4) P = 0.19
Star: 336 (3) P = 0.19
Star: 731 (1) P = 0.24
Star: 1088 (2) P = 0.25
Star: 4102 (3) P = 0.26
Star: 1146 (2) P = 0.27
Star: 303 (4) P = 0.29
Star: 3045 (3) P = 0.31
Star: 3453 (3) P = 0.35
Star: 2225 (3) P = 0.35
Star: 1903 (4) P = 0.38
Star: 1643 (1) P = 0.39
Star: 895 (4) P = 0.41
Star: 3407 (3) P = 0.41
PNM
PSM
PM
δV
−0.1
0.1
0
0.5
1.0
Phase

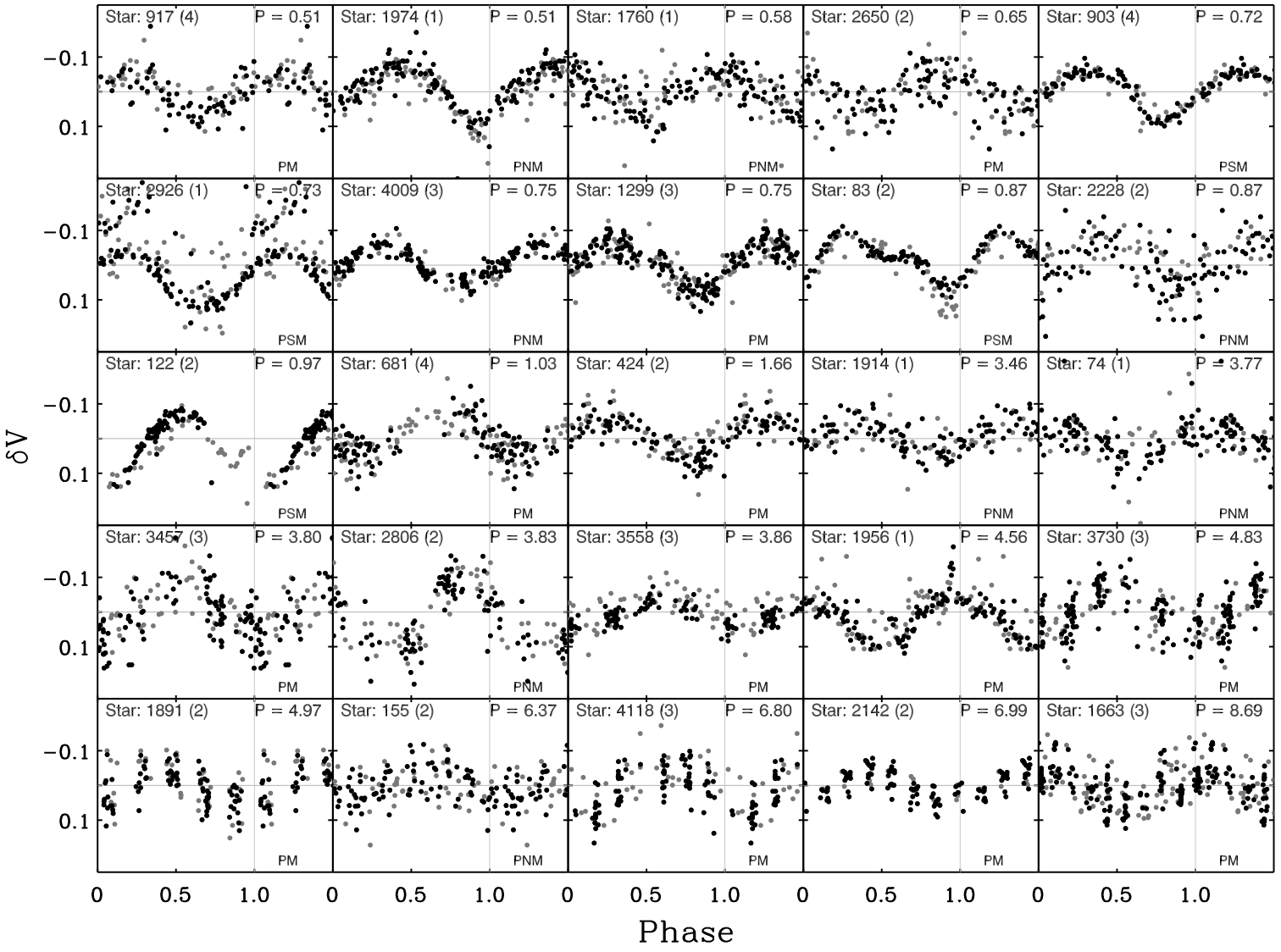
Star: 917 (4) P = 0.51
Star: 1974 (1) P = 0.51
Star: 1760 (1) P = 0.58
Star: 2650 (2) P = 0.65
Star: 903 (4) P = 0.72
Star: 2926 (1) P = 0.73
Star: 4009 (3) P = 0.75
Star: 1299 (3) P = 0.75
Star: 83 (2) P = 0.87
Star: 2228 (2) P = 0.87
Star: 122 (2) P = 0.97
Star: 681 (4) P = 1.03
Star: 424 (2) P = 1.66
Star: 1914 (1) P = 3.46
Star: 74 (1) P = 3.77
Star: 3457 (3) P = 3.80
Star: 2806 (2) P = 3.83
Star: 3558 (3) P = 3.86
Star: 1956 (1) P = 4.56
Star: 3730 (3) P = 4.83
Star: 1891 (2) P = 4.97
Star: 155 (2) P = 6.37
Star: 4118 (3) P = 6.80
Star: 2142 (2) P = 6.99
Star: 1663 (3) P = 8.69
PM
PNM
PSM
−0.1
0.1
δV
0
0.5
1.0
Phase

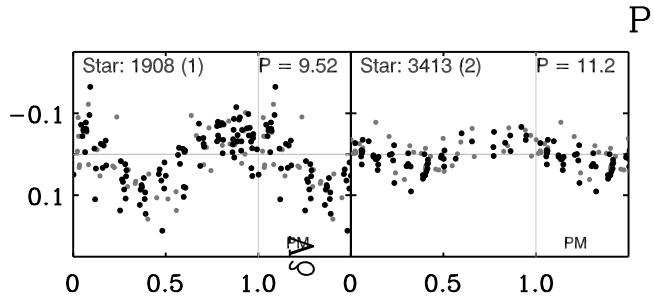
Phase
Star: 1908 (1)
P = 9.52
Star: 3413 (2)
P = 11.2
−0.1
0.1
V−I
PM
PM
0
0.5
1.0
0
0.5
1.0

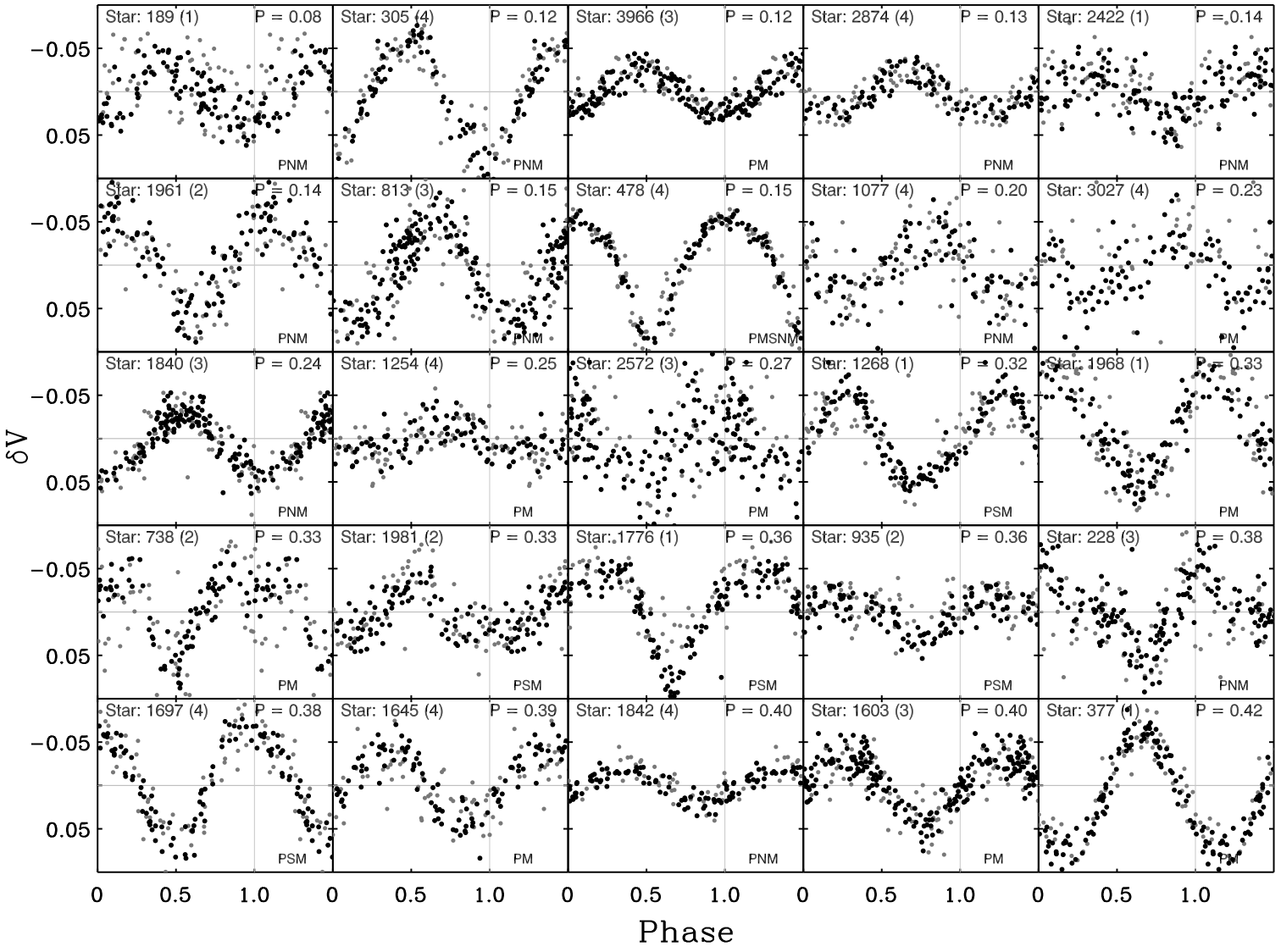
Star: 189 (1) P = 0.08 PNM
Star: 305 (4) P = 0.12 PNM
Star: 3966 (3) P = 0.12 PM
Star: 2874 (4) P = 0.13 PNM
Star: 2422 (1) P = 0.14 PNM
Star: 1961 (2) P = 0.14 PNM
Star: 813 (3) P = 0.15 PNM
Star: 478 (4) P = 0.15 PMSNM
Star: 1077 (4) P = 0.20 PNM
Star: 3027 (4) P = 0.23 PM
Star: 1840 (3) P = 0.24 PNM
Star: 1254 (4) P = 0.25 PM
Star: 2572 (3) P = 0.27 PM
Star: 1268 (1) P = 0.32 PSM
Star: 1968 (1) P = 0.33 PM
Star: 738 (2) P = 0.33 PM
Star: 1981 (2) P = 0.33 PSM
Star: 1776 (1) P = 0.36 PSM
Star: 935 (2) P = 0.36 PSM
Star: 228 (3) P = 0.38 PNM
Star: 1697 (4) P = 0.38 PSM
Star: 1645 (4) P = 0.39 PM
Star: 1842 (4) P = 0.40 PNM
Star: 1603 (3) P = 0.40 PM
Star: 377 (4) P = 0.42 PM
−0.05
0.05
δV
0
0.5
1.0
Phase

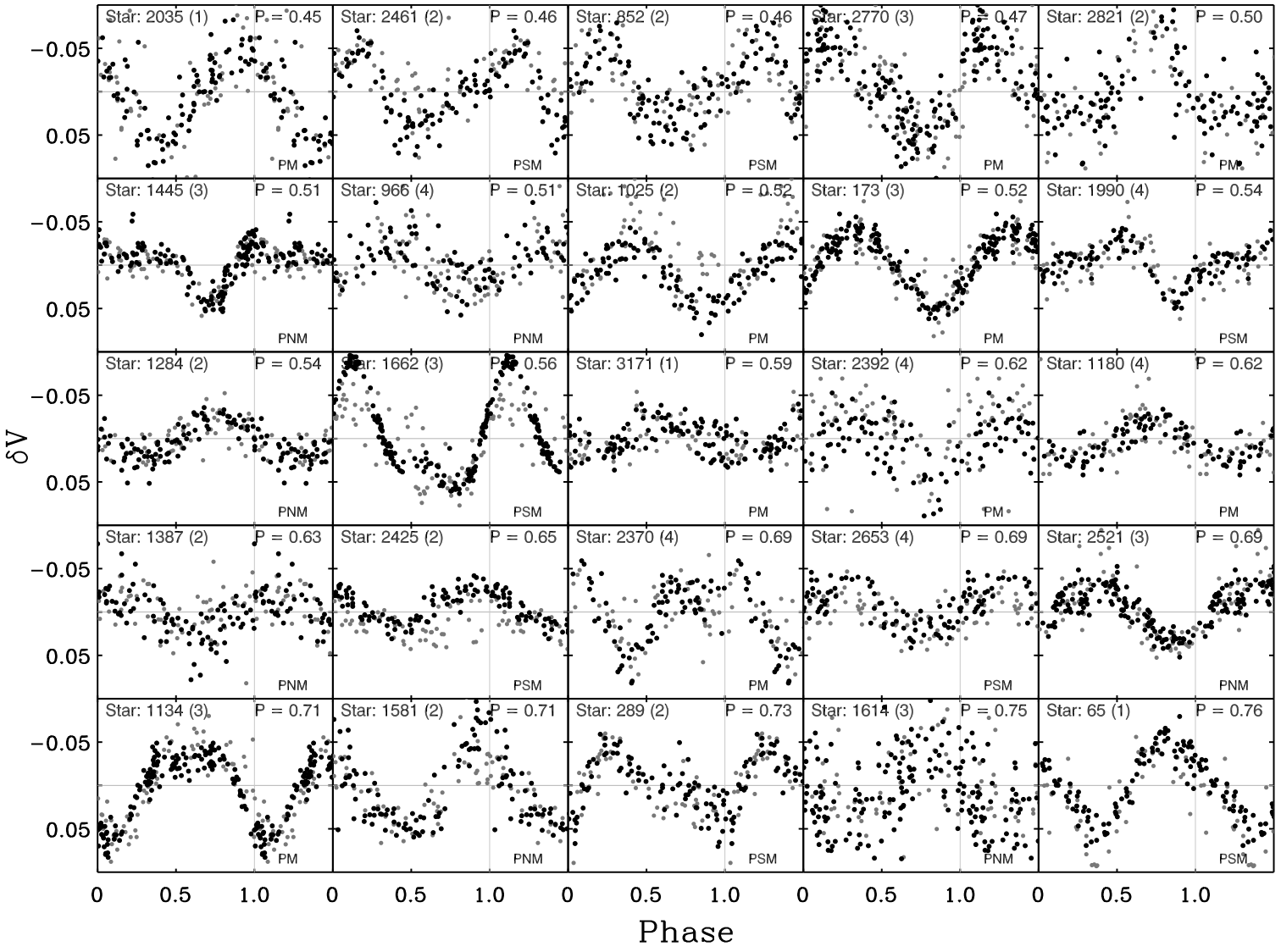
Star: 2035 (1) P = 0.45
Star: 2461 (2) P = 0.46
Star: 852 (2) P = 0.46
Star: 2770 (3) P = 0.47
Star: 2821 (2) P = 0.50
Star: 1445 (3) P = 0.51
Star: 966 (4) P = 0.51
Star: 1025 (2) P = 0.52
Star: 173 (3) P = 0.52
Star: 1990 (4) P = 0.54
Star: 1284 (2) P = 0.54
Star: 1662 (3) P = 0.56
Star: 3171 (1) P = 0.59
Star: 2392 (4) P = 0.62
Star: 1180 (4) P = 0.62
Star: 1387 (2) P = 0.63
Star: 2425 (2) P = 0.65
Star: 2370 (4) P = 0.69
Star: 2653 (4) P = 0.69
Star: 2521 (3) P = 0.69
Star: 1134 (3) P = 0.71
Star: 1581 (2) P = 0.71
Star: 289 (2) P = 0.73
Star: 1614 (3) P = 0.75
Star: 65 (1) P = 0.76
PM
PSM
PNM
−0.05
0.05
δV
0
0.5
1.0
Phase

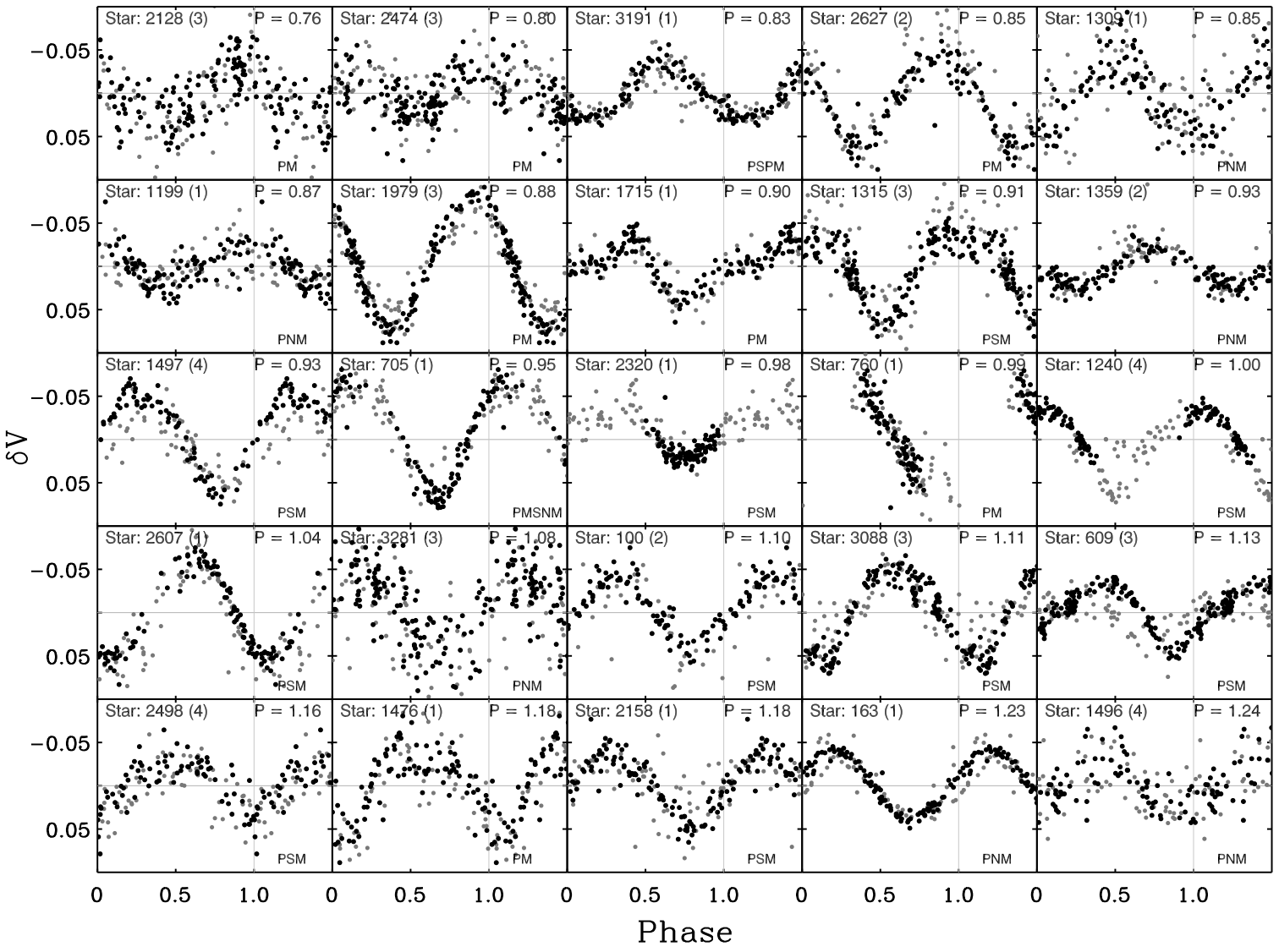
Star: 2128 (3) P = 0.76 PM
Star: 2474 (3) P = 0.80 PM
Star: 3191 (1) P = 0.83 PSPM
Star: 2627 (2) P = 0.85 PM
Star: 1309 (1) P = 0.85 PNM
Star: 1199 (1) P = 0.87 PNM
Star: 1979 (3) P = 0.88 PM
Star: 1715 (1) P = 0.90 PM
Star: 1315 (3) P = 0.91 PSM
Star: 1359 (2) P = 0.93 PNM
Star: 1497 (4) P = 0.93 PSM
Star: 705 (1) P = 0.95 PMSNM
Star: 2320 (1) P = 0.98 PSM
Star: 760 (1) P = 0.99 PM
Star: 1240 (4) P = 1.00 PSM
Star: 2607 (1) P = 1.04 PSM
Star: 3281 (3) P = 1.08 PNM
Star: 100 (2) P = 1.10 PSM
Star: 3088 (3) P = 1.11 PSM
Star: 609 (3) P = 1.13 PSM
Star: 2498 (4) P = 1.16 PSM
Star: 1476 (1) P = 1.18 PM
Star: 2158 (1) P = 1.18 PSM
Star: 163 (1) P = 1.23 PNM
Star: 1496 (4) P = 1.24 PNM
−0.05
0.05
δV
0
0.5
1.0
Phase

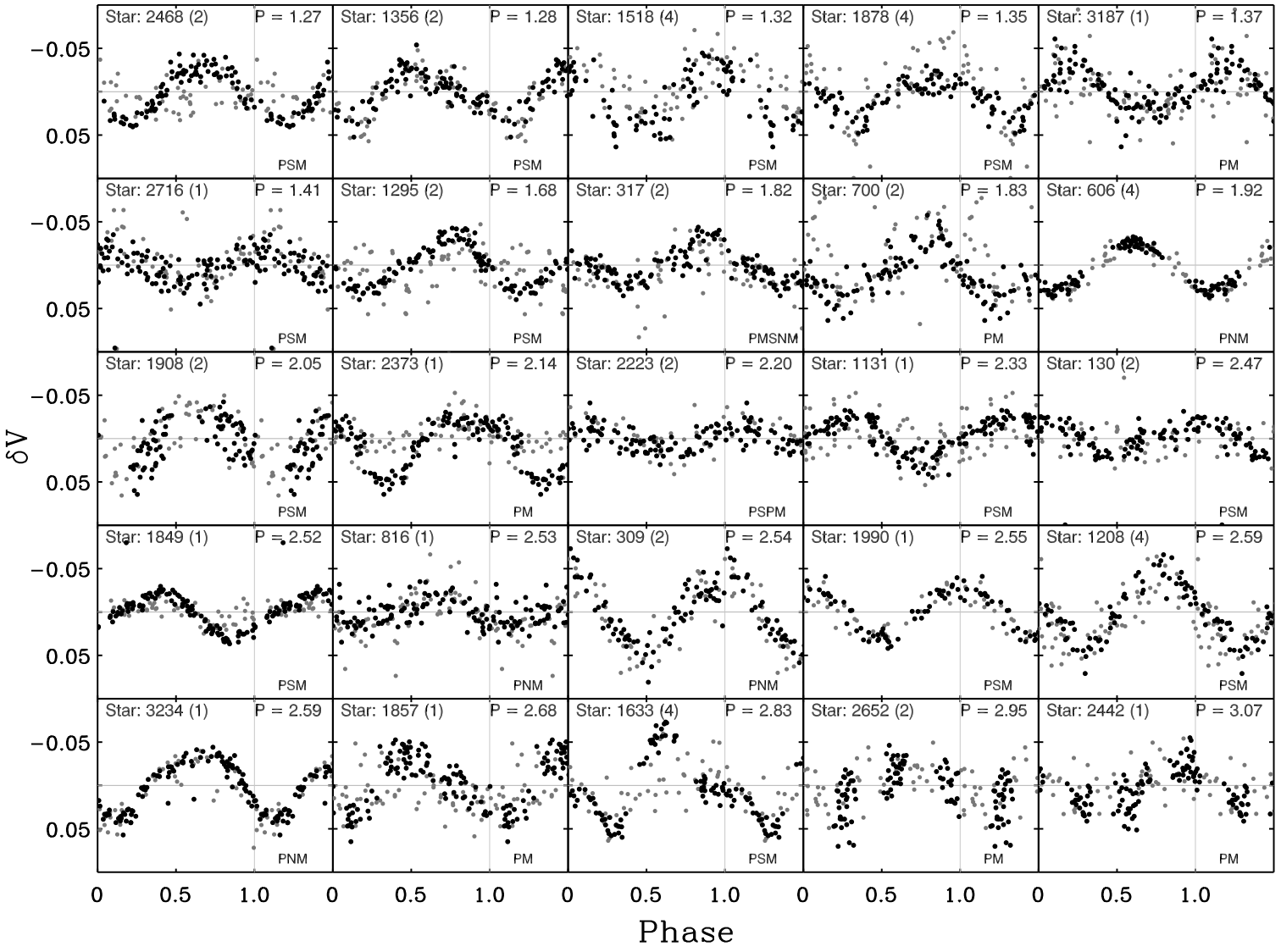
Star: 2468 (2) P = 1.27
Star: 1356 (2) P = 1.28
Star: 1518 (4) P = 1.32
Star: 1878 (4) P = 1.35
Star: 3187 (1) P = 1.37
Star: 2716 (1) P = 1.41
Star: 1295 (2) P = 1.68
Star: 317 (2) P = 1.82
Star: 700 (2) P = 1.83
Star: 606 (4) P = 1.92
Star: 1908 (2) P = 2.05
Star: 2373 (1) P = 2.14
Star: 2223 (2) P = 2.20
Star: 1131 (1) P = 2.33
Star: 130 (2) P = 2.47
Star: 1849 (1) P = 2.52
Star: 816 (1) P = 2.53
Star: 309 (2) P = 2.54
Star: 1990 (1) P = 2.55
Star: 1208 (4) P = 2.59
Star: 3234 (1) P = 2.59
Star: 1857 (1) P = 2.68
Star: 1633 (4) P = 2.83
Star: 2652 (2) P = 2.95
Star: 2442 (1) P = 3.07
PSM
PM
PMSNM
PNM
PSPM
−0.05
0.05
δV
0
0.5
1.0
Phase

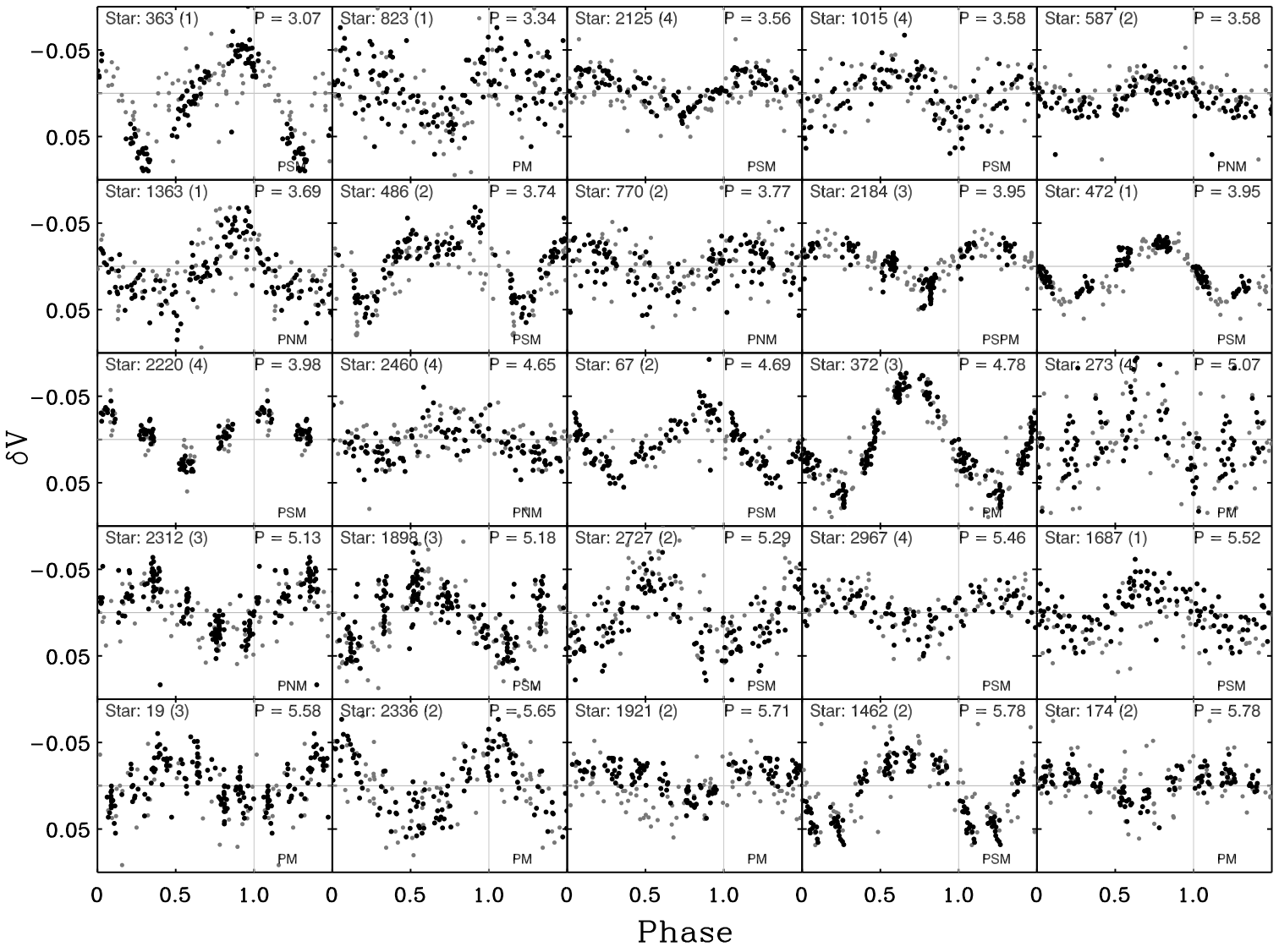
Star: 363 (1) P = 3.07
Star: 823 (1) P = 3.34
Star: 2125 (4) P = 3.56
Star: 1015 (4) P = 3.58
Star: 587 (2) P = 3.58
Star: 1363 (1) P = 3.69
Star: 486 (2) P = 3.74
Star: 770 (2) P = 3.77
Star: 2184 (3) P = 3.95
Star: 472 (1) P = 3.95
Star: 2220 (4) P = 3.98
Star: 2460 (4) P = 4.65
Star: 67 (2) P = 4.69
Star: 372 (3) P = 4.78
Star: 273 (4) P = 5.07
Star: 2312 (3) P = 5.13
Star: 1898 (3) P = 5.18
Star: 2727 (2) P = 5.29
Star: 2967 (4) P = 5.46
Star: 1687 (1) P = 5.52
Star: 19 (3) P = 5.58
Star: 2336 (2) P = 5.65
Star: 1921 (2) P = 5.71
Star: 1462 (2) P = 5.78
Star: 174 (2) P = 5.78
PSM
PM
PNM
PSPM
−0.05
0.05
δV
0
0.5
1.0
Phase

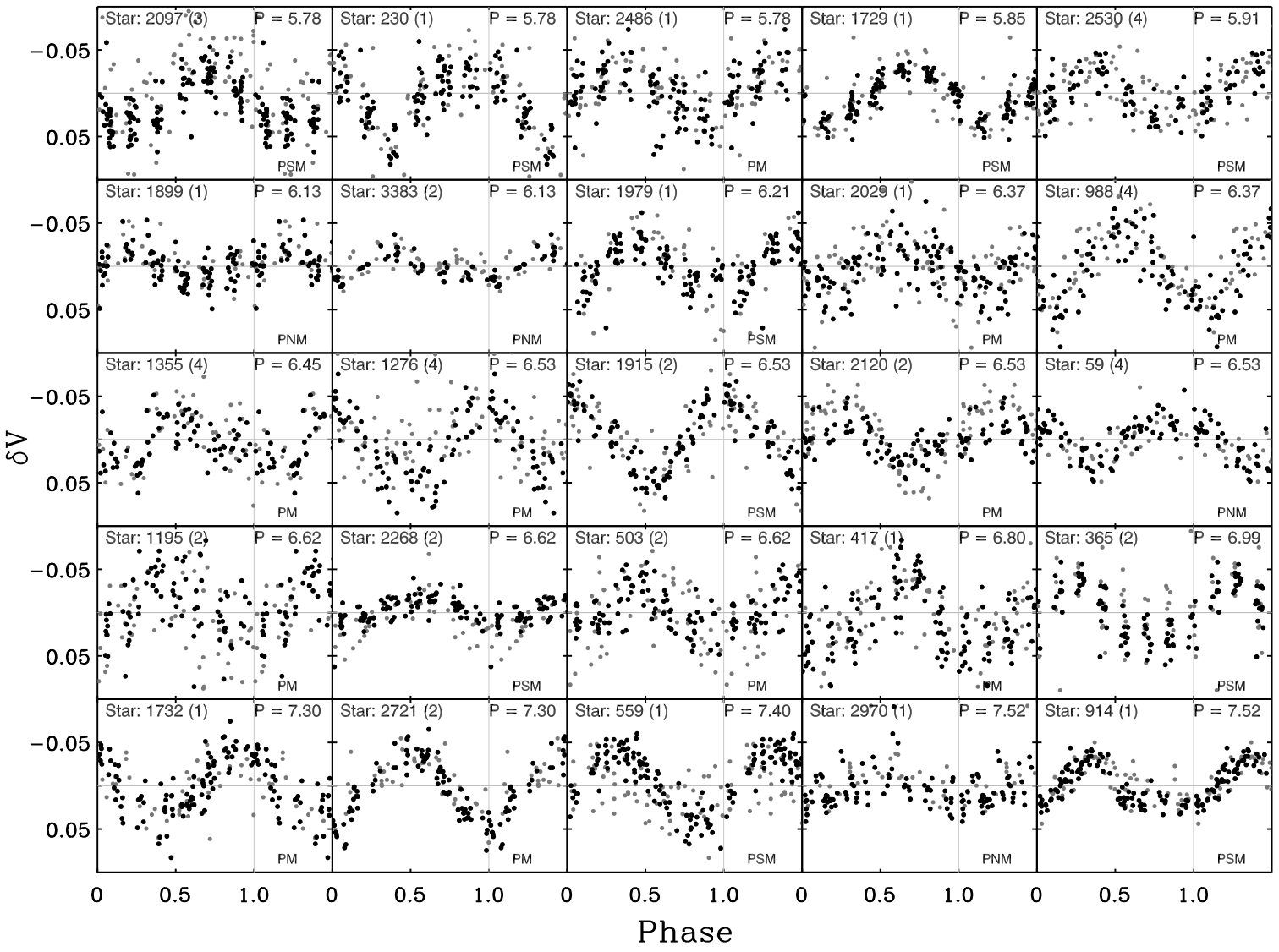
Star: 2097 (3) P = 5.78
Star: 230 (1) P = 5.78
Star: 2486 (1) P = 5.78
Star: 1729 (1) P = 5.85
Star: 2530 (4) P = 5.91
Star: 1899 (1) P = 6.13
Star: 3383 (2) P = 6.13
Star: 1979 (1) P = 6.21
Star: 2029 (1) P = 6.37
Star: 988 (4) P = 6.37
Star: 1355 (4) P = 6.45
Star: 1276 (4) P = 6.53
Star: 1915 (2) P = 6.53
Star: 2120 (2) P = 6.53
Star: 59 (4) P = 6.53
Star: 1195 (2) P = 6.62
Star: 2268 (2) P = 6.62
Star: 503 (2) P = 6.62
Star: 417 (1) P = 6.80
Star: 365 (2) P = 6.99
Star: 1732 (1) P = 7.30
Star: 2721 (2) P = 7.30
Star: 559 (1) P = 7.40
Star: 2970 (1) P = 7.52
Star: 914 (1) P = 7.52
PSM
PNM
PM
−0.05
0.05
δV
0
0.5
1.0
Phase

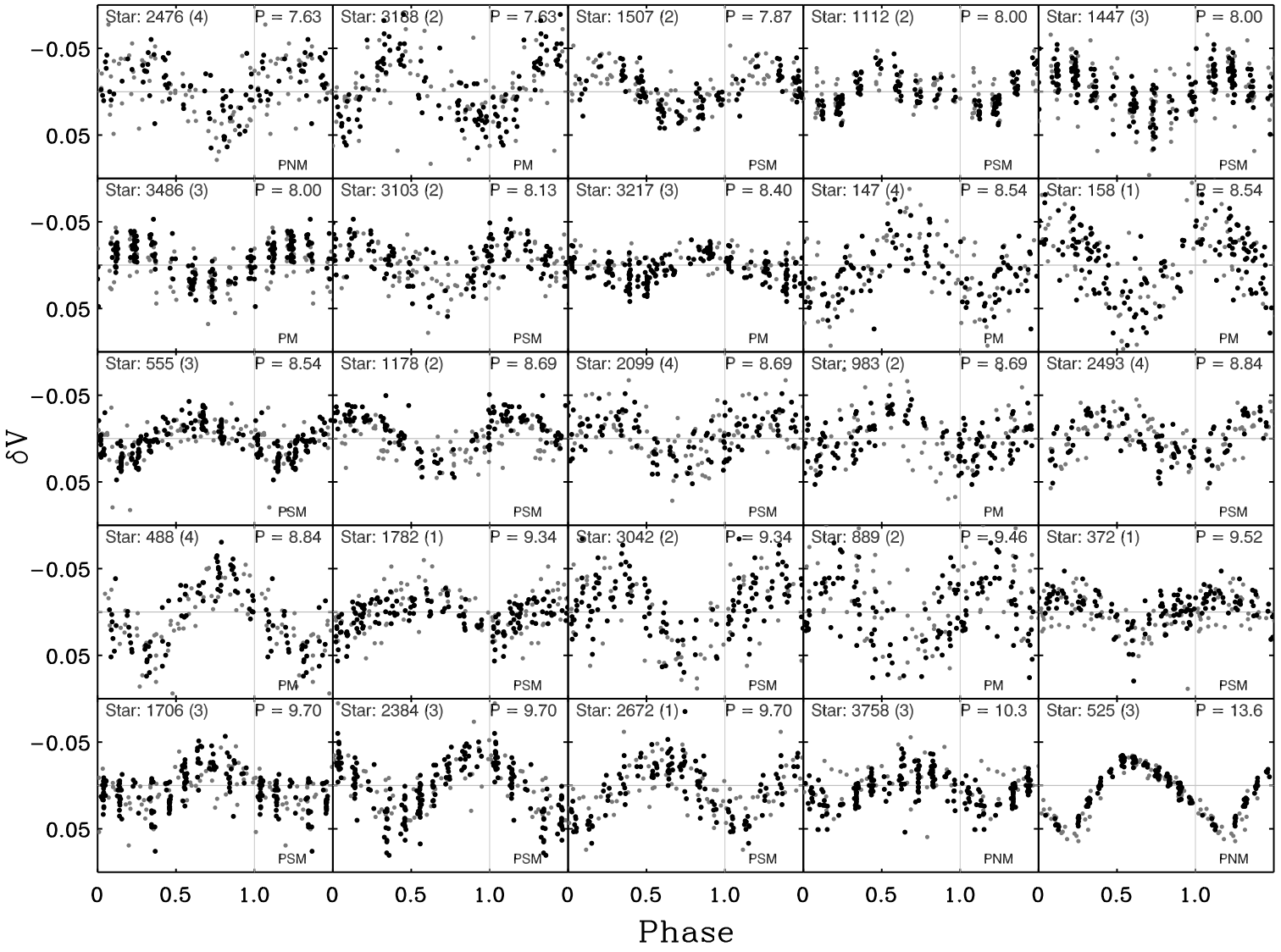
Star: 2476 (4) P = 7.63
Star: 3188 (2) P = 7.63
Star: 1507 (2) P = 7.87
Star: 1112 (2) P = 8.00
Star: 1447 (3) P = 8.00
Star: 3486 (3) P = 8.00
Star: 3103 (2) P = 8.13
Star: 3217 (3) P = 8.40
Star: 147 (4) P = 8.54
Star: 158 (1) P = 8.54
Star: 555 (3) P = 8.54
Star: 1178 (2) P = 8.69
Star: 2099 (4) P = 8.69
Star: 983 (2) P = 8.69
Star: 2493 (4) P = 8.84
Star: 488 (4) P = 8.84
Star: 1782 (1) P = 9.34
Star: 3042 (2) P = 9.34
Star: 889 (2) P = 9.46
Star: 372 (1) P = 9.52
Star: 1706 (3) P = 9.70
Star: 2384 (3) P = 9.70
Star: 2672 (1) P = 9.70
Star: 3758 (3) P = 10.3
Star: 525 (3) P = 13.6
PNM
PM
PSM
−0.05
0.05
δV
0
0.5
1.0
Phase

−0.05
0.05
0
0.5
1.0
0
0.5
1.0
Star: 955 (1)
P = 15.3
PM
Star: 115
P = 58.4
PNM
δV
Phase

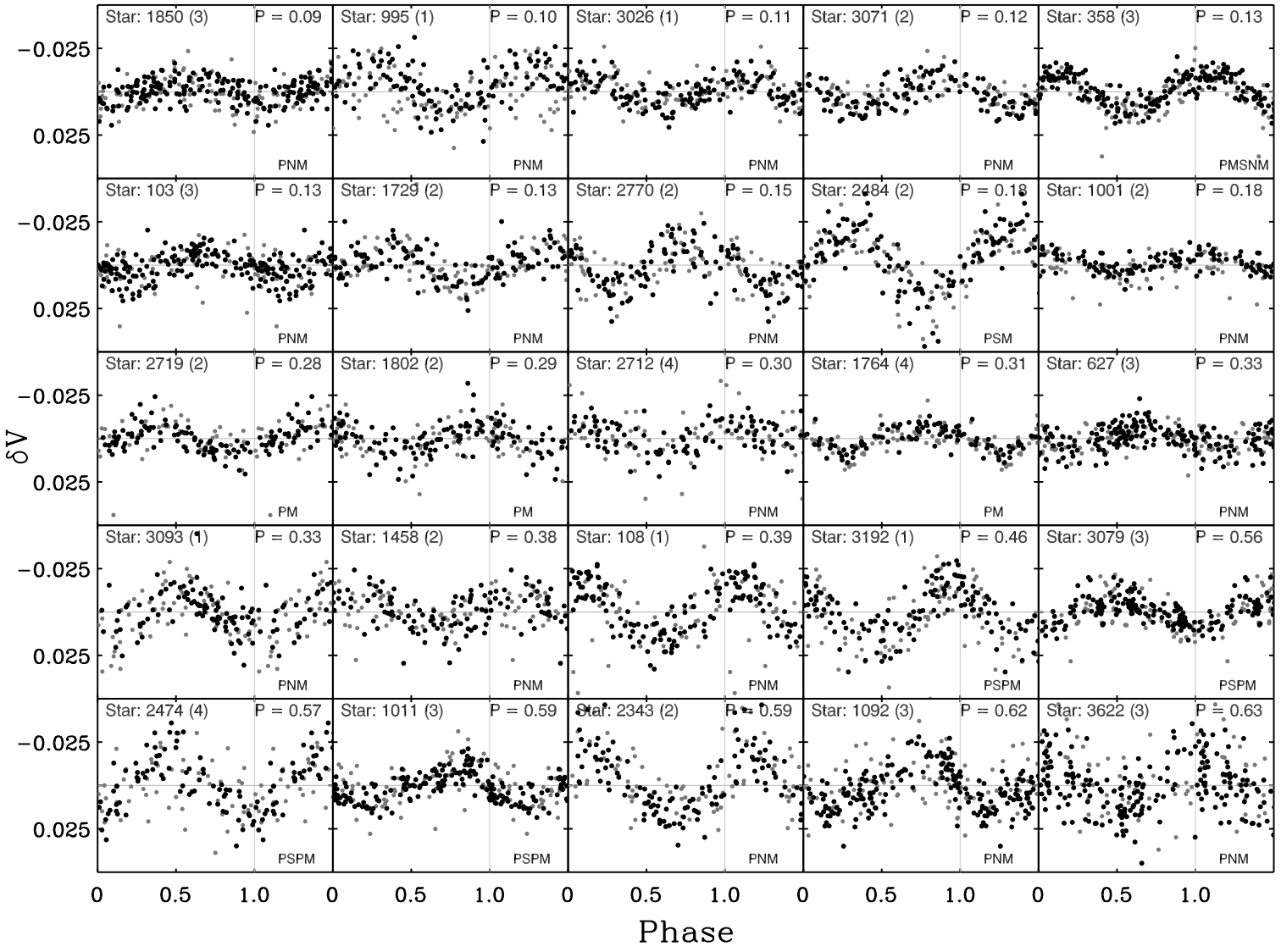
Star: 1850 (3) P = 0.09
Star: 995 (1) P = 0.10
Star: 3026 (1) P = 0.11
Star: 3071 (2) P = 0.12
Star: 358 (3) P = 0.13
Star: 103 (3) P = 0.13
Star: 1729 (2) P = 0.13
Star: 2770 (2) P = 0.15
Star: 2484 (2) P = 0.18
Star: 1001 (2) P = 0.18
Star: 2719 (2) P = 0.28
Star: 1802 (2) P = 0.29
Star: 2712 (4) P = 0.30
Star: 1764 (4) P = 0.31
Star: 627 (3) P = 0.33
Star: 3093 (1) P = 0.33
Star: 1458 (2) P = 0.38
Star: 108 (1) P = 0.39
Star: 3192 (1) P = 0.46
Star: 3079 (3) P = 0.56
Star: 2474 (4) P = 0.57
Star: 1011 (3) P = 0.59
Star: 2343 (2) P = 0.59
Star: 1092 (3) P = 0.62
Star: 3622 (3) P = 0.63
PNM
PMSNM
PSM
PM
PSPM
−0.025
0.025
δV
0
0.5
1.0
Phase

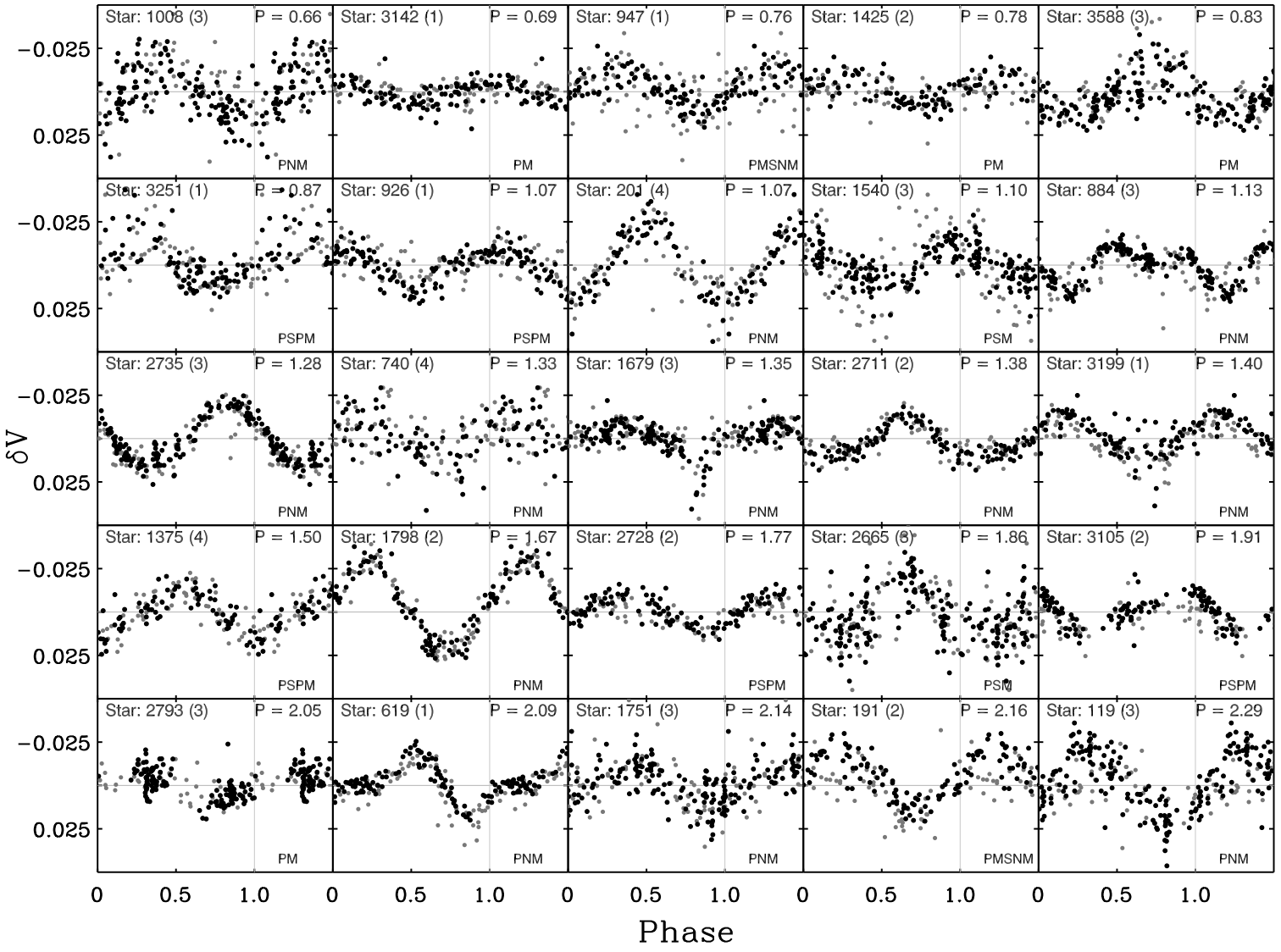
Star: 1008 (3) P = 0.66 PNM
Star: 3142 (1) P = 0.69 PM
Star: 947 (1) P = 0.76 PMSNM
Star: 1425 (2) P = 0.78 PM
Star: 3588 (3) P = 0.83 PM
Star: 3251 (1) P = 0.87 PSPM
Star: 926 (1) P = 1.07 PSPM
Star: 201 (4) P = 1.07 PNM
Star: 1540 (3) P = 1.10 PSM
Star: 884 (3) P = 1.13 PNM
Star: 2735 (3) P = 1.28 PNM
Star: 740 (4) P = 1.33 PNM
Star: 1679 (3) P = 1.35 PNM
Star: 2711 (2) P = 1.38 PNM
Star: 3199 (1) P = 1.40 PNM
Star: 1375 (4) P = 1.50 PSPM
Star: 1798 (2) P = 1.67 PNM
Star: 2728 (2) P = 1.77 PSPM
Star: 2665 (8) P = 1.86 PSM
Star: 3105 (2) P = 1.91 PSPM
Star: 2793 (3) P = 2.05 PM
Star: 619 (1) P = 2.09 PNM
Star: 1751 (3) P = 2.14 PNM
Star: 191 (2) P = 2.16 PMSNM
Star: 119 (3) P = 2.29 PNM
−0.025
0.025
δV
0
0.5
1.0
Phase

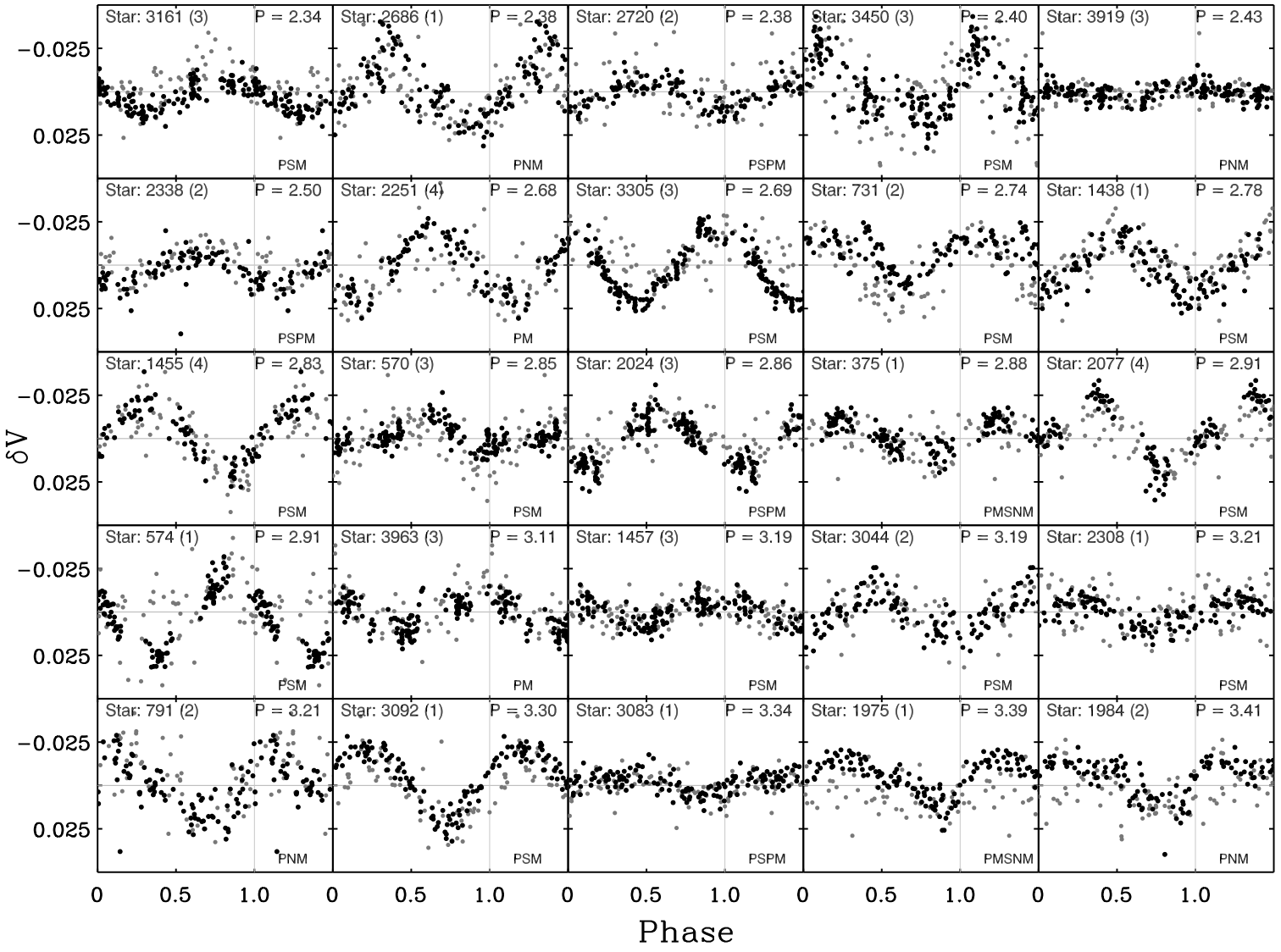
Star: 3161 (3) P = 2.34
Star: 2686 (1) P = 2.38
Star: 2720 (2) P = 2.38
Star: 3450 (3) P = 2.40
Star: 3919 (3) P = 2.43
Star: 2338 (2) P = 2.50
Star: 2251 (4) P = 2.68
Star: 3305 (3) P = 2.69
Star: 731 (2) P = 2.74
Star: 1438 (1) P = 2.78
Star: 1455 (4) P = 2.83
Star: 570 (3) P = 2.85
Star: 2024 (3) P = 2.86
Star: 375 (1) P = 2.88
Star: 2077 (4) P = 2.91
Star: 574 (1) P = 2.91
Star: 3963 (3) P = 3.11
Star: 1457 (3) P = 3.19
Star: 3044 (2) P = 3.19
Star: 2308 (1) P = 3.21
Star: 791 (2) P = 3.21
Star: 3092 (1) P = 3.30
Star: 3083 (1) P = 3.34
Star: 1975 (1) P = 3.39
Star: 1984 (2) P = 3.41
PSM
PNM
PSPM
PM
PMSNM
−0.025
0.025
δV
0
0.5
1.0
Phase

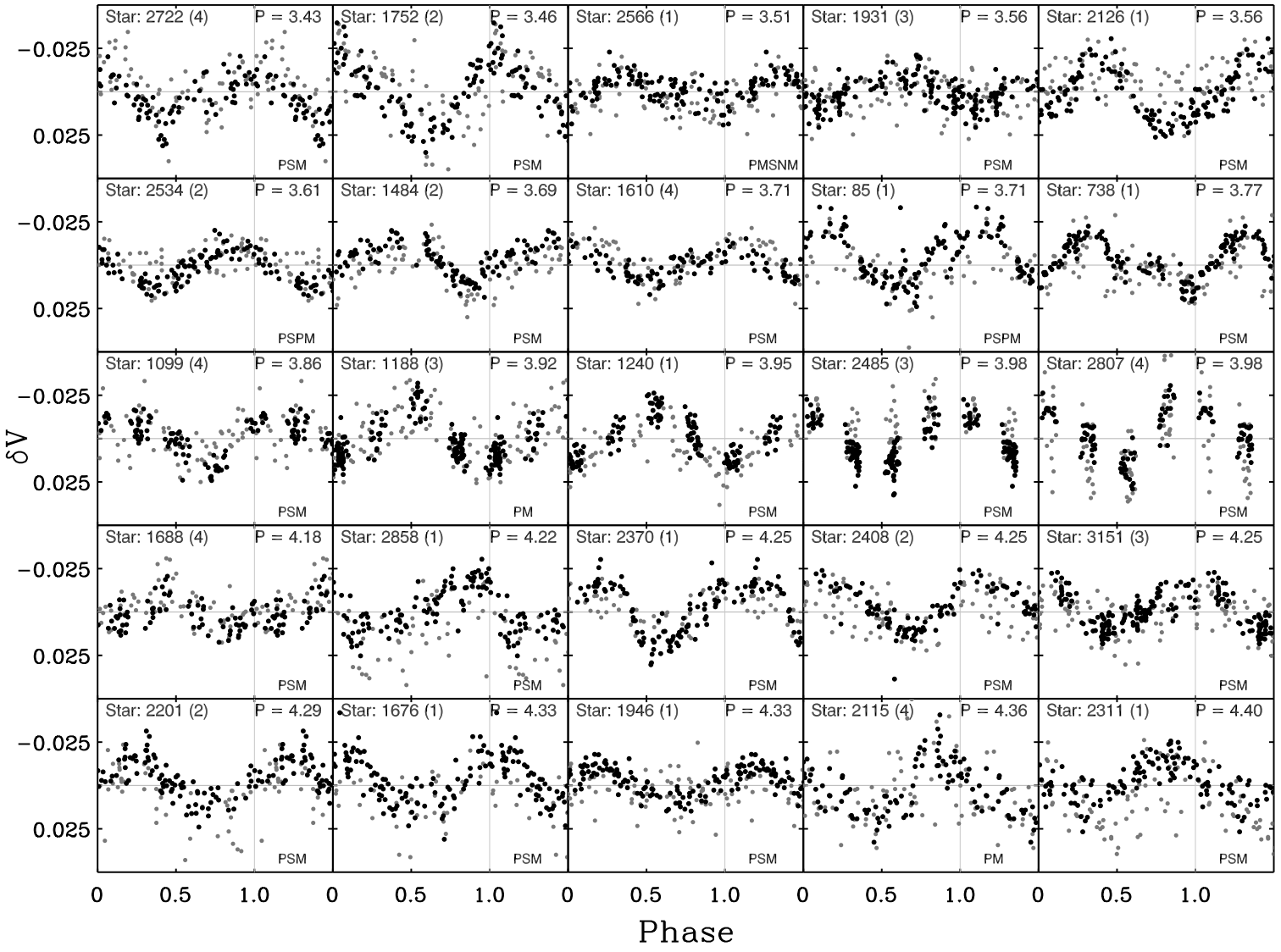
Star: 2722 (4) P = 3.43
Star: 1752 (2) P = 3.46
Star: 2566 (1) P = 3.51
Star: 1931 (3) P = 3.56
Star: 2126 (1) P = 3.56
Star: 2534 (2) P = 3.61
Star: 1484 (2) P = 3.69
Star: 1610 (4) P = 3.71
Star: 85 (1) P = 3.71
Star: 738 (1) P = 3.77
Star: 1099 (4) P = 3.86
Star: 1188 (3) P = 3.92
Star: 1240 (1) P = 3.95
Star: 2485 (3) P = 3.98
Star: 2807 (4) P = 3.98
Star: 1688 (4) P = 4.18
Star: 2858 (1) P = 4.22
Star: 2370 (1) P = 4.25
Star: 2408 (2) P = 4.25
Star: 3151 (3) P = 4.25
Star: 2201 (2) P = 4.29
Star: 1676 (1) P = 4.33
Star: 1946 (1) P = 4.33
Star: 2115 (4) P = 4.36
Star: 2311 (1) P = 4.40
PSM
PMSNM
PSPM
PM
−0.025
0.025
δV
0
0.5
1.0
Phase

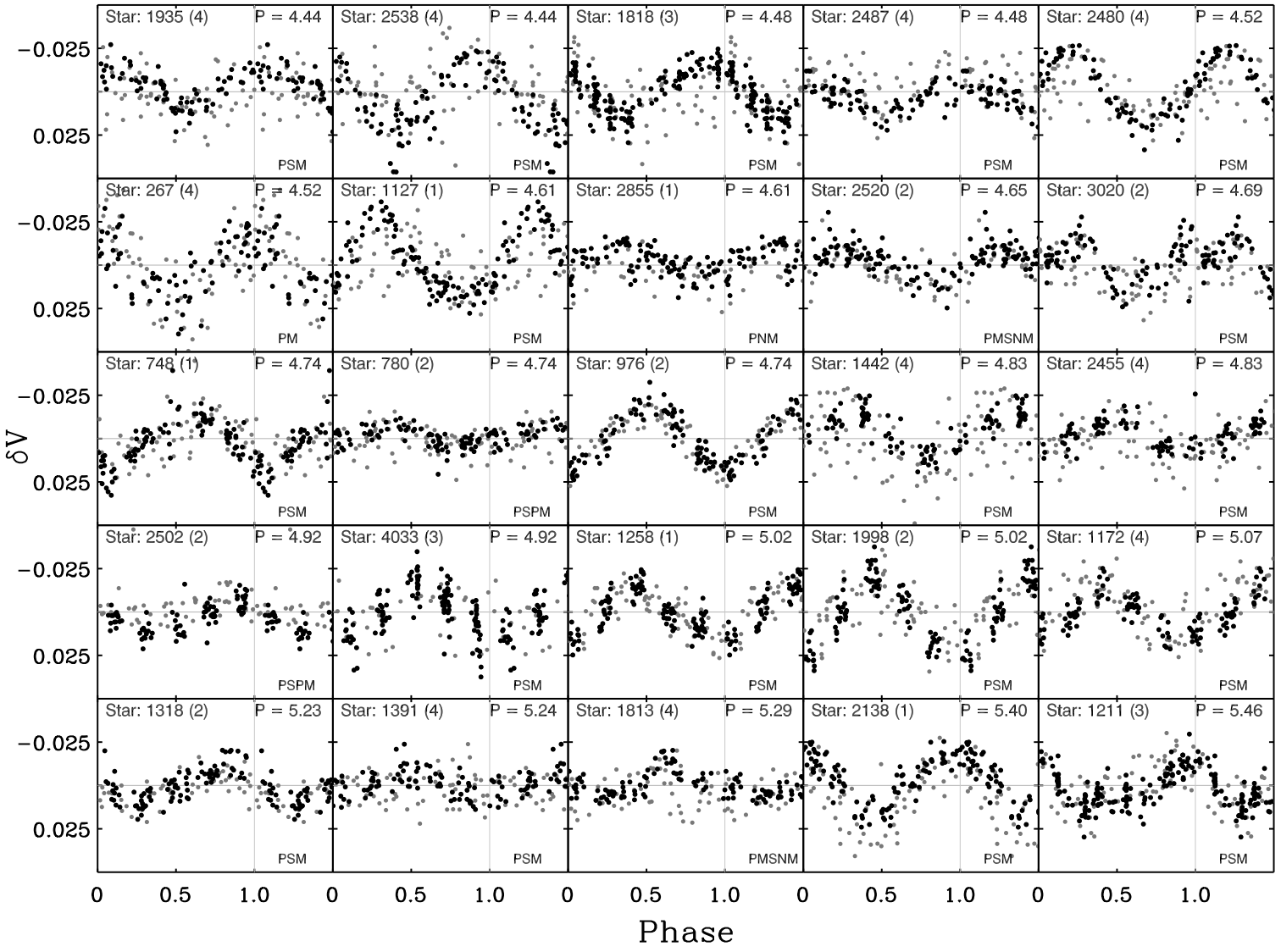
Star: 1935 (4) P = 4.44
Star: 2538 (4) P = 4.44
Star: 1818 (3) P = 4.48
Star: 2487 (4) P = 4.48
Star: 2480 (4) P = 4.52
Star: 267 (4) P = 4.52
Star: 1127 (1) P = 4.61
Star: 2855 (1) P = 4.61
Star: 2520 (2) P = 4.65
Star: 3020 (2) P = 4.69
Star: 748 (1) P = 4.74
Star: 780 (2) P = 4.74
Star: 976 (2) P = 4.74
Star: 1442 (4) P = 4.83
Star: 2455 (4) P = 4.83
Star: 2502 (2) P = 4.92
Star: 4033 (3) P = 4.92
Star: 1258 (1) P = 5.02
Star: 1998 (2) P = 5.02
Star: 1172 (4) P = 5.07
Star: 1318 (2) P = 5.23
Star: 1391 (4) P = 5.24
Star: 1813 (4) P = 5.29
Star: 2138 (1) P = 5.40
Star: 1211 (3) P = 5.46
PSM
PM
PNM
PMSNM
PSPM
−0.025
0.025
δV
0
0.5
1.0
Phase

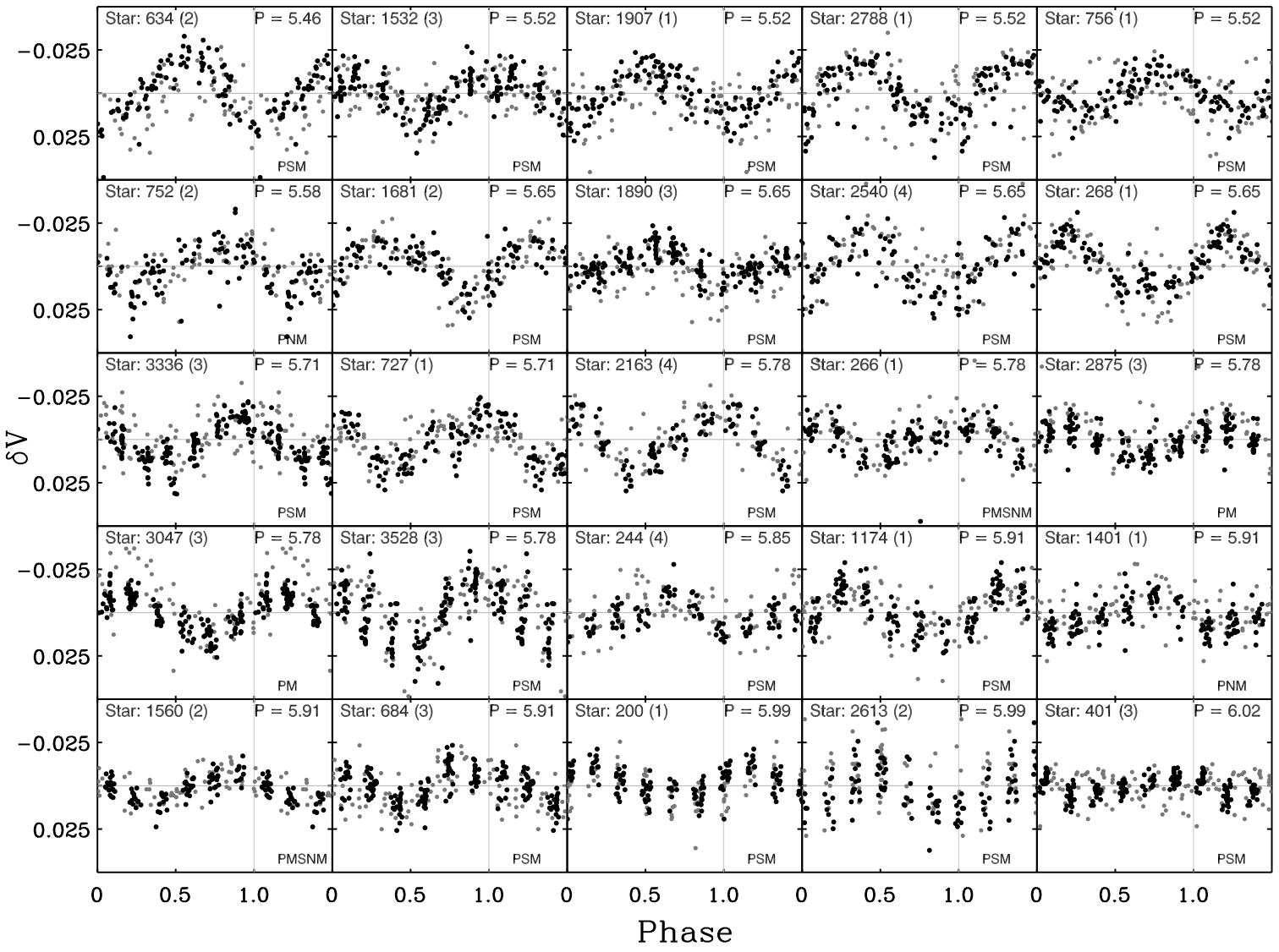
Star: 634 (2) P = 5.46
Star: 1532 (3) P = 5.52
Star: 1907 (1) P = 5.52
Star: 2788 (1) P = 5.52
Star: 756 (1) P = 5.52
Star: 752 (2) P = 5.58
Star: 1681 (2) P = 5.65
Star: 1890 (3) P = 5.65
Star: 2540 (4) P = 5.65
Star: 268 (1) P = 5.65
Star: 3336 (3) P = 5.71
Star: 727 (1) P = 5.71
Star: 2163 (4) P = 5.78
Star: 266 (1) P = 5.78
Star: 2875 (3) P = 5.78
Star: 3047 (3) P = 5.78
Star: 3528 (3) P = 5.78
Star: 244 (4) P = 5.85
Star: 1174 (1) P = 5.91
Star: 1401 (1) P = 5.91
Star: 1560 (2) P = 5.91
Star: 684 (3) P = 5.91
Star: 200 (1) P = 5.99
Star: 2613 (2) P = 5.99
Star: 401 (3) P = 6.02
PSM
PNM
PMSNM
PM
−0.025
0.025
δV
0
0.5
1.0
Phase

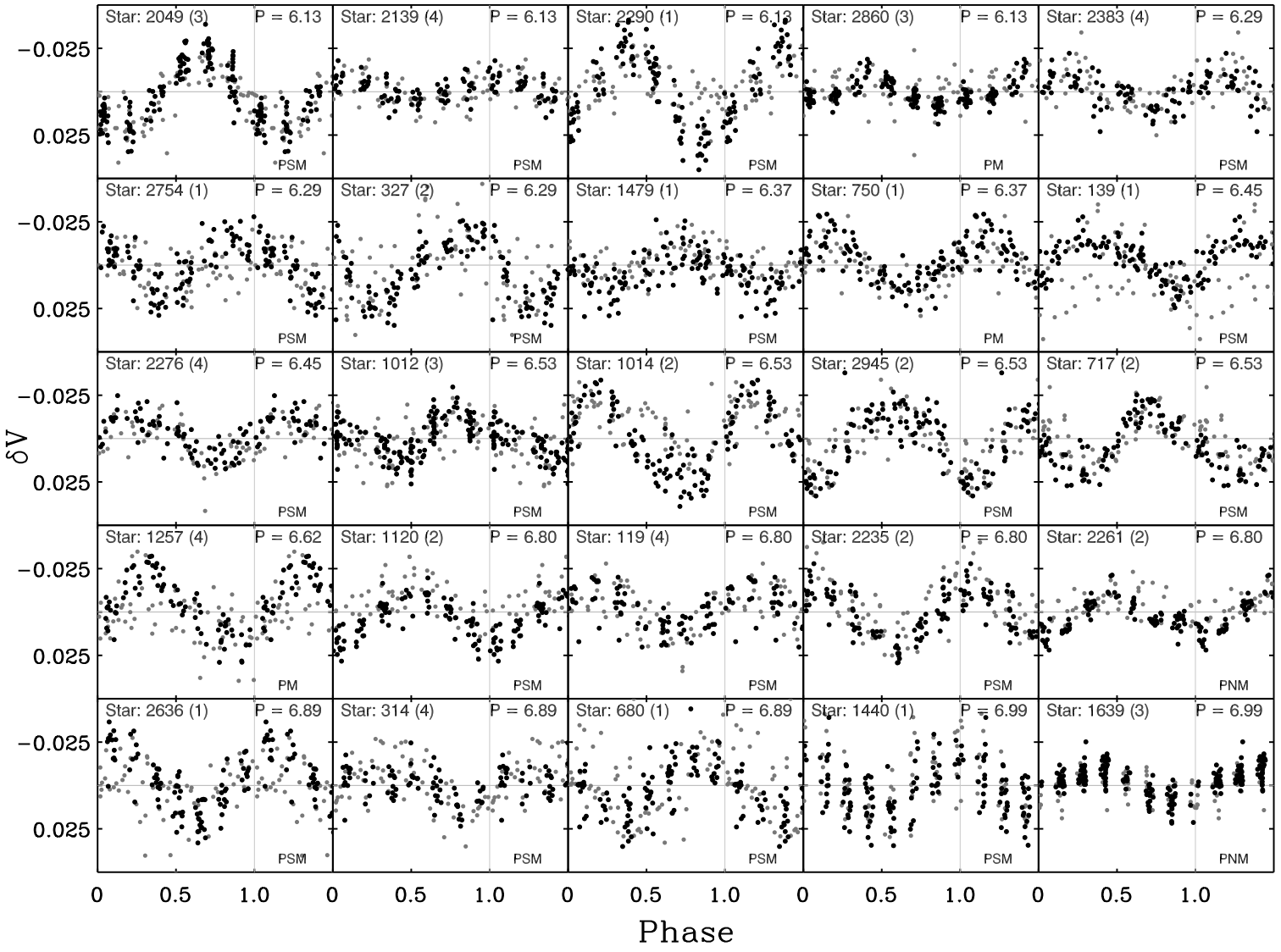
Star: 2049 (3) P = 6.13
Star: 2139 (4) P = 6.13
Star: 2290 (1) P = 6.13
Star: 2860 (3) P = 6.13
Star: 2383 (4) P = 6.29
Star: 2754 (1) P = 6.29
Star: 327 (2) P = 6.29
Star: 1479 (1) P = 6.37
Star: 750 (1) P = 6.37
Star: 139 (1) P = 6.45
Star: 2276 (4) P = 6.45
Star: 1012 (3) P = 6.53
Star: 1014 (2) P = 6.53
Star: 2945 (2) P = 6.53
Star: 717 (2) P = 6.53
Star: 1257 (4) P = 6.62
Star: 1120 (2) P = 6.80
Star: 119 (4) P = 6.80
Star: 2235 (2) P = 6.80
Star: 2261 (2) P = 6.80
Star: 2636 (1) P = 6.89
Star: 314 (4) P = 6.89
Star: 680 (1) P = 6.89
Star: 1440 (1) P = 6.99
Star: 1639 (3) P = 6.99
PSM
PM
PNM
−0.025
0.025
δV
0
0.5
1.0
Phase

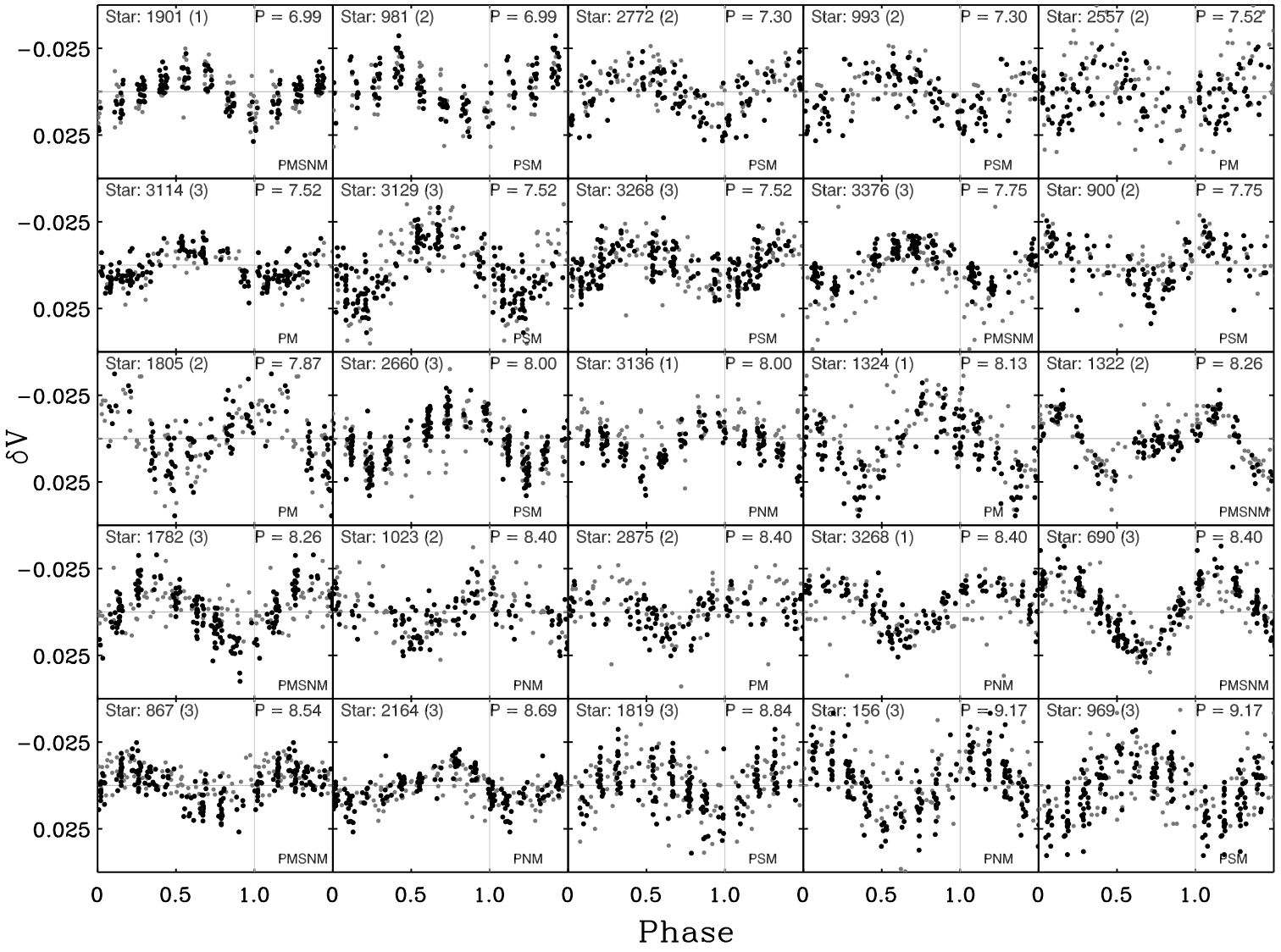
Star: 1901 (1) P = 6.99
Star: 981 (2) P = 6.99
Star: 2772 (2) P = 7.30
Star: 993 (2) P = 7.30
Star: 2557 (2) P = 7.52
Star: 3114 (3) P = 7.52
Star: 3129 (3) P = 7.52
Star: 3268 (3) P = 7.52
Star: 3376 (3) P = 7.75
Star: 900 (2) P = 7.75
Star: 1805 (2) P = 7.87
Star: 2660 (3) P = 8.00
Star: 3136 (1) P = 8.00
Star: 1324 (1) P = 8.13
Star: 1322 (2) P = 8.26
Star: 1782 (3) P = 8.26
Star: 1023 (2) P = 8.40
Star: 2875 (2) P = 8.40
Star: 3268 (1) P = 8.40
Star: 690 (3) P = 8.40
Star: 867 (3) P = 8.54
Star: 2164 (3) P = 8.69
Star: 1819 (3) P = 8.84
Star: 156 (3) P = 9.17
Star: 969 (3) P = 9.17
PMSNM
PSM
PM
PNM
−0.025
0.025
δV
0
0.5
1.0
Phase

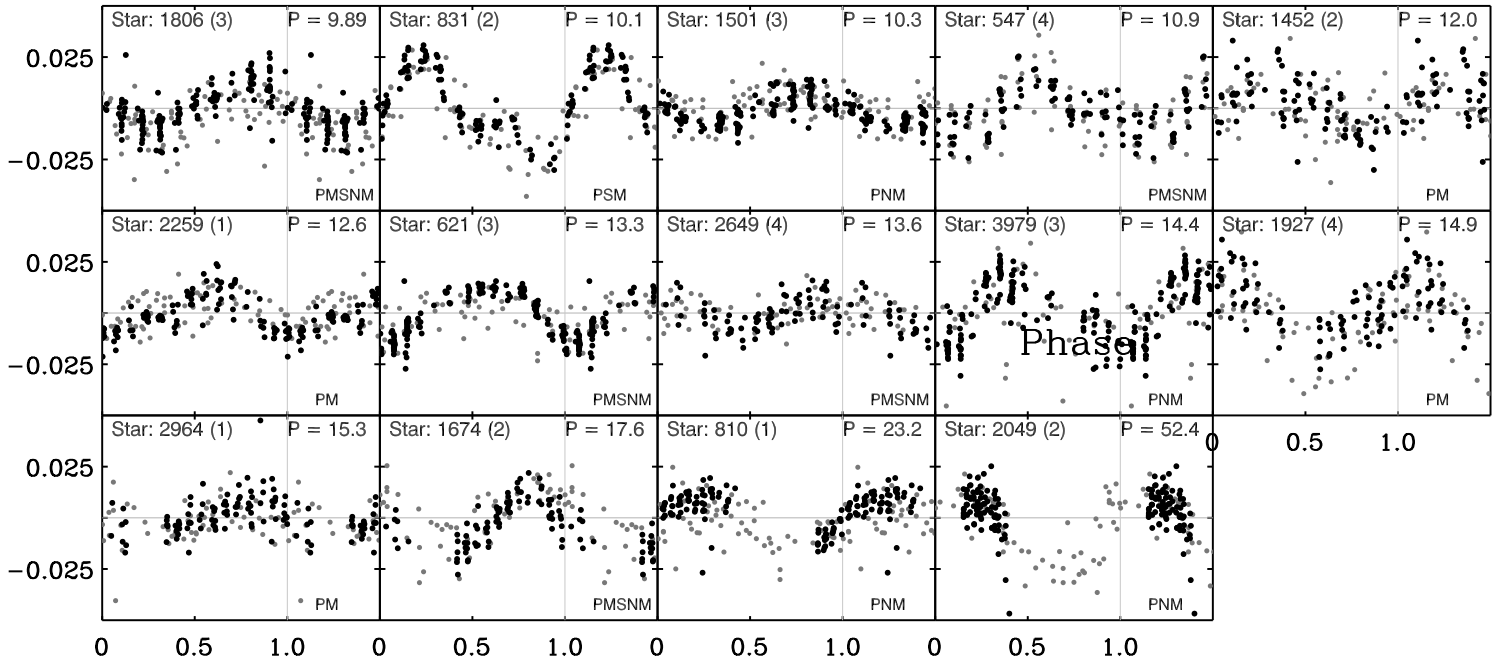
Star: 1806 (3) P = 9.89 PMSNM
Star: 831 (2) P = 10.1 PSM
Star: 1501 (3) P = 10.3 PNM
Star: 547 (4) P = 10.9 PMSNM
Star: 1452 (2) P = 12.0 PM
Star: 2259 (1) P = 12.6 PM
Star: 621 (3) P = 13.3 PMSNM
Star: 2649 (4) P = 13.6 PMSNM
Star: 3979 (3) P = 14.4 PNM
Star: 1927 (4) P = 14.9 PM
Star: 2964 (1) P = 15.3 PM
Star: 1674 (2) P = 17.6 PMSNM
Star: 810 (1) P = 23.2 PNM
Star: 2049 (2) P = 52.4 PNM
0.025
−0.025
0
0.5
1.0
Phase

Appendix B

DATA FOR ROTATOR SAMPLE IN M35

This appendix presents in Table 1 the astrometric, photometric, and spectroscopic (radial-velocity; RV) data for the 443 rotators in the field of M35. The stars are sorted with respect to rotation period (column 4).

Table B.1:: Data for rotator sample in M35

ID	**RA** ^{o}	**DEC** ^{o}	P_r **Days**	**U**	**B**	**V**	**R**	**I**	N_{RV}	$\bar{RV}$ $km\ s^{-1}$	σ_{RV} $km\ s^{-1}$	P_{RV} **%**	P_{PM} **%**
189	92.113058	24.354480	0.088	16.544	16.422	15.802	15.440	15.049	...	...	...	...	...
1850	92.134099	24.259229	0.095	16.414	16.282	15.613	15.173	14.720	...	...	...	...	...
995	92.179989	24.500319	0.107	...	17.150	16.504	16.089	15.618	...	...	...	...	...
3026	92.180341	24.623497	0.111	...	16.135	15.487	15.066	14.631	...	...	...	...	...
305	92.578988	24.054961	0.126	...	18.265	17.337	16.667	16.037	...	...	...	...	...
3966	92.098674	24.097875	0.127	...	13.430	12.891	12.559	12.192	1	7.16	0	0	95
2713	92.183529	24.609518	0.127	...	...	19.612	18.856	18.219	...	...	...	...	...
3071	92.281328	24.397062	0.127	16.364	16.088	15.420	14.995	14.511	...	...	...	...	...
358	92.060631	24.052470	0.130	...	15.392	14.757	14.373	13.922	3	15.32	0.08	0	...
1729	92.482243	24.573235	0.132	...	16.467	15.790	15.348	14.877	...	...	...	...	...
2787	92.562644	24.550633	0.133	...	...	19.695	18.971	18.250	...	...	...	...	...
2874	92.562988	24.173453	0.138	...	13.813	13.113	12.701	12.227	...	...	...	...	...
2422	92.065518	24.523284	0.140	...	18.252	17.516	17.011	16.531	...	...	...	...	...
1916	92.199079	24.269366	0.142	...	19.585	18.558	17.882	17.168	...	...	...	...	...
2056	92.415855	24.622555	0.147	...	...	18.793	18.008	17.299	...	...	...	...	...
1542	92.234091	24.616241	0.148	...	...	18.507	17.890	17.211	...	...	...	...	...
1961	92.316948	24.608539	0.148	...	19.035	18.230	17.669	17.126	...	...	...	...	...
2770	92.481407	24.545228	0.154	...	16.375	15.671	15.213	14.753	...	...	...	...	...
813	92.248611	24.107586	0.157	...	...	18.336	17.647	16.984	...	...	...	...	...
478	92.507756	24.097187	0.158	...	16.742	15.929	15.352	14.780	3	0.85	1.36	0	...
141	92.083710	24.020058	0.163	...	...	...	...	...	...	...	...	...	...
740	92.545251	24.424651	0.164	...	17.942	16.982	16.424	15.881	...	...	...	...	...
2436	92.568450	24.267544	0.178	...	18.719	17.935	17.318	16.732	...	...	...	...	...
575	91.919122	24.084354	0.181	...	19.078	18.276	17.731	17.158	...	...	...	...	...
2484	92.511957	24.430964	0.185	...	17.575	16.555	15.914	15.279	1	1.50	0	0	...
3796	92.114152	24.204246	0.194	...	18.811	17.955	17.388	16.798	...	...	...	...	...
397	92.489225	24.077479	0.195	...	...	18.000	17.296	16.611	...	...	...	...	...

Continued on Next Page...

Table B.1 – Continued

ID	**RA** $h\ \ m\ \ s$	**DEC** $^o\ \ '\ \ ''$	P_r **Days**	**U**	**B**	**V**	**R**	**I**	N_{RV}	$\bar{RV}$ $km\ s^{-1}$	σ_{RV} $km\ s^{-1}$	P_{RV} %	P_{PM} %
336	92.065804	24.049766	0.197	...	...	19.277	18.671	18.024	...	...	...	...	...
1077	92.489599	24.224998	0.202	...	19.185	18.262	17.584	16.857	...	...	...	...	...
3027	92.254734	24.300157	0.236	...	19.248	17.907	17.067	16.281	1	133.01	0	0	...
1840	92.053892	24.260351	0.240	18.088	17.884	17.300	16.905	16.460	...	...	...	...	...
731	92.132759	24.450738	0.244	...	19.301	17.924	17.084	16.264	1	-12.92	0	1	...
1088	92.295402	24.480767	0.259	...	...	19.692	18.924	18.319	...	...	...	...	...
2572	92.077098	24.077953	0.273	...	...	19.046	18.016	16.864	...	...	...	...	...
1146	92.394638	24.489595	0.277	...	...	18.901	17.863	16.844	...	...	...	...	...
2719	92.294801	24.523176	0.288	...	13.827	13.242	12.908	12.510	...	...	...	...	...
303	92.524280	24.055947	0.296	...	...	19.510	18.417	17.260	...	...	...	...	...
1802	92.339067	24.584038	0.297	...	13.787	13.211	12.892	12.490	...	...	...	...	...
2712	92.273068	24.227412	0.302	16.928	16.762	16.069	15.648	15.202	...	...	...	...	...
1764	92.451012	24.060802	0.318	...	15.248	14.576	14.178	13.699	1	14.98	0	0	...
3045	91.945761	24.202459	0.319	...	18.995	17.643	16.838	16.064	1	-2.06	0	0	...
1268	92.162259	24.555135	0.324	...	18.245	17.025	16.310	15.615	1	-6.54	0	88	...
1968	92.063314	24.397054	0.330	...	...	18.087	17.085	16.141	...	...	...	...	...
738	92.473507	24.424594	0.335	...	19.301	17.911	17.092	16.233	...	...	...	...	...
3093	92.234076	24.393724	0.337	15.968	15.718	15.091	14.694	14.272	...	...	...	...	...
1981	92.335445	24.610730	0.337	...	18.964	17.601	16.788	15.927	1	-6.58	0	88	...
3453	92.053804	24.296638	0.352	18.333	17.653	16.574	15.931	15.325	...	...	...	...	...
2225	92.212895	24.315928	0.358	...	19.348	18.059	17.155	16.319	...	...	...	...	...
1776	92.155876	24.345399	0.360	...	18.674	17.391	16.558	15.827	1	-12.52	0	4	...
935	92.429221	24.456933	0.367	...	18.699	17.281	16.461	15.609	1	-2.52	0	0	...
1458	92.360605	24.535450	0.381	...	17.031	16.268	15.787	15.247	...	...	...	...	...
228	92.273399	24.028495	0.382	...	17.715	16.989	16.480	15.981	...	...	...	...	...
1697	92.514129	24.035196	0.384	...	18.660	17.440	16.651	15.825	1	-9.24	0	91	...
1903	92.309464	24.107633	0.387	...	18.219	17.285	16.564	15.772	...	...	...	...	...
1645	92.543297	24.018063	0.393	...	18.646	17.313	16.539	15.765	...	...	...	...	...
1643	92.136100	24.644691	0.394	...	...	18.761	17.774	16.799	...	...	...	...	...

Continued on Next Page...

Table B.1 – Continued

ID	**RA** $h\ \ m\ \ s$	**DEC** $^o\ \ '\ \ ''$	P_r **Days**	**U**	**B**	**V**	**R**	**I**	N_{RV}	$\bar{RV}$ $km\ s^{-1}$	σ_{RV} $km\ s^{-1}$	P_{RV} %	P_{PM} %
108	92.004253	24.337935	0.397	...	16.866	16.232	15.864	15.446	...	...	...	...	...
1842	92.271032	24.089563	0.403	...	16.968	16.343	15.925	15.438	...	...	...	...	...
1603	92.174651	24.218581	0.405	...	18.466	17.235	16.461	15.739	...	...	...	...	...
895	92.597244	24.182369	0.412	...	...	18.241	17.313	16.413	...	...	...	...	...
3407	92.267530	24.279768	0.419	...	...	19.159	18.083	17.048	...	...	...	...	...
377	92.069086	24.390419	0.427	19.153	18.202	17.033	16.343	15.632	...	...	...	...	...
2035	91.966168	24.417218	0.450	...	...	18.469	17.527	16.628	...	...	...	...	...
2461	92.297773	24.423355	0.460	...	18.703	17.456	16.680	15.947	1	-10.24	0	79	...
852	92.344674	24.441688	0.464	...	19.435	18.017	17.130	16.328	1	-13.59	0	0	...
3192	92.209893	24.537094	0.467	...	13.978	13.401	13.029	12.657	2	-6.38	1.02	86	99
2770	92.140602	24.123153	0.479	...	...	18.673	17.724	16.783	...	...	...	...	...
2821	92.250792	24.561762	0.503	...	...	18.304	17.401	16.478	...	...	...	...	...
917	92.270854	24.196216	0.511	...	...	18.552	17.629	16.660	...	...	...	...	...
1445	92.200837	24.196395	0.512	...	18.550	17.100	16.199	15.339	1	-28.75	0	0	...
966	92.521790	24.200807	0.513	...	17.910	17.113	16.634	16.134	...	...	...	...	...
1974	92.248929	24.397959	0.516	...	...	18.180	17.372	16.598	...	...	...	...	...
1025	92.371989	24.472273	0.520	...	18.689	17.425	16.691	16.007	1	30.63	0	0	...
173	92.085814	24.024817	0.527	...	18.180	17.130	16.430	15.735	...	...	...	...	...
1990	92.281089	24.136417	0.543	...	17.524	16.486	15.860	15.210	1	-9.05	0	92	...
1284	92.501491	24.509136	0.547	...	17.221	16.443	15.959	15.439	...	...	...	...	...
3079	92.252066	24.199974	0.560	15.587	15.394	14.536	14.004	13.497	3	-7.87	0.22	94	...
1662	92.105889	24.230504	0.569	17.646	17.110	16.102	15.518	14.942	5	-9.78	4.72	87	...
2474	92.321101	24.286815	0.579	13.935	13.809	13.313	12.994	12.645	1	-9.16	0	92	...
1760	92.159577	24.341939	0.582	...	...	18.787	17.960	17.147	...	...	...	...	...
3037	92.054646	24.195314	0.593	17.133	16.970	16.289	15.865	15.412	...	...	...	...	...
1011	92.019577	24.140633	0.596	...	15.184	14.486	14.073	13.603	4	-10.39	0.53	76	91
2343	92.316004	24.384965	0.596	16.713	16.586	15.945	15.536	15.113	...	...	...	...	...
3171	91.971546	24.353596	0.596	...	13.557	13.105	12.834	12.544	1	-5.51	0	65	94
2392	92.307321	24.263274	0.622	...	...	17.997	17.160	16.271	...	...	...	...	...

Continued on Next Page...

Table B.1 – Continued

ID	**RA** $h\ \ m\ \ s$	**DEC** $^o\ \ '\ \ ''$	P_r **Days**	**U**	**B**	**V**	**R**	**I**	N_{RV}	$\bar{RV}$ $km\ s^{-1}$	σ_{RV} $km\ s^{-1}$	P_{RV} %	P_{PM} %
1092	92.023613	24.151637	0.623	...	17.403	16.640	16.175	15.695	...	...	...	...	...
1180	92.406648	24.249552	0.629	18.720	18.023	16.842	16.124	15.427	1	-12.00	0	13	...
1387	92.439398	24.524914	0.630	...	18.171	17.494	17.016	16.466	...	...	...	...	...
3622	91.953961	24.090427	0.636	...	18.086	17.348	16.851	16.327	...	...	...	...	...
2650	92.286030	24.496408	0.651	...	...	19.138	18.075	17.050	...	...	...	...	...
2425	92.512817	24.410634	0.653	...	17.280	16.250	15.611	14.973	3	-7.33	0.40	93	...
1008	91.975955	24.141571	0.661	...	17.756	17.054	16.604	16.121	...	...	...	...	...
361	92.406037	24.071854	0.688	...	17.064	16.328	15.920	15.418	...	...	...	...	...
2370	92.280921	24.256775	0.690	19.169	18.057	16.813	16.012	15.289	...	...	...	...	...
3142	92.158349	24.595711	0.690	...	13.791	13.282	12.952	12.630	1	-3.13	0	1	40
2653	92.353429	24.135622	0.697	...	18.878	17.486	16.677	15.856	1	-5.21	0	53	...
2521	92.140931	24.062530	0.698	...	16.979	16.314	15.882	15.450	...	...	...	...	...
1134	92.226064	24.150385	0.715	...	18.102	16.957	16.257	15.585	...	...	...	...	...
1581	92.416742	24.552771	0.715	...	17.703	16.967	16.510	15.999	...	...	...	...	...
903	92.273651	24.193193	0.728	...	18.464	17.270	16.509	15.850	1	-12.84	0	2	...
289	92.327159	24.359454	0.738	...	19.210	17.781	16.960	16.188	1	-2.66	0	0	...
2926	92.063474	24.468152	0.738	...	18.558	17.393	16.610	15.943	1	-6.03	0	80	...
4009	92.103584	23.988434	0.753	...	...	...	...	...	...	...	...	...	...
1299	92.224155	24.174459	0.754	...	...	18.302	17.389	16.541	...	...	...	...	...
1614	91.965730	24.225989	0.755	...	...	18.947	18.258	17.572	...	...	...	...	...
65	92.053486	24.330225	0.764	19.246	18.341	17.139	16.440	15.715	1	-7.72	0	94	...
2128	92.247988	24.300003	0.765	...	...	18.386	17.448	16.591	...	...	...	...	...
947	92.176675	24.488815	0.765	14.956	14.820	14.166	13.775	13.352	3	5.99	0.79	0	...
1425	92.335560	24.530776	0.781	...	13.504	12.896	12.546	12.159	1	14.20	0	0	...
2474	92.127706	24.052400	0.809	...	19.268	18.078	17.240	16.401	...	...	...	...	...
3191	92.190163	24.532452	0.830	...	14.249	13.618	13.232	12.811	3	-8.68	0.33	93	98
3588	91.953669	24.030691	0.832	...	15.500	14.854	14.460	14.022	...	...	...	...	...
2627	92.578723	24.486189	0.851	...	18.538	17.317	16.550	15.736	...	...	...	...	...
1309	92.091277	24.564000	0.859	...	18.588	17.778	17.266	16.688	...	...	...	...	...

Continued on Next Page...

Table B.1 – Continued

ID	RA	DEC	P_r	U	B	V	R	I	N_{RV}	$\bar{RV}$	σ_{RV}	P_{RV}	P_{PM}
	h m s	^{o} $'$ $''$	Days							$km\ s^{-1}$	$km\ s^{-1}$	%	%
83	92.467740	24.328546	0.872	...	18.452	17.248	16.498	15.769	1	-7.18	0	92	...
1199	92.119964	24.542256	0.874	...	17.162	16.470	15.988	15.492	...	...	...	...	...
2228	92.290211	24.346341	0.877	...	...	19.386	18.635	17.905	...	...	...	...	...
3251	92.166119	24.453221	0.878	13.878	13.779	13.290	12.990	12.647	1	-6.90	0	91	...
1979	92.257994	24.276333	0.881	18.036	17.489	16.356	15.666	15.018	1	12.14	0	0	...
1715	92.078236	24.330311	0.901	18.535	17.918	16.834	16.173	15.542	1	-11.44	0	34	...
1315	92.019058	24.182679	0.914	...	18.749	17.471	16.711	15.994	1	-9.93	0	85	...
1359	92.287519	24.521765	0.932	...	18.206	16.731	15.907	15.055	...	...	...	...	...
1497	92.477204	24.305461	0.932	...	17.693	16.574	15.928	15.277	3	-8.50	0.91	94	...
705	92.008521	24.446521	0.952	...	17.543	16.500	15.882	15.246	3	-4.17	2.22	11	...
1648	91.990358	24.313890	0.959	...	18.260	17.589	17.153	16.716	...	...	...	...	...
122	92.286693	24.334872	0.970	18.762	18.013	16.898	16.175	15.516	1	-9.00	0	92	...
2320	92.178619	24.494160	0.984	17.458	16.829	15.786	15.154	14.521	3	-9.14	0.53	92	...
760	92.223544	24.454640	0.994	...	18.174	16.976	16.267	15.551	1	-2.37	0	0	...
1240	92.559623	24.256574	1.00	...	17.024	16.026	15.445	14.862	3	-7.85	0.93	94	...
2582	92.394822	24.469891	1.02	14.079	13.903	13.375	13.053	12.665	1	-7.32	0	93	...
2607	92.247535	24.576527	1.04	...	17.939	16.880	16.196	15.534	1	-10.01	0	84	...
926	92.122260	24.483395	1.07	15.311	15.185	14.452	13.982	13.513	15	-8.69	4.38	93	99
201	92.373561	24.040211	1.07	...	16.960	16.332	15.864	15.397	...	...	...	...	...
3281	92.241724	24.251699	1.08	...	...	18.687	17.830	17.020	...	...	...	...	...
100	92.260479	24.331080	1.10	17.947	17.372	16.279	15.597	14.919	11	-8.38	5.48	94	...
1540	92.115113	24.210352	1.10	17.992	17.417	16.339	15.714	15.113	3	-5.82	0.52	75	...
3088	92.073926	24.207081	1.11	16.678	16.246	15.299	14.722	14.171	3	-7.25	1.84	92	...
884	91.962244	24.125567	1.13	...	14.238	13.946	13.753	13.529	...	...	...	...	...
609	92.082631	24.084017	1.13	...	16.529	15.638	15.121	14.621	3	-7.63	0.60	93	...
2498	92.385993	24.289693	1.16	...	18.804	17.295	16.394	15.530	1	-10.68	0	67	...
1476	92.056225	24.601142	1.18	...	19.218	17.988	17.207	16.367	...	...	...	...	...
2158	92.145291	24.449694	1.18	18.781	17.878	16.751	16.114	15.486	1	-8.43	0	94	...
163	92.041544	24.350173	1.23	16.582	15.724	14.712	14.107	13.543	1	46.59	0	0	...

Continued on Next Page...

Table B.1 – Continued

ID	**RA** $h\ \ m\ \ s$	**DEC** $^o\ \ '\ \ ''$	P_r **Days**	**U**	**B**	**V**	**R**	**I**	N_{RV}	$\bar{RV}$ $km\ s^{-1}$	σ_{RV} $km\ s^{-1}$	P_{RV} %	P_{PM} %
1496	92.562022	24.302400	1.24	...	18.094	17.362	16.916	16.539	...	...	...	...	...
2468	92.369944	24.425855	1.27	17.001	16.622	15.669	15.115	14.568	3	-8.92	0.77	93	...
2735	92.158374	24.113417	1.28	...	14.352	13.939	13.692	13.449	...	...	...	...	...
1356	92.348176	24.520982	1.28	...	17.080	15.918	15.271	14.597	4	-9.03	2.32	92	...
1518	92.341612	24.313858	1.32	17.638	16.970	15.849	15.179	14.557	4	-5.61	0.73	69	...
740	92.495495	24.150748	1.33	...	17.772	16.966	16.398	15.837	...	...	...	...	...
1679	92.230406	24.230442	1.35	15.743	15.486	14.975	14.651	14.286	...	...	...	...	...
1878	92.288075	24.100821	1.35	...	17.290	16.216	15.627	15.010	3	-10.03	0.61	83	...
3187	92.190057	24.483426	1.37	...	17.799	16.672	16.013	15.382	1	-11.49	0	32	...
2711	92.319713	24.520569	1.38	...	15.178	14.805	14.557	14.302	...	...	...	...	...
3199	92.253615	24.625194	1.40	...	13.837	13.553	13.384	13.171	...	...	...	...	...
2716	92.222103	24.610106	1.41	...	18.861	17.662	16.876	16.135	1	-11.04	0	53	...
1375	92.507310	24.281335	1.50	...	15.251	14.498	14.051	13.626	3	-9.55	0.94	89	79
424	92.301414	24.381086	1.66	...	...	18.417	17.420	16.466	...	...	...	...	...
1798	92.461709	24.582870	1.67	...	15.652	15.268	14.990	14.676	...	...	...	...	...
1295	92.388022	24.511436	1.68	...	16.588	15.607	15.046	14.486	8	-9.49	1.50	90	...
2728	92.292794	24.528983	1.77	...	15.393	14.635	14.190	13.734	4	-7.43	0.25	93	95
317	92.549127	24.361531	1.82	...	15.171	14.518	14.102	13.696	4	8.94	0.86	0	58
2665	92.104196	24.101740	1.86	...	18.590	17.298	16.581	15.874	1	-9.26	0	91	...
3105	92.281839	24.464903	1.91	15.359	15.251	14.539	14.109	13.682	6	-8.61	0.92	93	...
606	92.508625	24.124315	1.92	...	15.293	14.947	14.678	14.426	...	...	...	...	...
1908	92.341345	24.599630	2.05	...	17.202	16.074	15.430	14.734	3	-8.27	1.44	94	...
2793	91.934709	24.134355	2.05	...	15.934	15.133	14.698	14.205	2	25.42	106.47	0	...
619	92.153117	24.429995	2.09	14.325	14.368	14.072	13.837	13.572	...	...	...	...	...
1751	92.229426	24.240409	2.14	17.232	16.937	16.162	15.739	15.321	...	...	...	...	...
2373	92.197433	24.506929	2.14	...	17.706	16.645	15.985	15.350	1	-11.14	0	48	...
191	92.468889	24.345694	2.16	...	16.611	15.746	15.208	14.683	3	21.81	0.49	0	...
2223	92.260770	24.345754	2.20	14.353	14.219	13.616	13.236	12.829	32	-8.30	21.44	94	...
119	92.108585	24.015724	2.29	...	17.639	16.658	16.040	15.481	...	...	...	...	...

Continued on Next Page...

Table B.1 – Continued

ID	**RA** $h\ \ m\ \ s$	**DEC** $^o\ \ '\ \ ''$	P_r **Days**	**U**	**B**	**V**	**R**	**I**	N_{RV}	$\bar{RV}$ $km\ s^{-1}$	σ_{RV} $km\ s^{-1}$	P_{RV} %	P_{PM} %
1131	92.157857	24.529309	2.33	...	17.009	15.954	15.325	14.678	14	-8.07	34.54	94	...
3161	92.013667	24.223760	2.34	15.488	15.428	14.710	14.256	13.819	4	-9.27	0.60	91	...
2686	92.187448	24.601842	2.38	...	14.557	13.964	13.610	13.255	1	24.20	0	0	5
2720	92.311874	24.523107	2.38	...	15.724	14.927	14.447	13.972	1	-7.91	0	94	94
3450	92.264680	24.289861	2.40	17.637	17.047	15.951	15.287	14.669	19	-7.05	13.28	91	...
2338	92.286801	24.382087	2.50	15.560	15.447	14.696	14.233	13.766	4	-9.09	0.21	92	...
1849	92.084076	24.364310	2.52	15.736	15.603	14.859	14.402	13.956	15	-8.15	2.11	94	...
816	92.165184	24.464347	2.53	18.543	18.159	17.206	16.626	16.066	...	...	...	...	...
309	92.537986	24.360652	2.54	...	18.737	17.571	16.863	16.168	...	...	...	...	...
1990	91.913626	24.402348	2.55	...	15.504	14.743	14.304	13.840	3	-7.80	0.62	94	...
1208	92.597958	24.249337	2.59	...	16.314	15.354	14.927	14.304	4	-9.14	0.04	92	...
3234	91.966434	24.568866	2.59	...	13.015	12.823	12.683	12.514	...	...	...	...	...
1857	92.219030	24.366700	2.68	19.056	18.371	17.208	16.495	15.761	1	11.16	0	0	...
2251	92.350547	24.216637	2.68	16.250	16.052	15.204	14.682	14.181	...	...	...	...	...
3305	92.043853	24.263809	2.69	15.674	15.550	14.793	14.345	13.900	3	-6.80	0.72	90	...
731	92.559174	24.423202	2.74	...	15.762	14.979	14.497	14.066	14	-9.84	1.27	86	...
1438	92.213613	24.592012	2.78	...	14.974	14.155	13.682	13.196	3	-8.20	0.88	94	...
1455	92.481794	24.295939	2.83	...	15.900	15.020	14.509	13.990	18	-7.53	17.78	93	...
1633	92.387951	24.019141	2.83	...	17.423	16.332	15.685	15.091	3	-8.75	1.97	93	...
570	92.103076	24.078137	2.85	...	15.473	14.763	14.312	13.891	3	-8.58	0.53	93	...
2024	92.174192	24.284492	2.86	15.833	15.661	14.882	14.410	13.947	5	-7.37	0.23	93	...
375	92.172431	24.389346	2.88	15.837	15.613	14.763	14.263	13.765	3	5.71	0.43	0	...
2077	92.488861	24.158915	2.91	...	15.933	15.043	14.481	13.938	1	-9.77	0	87	...
574	92.064235	24.424163	2.91	16.281	15.938	15.123	14.687	14.199	15	-5.97	1.76	79	...
2652	92.284825	24.496917	2.95	...	...	18.034	17.077	16.134	...	...	...	...	...
2442	91.988691	24.530975	3.07	...	18.392	17.187	16.514	15.811	1	73.73	0	0	...
363	92.062833	24.387815	3.07	...	18.275	17.114	16.407	15.722	1	-15.89	0	0	...
3963	92.153272	24.036777	3.11	...	13.393	12.988	12.741	12.443	1	-2.61	0	0	72
1457	92.255273	24.196007	3.19	16.301	15.971	15.029	14.465	13.917	3	-7.88	0.25	94	...

Continued on Next Page...

Table B.1 – Continued

ID	**RA** $h\ \ m\ \ s$	**DEC** $^o\ \ '\ \ ''$	P_r **Days**	**U**	**B**	**V**	**R**	**I**	N_{RV}	$\bar{RV}$ $km\ s^{-1}$	σ_{RV} $km\ s^{-1}$	P_{RV} %	P_{PM} %
3044	92.413251	24.329701	3.19	16.210	15.940	15.059	14.530	14.028	3	-7.20	0.36	92	...
2308	92.113734	24.491755	3.21	16.393	16.096	15.217	14.693	14.183	3	-8.53	0.16	94	...
791	92.456746	24.433583	3.21	...	17.734	16.753	16.152	15.580	...	...	...	...	...
3092	91.978498	24.395161	3.30	...	15.800	15.028	14.569	14.129	16	-8.80	2.37	93	...
3083	91.992795	24.383520	3.34	...	15.226	14.543	14.154	13.733	4	-7.60	0.14	93	96
823	92.225014	24.465782	3.34	...	...	18.507	17.550	16.678	...	...	...	...	...
1975	91.954222	24.399860	3.39	...	15.657	14.867	14.399	13.962	3	14.80	0.39	0	...
1984	92.456668	24.610300	3.41	...	15.966	14.830	14.163	13.556	2	18.16	0.53	0	...
2722	92.546467	24.233778	3.43	...	16.130	15.278	14.742	14.251	3	-7.67	0.44	94	...
1752	92.534647	24.575550	3.46	...	16.944	15.886	15.253	14.612	3	-7.78	0.82	94	...
1914	91.917076	24.383993	3.46	...	...	18.512	17.835	17.198	...	...	...	...	...
2566	92.049969	24.565758	3.51	...	16.168	15.266	14.705	14.142	7	34.65	13.92	0	...
2125	92.314884	24.178377	3.56	17.082	16.501	15.467	14.858	14.295	37	-5.93	8.58	78	...
2126	92.126237	24.441231	3.56	16.125	15.906	15.095	14.623	14.154	3	-7.87	0.30	94	...
1015	92.293266	24.217595	3.58	...	19.378	17.816	16.909	16.055	1	-4.78	0	33	...
2534	92.466089	24.450140	3.61	...	15.720	14.805	14.256	13.753	3	-8.85	0.23	93	67
1363	92.020983	24.578153	3.69	...	18.967	17.777	17.078	16.345	...	...	...	...	...
1484	92.447848	24.538892	3.69	...	16.172	15.308	14.809	14.289	3	-8.82	0.23	93	...
1610	92.371625	24.011765	3.71	...	15.777	14.984	14.510	14.058	3	-9.82	0.23	86	...
85	92.187953	24.332271	3.71	16.258	15.905	14.944	14.393	13.845	6	-7.97	0.32	94	...
486	92.359760	24.388770	3.74	18.008	17.364	16.284	15.664	15.078	3	-7.93	0.47	94	...
738	92.049226	24.451988	3.77	16.158	15.947	15.168	14.701	14.261	3	-8.09	0.58	94	...
770	92.417986	24.429521	3.77	...	19.152	18.182	17.552	16.995	...	...	...	...	...
3457	92.039842	24.298267	3.80	...	...	19.443	18.367	17.226	...	...	...	...	...
2806	92.428134	24.556982	3.83	...	...	19.114	18.336	17.507	...	...	...	...	...
1099	92.505333	24.228629	3.86	...	15.941	15.158	14.666	14.216	3	-7.79	0.05	94	...
3558	92.174366	24.318673	3.86	...	19.219	17.771	16.935	16.196	...	...	...	...	...
1188	92.111246	24.161094	3.92	16.307	16.052	15.145	14.599	14.054	...	...	...	...	...
1240	92.032904	24.549485	3.95	...	15.983	15.178	14.707	14.268	3	-7.68	0.23	94	...

Continued on Next Page...

Table B.1 – Continued

ID	**RA** $h\ m\ s$	**DEC** $^o\ '\ ''$	P_r **Days**	**U**	**B**	**V**	**R**	**I**	N_{RV}	$\bar{RV}$ $km\ s^{-1}$	σ_{RV} $km\ s^{-1}$	P_{RV} %	P_{PM} %
2184	92.029437	24.313865	3.95	16.187	15.968	15.146	14.668	14.212	1	-6.49	0	87	72
472	92.043528	24.406614	3.95	16.611	16.283	15.441	14.938	14.467	3	-7.26	0.10	92	...
2220	92.267763	24.211646	3.98	16.491	16.186	15.306	14.777	14.283	3	-8.08	0.05	94	...
2485	92.218491	24.051748	3.98	...	15.820	15.064	14.616	14.178	3	-8.09	0.51	94	...
2807	92.382945	24.177319	3.98	16.243	15.923	15.014	14.465	13.946	22	-8.10	5.75	94	...
465	92.194624	24.063037	4.15	...	...	18.583	17.616	16.696	...	...	...	...	...
2858	91.969182	24.333996	4.22	...	15.945	15.171	14.703	14.270	3	-7.03	0.19	91	...
2370	91.934877	24.507273	4.25	...	16.058	15.234	14.742	14.245	16	-7.03	5.00	91	...
2408	92.543905	24.404000	4.25	...	16.171	15.330	14.807	14.350	5	-8.90	1.19	93	...
3151	92.261162	24.214189	4.25	16.924	16.527	15.561	14.994	14.462	3	-7.55	0.32	93	...
2201	92.507305	24.336692	4.29	...	16.226	15.347	14.846	14.333	3	-8.71	0.43	93	...
1676	92.138243	24.320342	4.33	16.372	16.110	15.280	14.799	14.315	3	-8.21	0.39	94	...
1946	92.217645	24.391151	4.33	16.219	16.003	15.150	14.653	14.144	3	-9.46	0.04	90	...
2115	92.488540	24.171030	4.36	...	16.906	15.834	15.192	14.571	...	...	...	...	...
2311	92.258959	24.492007	4.40	17.393	16.810	15.863	15.296	14.753	3	-7.51	0.76	93	...
1935	92.380118	24.117458	4.44	...	15.992	15.151	14.663	14.191	3	-8.08	0.67	94	...
2538	92.392241	24.302521	4.44	17.000	16.568	15.599	15.020	14.449	3	-6.61	0.34	88	...
1818	92.239187	24.251397	4.48	16.950	16.581	15.619	15.049	14.480	3	-9.01	0.41	92	...
2487	92.341232	24.288057	4.48	16.684	16.352	15.458	14.946	14.435	4	-8.71	0.43	93	...
2480	92.458636	24.284114	4.52	...	16.534	15.574	15.031	14.503	3	-9.02	0.34	92	...
267	92.529789	24.048719	4.52	...	18.067	16.837	16.168	15.510	1	19.22	0	0	...
1956	92.177207	24.393676	4.56	18.890	18.128	16.972	16.267	15.590	1	2.18	0	0	...
1127	92.194237	24.528621	4.61	...	16.472	15.561	14.997	14.453	3	-7.90	1.03	94	...
2855	92.078440	24.321916	4.61	16.977	15.922	14.148	13.200	12.303	...	...	...	...	...
2460	92.347823	24.282427	4.65	18.969	18.500	17.536	16.933	16.339	...	...	...	...	...
2520	92.276633	24.444927	4.65	17.244	16.819	15.827	15.247	14.690	17	-0.67	16.26	0	...
3020	92.488673	24.630527	4.69	...	16.640	15.688	15.158	14.573	3	-8.45	0.13	94	...
67	92.262774	24.326725	4.69	17.149	16.752	15.750	15.166	14.600	14	-9.24	9.05	91	...
748	92.235082	24.452950	4.74	16.745	16.409	15.509	14.990	14.494	3	-6.24	0.07	84	...

Continued on Next Page...

Table B.1 – Continued

ID	**RA** $h\ \ m\ \ s$	**DEC** $^o\ \ '\ \ ''$	P_r **Days**	**U**	**B**	**V**	**R**	**I**	N_{RV}	$\bar{RV}$ $km\ s^{-1}$	σ_{RV} $km\ s^{-1}$	P_{RV} %	P_{PM} %
976	92.380909	24.463800	4.74	16.303	16.029	15.191	14.691	14.234	3	-8.05	0.30	94	...
372	92.031770	24.054656	4.78	...	18.013	16.892	16.210	15.590	...	...	...	...	...
1442	92.519612	24.292992	4.83	...	16.314	15.412	14.926	14.453	3	-7.40	0.16	93	...
2455	92.412526	24.278934	4.83	16.933	16.526	15.613	15.063	14.539	4	-7.38	0.42	93	...
3730	92.145669	24.285589	4.83	...	...	19.087	18.062	17.015	...	...	...	...	...
3533	92.230660	24.308635	4.92	18.951	18.517	17.407	16.802	16.169	...	...	...	...	...
4033	92.098591	23.993092	4.92	...	16.560	15.668	15.180	14.690	1	-7.61	0	93	...
1891	92.375305	24.597189	4.97	...	...	18.874	17.889	16.849	...	...	...	...	...
1258	92.115455	24.553257	5.02	...	16.742	15.759	15.222	14.691	5	-8.41	1.05	94	...
1998	92.422425	24.612290	5.02	...	16.549	15.650	15.110	14.548	3	-8.27	0.62	94	...
1172	92.495023	24.245351	5.07	...	16.419	15.484	14.927	14.405	3	-9.20	0.30	91	...
273	92.377013	24.054506	5.07	...	...	18.746	17.706	16.756	...	...	...	...	...
2312	92.197046	24.009344	5.13	...	18.334	17.266	16.676	16.079	...	...	...	...	...
1898	92.238451	24.264810	5.18	...	19.268	17.830	16.987	16.204	1	-11.64	0	25	...
1318	92.331866	24.514651	5.23	...	16.685	15.725	15.171	14.633	3	-7.56	0.35	93	...
1391	92.330170	24.289553	5.24	16.820	16.457	15.533	14.992	14.459	17	-8.86	6.83	93	...
2727	92.561020	24.526261	5.29	...	19.576	18.129	17.223	16.416	1	1.52	0	0	...
2138	92.179039	24.442804	5.40	17.059	16.635	15.664	15.099	14.551	3	-9.51	0.37	89	...
1211	92.198349	24.161734	5.46	17.105	16.716	15.764	15.213	14.702	1	-7.33	0	93	...
2967	92.484785	23.993084	5.46	...	17.599	16.448	15.793	15.032	2	-6.48	1.34	87	...
634	92.431021	24.409375	5.46	16.710	16.379	15.483	14.986	14.505	3	-7.97	0.48	94	...
1532	92.272437	24.205003	5.52	17.365	16.828	15.843	15.283	14.759	3	-7.91	0.33	94	...
1687	92.165483	24.323363	5.52	...	18.900	17.531	16.747	16.034	1	-6.54	0	88	...
1907	92.187057	24.381290	5.52	17.685	16.996	15.904	15.255	14.655	3	-8.90	0.40	93	...
2788	92.200364	24.630557	5.52	...	16.620	15.689	15.176	14.729	3	-8.37	0.53	94	...
756	92.146254	24.454718	5.52	17.145	16.634	15.639	15.048	14.495	3	-9.15	0.46	92	...
19	92.239391	23.993396	5.58	...	18.155	16.986	16.290	15.640	...	...	...	...	...
752	92.360601	24.426949	5.58	17.805	17.491	16.563	16.010	15.458	...	...	...	...	...
1681	92.345336	24.568457	5.65	...	17.058	16.044	15.454	14.831	3	-8.82	0.32	93	...

Continued on Next Page...

Table B.1 – Continued

ID	RA	DEC	P_r	U	B	V	R	I	N_{RV}	$\bar{RV}$	σ_{RV}	P_{RV}	P_{PM}
	h m s	^{o} $'$ $''$	Days							$km\ s^{-1}$	$km\ s^{-1}$	%	%
1890	92.073695	24.268103	5.65	17.101	16.677	15.759	15.229	14.736	3	-9.46	0.45	90	...
2336	92.398652	24.381438	5.65	...	...	18.283	17.306	16.500	...	...	...	...	...
2540	92.341012	24.305886	5.65	17.505	16.963	15.955	15.375	14.841	3	-8.66	0.11	93	...
268	92.155376	24.371622	5.65	17.412	16.905	15.904	15.341	14.803	3	-8.16	0.65	94	...
1921	92.405590	24.601551	5.71	...	17.698	16.608	15.969	15.332	...	...	...	...	...
3336	92.180894	24.268684	5.71	17.242	16.776	15.801	15.265	14.736	3	-9.24	0.38	91	...
727	92.071007	24.450550	5.71	17.156	16.660	15.742	15.198	14.712	3	-7.67	0.18	94	...
1462	92.375181	24.535693	5.78	...	18.368	17.119	16.392	15.705	1	-6.66	0	89	...
2097	92.194104	24.295939	5.78	...	18.630	17.351	16.566	15.819	1	-13.30	0	0	...
2163	92.298710	24.189981	5.78	17.331	16.890	15.902	15.349	14.828	3	-8.95	0.13	93	...
230	92.027841	24.363983	5.78	...	19.572	18.106	17.224	16.446	1	-8.76	0	93	...
266	92.128491	24.371558	5.78	17.870	17.351	16.308	15.711	15.148	3	18.47	1.46	0	...
2875	91.955963	24.153696	5.78	...	16.863	15.927	15.393	14.905	...	...	...	...	...
3047	91.982002	24.200965	5.78	...	16.819	15.864	15.300	14.786	...	...	...	...	...
3528	92.246039	24.306946	5.78	17.570	17.057	16.008	15.399	14.843	3	-9.17	0.71	92	...
1729	92.147564	24.333129	5.85	18.753	17.920	16.763	16.082	15.454	1	-8.60	0	93	...
244	92.393596	24.047974	5.85	...	16.591	15.658	15.142	14.604	3	-7.57	1.28	93	...
1174	92.258034	24.535765	5.91	...	16.928	15.978	15.398	14.856	3	-7.36	0.22	93	...
1401	92.042368	24.585602	5.91	...	17.146	16.306	15.792	15.266	...	...	...	...	...
1560	92.515730	24.548530	5.91	...	15.843	15.061	14.580	14.108	3	21.40	0.34	0	...
2530	92.317080	24.300914	5.91	...	18.463	17.220	16.452	15.804	1	-9.55	0	89	...
684	92.138676	24.092649	5.91	...	16.807	15.856	15.343	14.806	3	-7.74	0.12	94	...
200	92.050194	24.357433	5.99	17.370	16.811	15.849	15.312	14.795	3	-8.36	0.14	94	...
2613	92.411878	24.481590	5.99	...	17.850	16.668	16.013	15.363	1	-8.26	0	94	...
401	92.226689	24.052228	6.02	...	15.733	14.968	14.516	14.059	19	-7.45	17.53	93	...
2049	92.171100	24.289074	6.13	17.635	17.053	16.042	15.470	14.947	3	-8.63	0.77	93	...
2290	92.124232	24.488279	6.13	17.932	17.271	16.197	15.578	15.026	3	-8.09	0.51	94	...
1979	91.931532	24.400440	6.21	...	18.397	17.087	16.258	15.476	1	-6.15	0	82	...
2754	92.165267	24.620922	6.29	...	16.866	15.940	15.410	14.883	3	-7.97	0.61	94	...

Continued on Next Page...

Table B.1 – Continued

ID	**RA** $h\ \ m\ \ s$	**DEC** $^o\ \ '\ \ ''$	P_r **Days**	**U**	**B**	**V**	**R**	**I**	N_{RV}	$\bar{RV}$ $km\ s^{-1}$	σ_{RV} $km\ s^{-1}$	P_{RV} %	P_{PM} %
327	92.371614	24.364224	6.29	18.086	17.345	16.263	15.654	15.090	4	-8.71	0.94	93	...
1479	92.199972	24.600607	6.37	...	16.861	15.922	15.388	14.871	3	-8.87	0.23	93	...
2029	92.254450	24.414773	6.37	...	...	18.306	17.396	16.576	...	...	...	...	...
750	91.959321	24.454900	6.37	...	17.355	16.308	15.658	15.051	...	...	...	...	...
988	92.278104	24.212562	6.37	...	19.403	17.903	17.019	16.257	...	...	...	...	...
1355	92.276293	24.284768	6.45	...	19.299	17.730	16.810	15.933	...	...	...	...	...
139	92.134004	24.343413	6.45	17.654	17.091	16.058	15.492	14.963	4	-7.24	0.49	92	...
2276	92.308633	24.226871	6.45	17.667	17.070	16.047	15.469	14.936	3	-8.50	0.90	94	...
1012	92.143540	24.137204	6.53	...	17.118	16.119	15.555	15.018	3	-7.00	0.45	91	...
1014	92.532623	24.469748	6.53	...	17.548	16.468	15.776	15.184	3	-7.60	0.56	93	...
1276	92.378055	24.267989	6.53	...	...	18.255	17.266	16.278	...	...	...	...	...
1915	92.581141	24.599333	6.53	...	18.880	17.550	16.754	15.982	1	-10.76	0	64	...
2120	92.472203	24.633322	6.53	...	18.397	17.154	16.435	15.744	...	...	...	...	...
2945	92.382907	24.604010	6.53	...	17.315	16.242	15.657	15.055	3	-8.37	0.54	94	...
59	92.259821	24.014149	6.53	...	17.939	16.914	16.296	15.683	...	...	...	...	...
717	92.387498	24.421601	6.53	17.935	17.210	16.170	15.560	15.008	3	-9.26	0.51	91	...
1195	92.490651	24.496003	6.62	...	...	18.769	17.719	16.805	...	...	...	...	...
1257	92.456015	24.263100	6.62	...	17.673	16.518	15.856	15.246	...	...	...	...	...
2268	92.277023	24.358399	6.62	18.233	17.480	16.373	15.736	15.168	3	-8.15	0.66	94	...
1120	92.311747	24.486227	6.80	...	17.243	16.225	15.636	15.107	3	-8.90	0.49	93	...
119	92.417821	24.021309	6.80	...	17.364	16.295	15.677	15.116	3	-8.28	0.39	94	...
2235	92.427465	24.347773	6.80	18.487	17.606	16.495	15.845	15.230	6	-8.05	1.35	94	...
2261	92.404832	24.356348	6.80	14.390	14.012	13.221	12.763	12.341	1	-2.08	0	0	...
4118	92.281150	24.142690	6.80	...	...	19.324	18.271	17.141	...	...	...	...	...
417	92.212765	24.397274	6.80	...	...	18.370	17.418	16.562	...	...	...	...	...
2636	92.262781	24.582357	6.89	...	17.088	16.065	15.488	14.886	3	-7.71	0.34	94	...
314	92.448052	24.060362	6.89	...	17.654	16.488	15.796	15.183	1	-8.82	0	93	...
680	92.069916	24.440804	6.89	...	18.213	17.038	16.327	15.701	1	-5.89	0	77	...
1440	92.031092	24.593259	6.99	...	18.352	17.098	16.381	15.710	1	-6.73	0	89	...

Continued on Next Page...

Table B.1 – Continued

ID	**RA** $h\ \ m\ \ s$	**DEC** $^o\ \ '\ \ ''$	P_r **Days**	**U**	**B**	**V**	**R**	**I**	N_{RV}	$\bar{RV}$ $km\ s^{-1}$	σ_{RV} $km\ s^{-1}$	P_{RV} %	P_{PM} %
1639	92.148934	24.225409	6.99	16.706	16.569	15.758	15.280	14.810	...	...	...	...	...
1901	92.184632	24.379756	6.99	17.738	16.907	15.765	15.118	14.514	16	-13.63	16.77	0	...
2142	92.281048	24.318199	6.99	...	...	18.562	17.590	16.701	...	...	...	...	...
365	92.585339	24.369701	6.99	...	18.632	17.343	16.559	15.830	1	-8.64	0	93	...
981	92.361654	24.465254	6.99	18.486	17.604	16.477	15.844	15.278	3	-8.71	0.11	93	...
1732	91.992213	24.336343	7.30	...	19.286	17.892	17.072	16.306	...	...	...	...	...
2721	92.277258	24.523899	7.30	...	19.016	17.695	16.893	16.095	...	...	...	...	...
2772	92.578172	24.545756	7.30	...	17.848	16.669	15.978	15.342	1	-9.37	0	90	...
993	92.294383	24.467769	7.30	18.564	17.675	16.531	15.894	15.334	6	-7.68	1.38	94	...
559	92.136657	24.419890	7.40	...	18.957	17.590	16.770	16.058	1	-15.73	0	0	...
2557	92.414169	24.456518	7.52	18.914	17.875	16.724	16.054	15.454	...	...	...	...	...
2970	91.917606	24.561253	7.52	...	17.365	16.657	16.203	15.762	...	...	...	...	...
3114	91.921921	24.216804	7.52	...	15.078	14.249	13.765	13.324	2	14.50	0.20	0	...
3129	92.107695	24.214937	7.52	19.086	18.051	16.867	16.166	15.566	1	-7.46	0	93	...
3268	92.093000	24.250697	7.52	18.419	17.586	16.502	15.866	15.301	1	-7.70	0	94	...
914	92.013110	24.481843	7.52	...	17.783	16.679	16.018	15.451	1	-9.09	0	92	...
2476	92.600402	24.279184	7.63	...	...	18.061	17.196	16.487	...	...	...	...	...
3188	92.434352	24.415091	7.63	...	...	18.391	17.441	16.580	...	...	...	...	...
3376	92.260189	24.273723	7.75	15.471	15.153	14.309	13.815	13.361	6	-3.31	0.50	1	...
900	92.328372	24.451400	7.75	18.651	17.678	16.566	15.931	15.383	1	-7.23	0	92	...
1507	92.559152	24.541760	7.87	...	18.264	17.004	16.313	15.626	1	-6.86	0	90	...
1805	92.520487	24.583080	7.87	...	18.055	16.858	16.184	15.513	...	...	...	...	...
1112	92.563399	24.483036	8.00	...	18.389	17.075	16.333	15.635	1	-9.53	0	89	...
1447	92.169971	24.197375	8.00	...	19.027	17.639	16.819	16.109	1	-6.13	0	82	...
2660	92.205085	24.097330	8.00	...	17.648	16.572	15.923	15.365	3	-6.17	0.66	83	...
3136	92.242356	24.553220	8.00	...	14.673	13.818	13.318	12.832	1	-1.76	0	0	...
3486	92.201156	24.299744	8.00	...	18.470	17.134	16.381	15.721	...	...	...	...	...
1324	92.014042	24.569422	8.13	...	18.141	16.958	16.257	15.644	...	...	...	...	...
3103	92.385452	24.456611	8.13	...	19.171	17.845	17.021	16.227	1	-4.47	0	20	...

Continued on Next Page...

Table B.1 – Continued

ID	**RA** $h\ \ m\ \ s$	**DEC** $^o\ \ '\ \ ''$	P_r **Days**	**U**	**B**	**V**	**R**	**I**	N_{RV}	$\bar{RV}$ $km\ s^{-1}$	σ_{RV} $km\ s^{-1}$	P_{RV} %	P_{PM} %
1322	92.550808	24.513923	8.26	...	16.531	15.464	14.839	14.251	3	-17.81	0.41	0	...
143	92.121425	24.019286	8.26	...	...	18.971	17.937	16.938	...	...	...	...	...
1782	92.245669	24.244902	8.26	18.361	17.410	16.203	15.497	14.868	5	-12.04	7.01	12	...
1023	92.323217	24.472350	8.40	17.471	17.246	16.673	16.360	16.017	...	...	...	...	...
2875	92.509021	24.577026	8.40	...	17.759	16.654	16.045	15.429	1	22.23	0	0	...
3217	91.920024	24.239827	8.40	...	17.806	16.701	16.049	15.400	...	...	...	...	...
3268	92.040793	24.574577	8.40	...	13.725	12.877	12.386	11.944	...	...	...	...	...
690	92.039706	24.097294	8.40	...	16.077	15.107	14.561	14.036	3	17.70	0.26	0	...
147	92.383504	24.026391	8.54	...	...	18.320	17.389	16.497	...	...	...	...	...
158	92.151274	24.348176	8.54	...	...	18.429	17.442	16.621	...	...	...	...	...
555	92.025074	24.078343	8.54	...	18.338	17.184	16.466	15.818	1	-5.18	0	52	...
867	92.090140	24.119385	8.54	...	16.284	15.508	15.046	14.585	3	11.28	0.12	0	...
1178	92.476009	24.494279	8.69	...	18.481	17.146	16.404	15.718	1	-6.89	0	91	...
2099	92.463615	24.167184	8.69	...	19.250	17.732	16.923	16.114	1	-9.38	0	90	...
2164	92.146723	24.306670	8.69	15.893	14.937	13.885	13.278	12.745	...	...	...	...	...
983	92.343925	24.465509	8.69	...	19.039	17.661	16.849	16.141	...	...	...	...	...
1819	92.097108	24.255633	8.84	...	18.387	17.105	16.400	15.777	1	-7.58	0	93	...
2493	92.508021	24.285541	8.84	...	18.987	17.612	16.791	16.074	1	-8.48	0	94	...
488	92.352092	24.103556	8.84	...	...	17.796	16.935	16.228	...	...	...	...	...
156	92.065349	24.022777	9.17	...	18.047	16.971	16.334	15.726	...	...	...	...	...
225	92.363810	24.351201	9.17	...	...	18.769	17.747	16.825	...	...	...	...	...
969	92.199916	24.129819	9.17	...	18.429	17.184	16.381	15.623	1	-4.38	0	17	...
1782	92.081835	24.347535	9.34	...	18.836	17.484	16.702	16.005	1	-9.46	0	90	...
3042	92.545709	24.326083	9.34	...	19.054	17.727	16.885	16.157	1	-9.68	0	88	...
889	92.463940	24.447843	9.46	...	...	18.765	17.729	16.779	...	...	...	...	...
1908	92.244243	24.381119	9.52	...	...	19.022	17.998	16.992	...	...	...	...	...
372	92.187587	24.388514	9.52	...	18.762	17.456	16.618	15.960	1	-4.99	0	43	...
1706	92.216396	24.234655	9.70	...	19.098	17.688	16.829	16.109	1	-9.33	0	91	...
2384	91.954111	24.034109	9.70	...	19.044	17.716	16.900	16.157	1	-8.07	0	94	...

Continued on Next Page...

Table B.1 – Continued

ID	**RA** $h\ \ m\ \ s$	**DEC** $^o\ \ '\ \ ''$	P_r **Days**	**U**	**B**	**V**	**R**	**I**	N_{RV}	$\bar{RV}$ $km\ s^{-1}$	σ_{RV} $km\ s^{-1}$	P_{RV} %	P_{PM} %
2672	91.977295	24.597143	9.70	...	18.878	17.635	16.837	16.137	1	-7.35	0	93	...
1806	92.102174	24.252754	9.89	17.872	17.141	16.106	15.548	15.012	3	-18.54	0.06	0	...
831	92.351489	24.438902	10.1	16.513	16.219	15.341	14.833	14.331	22	-7.36	28.39	93	...
1501	92.237595	24.201332	10.3	17.518	16.398	15.252	14.572	13.997	4	7.31	0.18	0	...
3758	92.104379	24.000950	10.3	...	18.613	17.543	16.954	16.376	...	...	...	...	...
547	92.548688	24.110287	10.9	...	16.542	15.590	15.030	14.505	3	24.97	0.53	0	...
798	92.044324	24.463038	11.4	...	...	18.442	17.515	16.675	...	...	...	...	...
1452	92.488221	24.534270	12.0	...	17.748	16.579	15.875	15.266	...	...	...	...	...
2259	92.251613	24.479262	12.6	15.756	15.215	14.323	13.779	13.279	2	-16.02	0.41	0	...
621	91.948527	24.090235	13.3	...	14.810	13.934	13.468	13.029	4	13.57	0.23	0	...
525	91.958165	24.077140	13.6	...	15.910	14.400	13.569	12.726	...	...	...	...	...
3979	91.962789	24.308025	14.4	...	13.842	12.997	12.504	12.062	1	49.71	0	0	...
1927	92.455431	24.113982	14.9	...	18.137	16.973	16.283	15.651	...	...	...	...	...
2964	92.071134	24.549330	15.3	...	16.481	15.535	14.987	14.467	...	...	...	...	...
955	92.111525	24.490206	15.3	...	17.834	16.682	16.001	15.380	1	27.17	0	0	...
1674	92.575255	24.565179	17.6	...	16.819	15.800	15.172	14.596	3	30.20	0.37	0	...
810	92.149304	24.463598	23.2	16.015	15.165	14.165	13.574	13.048	2	21.82	0.04	0	...
2906	92.520773	24.284515	25.5	...	14.619	12.677	11.112	...	...	...	...	...	...
2049	92.528159	24.620884	52.4	...	17.174	15.782	14.971	14.077	...	...	...	...	...
1152	92.125174	24.532799	58.4	...	18.978	17.356	16.361	15.457	1	-16.40	0	0	...

Appendix C

THE ROTATION PERIOD DISTRIBUTION OF THE NON-MEMBERS

In this section, we display and briefly comment upon the rotation period distribution of the non-members, which are presumably mostly background stars belonging to the Galactic disk. Unlike the M35 stars we do not know either the age, distance, or mass for these stars. We will therefore not try to draw any conclusions from a comparison between the two distributions but simply comment on distinct features in the period distribution of the 133 non-members shown in Figure C.1. First, periods are detected over the same range ($\sim$ 0.1 - 15 days) as for the 150 Myr cluster members. Second, there appear to be no indication of a bimodal distribution, but rather a distribution with a peak of ultra fast rotators and a long tail of periods to beyond 15 days. Third, and most strikingly, as shown by the 0.1 day resolution of the insert in Figure C.1, the non-member distribution exhibit a very distinct peak at rotation periods between 0.1 and 0.2 days. By inspecting of the phased light curves in Appendix A the reader can convince her or himself that the vast majority of these stars show very well defined photometric variability with with peak-to-peak amplitudes of $0\overset{\mathrm{m}}{.}1$ or higher.

These stars may be contact binaries of the W UMa-type although such binaries typically have orbital periods of order 0.2-0.5 days. We have not yet carefully considered the nature of these stars.

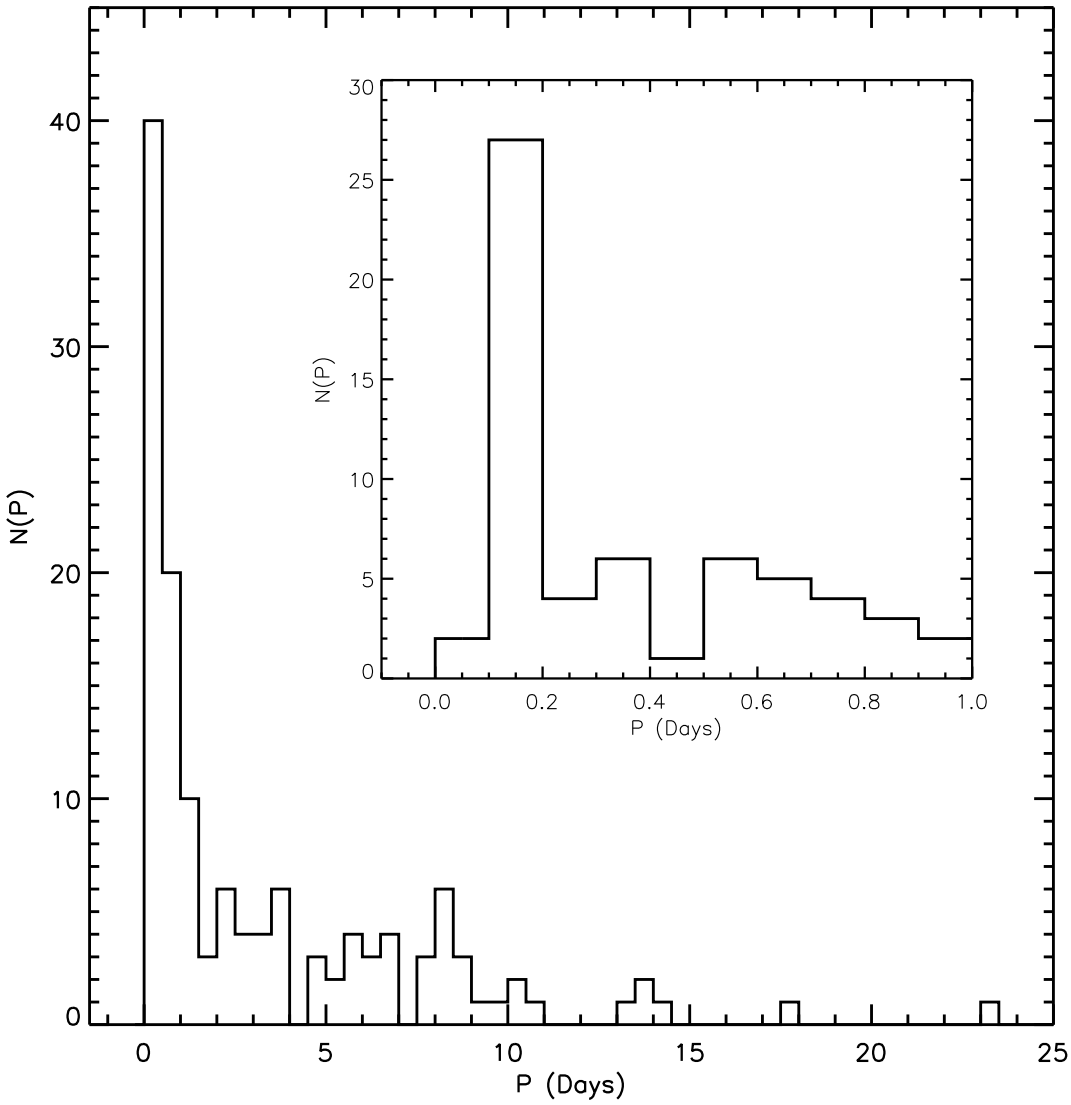

Fig. C.1.— The rotation period distribution of the 133 radial-velocity and/or photometric non-members. The insert shows the distribution of periods less than 1 day with increased resolution of 0.1 day.